The Cocaine-Binding Aptamer: A Thermodynamic and Structural Overview of Specific and Non-Specific Binding Interactions

OREN REINSTEIN

A DISSERTATION SUBMITTED TO

THE FACULTY OF GRADUATE STUDIES

IN PARTIAL FULFILLMENT OF THE REQUIREMENTS

FOR THE DEGREE OF

DOCTOR OF PHILOSOPHY

GRADUATE PROGRAM IN CHEMISTRY

YORK UNIVERSITY

TORONTO, ONTARIO

April 2016

Abstract

Isothermal Titration Calorimetry (ITC) studies were conducted wherein variances in the heat capacity of binding (ΔC_p) among variants of the cocaine-binding aptamer were suggestive of two distinct binding mechanisms. Aptamer variants containing 6 base pairs in stem 1 are pre-folded and show little change in secondary structure with ligand binding. Aptamer variants with 3 base pairs in stem 1 are mostly unfolded and exhibit conformational changes that take place with ligand binding.

ITC studies were extended to aptamer variants containing single nucleotide mutations and truncated stems. A relationship between nucleotide identity vs binding affinity was established while also noting that mutations within the aptamer core result in the switch of binding specificity from alkaloids to steroids. This altered specificity was most notable when one of two GA mismatched pairs in the aptamer core was converted to the Watson-Crick GC pair. Simultaneous mutation of both GA base pairs resulted in no detectable binding. Additional ITC and NMR spectroscopy studies demonstrated that the binding mechanism of steroid-binding aptamer constructs is nearly identical to that of cocaine-binding constructs. Conformational changes were noted for steroid-binding constructs with 4 base pairs in stem 1, as opposed to 3 base pairs as in cocaine-binding constructs.

Combined ITC and NMR spectroscopy studies characterized the high affinity interaction of the cocaine-binding aptamer with quinine, showing a 30 – 40 fold increased affinity over cocaine. The binding mechanism with quinine was shown to be identical to that of cocaine, utilizing the same binding site while electrostatic interactions contributed only about 6% of the binding free energy. Fluorescence spectroscopy revealed that the aptamer is structurally stable at very high concentrations of urea. MN4 and MN19 both demonstrated high resistance to chemical denaturation with concentrations of urea reaching 6 M and 4.4 M, respectively.

A final ITC study confirmed the bifunctionality of modified cocaine-binding aptamers. A titration of an equimolar mixture of deoxycholic acid (DCA) and cocaine had an enthalpy of (-32.5 ± 0.2) kcal mol^{-1}. This is comparable to the sum of enthalpies for independent titrations of cocaine and DCA at (-12 ± 5) and (-11 ± 2) kcal mol^{-1}, respectively.

Acknowledgements

I would like to wholeheartedly thank Professor Philip E. Johnson for providing me with such an amazing opportunity. What began as but a few months of research to end off my undergraduate career blossomed into so much more than anyone could have imagined. I have gained so much confidence, motivation, insight, and most importantly, creativity throughout this unbelievable journey. None of this would have been possible without your guidance and extreme patience at every step. I certainly have a very different outlook on the world today than I did when I first began, and in the end, I owe so much of it to you.

To my dearest father and mother, is it even possible for me to think of a moment where you weren't there for me? The support you've given me through this journey is already more than I could have ever asked for. At many times, the going got rough, and your advice always kept me strong. Father, you always quoted how fortunate we are that we have food on our table and a roof above our heads. When things were looking down, this was never a falsehood and would help maintain perspective so well that my shortcomings felt as mere seconds in the history of time. Mother, your care, compassion, and understanding for those around you have had such a huge impact on the positive attitude that I am able to maintain. Following your example, I have been able to forge and maintain amazing new friendships along the way and each one has been instrumental to my success. So I dedicate this thesis to the both of you and our beloved family.

To my brother, you've come to know me so well. My hopes, my dreams, and how "later" might be the most common word in my vocabulary. They say that a healthy mind is a healthy body however, it is ever more apparent that the reverse may be equally true and I have you to thank for helping me attain at least some of my desired physical goals. Seeing your successes has always been motivation for me and I am fortunate to have such a wonderful brother as you.

To Sergey Krylov and Gerald Audette, your works are truly inspirational and I am grateful for what I have learned from both of you. My deepest thanks for taking the time to discuss my research and all the support and guidance you have provided throughout this project.

To Howard Hunter, I cannot thank you enough for your time and endless patience in teaching me how to work with the NMR. I truly appreciate the support you provided and could not have asked for more.

To Miguel Neves and Sherry Boodram, my sincere thanks for taking the time to share your knowledge with me. Seeing you both graduate still serves as inspiration for me. Sina Haftchenary, 11 years of friendship and going! Words can't describe the experiences we have shared and I hope the future will hold many more adventures. Thank you for all your support and insight. Julia Bao, I truly admire your creativity and hope it brings you all that you desire. Thank you for your time, knowledge, and patience. Your support saved me countless hours throughout this project. Ekaterina Smirnova and Jamie Kwan, thank you for taking the time to show me some useful laboratory techniques. Parts of this project would have been extremely difficult if not for your support. Agnesa Shala, your input to parts of this work is greatly appreciated. To current members of the Johnson lab, I appreciate the meaningful discussions and thank you for some truly memorable moments.

Contributions of Authors

This dissertation is an assembly of research from 4 peer-reviewed publications as well as a compilation of data from unpublished research projects. Chapters 2 – 4 outline research largely from my own published works. Chapters 5 and 6 present results that have not yet been published. The introduction is an original production outlining a brief history of aptamers including the production and use of the cocaine-binding aptamer. The final chapter contains my own concluding remarks and future directions for this work.

Chapter 2: Research discussed in this chapter has been published in the journal *Biochemistry* (Neves et al. 2010). My contributions to this work include applications of ITC and data analysis in establishing the change in heat capacity of binding (ΔC_p) for the MN6 aptamer with cocaine. I also conducted the 1D ^{1}H-NMR experiments for MN6. NMR data was processed by Dr. Philip Johnson. Research on MN1, MN4, and MN19 aptamers was conducted by Miguel A. Neves, including ITC derived thermodynamics of binding, 1D ^{1}H-NMR, 2D-NOESY NMR, and UV thermal melts. For clarification: research outlined in this chapter took place during my undergraduate research project but all data analysis and conclusions were established within my graduate studies.

Chapter 3: Research presented in this chapter has been published in the journals *Biochemistry* (Neves et al. 2011) and *Biophysical Chemistry* (Reinstein et al. 2010). My contributions to the biochemistry publication include ITC derived binding thermodynamics and data analysis of WC, rWC, MN2, MN8, MN9, MN10, MN11, and MN12 aptamers. I performed additional analysis on WC to derive ΔC_p of binding with deoxycholic acid. With the exception of the rWC aptamer, data here was obtained as part of my undergraduate research project, however, data analysis and conclusions were established within my graduate studies. I also completed the data analysis of the MS2 aptamer to establish ΔC_p. ITC derived binding thermodynamics of binding and NMR data for MS1 and MS2 aptamers were obtained by Makbul Saad with the aid of Miguel A. Neves. NMR imino assignments were completed by Dr. Philip Johnson. DOSY-NMR studies were conducted Dr. Patrick Groves. SAXS studies were conducted by Dr. Matthew Wilce and Simone A. Beckham. My contributions to the biophysical chemistry publication include ITC derived binding thermodynamics for the aptamers previously listed and MN18 (undergraduate

research project). ITC derived binding thermodynamics for several aptamer variants, buffer pH and ion concentration studies as well as NMR studies were conducted by Miguel A. Neves. ITC derived binding thermodynamics of MS3 and MS4 aptamers were obtained by Makbul Saad with the aid of Miguel A. Neves. Agnasa Shala suggested development of the MN21 aptamer with lengthened stems. I was responsible for proceeding with ITC experiments using MN21 and subsequent data analysis.

Chapter 4: The research contained in this chapter has been published in the journal *Biochemistry* (Reinstein et al. 2013). I performed the initial ITC and 1D ^{1}H-NMR experiments used to study MN4 and MN19 binding to quinine. I also conducted the ITC competitive binding studies and analyzed the data therein. The 2D-NOESY spectrum was obtained by me with the aid of Dr. Philip Johnson. In all spectra, imino protons were assigned by Dr. Philip Johnson. MN4 and MN19 ΔC_p data was obtained by Mina Yoo and Chris Han with my aid. Electrostatics of binding was the work of Tsering Palmo with my aid. I also performed ITC binding studies for aptamers in different buffers and with ions of varying size and charge. SAXS data was obtained and analyzed by Dr. Matthew Wilce and Simone A. Beckham.

Chapter 5: This chapter outlines research that has not yet been published. All ITC binding studies, 1D ^{1}H-NMR, fluorescence spectroscopy experiments, and data analysis contained therein were conducted by me.

Chapter 6: This chapter also presents research that has not yet been published. Initial studies using the "AND" and "OR" aptamers were the work of Kristina Bauer, with my aid. I followed up with additional ITC studies testing aptamer bifunctionality and data analysis.

Table of Contents

List of Tables

Chapter 1

Chapter 2

Chapter 3

Chapter 4

Chapter 6

List of Figures

Chapter 1

Chapter 2

Chapter 3

Chapter 4

Chapter 5

Chapter 6

Chapter 8

List of Abbreviations

Buffer A	20 mM TRIS (pH 7.4), 140 mM NaCl, 5 mM KCl	nbd	No Detectable Binding
cDNA	Complementary DNA	NMR	Nuclear Magnetic Resonance Spectroscopy
ΔCp	Change in Heat Capacity	NOESY	Nuclear Overhauser Enhancement Spectroscopy
ΔG	Change in Free Energy	PCR	Polymerase Chain Reaction
ΔH	Change in Enthalpy	PDDF	Pair Distance Distribution Function
ΔS	Change in Entropy	Rg	Radius of Gyration
DCA	Deoxycholic Acid	Rh	Radius of Hydration
DNA	Deoxyribonucleic acid	RNA	Ribonucleic Acid
DOSY	Diffusion Ordered Spectroscopy	RT-PCR	Reverse Transcription Polymerase Chain Reaction
Dt	Translational Diffusion Coefficient	SAXS	Small Angle X-Ray Scattering
HEPES	N-(2- hydroxyethyl)piperazine-N′-ethanesulfonic acid	SELEX	Systematic Evolution of Ligands by Exponential Enrichment
ITC	Isothermal Titration Calorimetry	ssDNA	Single Stranded DNA
Ka	Binding Association Constant	τm	Mixing Time
Kd	Binding Dissociation Constant	TRIS	Tris(hydroxymethyl)aminomethane
MN#	A series of alkaloid-binding aptamers	QELS	Quasi-Elastic Light Scattering
MNS4.1	The Cocaine-Binding Aptamer (originally isolated)	vwb	Very Weak Binding
MS#	A series of steroid-binding aptamers	WC	Watson Crick

1 Introduction

1.1 The Development of Aptamers

1.1.1 Aptamer History: From Concept to Reality

Aptamers were conceptualized long before their actual discovery. The work of Sol Spiegelman and collaborators nearly half a century ago would build the foundation for what we know today as Systematic Evolution of Ligands by EXponential enrichment abbreviated "SELEX". In experiments dealing with the Qβ bacteriophage replicase protein, an RNA-dependent RNA polymerase, selective pressure leading to the fastest and most efficient products yielded RNAs that were truncated variants of the Qβ genome. Interestingly, these variants retained all the necessary secondary and tertiary structure elements needed for high affinity interactions with the replicase protein.[1,2] It could be said that the resultant RNA products were both aptamers and substrates for the polymerase.

Spiegleman's work however, would not have been able to outline a clear-cut method for the selection of aptamers like the one that exists today. The major barrier at the time was the amplification process itself. More specifically, a major setback was that a sequence of interest would first have to be inserted into a vector. Such exogenous RNA sequences would be removed far too quickly under selection pressure, favouring instead those sequences that could be replicated more quickly and bind more tightly to the polymerase. Research on this subject was well demonstrated by Fred Kramer and colleagues in which an exogenous RNA sequence, a ribozyme to be specific, incorporated into the Qβ genome and was amplified nearly 300-fold.[3] While this result is very significant and laid the ground work for amplification of short sequences of interest, it was shown that the Qβ replicase protein could amplify the Qβ genome by nearly 10^5 fold in roughly the same time frame as the genome with the ribozyme sequence incorporated.[4] The drop off in amplification here makes it quite clear that the method could benefit from major enhancements, namely, enhancements that could make the amplification process independent of the sequence being amplified.

The advent of polymerase chain reaction (PCR) would ultimately serve as the key ingredient needed for synthesis of large oligonucleotide libraries needed for the generation of aptamers. This

is where the works of Larry Gold and Jack Szostak would shine and for the first time, reveal how *in-vitro* evolution of RNAs could lead to RNA products exhibiting both high selectivity and high affinity interactions with a variety of target molecules. Craig Tuerk and Larry Gold used what they were the first to describe as SELEX, to yield two RNA sequences (just 8 nucleotides as part of a larger gene 43 translational operator in bacteriophage T4) that exhibited high affinity for gp43, the gene 43 translation protein. One being the wild type sequence, the other being a quadruple mutant that yielded a shorter loop region. Interestingly, the mutant sequence bound with same affinity as the wild type sequence.[5] These results were quite profound in that they demonstrated for the first time that tight binding RNA molecules could be isolated from large pool of randomized oligonucleotide sequences. To quote Larry Gold and Craig Tuerk, this truly was "the beginning of evolution in a test tube".[5]

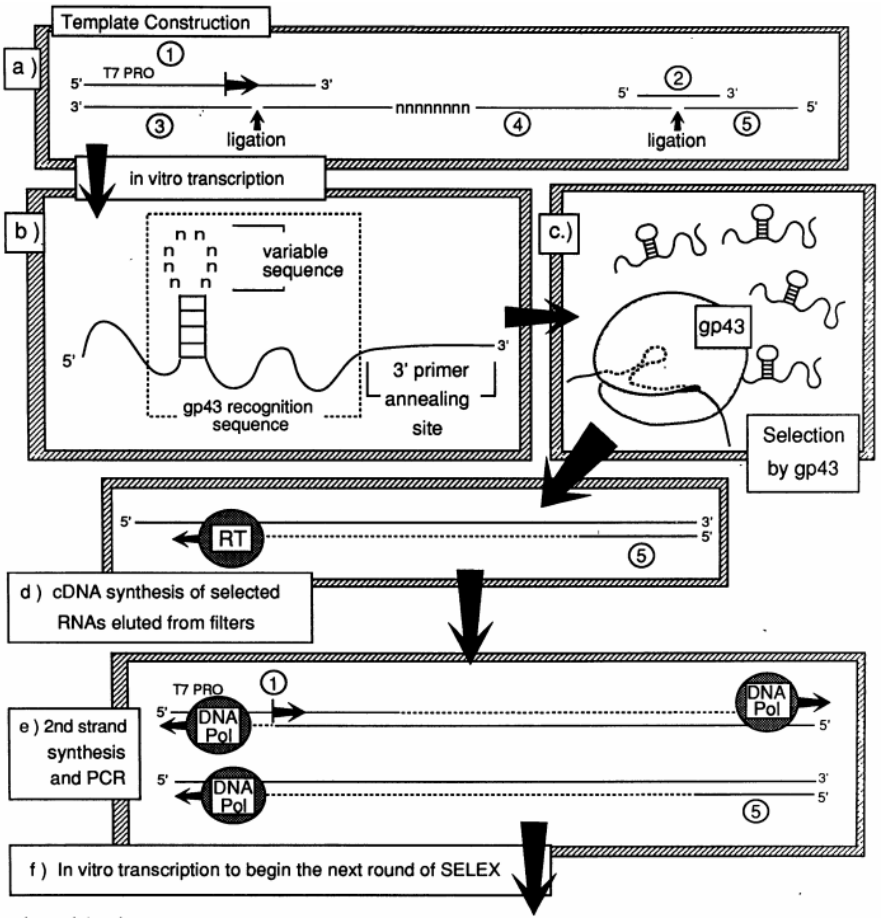

Figure 1.1: The original schematic of the SELEX procedure outlined by Tuerk and Gold demonstrating repeated rounds of selection and amplification. (Obtained from ref. 5)

Research conducted by Jack Szostak and Andrew Ellington would arrive at very much the same conclusion as Tuerk and Gold and not more than a month apart. Szostak and Ellington applied a method of *in vitro* selection nearly identical to the SELEX scheme shown in Figure 1.1. This was done in an effort to calculate the frequency in which RNAs from a randomized pool of oligonucleotides were capable of folding up in a manner that would result in high affinity interactions with a target molecule and/or catalytic activity.[6]

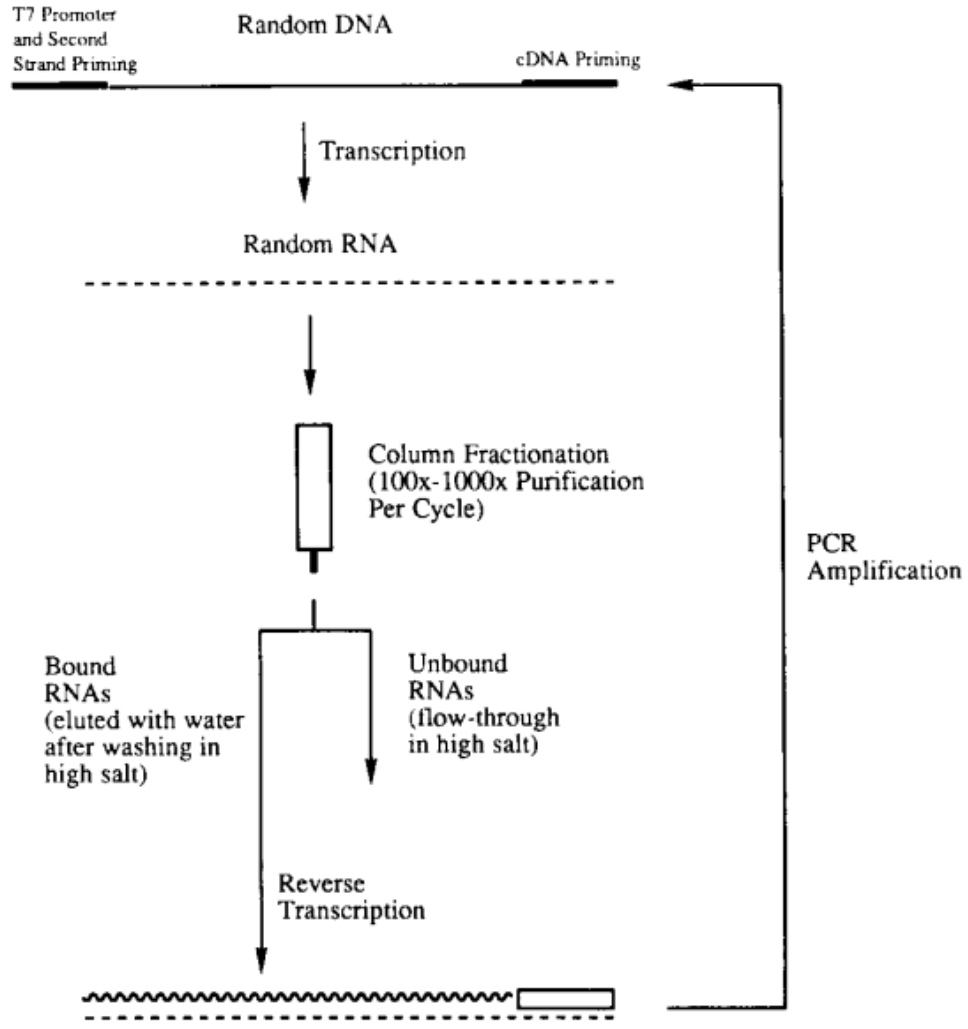

Figure 1.2: The original schematic of the in-vitro selection approach used by Szostak and Ellington illustrating selection and amplification steps applied to an initial pool of random RNAs. (Obtained from ref. 6)

It is thought that the probability of finding high affinity or catalytic sequences within a randomized pool of oligonucleotides is quite low (for a sizable pool of roughly 10^{15} oligos). While

this is indeed true and ever more so as sequence length increases, it was discovered that after numerous selection rounds, different isolates converged on specific sequences which were verified to interact with the ligand at the binding site. These conserved sequences consisted of 22 nucleotides. A rough calculation revealed that a 22-mer could have one of 10^{13} different possible sequence arrangements. Szostak and Ellington began their selection process with nearly this many 100-mers, which meant that it was quite likely that every single 22-mer combination would be present in the initial pool. In conclusion, they were able to estimate approximately 100 – 1000 different sequences which would ultimately be able to fit the small dye molecules for which their RNAs were being selected.[6] These results, once again, demonstrated that high affinity oligonucleotides could be seemingly isolated from a large pool of randomized sequences under selective pressure. It was at this point that Szostak coined the term "aptamer", rooted in the greek word *aptus*, meaning "to fit".[7]

This research did, however, leave some very interesting open ended questions. It was suggested that even with the current method of *in vitro* selection, estimating the number of fundamentally different classes of structures capable of carrying out a given binding or catalytic function might be a rather daunting task. However, the answer to such a question would shed an enormous light on the origin of life and the RNA world hypothesis.[7]

Much of the work leading up to the development of aptamers seems to bear one common aspect, finding the means by which we can study the origin of life. Our knowledge of oligonucleotides has advanced substantially over the last century but our understanding is far from complete. Perhaps the most puzzling remains the various catalytic functions of oligonucleotides that we are still completely unaware of. Simply by the history, it is apparent that there is still a lot left to discover. The existence of functional RNAs was not even proven until the pioneering work of Cech and Altman in the early 80s.[8,9] However, the existence of such RNAs were postulated as early as 1967.[10] What is undoubtedly clear though, is that with the discovery of aptamers, we have gained an invaluable tool by which our ability to study nucleic acids has been greatly accelerated. We are essentially at liberty to ask anything we desire of nucleic acids and this has opened the door wide open for our investigation into the origin of life.

1.1.2 Systematic Evolution of Ligands by Exponential Enrichment

The fundamental steps within the SELEX procedure outlined by Tuerk and Gold remains quite consistent into modern day selection of aptamers. While new modifications have worked their way into the procedure with aims to boost efficiency, the basic steps applied in SELEX have remained mostly unchanged.[12]

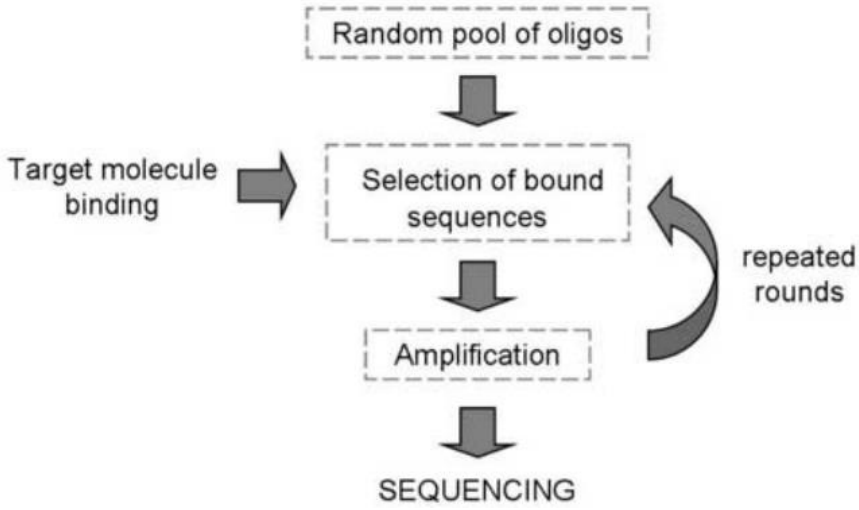

Figure 1.3: A generalized representation of SELEX outlining the repeated rounds of selection and amplification of sequences which originate from a random pool of oligonucleotides. (Obtained from ref. 11)

The scheme presented in Figure 1.3 is the standard procedure used for the production of specific and high affinity aptamers to a desired target molecule. The process typically begins with a random pool of approximately 10^{15} different sequences. Selection pressure is then applied by exposing the pool to a target molecule. Sequences with moderate to high affinity to the target will generally remain present during a wash off step in which sequences with weak or no binding interactions are removed from the pool. The resultant pool is then amplified by means of PCR. Beyond this, the amplified sequences may be subject to repeated rounds of selection and amplification anywhere from 4 – 20 times.[12] As noted in some of the earliest experiments with aptamers, using SELEX is more than likely to result in multiple aptamer constructs which interact with the target molecule. Ultimately, the size of the initial pool and the complexity and size of the target molecule govern the number of potential solutions available for the problem.

1.1.2.1 Building an oligonucleotide library

It may sound strange to point out that a large pool of random oligonucleotides sequences needs to be carefully chosen, but this is indeed something that needs to be considered for initiating SELEX. Analogous to fitting an unknown function using an iterative algorithm, SELEX also requires a bare minimum set of conditions to be effective. This begins with the size of the library being constructed. A typical aptamer screen begins SELEX with an oligonucleotide pool consisting of at least 10^{15} different sequences. The rationale here is that with such a complex pool of oligos, the sequence space being probed contains aptamers up to 25 nucleotides long. In fact, libraries of up to 10^{20} sequences are attainable[14], but not entirely practical when smaller libraries are already quite diverse. One would preferentially saturate the available sequence space so as to ensure that the target molecule being fit has one, multiple, or no solutions.[13]

Furthermore, oligonucleotide libraries are typically constructed of all 4 DNA bases. During synthesis, it is often advantageous to supply the bases in a 1:1:1:1 ratio as this would ensure the greatest sequence diversity in the sample. Any bias introduced to this condition would affect the presence of homopolymeric sequences in an exponential manner[5] where such sequences have just as much potential for establishing high affinity interactions with a target molecule.[17] A few studies did demonstrate that catalytic RNAs could indeed be isolated from pools constructed of as few as 2 of the bases. The results indicated however, that RNAs constructed of 2 bases had catalytic rates far lower than those consisting of all 4 bases.[15,16]

With these constraints in place, sequence libraries are generally constructed of a randomized ssDNA sequence anywhere from 20 – 80 nucleotides long. Flanking the 3' and 5' regions are 18 – 21 nucleotides of specific sequences necessary for primer binding during the PCR process. Keeping the randomized sequence short can be more efficient as previous research has indicated that aptamers isolated through SELEX tend to be truncated variants of those introduced in the initial pool.[18] Furthermore, binding domains within an oligonucleotide generally only make up a fraction of the full sequence length. This implies that longer sequences can be characterized as short individual domains that may or may not interact cooperatively in binding a target molecule.[5,6,13,19-26]

1.1.2.2 Introducing a Target Molecule

There are no specific restrictions in selecting a target molecule for SELEX. It is well researched that aptamers can be selected for just about any molecule of interest.[19,27-29] However, there are some precautions that need to be taken to maintain a high level of efficiency. Aptamers, being oligonucleotides, are inherently anionic and also contain numerous hydrogen bond acceptor and donor groups. Such properties make aptamer selection for positively charged small molecules far easier than for molecules that are more bulky, negatively charged, or have mostly hydrophobic character. While the DNA bases do possess some hydrophobic character due to planar aromatic bases which are typically involved in stacking interactions, DNA remains a polar molecule and better suited for interactions with other polar molecules in polar solvents. This is not to say that all bulky hydrophobic or negatively charged targets must be excluded. Rather, the weak affinity established by aptamers to these targets makes them much more difficult to isolate, but certainly within the realm of possiblities.[30-32]

The extreme versatility of aptamers has been one of the fundamental reasons for their extensive investigation. This versatility is demonstrated by the aptamers that have already been selected to bind inorganic components (metal ions), small molecules (organic dyes, cofactors, alkaloids, antibiotics), individual nucleotides and nucleic acids, individual amino acids, peptides, and whole proteins, carbohydrates, lipids[33] and many higher order structures (spores, viral capsids, whole cells).[19]

Other important factors tied to overall SELEX efficiency include the purity and abundance of the target molecule. Impure samples can easily yield aptamers for unintended targets and a major goal through SELEX includes elimination of non-specific binding. The selection step generally proceeds by immobilizing the target molecule within a column. Non-binding sequences elute out while sequences with high affinity for the target molecule are removed in wash off step using salt or chemical denaturant. Under optimal conditions, non-specific and non-binding sequences can be removed from the nucleotide pool quite early.

1.1.2.3 Amplification of High Affinity Sequences

Sequences remaining in the oligonucleotide pool are amplified using PCR. The amplification step is crucial for regenerating a sizable pool of sequences with higher affinity for the target molecule. In cases where an RNA aptamer is desired, reverse transcription PCR (RT-PCR) is applied to convert the RNAs to their corresponding cDNAs which can then be used in standard PCR methods. This process for RNA aptamers means that a T7 promoter site would be required at the 5' end of the sequence. ssDNA aptamers need only be amplified using standard PCR protocols.[5,6,19]

PCR is one of the core protocols that has made SELEX so successful. However, as with all steps within the SELEX procedure, PCR must likewise be optimized. Numerous PCR protocols have been established and can be applied as part of SELEX.[34-37] However, some noteworthy differences exist between applying PCR to amplify a homogenous oligonucleotide sample versus an oligonucleotide library. Studies have shown that the PCR process for a homogenous oligonucleotide sample ends when primers are used up. Oligonucleotide libraries on the other hand, give rise to certain by-products that occur with primers still in excess. Optimizations applied to prevent such by-product formation include using shorter sequences as well as modification of primer design and location of primer hybridization sites. Furthermore, increased concentrations of polymerase favour product formation over by-product formation.[38,39] Following regeneration of a sizable high affinity oligonucleotide pool, the iterative process is applied.

1.1.2.4 Iterations and Sequencing

The iterative procedure employed within SELEX is what makes the technique such a powerful tool for the isolation of high affinity aptamers for selected molecules. By executing consecutive rounds of amplification and selection, the existing pool of oligonucleotides subsequently loses diversity as it begins to converge on sequences critical for binding. Aptamers exhibiting high affinity and specificity have been isolated from as few as 6 to as many as 20 or more rounds of amplification and selection. The number of iterations required is fairly dependent on the type of target as well as selection stringency.[19] The end of SELEX is typically signalled when sequences with higher affinity fail to be generated by additional rounds of amplification and selection. The resultant sequences are then isolated and sequenced. It is quite common to find anywhere from 1

to 10^6 aptamer candidates for a selected target following SELEX.[40] It is also worth pointing out that while SELEX has had an excellent track record of success, it does have its own shortcomings which are not limited to aptamer biostability, cross reactivity, and by-product formation.[41-44] Furthermore, highly stringent selection conditions or sub-optimal conditions in any of the criteria listed previously could result in no identifiable aptamer for a selected target.

1.2 Advances in Aptamer Screening

1.2.1 Modifications to Oligonucleotide Libraries

Perhaps one of the most pressing matters with respect to oligonucleotide libraries is linked to the length of sequences used. Aptamer screens rely on the ability of random oligonucleotide sequences to fold up into a functional and/or catalytic 3 dimensional structures.[45-47] It is tempting to incorporate longer sequences within an oligonucleotide library as these sequences would undoubtedly have higher chances of including a motif capable of binding a target. Unfortunately, the amount of sequence space generated for lengthy oligonucleotides increases exponentially to the point that saturating the sequence space of any oligo longer than 34 nucleotides long simply becomes unfeasible if not due to solubility limits alone. Where longer sequences are required though, the drawback becomes quite apparent; the method relies on isolating a high affinity sequence which may not even be present in the library to begin with. Luckily, sequences necessary for binding typically comprise only a fraction of the original sequence where high affinity sequences as short as 11 nucleotides have been identified as in the case of the DNA aptamer selected against the Lup an 1 Food Allergen.[48] Longer sequences, such as the 154 nucleotides necessary for cleavage in the *Neurospora* VS RNA, have also been identified.[49] Within such large domains however, key nucleotides have been identified as being critical for catalysis[50], further reinforcing the notion that long sequences are not a necessity for producing highly selective, high affinity aptamers.

Another component of oligonucleotide libraries and aptamers as a whole include their biostability. Numerous research studies have been devoted to isolating aptamers that are resistant to nuclease degradation as this not only affects isolated aptamers, but the diversity of the oligonucleotide library itself.[51-54] To this respect, modifications can be applied to just about any part of the nucleotide to increase its resistance to nucleases. Thioaptamers have been developed by

modifications to the phosphate backbone in which a non-bridging oxygen is replaced by sulfur.[51] For RNA aptamers, modifications to ribose sugars which replace the 2' OH with less reactive groups such as halogens, methyl, amine, or methoxy groups, all of which impart excellent nuclease resistance.[52,53] Finally, perhaps less for the purpose of biostability, modifications to the nucleobases can give rise to new functionality in selected aptamers. Substitutions to C-5 in pyrimidines and C-8 in purines with aminoacyl motifs (such as arginyl, histidyl, lysyl, phenylalanyl, tryptophanyl, leucyl, prolyl, glutaminyl, seryl, *O*-benzyl seryl or threonyl) can easily alter affinity and specificity where some studies report having isolated such modified aptamers against anionic targets.[54]

1.2.2 Improvements in Selection Strategies

The partitioning of binding aptamer sequences from non-binding ones is absolutely essential to the success of SELEX. Immobilization of targets on Sepharose or Agarose columns has been standard procedure[55-57] but does present its own challenges. It is more than likely that large oligonucleotide libraries contain some sequences that will inevitably bind to the column material and/or linker regions of immobilized molecules. These sequences can be persistent and eventually contaminate the pool with aptamers for an unintended target. To handle this issue, negative selection procedures are now quite commonly employed wherein aptamers are exposed to undesired targets at some selection steps. This allows for the separation of aptamers which bind these undesired targets followed by their removal from the pool in subsequent wash-off procedures.[58,59]

Another issue that has been brought to light more recently involves immobilized targets. It is apparent that a target molecule attached by a linker region to a surface is unlikely to have all surfaces accessible for binding interactions during the selection step.[60] While this has by no means been extremely detrimental, selection can be far more efficient when aptamers can probe the entire surface of a target. A number of ways in which this has been achieved include first and foremost, not using immobilization at all. Where a protein is the intended target, simply allowing aptamer sequences and the target protein enough time to mix can allow for separation using affinity chromatography protocols.[19] One study has demonstrated such separation where proteins and aptamer-protein complexes adhere to cyanogen bromide activated sepharose while free

aptamers do not.[215] Magnetic beads have also been applied with similar intent of increasing surface accessibility of the target.[61]

The most recent advances have incorporated several new methods within the SELEX procedure and are not limited to Capillary Electrophoresis (CE), Mass Spectrometry (MS), Flow Cytometry (FC) and Surface Plasmon Resonance (SPR).[62-65,216] The SPR study is demonstrated in more detail in Figure 1.4 shown below.

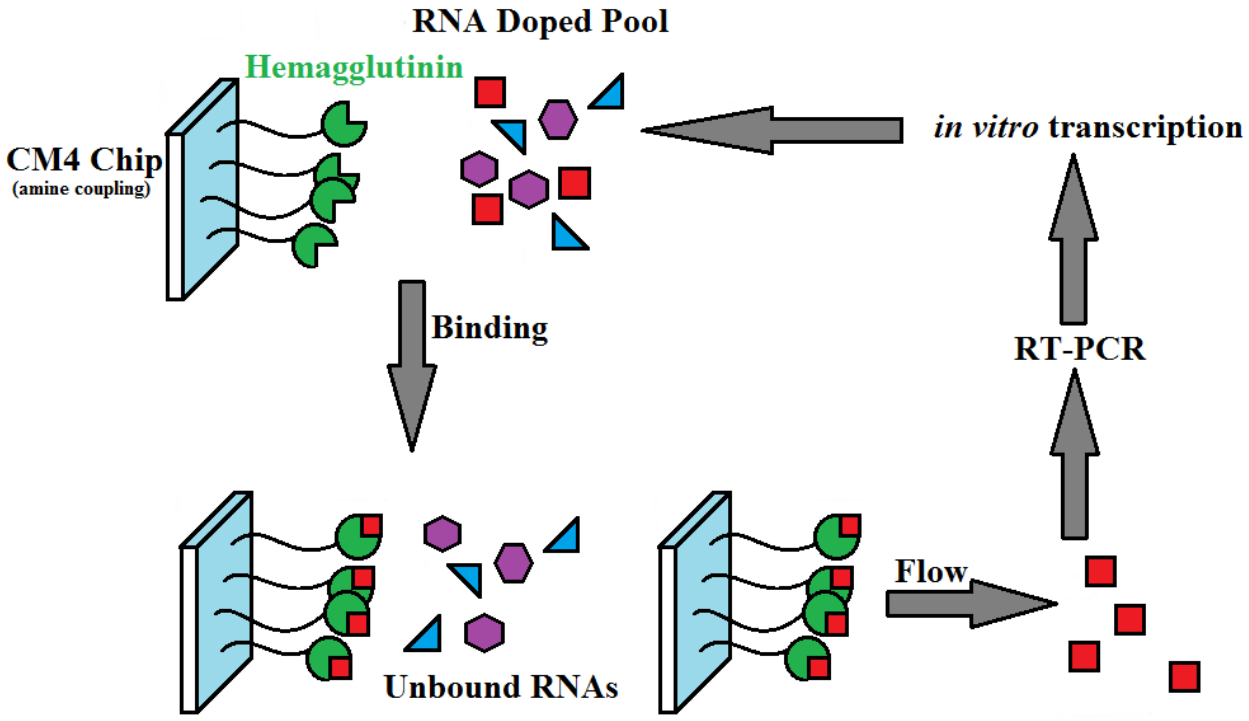

Figure 1.4: A schematic for a SELEX protocol using Surface Plasmon Resonance for the selection of an anti-hemagglutinin aptamer. Adapted from ref. 216

1.2.3 Improvements in Amplification

While PCR is one of the most critical steps in the SELEX process, it can also lead to undesired products. Previously noted were the potential by-products that accumulate as a result of performing PCR on DNA libraries. This is largely attributed to product-product and primer-product hybridization.[38] However, it is also quite possible that sequences following a selection step fold into conformations that simply make their amplification rather difficult. This is especially true of sequences exhibiting tandem repeats, documented to result in replication

slippage.[66] Despite these pitfalls, PCR has also come a long way with numerous enhancements which include use of various organic additives (DMSO, glycerol, formamide and other low molecular weight amides) and nanoparticles (TiO_2, ZnO) which have shown to greatly improve PCR specificity.[217,218] Such enhancements are becoming far more common within the SELEX protocol. To address the formation of by-products, asymmetric PCR employed in some studies seems to have partially alleviated the issue by greatly reducing the aforementioned PCR by-products which could typically result in poor yield.[67-69] Other studies have scrutinized the effects of primer design in PCR as well as suggesting that the target molecule may also be another key factor in determining extent of by-product formation.[70]

1.2.4 Additional Considerations for Successful Aptamer Production

It is apparent that accounting for every sequence contained within an oligonucleotide library is currently an impossibility. However, sometimes the solution to such a problem need not be so complex. In light of all the advancements and refinements at every step of SELEX, simply starting up the procedure from the beginning may be the simplest approach to isolating an aptamer where one had initially failed to be identified. A potential binding candidate lost for whatever reason may turn up in repeated trials and it would hardly be surprising given the sensitive nature of the technique.

1.3 Applications of Aptamers

The field of aptamers has grown substantially since their initial discovery. The potential for aptamers is virtually limitless and this has sparked interest on both the academic and commercial forefronts. Major academic investigations seek to use aptamers in the development of novel techniques.[13] Perhaps one of the most heavily investigated areas involves the use of aptamers as biosensors. More recently, their uses in nanotechology has also been investigated.[71] However, many studies of aptamers are undertaken to gain further insight into RNA in the early world.[7,13] Commercial interest in aptamers lay mostly in therapeutic aspects. Aptamers can exhibit very high affinity and specificity for targets making them ideal candidates for pharmaceuticals and drug delivery.[12,72]

1.3.1 Aptamers as Therapeutic Agents

Aptamers have demonstrated such profound versatility that their applications in therapeutics have grown into a multi-million dollar industry.[73] With the ability to produce aptamers that bind to just about any target molecule, the therapeutic potential was recognized relatively fast. Not more than 2 years after the discovery of aptamers, a variety of targets of high medical importance were already being targeted.[74-76]

The development of aptamers with therapeutic properties relies on the ability of the aptamer to bind its target and inhibit its function. The development process in the generation and isolation of therapeutic aptamers is largely the same as with any other aptamer, following a standard SELEX protocol. However, therapeutic aptamers are ultimately designed for activity *in vivo* which comes with several new challenges. Biostability of aptamers must be improved for them to be effective for in vivo applications. Several aptamer enhancements were already reviewed in section 1.2.1, but beyond these small modifications, several new classes of aptamers have been developed which now make them very viable in therapeutic applications. The development of Spiegelmers, aptamer mirror images constructed almost entirely of L-nucleotides, provided sequences which carry out the same function as aptamers, but with profound biostability.[77] Spiegelmers can be further modified in a similar manner to standard aptamers for even greater biostability, but already show strong promise as therapeutic agents.[78,79]

The most recent advancement in aptamers includes their ability to be isolated based on kinetic parameters. Slow off-rate modified aptamers (SOMAmers) have been isolated for thousands of biologically relevant targets, many of which are human proteins, with affinities well into the picomolar range, rivaling the affinity exhibited by some antibodies.[80] The key modifications that make SOMAmers so effective are substitutions of hydrophobic components within the base. Here the C-5 position in uracil is typically modified to include such groups as benzylaminocarbonyl, naphthylmethylaminocarbonyl, tryptaminocarbonyl, and isobutylaminocarbonyl.[219] SOMAmers are able to more effectively form hydrophobic interactions with their target and are generally less polar than standard aptamers.[7,80,81] This optimization has made them extremely valuable and powerful tools in therapeutic applications.

Table 1.1: Aptamers in the clinic (adapted from ref. 82)				
Aptamer Name (Company Name)	**Composition**	**Target**	**Indication**	**Current Phase**
Pegaptanib sodium/Macugen (Pfizer/Eyetech)	2' O-methyl purine/2'-fluoro pyrimidine with two 2'-ribo purines conjugated to 40 kDa PEG, 3' inverted dT	Vascular endothelial growth factor (VEGF)	Age-related macular degeneration	Approved in the US and EU
AS1411/AGRO001 (Antisoma)	G-rich DNA	Nucleolin	Acute myeloid leukaemia	Phase II
REG1/RB006 plus RB007 (Regado Biosciences)	2'-ribo purine/2'-fluoro pyrimidine (RB006)/40 kDa PEG plus 2'-O-methyl antidote (RB007)	Coagulation factor Ixa	Percutaneous coronary intervention	Phase II
ARC1779 (Archemix)	DNA and 2'-O-methyl with a single phosphorothioate linkage conjugated to 20 KdA PEG, 3' inverted dT	A1 domain of Von Willebrand factor	Thrombotic microangiopathies and carotid artery disease	Phase II
NU172 (ARCA biopharma)	Unmodified DNA aptamer	Thrombin	Cardiopulmonary bypass to maintain steady state of anticoagulation	Phase I
ARC1905 (Ophthotech)	2'-ribo purine/2'-fluoro pyrimidine conjugated to 40 kDa PEG, 3' inverted dT	Complement component 5	Age-related macular degeneration	Phase I
E10030 (Ophthotech)	DNA and 2'-O-methyl 5'-conjugated to 40 kDa PEG, 3' inverted dT	Platelet-derived growth factor	Age-related macular degeneration	Phase I
NOX-A12 (NOXXON Pharma)	L-RNA with 3'-PEG	CXCL12	Multiple myeloma and non-Hodgkin's lymphoma	Phase I
NOX-E36 (NOXXON Pharma)	L-RNA with 3'-PEG	CCL2	Type 2 diabetes, diabetic nephropathy	Phase I

Table 1.1 lists several aptamers currently in clinical trials as well as one aptamer approved for the treatment of age-related macular degeneration, Macugen. With nearly thousands of other targets of therapeutic interest being investigated, the list is far from being exhaustive, but it does outline

how recent advances in the field have allowed for the production of highly viable therapeutic aptamers.

1.3.2 Aptamers as Biosensors

A large part of bioanalytical chemistry is focused on identifying the presence of an analyte in solution. Detection and quantification of analytes currently comes in a variety of forms. Fluorescent, colorimetric, and more recently, electrical signals, have all been viable methods applied within biosensing applications.[83-91] Antibodies have always been the gold standard in biosensing as they have very high affinity and specificity to their targets allowing for high sensitivity. However, recent advances in aptamers have given rise to an ever increasing number of biosensing applications in which aptamers are being substituted for antibodies.[92,93] Aptamers are slowly becoming an accepted standard due to their thermostability, biostability, ease of manufacture, and target binding versatility. Aptamers are also able to target several small molecules and ions such as ATP,[220] K^+,[221] cocaine,[118] and theophylline,[222] for which study by antibodies would not be feasible.[79,93,94] The property that makes aptamers so successful in biosensing applications is their ability to undergo conformational changes with binding of their targets.[96] Nearly all biosensing applications utilize structural transitions that take place when aptamers bind their targets to generate the signals needed for detection. For example, signalling by fluorescence can be attained in numerous ways, two of which are outlined in Figure 1.5. Typically, whole aptamers are made into molecular beacons, having both a fluorophore and quencher. Binding of the target would then either result in increased fluorescence intensity or quenching, dependent on the location of the fluorophore and quencher as well as the extent of conformational changes that take place.[97-99] Colorimetric biosensing with aptamers in the simplest case uses weakly binding dye molecules that are displaced in the presence of a higher affinity target such as cocaine.[100] Several other investigations have made use of scaffolds such as gold nanoparticles and electrodes for highly sensitive colorimetric and electrical biosensing.[101-103] Without a doubt, aptamers for biosensing purposes are plentiful. However, even with such an abundance of studies, the binding mechanisms utilized by many aptamers are ill-understood.

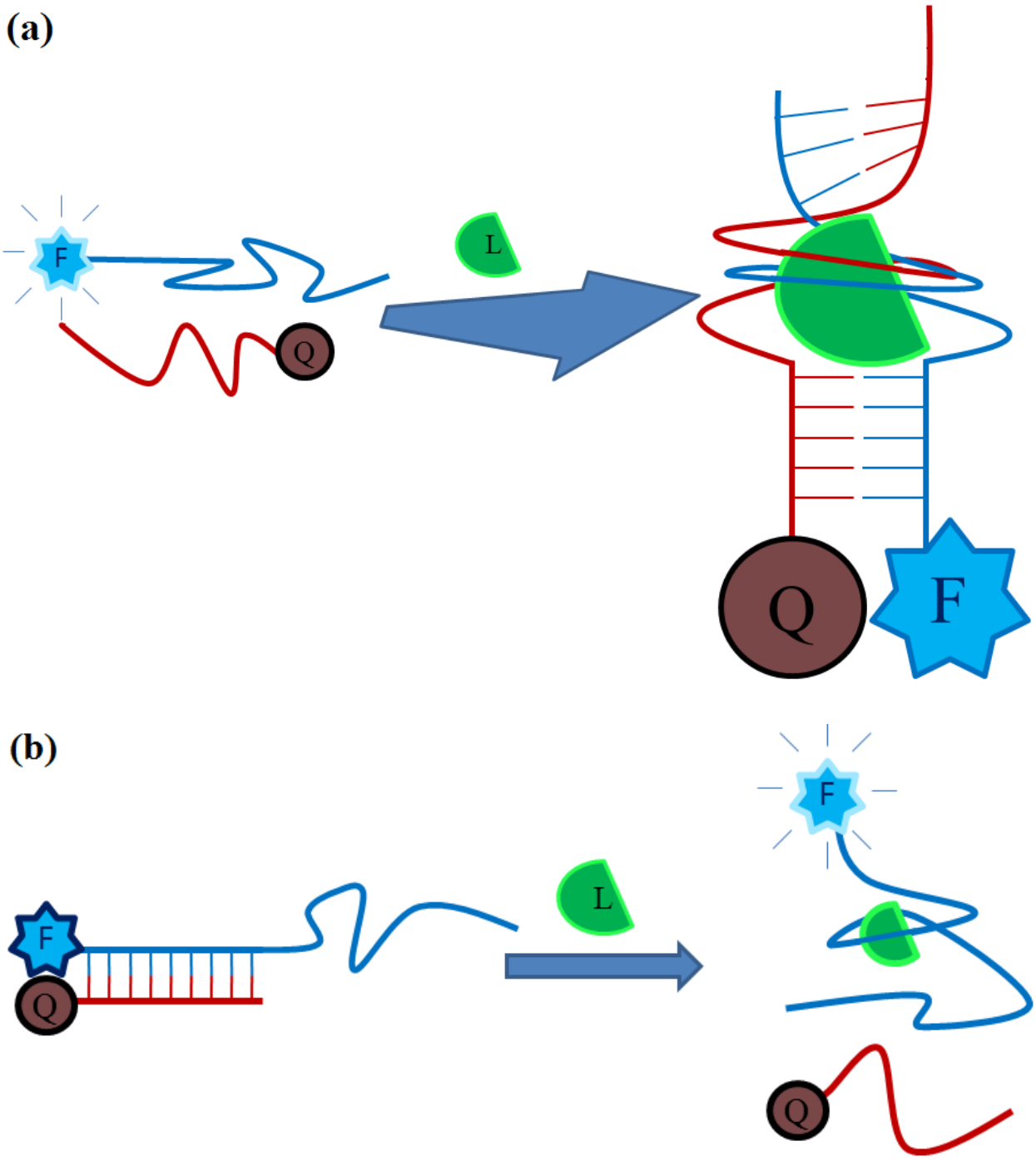

Figure 1.5: Fluorescence detection of a target molecule (F = fluorophore, Q = quencher, L = target). (a) A target molecule binds and induces conformational changes allowing hybridization of a "split" aptamer resulting in quenching of fluorescence. (b) An aptamer is bound by a short complimentary sequence which dissociates with binding of the target molecule generating a fluorescence signal. (Adapted from ref. 91)

1.3.3 Nature's Aptamers: Riboswitches

While aptamers appear to be purely the output of an experimental procedure, research conducted in the early 2000s revealed that nature also had its very own set of aptamers. Conserved sequences in the 5' untranslated region (UTR) of some prokaryotic mRNAs were discovered to be critical regulatory elements. These sequences are capable of folding into a variety of complex structures that could interact with small molecules and in doing so, exert regulatory control over downstream regions.[104-107] They were termed riboswitches to indicate their ability to exert a level of transcriptional and translational control in the presence of a small molecule metabolite. This implies that riboswitches utilize sequences very much similar to those developed *in vitro*, which undergo conformational changes with target binding. Such a case was observed for the Escherichia coli btuB mRNA, which operates as a metabolite-sensing genetic switch capable of inhibiting ribosome binding.[108] With some 5'-UTRs as long as 4500 nucleotides (invertebrates), 200 on average for humans and other diverse taxonomic classes,[109] binding of a metabolite can induce significant conformational changes at a distance, resulting in the observed regulation. More recent research makes it more evident that many organisms are likely to use riboswitches as regulatory elements encoded in the 5'-UTR. The 3'-UTR is also known to contain such regulatory elements where quite recently, the human riboswitch VEGFA, a metabolite-independent riboswitch, has been identified.[110] While our understanding of riboswitches is still quite limited, they may be one of the missing links that reinforces the notion of an early RNA world wherein structurally diverse RNAs were highly functional molecules.

1.4 The Cocaine-Binding Aptamer

1.4.1 Sequence and Structural Characteristics

The cocaine-binding aptamer is a DNA aptamer consisting of 3 stems built around a 3-way junction. The aptamer was selected using standard SELEX with cocaine as the target molecule.[111] The initially selected aptamer (MNS4.1) consists of 38 nucleotides, a majority of which are involved in Watson-Crick base pairing. That aptamer also contains 5 non-canonical base pairs, 3 G-A base pairs nearer the end of stem 1 and G-A and G-T base pairs in stem 3 (Figure 1.6). The ligand binding site is hypothesized to be at the 3 way junction. It was proposed that the aptamer exists in a partially folded state with stems 1 and 2 being mostly folded while stem 3 folds upon

binding of cocaine. This unfolded to folded transition is illustrated in Figure 1.7. Finally, the aptamer was selected to have selectivity for cocaine over its metabolites benzoylecgonine and ecgonine methyl ester.[111,112]

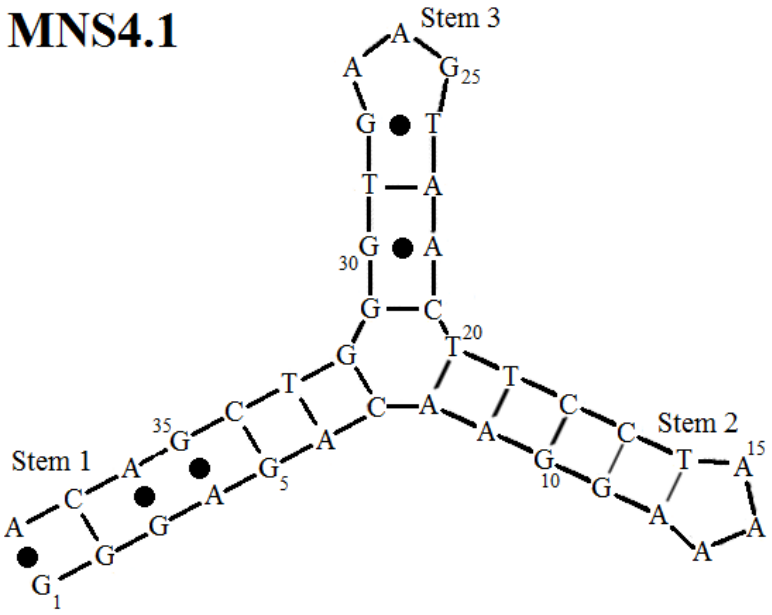

Figure 1.6: Secondary structure of the originally selected cocaine-binding aptamer (MNS4.1) based on mutation analysis. (Adapted from ref. 112)

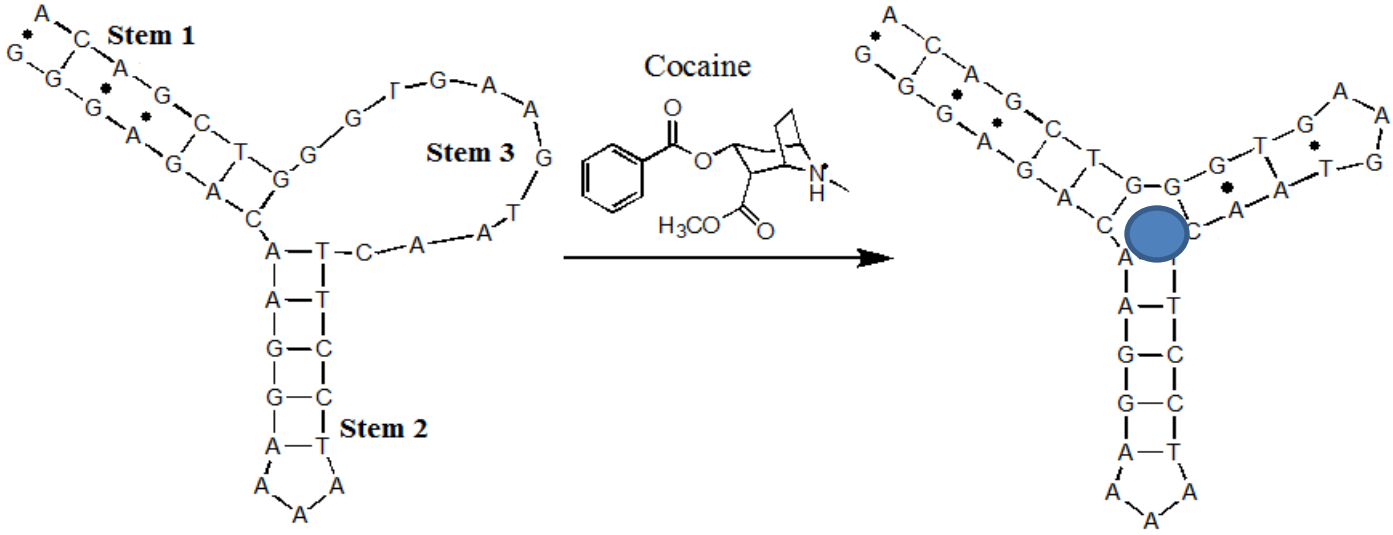

Figure 1.7: Binding mechanism proposed for the cocaine-binding aptamer. Stems 1 and 2 are completely folded in the absence of cocaine while stem 3 only folds upon binding. The blue circle shows the binding site of cocaine. (Adapted from ref. 100)

1.4.2 Why an Aptamer for Cocaine?

The cocaine-binding aptamer was initially selected for the purposes of demonstrating that aptamer subunits would be able to assemble in the presence of cocaine. "Split" aptamers of this nature have been reported to retain selectivity and affinity for their targets.[113] SELEX normally outputs an aptamer that consists of a single oligonucleotide chain which can contain fairly complex architecture (very common for long RNAs) connected by several loop segments. Studies on aptamers selected against thrombin and mammalian initiation factor 4A demonstrated that these aptamers not only contain multiple loop segments, but that these loop segments may also play a critical role in target affinity and specificity.[223,224] DNA aptamers with multiple stems also appear to be fairly common and have been selected to bind many different targets.[13] The work of Stojanovic et al. demonstrated that by splitting the cocaine-binding aptamer at the stem loops, such as those seen at the ends of stems 2 and 3 (Figure 1.6), the aptamer would assemble in the presence of cocaine and bind with a dissociation constant (K_d) of approximately 5 μM.[111] While the result reinforced previous findings, it also laid the groundwork for converting the aptamer into a fluorescent sensor for cocaine. A reason for using cocaine as the target molecule for this study was not specified. However, several points have made it a good candidate. Prior to the reported research, an anti-cocaine aptamer had not yet been isolated. Furthermore, cocaine is well-researched in nearly all respects, from its origin to its uses in medicine. Finally, cocaine also comes with a long history of use and abuse. With cocaine seizures amounting to nearly $137 M alone within Canada in 2013, a means for its easy and fast detection may be in high demand.[114,115]

1.4.3 A Brief History of Cocaine Biosensing

Since selection of the cocaine-binding aptamer in 2000, at least 70 independent biosensing studies have been conducted where fluorescence, colorimetric, or electrical signaling were used to detect the presence of cocaine in solution. In 2001, Stojanovic et al. used their initial findings to produce a variant of the cocaine-binding aptamer, F7.9D (Figure 1.8) which contained both a fluorophore attached at the 5' terminal and quencher attached at the 3' terminal. In the absence of cocaine, relatively high fluorescence was observed. On addition of cocaine, quenching of the fluorescence signal occurred, indicating that folding of the aptamer had taken place. The study demonstrated

that a ligand-induced stem closure mechanism could be engineered into the aptamer and allows the use of fluorescence as a means of detection of cocaine.[112]

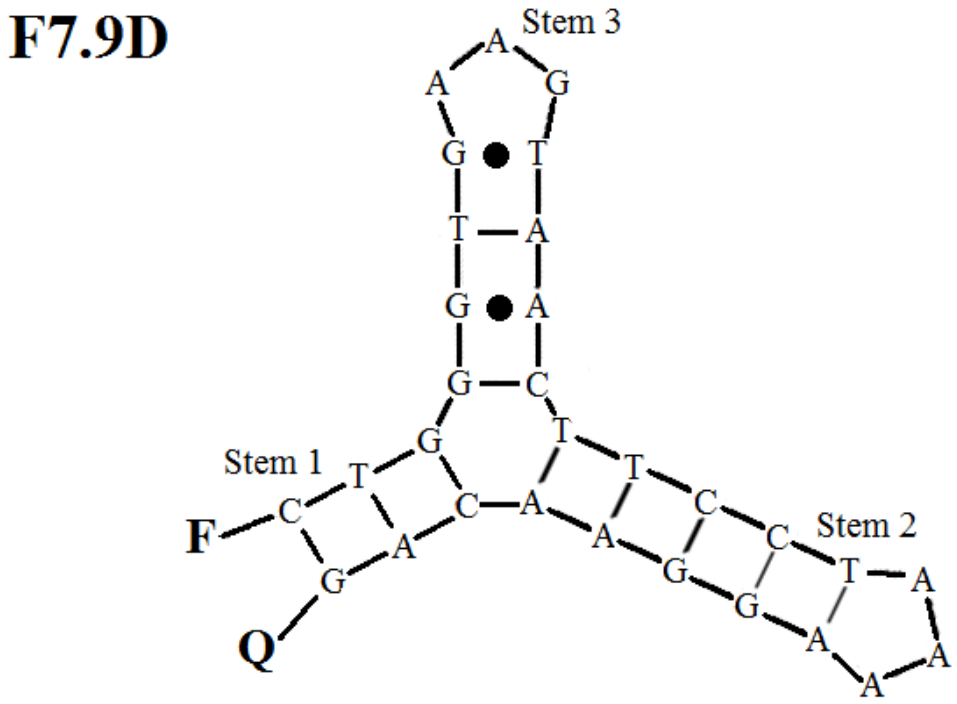

Figure 1.8: A modified cocaine-binding aptamer variant (F7.9D) where stem 1 has been shortened to 3 base pairs and includes a fluorophore (F) at the 5' and quencher (Q) at the 3'. (Adapted from ref. 112)

In 2002, Stojanovic and Landry demonstrated that the cocaine-binding aptamer could be used in the colorimetric detection of cocaine, a first for colorimetric biosensing. After screening several dye molecules for affinity to the aptamer, a weakly binding cyanine dye was shown to be displaced by the presence of cocaine giving rise to detectable intensity changes in the visible spectrum.[100] The study used the originally selected MNS4.1 aptamer and did not require any modifications. Although dye molecules were screened after the aptamer was produced, the findings presented in this work suggest that it might very well be possible to perform SELEX for aptamers which have affinity to both a target of interest and molecules which can be used for colorimetric signals.

A 2006 study by Baker et al. used a previously described scaffold known as an aptamer-based sensing platform, termed "E-AB" sensor, for the rapid detection of cocaine in a number of samples varying greatly in degree of purity. The F7.9D sequence was used with a linker at the 5' end for mounting to a small gold electrode and redox tag at the 3' end. Detectable electrical changes were observed when the aptamer was exposed to cocaine, attributed to folding of the aptamer due to binding. Results also showed the detectability of cocaine in blood serum and saliva using the E-AB sensor.[116] However, use of the cocaine-binding aptamer to detect cocaine present in serum for the purposes of criminal investigation might not be very feasible. With cocaine half-life at just 90 minutes in serum, the average dose of 250 mg[117] would be no longer detectable by means of an E-AB sensor in just 6 hours. In this case, an aptamer selective for cocaine metabolites (having much longer half-lives)[117] might be more effective.

Another 2006 study conducted by Liu and Lu made use of gold nanoparticles and aptamers to demonstrate colorimetric sensing of target molecules in solution. Their initial design used an adenosine aptamer and linker regions on the gold nanoparticles which allowed them to aggregate. In the presence of adenosine, the aggregates would disassemble, giving rise to a detectable change in the visible spectrum. The same design was extended to use the cocaine-binding aptamer with nearly identical results. Changes within the secondary structure of the aptamer would result in the disassembly of the aggregates. Having a detection limit at roughly 50 μM cocaine,[118] the method is not as sensitive as some of those outlined previously. It did however, allow for the rapid detection of cocaine, and much like the E-AB sensor, provided a generalizable scaffold with which just about any aptamer-target pair can be implemented.

In 2010, Yan et al. managed to greatly improve detection limits by using a chemiluminescence (CL) immunosensing platform. Using the adenosine and cocaine-binding aptamers, they were able to make use of magnetic beads and CL detection tools to verify the presence of cocaine with a detection limit in the range of 5 nM. Their technique also allowed simultaneous detection of several target molecules,[119] a huge advantage when thoughts of multi-drug screening come to mind. Perhaps the detection time was not the strongest aspect of the study, but as with other reports, the generalizability of the platform makes it an extremely versatile technique.

One study that seems to have improved on both detection limit and detection times was conducted by Kawano et al. also in 2010. Using nanopore amperometry and a split cocaine-binding aptamer

where one fragment contained a native sequence followed by a trail of 30 cytosines, concentrations of cocaine around 5 μM could be detected in approximately 60 seconds. Most conventional drug test kits have detection limits on this order of magnitude. Higher cocaine concentrations were detectable in shorter time periods, but all on the order of seconds.[120] Perhaps the greatest advantage of this method is not so much the major improvements in detection time, but the fact that no modifications had to be made to the aptamer itself. Although the native sequence may have been modified, no tags or linkers of any type had to be attached to the aptamer to allow for cocaine detection, making the whole platform a very viable approach at rapid and efficient detection of cocaine.

A more recent study completed in 2013 by Sheng et al.[121] reported detection of some of the lowest concentrations of cocaine to date. Using a 3-dimensional DNA nanostructure which incorporated the cocaine-binding aptamer, binding of cocaine altered the original pyramidal shape of the structure allowing a surface dependent redox reaction to take place. With the whole structure mounted to the surface of a gold electrode, an electrochemical signal was able to easily distinguish between the different structural states in a variety of different solutions, including serum. Accurate detection was performed on the order of 1 hour and the sensor was regenerated in approximately 3 hours. The limit of detection was calculated to be at a cocaine concentration of approximately 210 pM.[121] While the method requires tagging of DNA strands and a rather complex DNA architecture, the ultra-sensitivity is a substantial payoff. Such high sensitivity could allow for the detection of an average cocaine dose beyond 24 hours from serum. The outlined protocol in this study can also be generalized to function for just about any aptamer so long as sequence lengths are appropriate. If such high sensitivity is retained for a variety of aptamer-target pairs, an anti-benzoylecgonine aptamer could provide accurate detection of benzoylecgonine in urine samples up to 10 days beyond an average dose.[122]

It is quite evident that cocaine detection is becoming increasingly more efficient and accurate. The cocaine-binding aptamer itself has remained rather constant, but its application in so many different biosensing methods demonstrates how versatile the aptamer truly is. In essence, advancements in biosensing techniques have allowed for the use of the cocaine-bonding aptamer in novel ways that have led to more efficient detection. With many such biosensing techniques

being generalized, aptamers as a whole show great promise as powerful biosensors for a wide array of drug molecules.

1.4.4 Beyond Biosensing

While the cocaine-binding aptamer has its uses in drug detection and drug related research, numerous studies have been devoted to better understanding features of the aptamer itself as well as how the interaction with cocaine is established. Stem length, nucleotide positions, stem folding, strength of intermolecular forces, and secondary and tertiary structure are all highly important aspects that play a role in the affinity of the aptamer to cocaine.[123-127] Though a crystal structure has not yet been solved, a lot of structural information about the aptamer is known. The works of Stojanovic et al. revealed that the aptamer undergoes structural changes when binding cocaine.[100-112] This finding may very well be one of the leading causes for the surge in biosensing applications utilizing the cocaine-binding aptamer. Studies of cross-reactive arrays utilizing the cocaine-binding aptamer illustrated that the 3-way junction structure in itself is a powerful tool capable of distinguishing between various target molecules depending on the identity of nucleotides at the junction. This finding has its place in biosensing applications, but also revealed that specificity of the cocaine-binding aptamer can be altered with some variants binding steroid molecules as a result of a single nucleotide change at the binding site.[123,127]

Research by Cekan et al. focused specifically on structural aspects of the cocaine-binding aptamer. Results showed that the aptamer has stems 2 and 3 stacked coaxially with stem 1 being unfolded and quite mobile in the absence of cocaine. Upon binding, the 3 way junction is formed (Figure 1.9).[125]

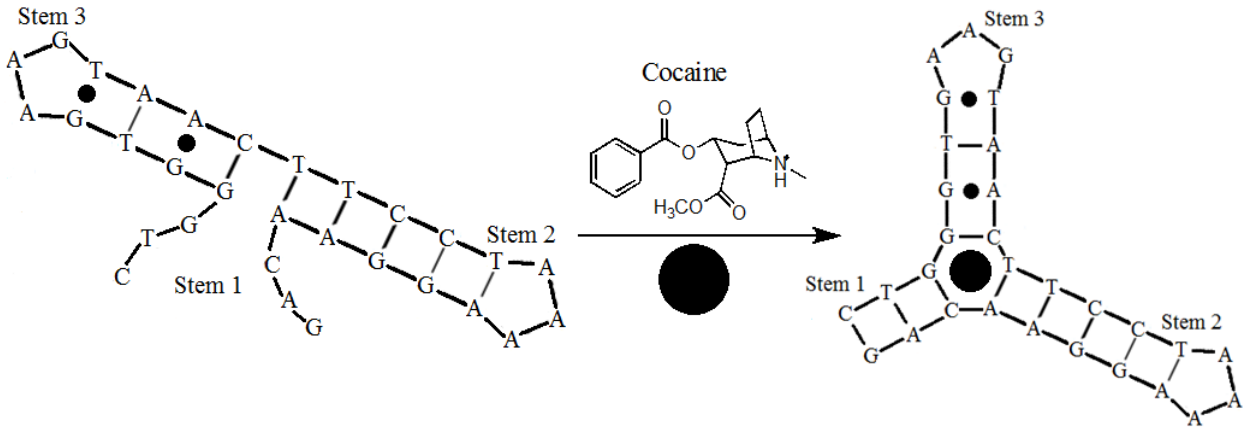

Figure 1.9: A variant of the cocaine-binding aptamer undergoes structural changes when binding cocaine. Cocaine binding drives the formation of the 3-way junction (adapted from ref. 125)

The proposed stem arrangements for the aptamer in the absence of cocaine shown in Figure 1.9 are not that unusual. Much research has shown that catalytic RNAs (ribozymes) contain coaxially arranged stems and bulges which are critical for their functionality.[128] While the existence of naturally occurring catalytic DNAs remains under question, it is not surprising that high affinity DNA aptamers contain at least some of the basic secondary structure elements found in catalytic RNAs. Under the induced fit mechanism, flexible regions within macromolecules are fairly crucial aspects in target binding. In light of all the research related to the cocaine-binding aptamer as well as aptamers in general, conformational changes such as folding may be a major driving force in target binding.

1.5 Essential Goals for this Research

Aptamers as a whole could be considered a gateway to studying the origin of life. The cocaine-binding aptamer is only one of the many aptamers developed to bind a target and it may seem futile to make any generalized statements about the behaviour of all oligonucleotides on account of just one. However, findings related to the cocaine-binding aptamer are nonetheless relevant and may certainly extend to at least multi-way junction structures. The natural evolution of oligonucleotides is a process which is postulated to have taken billions of years[129] and now studying this evolution process can be done in a matter of hours in the laboratory. This is certainly not to say that modern day RNA and DNA is an accurate representation of what may have existed eons ago. In fact, it is postulated that early RNA may have had a very different molecular arrangement, especially bases, which might have included a variety of adducts.[130] We can recognize that the structural and functional possibilities for early RNAs and oligos that followed were nearly limitless and that the cocaine-binding aptamer is simply a platform used to study the behaviour of a unique group contained within. Perhaps by understanding that catalytic oligonucleotides of the early world may have looked and functioned in ways completely foreign to what we know today, are we able to expand our horizons and bring to life new and creative methodologies that may just by chance, reveal a clue that steers investigators in the right direction. It is with much hope that the research outlined in this dissertation, having studied both aptamer

structure and thermodynamics of target binding, finds its use in practical applications of aptamers as well as development of aptamers by rational design.

2 Defining a Stem Length-Dependent Binding Mechanism for the Cocaine-Binding Aptamer

All of the content reported within this chapter has been published in the article listed below.[131] Results presented are from experiments conducted during my undergraduate research project, however data analysis and the discussion reported here are all part of my graduate work. Information on contributing authors is provided in the corresponding section.

- Neves M.A., Reinstein O., Johnson P.E. (2010) Defining a stem length-dependent binding mechanism for the cocaine-binding aptamer. A combined NMR and calorimetry study, *Biochemistry* **49** (39), 8478-8487.

2.1 Introduction

The content contained within this section pertains to structural elements of the cocaine-binding aptamer established purely by corresponding authors prior to my partaking in this research project. It is included here in order to explain the origin of the modified secondary structure of the aptamer used in figures to follow.

2.1.1 The Adaptive Binding Model

For many aptamers studied, particularly RNA aptamers, an adaptive binding mechanism has been proposed[132-135]. In this mechanism, the free state of the aptamer or region of an aptamer exists in an unfolded or partially unfolded state, with the active state, or ligand-binding conformation, being just one of the many structures present in solution. In the presence of the correct ligand, the functional conformations in the unbound state bind the ligand. This shifts the equilibrium to include more active states, which then go on to bind more ligand. This adaptive binding mechanism has been observed in the purine riboswitch[136]. However, the generality of an adaptive binding mechanism in nucleic acid-small molecule interactions is unknown. For example, the lysine riboswitch regulatory element appears to present a prefolded structure, showing little conformation change with ligand binding[137].

It was proposed that the cocaine-binding aptamer utilizes the adaptive binding mechanism as illustrated in Figures 1.6 and 1.8. Although a substantial amount of research suggests that the

aptamer does indeed utilize an adaptive binding model[96-103], evidence from a thermodynamic standpoint has not been provided. Additionally, much of the evidence comes from methods used to observed structural changes, but NMR spectroscopy, a method refined for structural analysis has not been conducted to further support these findings.

2.1.2 An NMR-Based Secondary Structure for the Cocaine-Binding Aptamer

Initial NMR spectroscopy studies on the cocaine-binding aptamer began with the MN1 (Figure 2.1) variant which excluded the terminal GA originally found in stem 1. These two nucleotides, making up the 5' and 3' termini, were presumed to be unpaired as they constitute a non-Watson-Crick base pair. Their flexibility would make them difficult to detect by NMR. Additionally, it was hypothesized that the absence of these two nucleotides would not adversely affect the binding ability of the aptamer as variants with stem 1 truncated are reported to retain high affinity for cocaine.[112]

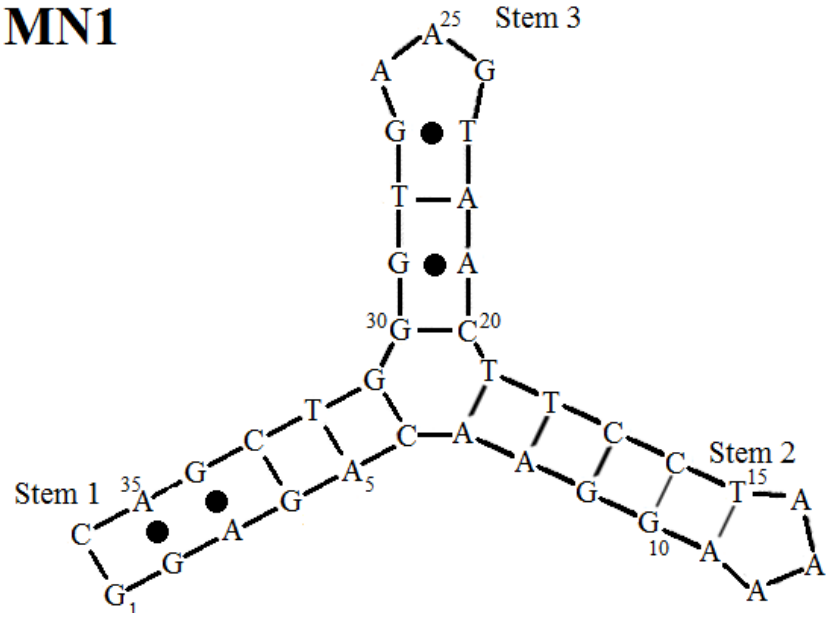

Figure 2.1: Assumed secondary structure of the MN1 aptamer prior to 2D NMR analysis.

The 1D ^{1}H-NMR spectrum of MN1 was initially promising as it showed roughly the expected number of resonances for a molecule with 14 base pairs (Figure 2.2). This indicated that all three stems are fully formed in MN1 even in the absence of ligand. However, spectra of 2D NMR experiments on MN1 were uniformly very poor, with few cross-peaks visible. Upon the addition

of cocaine, many resonances in MN1 change chemical shift and the peaks become sharper, but roughly the same number of resonances are observed. The 2D NMR experiments of cocaine-bound MN1 were still poor, and only partial assignments of the cocaine-bound conformation were obtained (Figure 2.2).

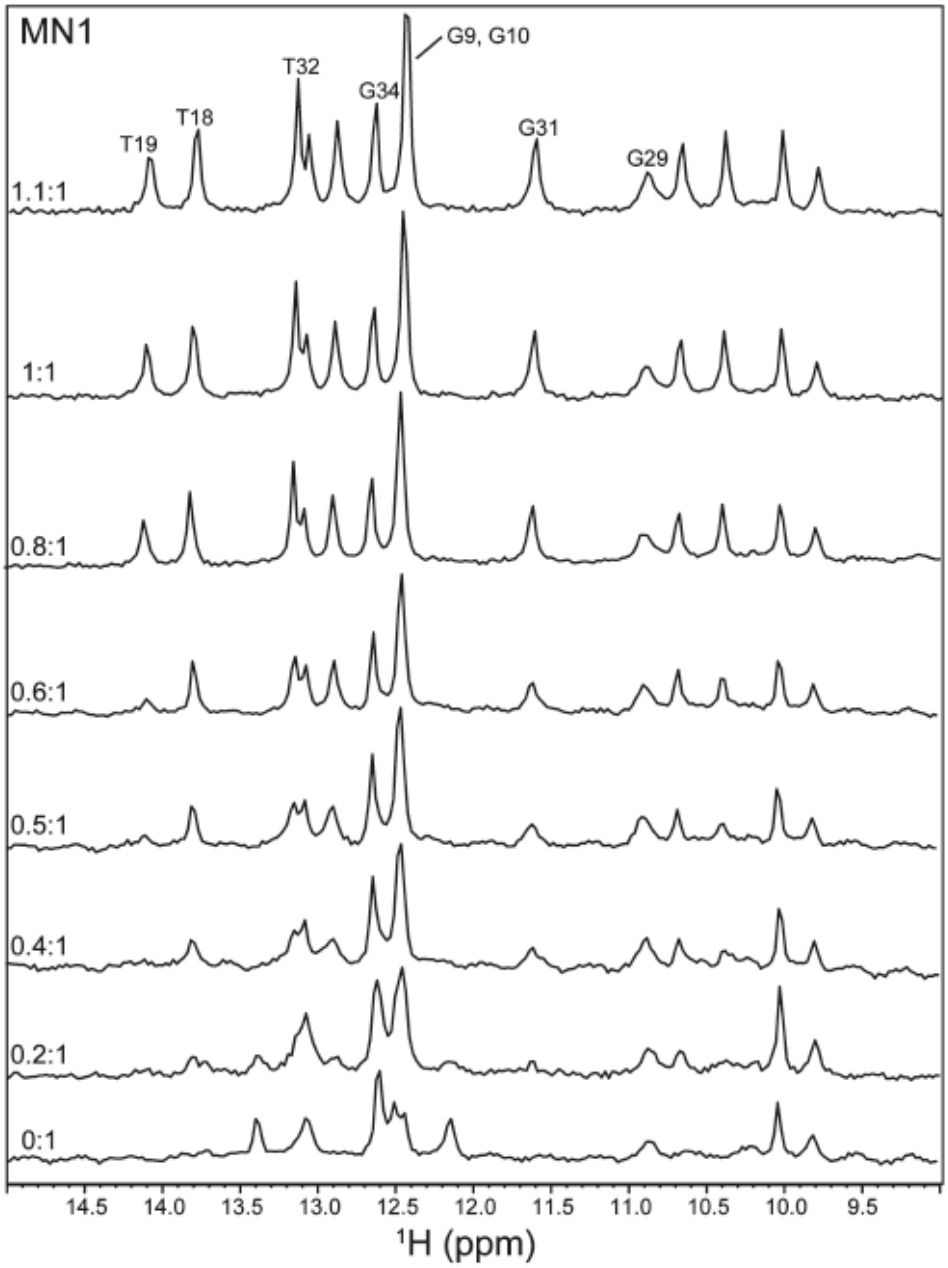

Figure 2.2: Cocaine binding by the MN1 aptamer monitored by 1D ^{1}H-NMR. Shown is the region of the NMR spectrum focusing on the imino resonances as a function of increasing cocaine concentration. Only partial imino assignments are provided. The spectrum was acquired in 90% H_2O/10% D_2O at 5 °C. The molar ratios of cocaine:aptamer are indicated.

In an attempt to rectify quality issues with 2D NMR spectra obtained for MN1, the MN4 aptamer was produced in which 3 of 4 non-canonical base pairs were converted to Watson-Crick base pairs (Figure 2.3). The GA pair nearest the 3-way junction was not changed.

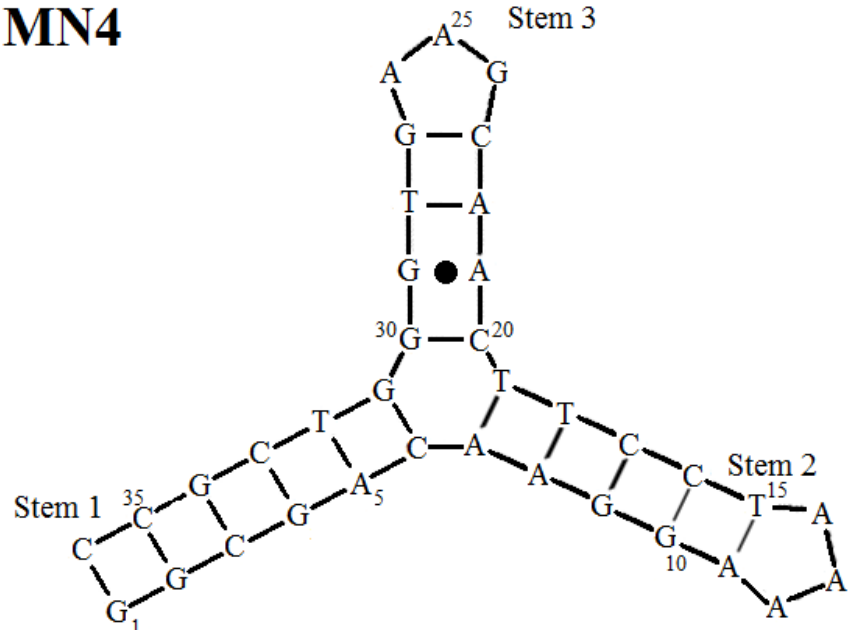

Figure 2.3: Assumed secondary structure of the MN4 aptamer prior to 2D NMR analysis.

In the cocaine-free conformation, the imino region of the ^{1}H-NMR spectrum of MN4, like MN1, contained the expected number of peaks for the number of base pairs, but the peaks in MN4 were much sharper than for free MN1. With cocaine binding, a number of peaks changed chemical shift and the sharpness of the peaks from MN4 increased further (Figure 2.4).

Assignments of the imino resonances in the unbound and cocaine-bound MN4 aptamer were readily obtained from 2D NOESY spectra of the aptamer in water (Figure 2.5). Complete assignments of the imino resonances of cocaine-bound MN4 were obtained with the exception of G1. The resonance from G1 is likely not present due to stem breathing motions as G1 is in the first base pair and is found at the base of stem 1. The three stems of MN4 each show a series of NOEs connecting adjacent base pairs but no inter stem NOEs are observed, suggesting that there are no base stacking interactions or close contact between base pairs across the junction. Additionally, in the cocaine-free spectrum of MN4, the imino resonance of T19 is not observed but is seen in the bound spectrum as the most downfield resonance.

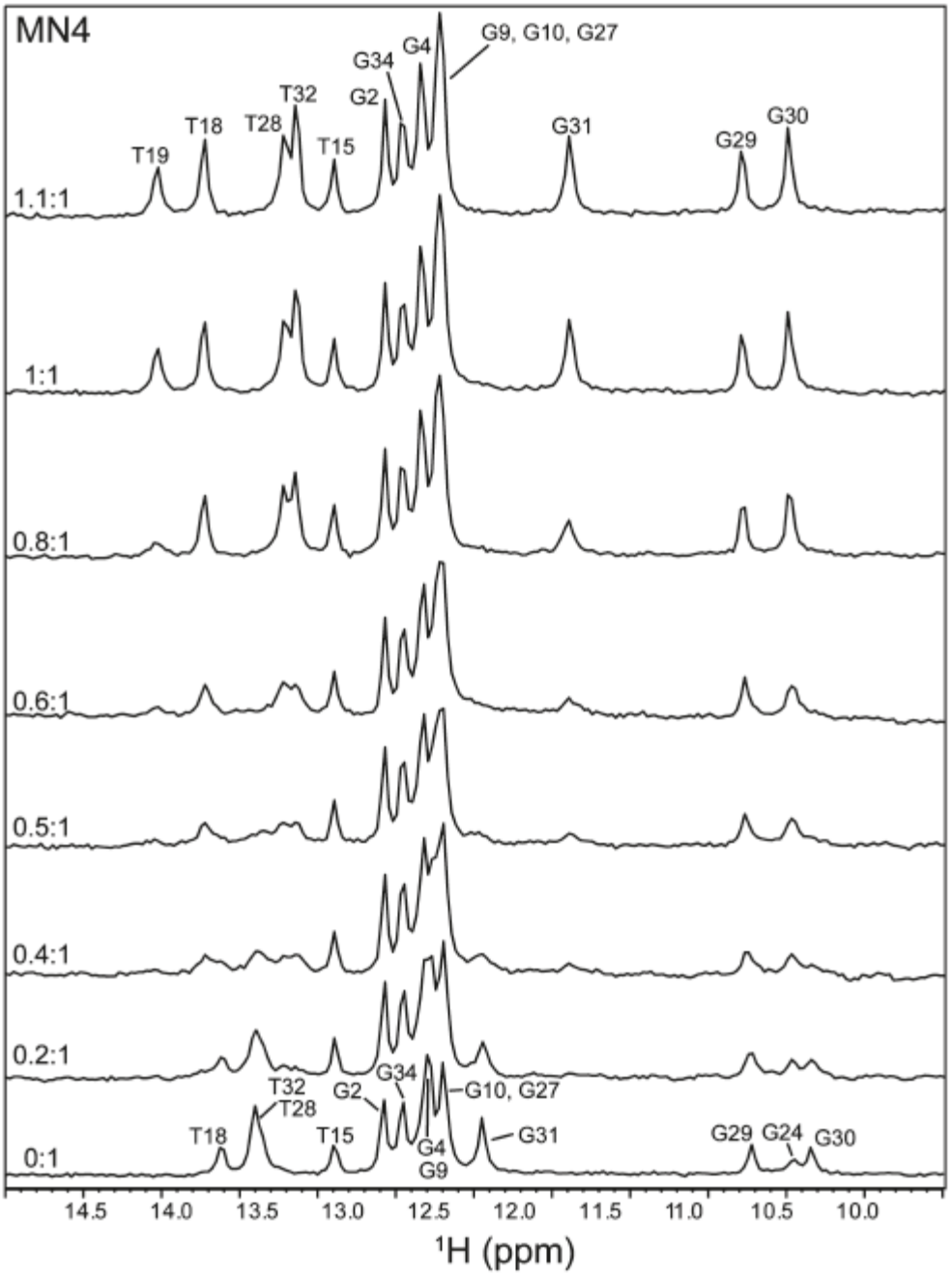

Figure 2.4: Cocaine binding by the MN4 aptamer monitored by 1D ^{1}H-NMR. All imino assignments are indicated. The spectrum was acquired in 90% H_2O/10% D_2O at 5 °C. The molar ratios of cocaine:aptamer are indicated.

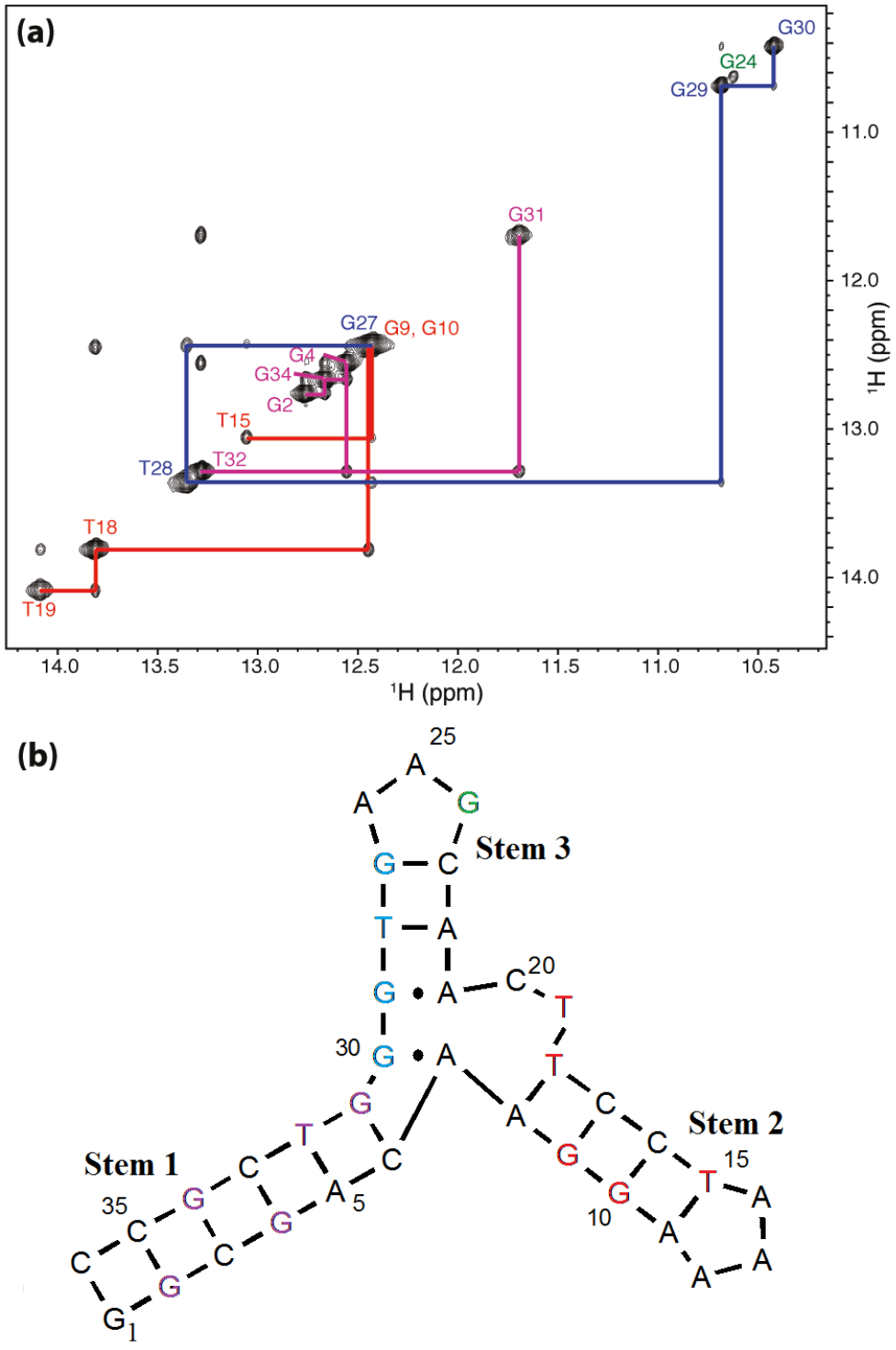

Figure 2.5: Imino proton assignments. (a) Imino-imino region of the 2D NOESY (τ_m = 200 ms) of cocaine bound MN4 in H_2O/D_2O (90%/10%) recorded at 5 °C. (b) Proposed secondary structure of the MN4. Nucleotides are color coded according to their location in the structure and correspond to the assignments provided in (a).

One feature immediately apparent in the imino region of the spectrum of the MN4 aptamer (Figure 2.4) is the presence of one weak and two strong upfield signals around 10.5 ppm. The weak peak is assigned to G24 in the triloop of stem 3. The two strong resonances show an NOE between them in the 2D NOESY spectrum. The upfield nature of these imino resonances indicates they do not arise from standard Watson-Crick base pairs but are in a chemical shift range typical for sheared GA base pairs.[137-141] From the original secondary structure prediction (Figure 2.3) it is expected that one imino peak is from a GA base pair and the most likely conclusion is that there are two adjacent GA base pairs in MN4 as shown in Figure 2.5b. Consistent with the proposed secondary structure for the cocaine-binding aptamer, the 1D ^{1}H-NMR spectrum of the imino region of a construct (WC), where all of the non-Watson-Crick base pairs in the original secondary structure were changed to be Watson-Crick base pairs, still shows the presence of a GA base pair in addition to the signal from G24 (Figure 2.7). Additional NMR based support for the presence of a sheared GA base pair (Figure 2.6b) is the observation of an NOE between the imino proton of G29 and the H8 proton of A21.

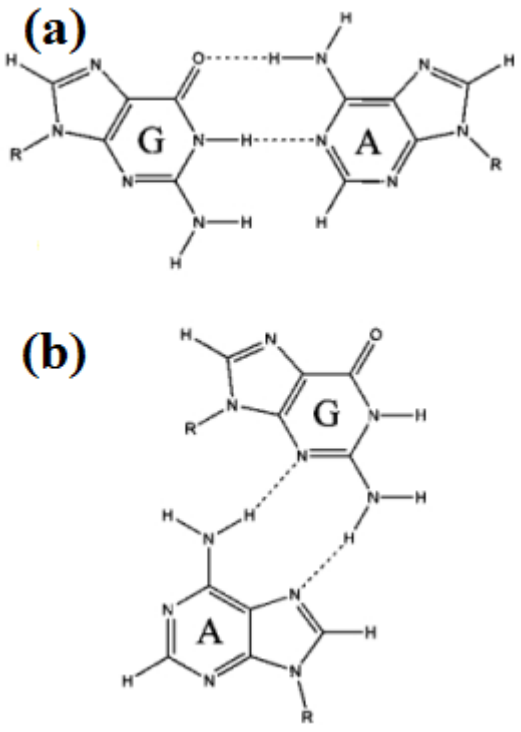

Figure 2.6: (a) GA base pair using Watson-Crick edge. (b) Sheared GA base pair arrangement utilizing Hoogsteen/sugar edge. Obtained from ref. 225

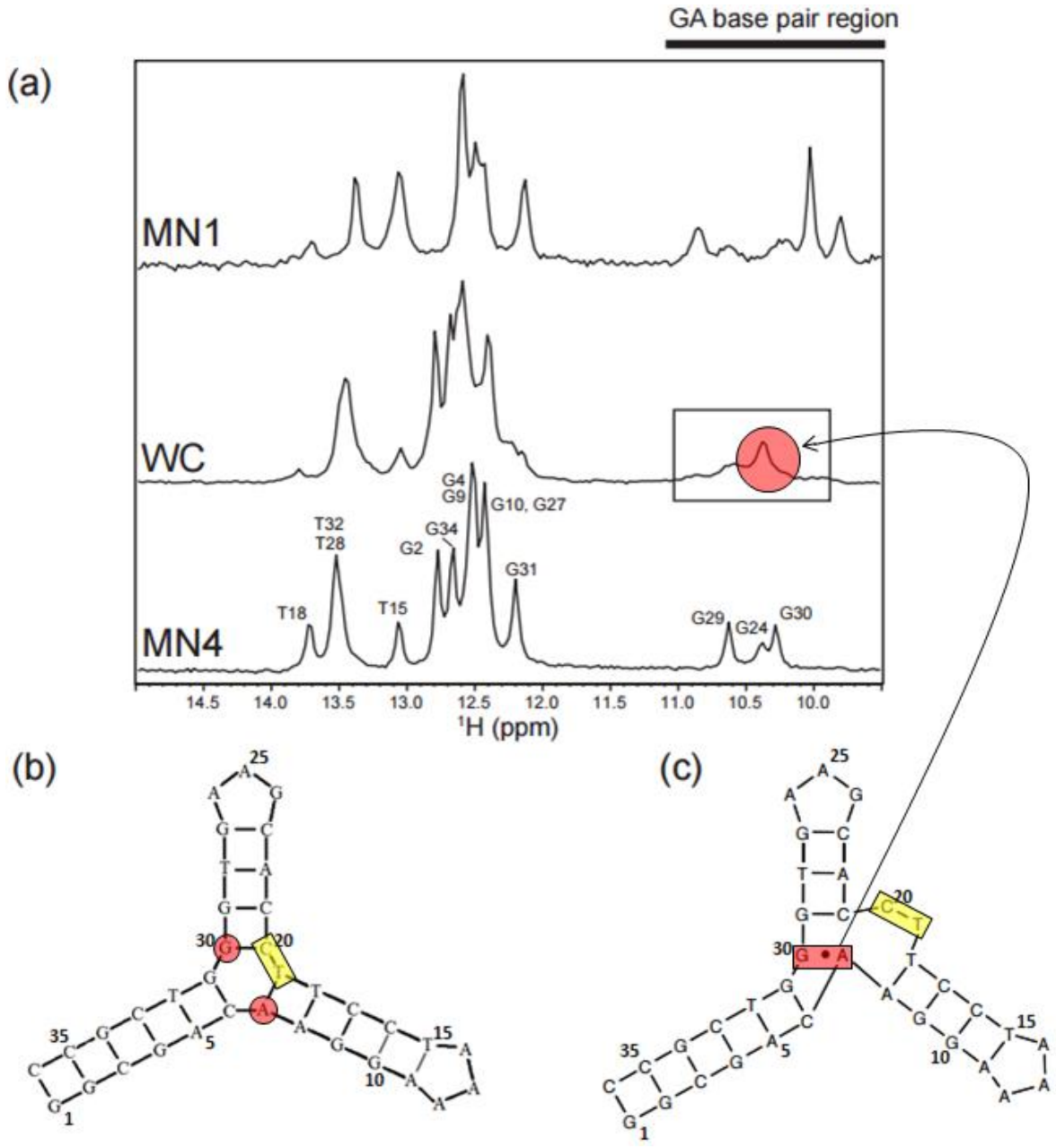

Figure 2.7: (a) 1D ^{1}H-NMR spectra showing the imino region of the WC construct and comparing it to that of the MN4 and MN1 constructs. All spectra are of the unbound aptamers. Boxed in the spectrum of WC is the region showing a GA base pair as well as the signal from G24. (b) Secondary structure of the cocaine-binding aptamer construct "WC" drawn in the previously proposed secondary structure configuration and (c) in the configuration presented here. Observation in (a) of the NMR signal of the GA base pair in the WC construct is only consistent with the secondary structure presented in (c).

2.2 Results

2.2.1 ITC-Derived Thermodynamics of Binding

Isothermal titration calorimetry was used to quantify the ligand binding affinity and thermodynamics of the cocaine-binding aptamer and a set of sequence variants (Figure 2.8). Table 2.1 summarizes the results of the thermodynamic analysis. Two sets of aptamers were analyzed, those with a long (6 base pairs) stem 1, MN1 and MN4, and those with a truncated (3 base pairs) stem 1, MN6 and MN19. Both sets of aptamers bind cocaine. The aptamers with a full-length stem 1 have tighter binding. In both pairs of aptamers, the change of a GT base pair to a GC base pair in stem 3 results in significantly tighter binding. For all aptamers, binding is enthalpically driven and entropically unfavorable under all of the conditions studied.

Table 2.1: Dissociation constant and thermodynamic parameters of cocaine binding for selected aptamer variants

Aptamer	K_d (μM)	ΔH (kcal mol^{-1})	-TΔS (kcal mol^{-1})
MN1	9.15 ± 0.09	-28.1 ± 0.7	21.1 ± 0.7
MN4	7 ± 1	-14.5 ± 0.4	7.6 ± 0.5
MN6	45.3 ± 0.5	-22.3 ± 1.6	16.5 ± 1.6
MN19	26.7 ± 0.7	-23.9 ± 0.9	17.7 ± 0.9

The ΔC_p for cocaine binding by MN4 was determined by measuring the enthalpy of binding at different temperatures over a temperature range of 10 - 50 °C (Figure 2.9). A complete table of ΔH and calculated ΔC_p values for all ITC experiments for MN4 is provided in Table 2.2. From a fit of the MN4 data to an equation that accounts for a temperature-dependent heat capacity change, ΔC_p was determined to be -558.8 cal mol^{-1} K^{-1}. Additionally, the value of $\Delta\varphi_p$ was determined to be 0.251 cal mol^{-1} K^{-2}, and ΔH was determined to be -19.4 kcal mol^{-1}. As the $\Delta\varphi_p$ value is small, it is possible to use a linear approximation to determine the value of ΔCp which was found to be to be (-557 ± 29) cal mol^{-1} K^{-1} and ΔH to be (-19 ± 1) kcal mol^{-1}.

For MN6, the measured enthalpy data from 5 to 25 °C results from two effects: (1) binding of ligand and (2) folding of the aptamer. At low temperatures (5 - 15 °C) folding of the aptamer is complete, and these effects result in a near linear fit of the enthalpy to the heat capacity equations to result in a ΔC_p of -918.6 cal mol^{-1} K^{-1}, a value of $\Delta\varphi_p$ of 1.6 cal mol^{-1} K^{-2}, and ΔH was

determined to be -33.4 kcal mol^{-1}. Similar to MN4, the value of $\Delta\varphi_p$ for MN6 is very small. When the data were fit to the linear approximation, the value of ΔC_p is determined to be (-922 ± 51) cal mol^{-1} K^{-1} and $\Delta H°$ to be (-30 ± 2) kcal mol^{-1}. At temperatures above 15° C, binding of ligand does not result in 100% folding of the aptamer. As temperature rises, an increasing percentage of the aptamer remains unfolded in the presence of ligand. This means less of the enthalpy of folding is added to the enthalpy of binding, resulting in a trend to larger (less negative) enthalpy values at temperatures over 15 °C. Consequently, the data acquired at 20 and 25 °C were not used in the data fitting to determine ΔC_p. A table of ΔH and calculated ΔC_p values for all ITC experiments for MN6 is provided in Table 2.3.

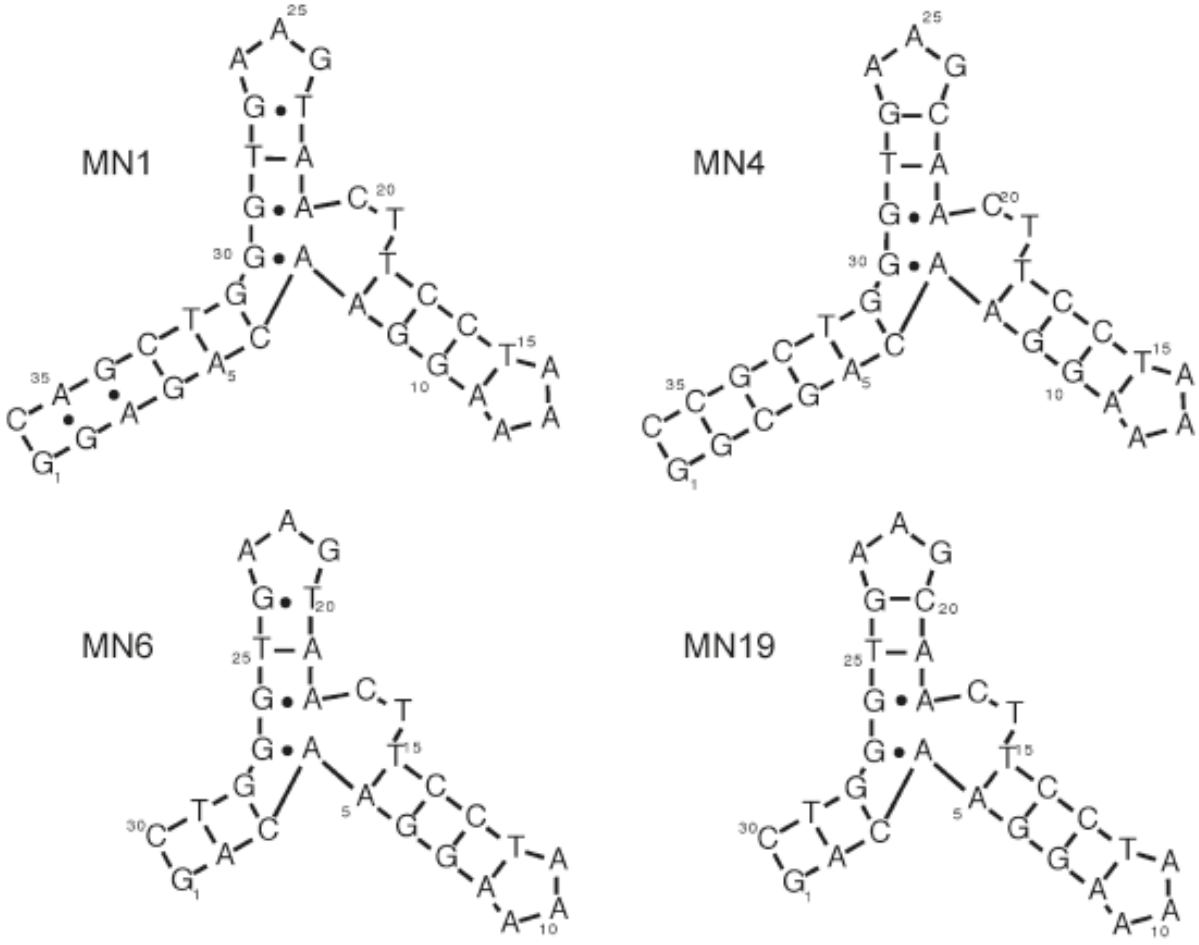

Figure 2.8: Secondary structure of the MN1, MN4, MN6, and MN19 aptamers drawn using the newly proposed secondary structure that includes the tandem GA mismatch.

Table 2.2: Temperature dependence of the binding enthalpy and the calculated change in heat capacity by the MN4 cocaine-binding aptamer as determined by isothermal titration calorimetry.[a]		
Temperature (°C)	**ΔH (kcal mol^{-1})**	**ΔC_p (kcal mol^{-1} K^{-1})**
10.023	-12.6 ± 0.4	-560
10.017	-12.1 ± 0.8	-560
10.199	-12.7 ± 0.2	-560
15.014	-11.7 ± 0.2	-560
15.015	-12.1 ± 0.3	-560
20.016	-14.7 ± 0.4	-560
20.029	-14.8 ± 0.4	-560
25.015	-19.9 ± 0.5	-560
30.049	-22.1 ± 1.5	-560
30.029	-22.1 ± 2.7	-560
37.026	-27.5 ± 7.5	-560
37.01	-25.8 ± 1.8	-560
40.02	-29.9 ± 2.6	-560
40.036	-29.4 ± 9.2	-560
50.121	-31.7 ± 14.9	-550
50.124	-32.5 ± 7.0	-550

Table 2.3: Temperature dependence of the binding enthalpy and the calculated change in heat capacity by the MN6 cocaine-binding aptamer as determined by isothermal titration calorimetry.[a] Data in bold were used in the fit to determine ΔC_p.		
Temperature (°C)	**ΔH (kcal mol^{-1})**	**ΔC_p (kcal mol^{-1} K^{-1})**
5.252	**-12.1 ± 0.6**	**-950**
7.516	**-14.6 ± 0.3**	**-950**
10.012	**-16.3 ± 0.3**	**-940**
10.011	**-16.8 ± 0.5**	**-940**
12.513	**-18.2 ± 1.4**	**-940**
12.516	**-18.1 ± 0.6**	**-940**
15.175	**-21.2 ± 0.7**	**-930**
15.012	**-21.4 ± 0.5**	**-930**
20.173	-23.4 ± 1.2	-930
20.051	-22.1 ± 1.5	-930
20.012	-21.2 ± 1.4	-930
25.021	-6.9 ± 0.9	-920
25.008	-9.4 ± 1.2	-920

[a]Data acquired in 20 mM TRIS (pH 7.4), 140 mM NaCl, 5 mM KCl (**Buffer A**). The error range reported is the standard measurement of error.

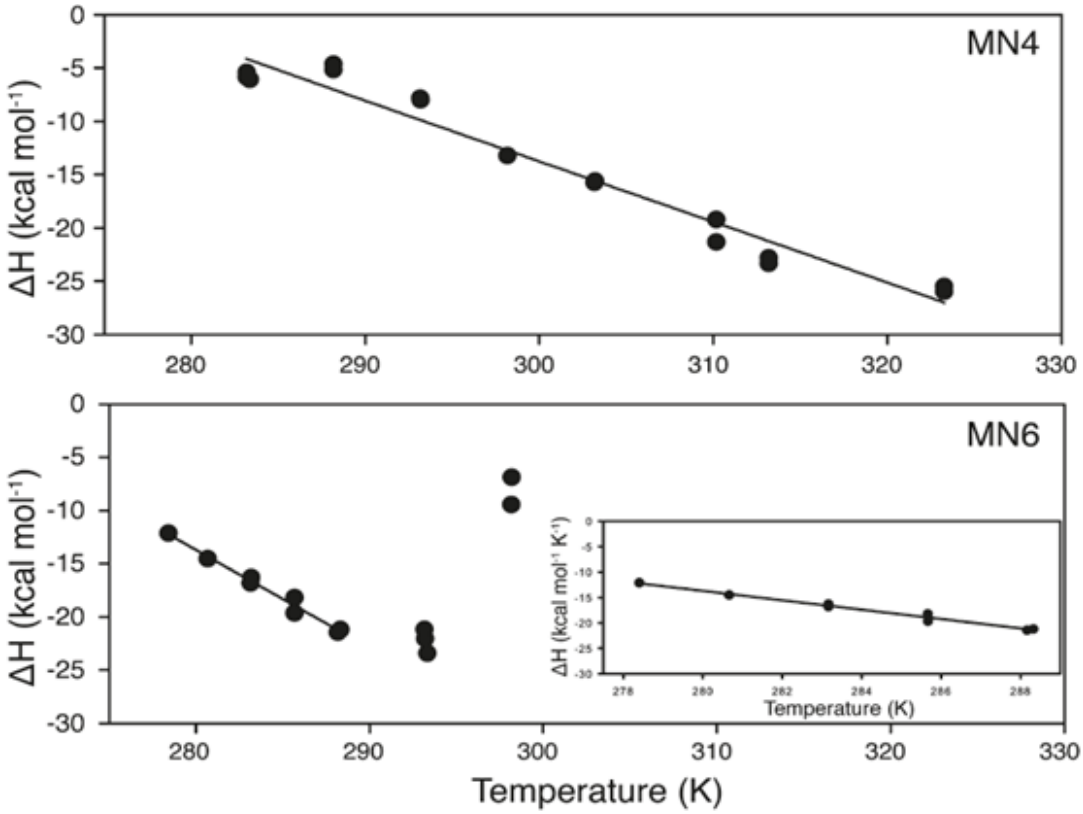

Figure 2.9: Temperature dependence of the enthalpy of cocaine binding for the MN4 and MN6 aptamers derived by ITC. The data values are shown as filled circles while the fit of the data to an equation that accounts for a temperature-dependent heat capacity change is the solid line. For MN6, only the low-temperature region where effects of aptamer unfolding do not contribute to the enthalpy was used in the fit (inset). Binding experiments were performed in Buffer A.

2.2.2 Folding Studied by NMR

For the two aptamers with the truncated stem 1, MN6 and MN19, the NMR spectrum of the free aptamer showed only a few very weak and very broad peaks in the imino region (Figures 2.9 and 2.10). The spectra of the free MN6 and MN19 aptamers are indicative of very little to no secondary structure being present. With the addition of cocaine, the 1D ^{1}H-NMR spectra of MN6 and MN19 dramatically change as numerous sharp peaks appear as the aptamer folds into a well-defined structure. The number of peaks in the bound spectrum of each aptamer is consistent with the number of base pairs expected in the secondary structure of the aptamers as shown in Figure 2.10.

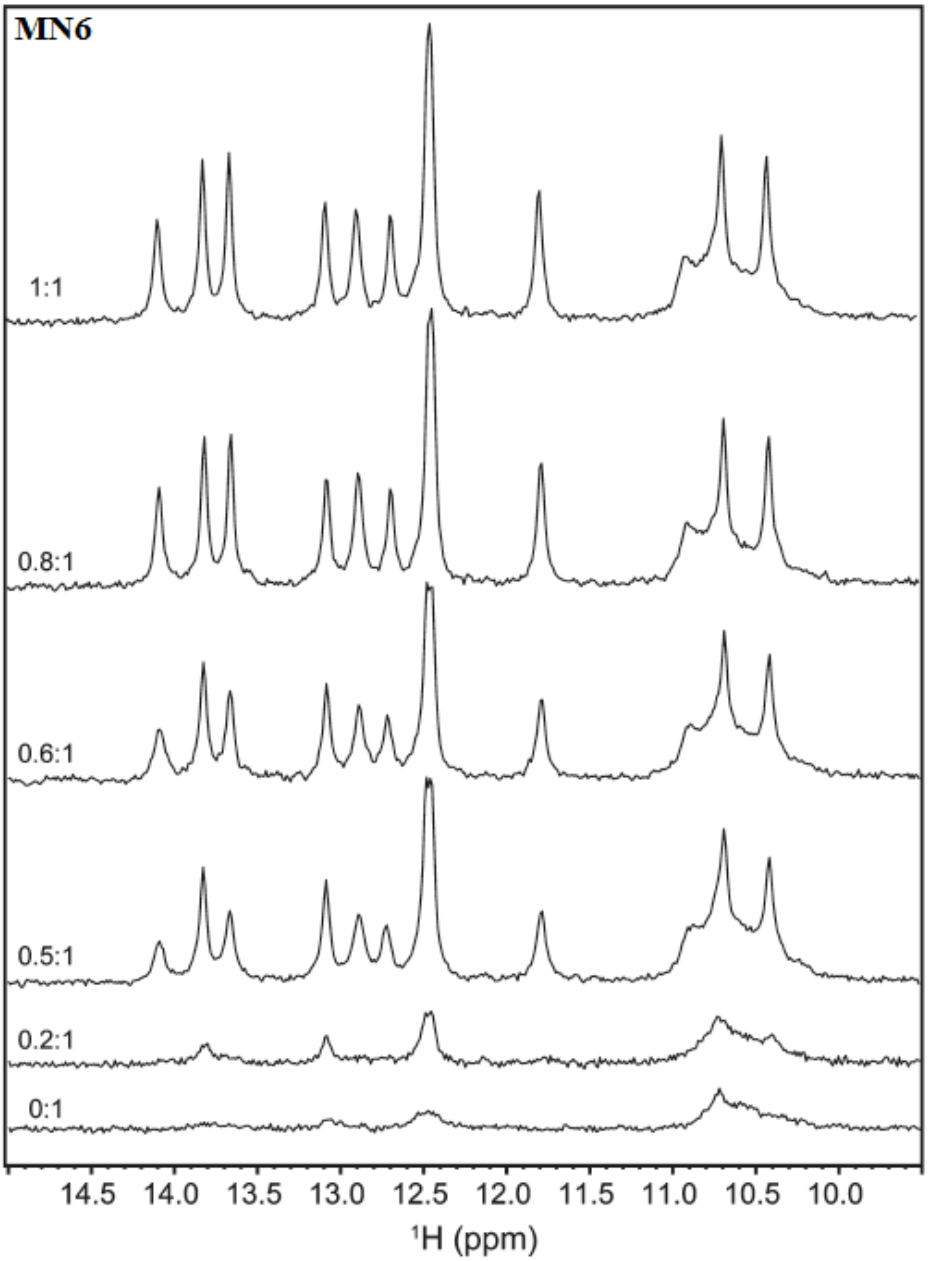

Figure 2.10: Cocaine binding by the MN6 aptamer monitored by 1D ^{1}H-NMR. Shown is the region of the NMR spectrum focusing on the imino resonances as a function of increasing cocaine concentration. Spectra were acquired in 90% H_2O/10% D_2O at 5 °C. The molar ratios of cocaine**:**aptamer are indicated.

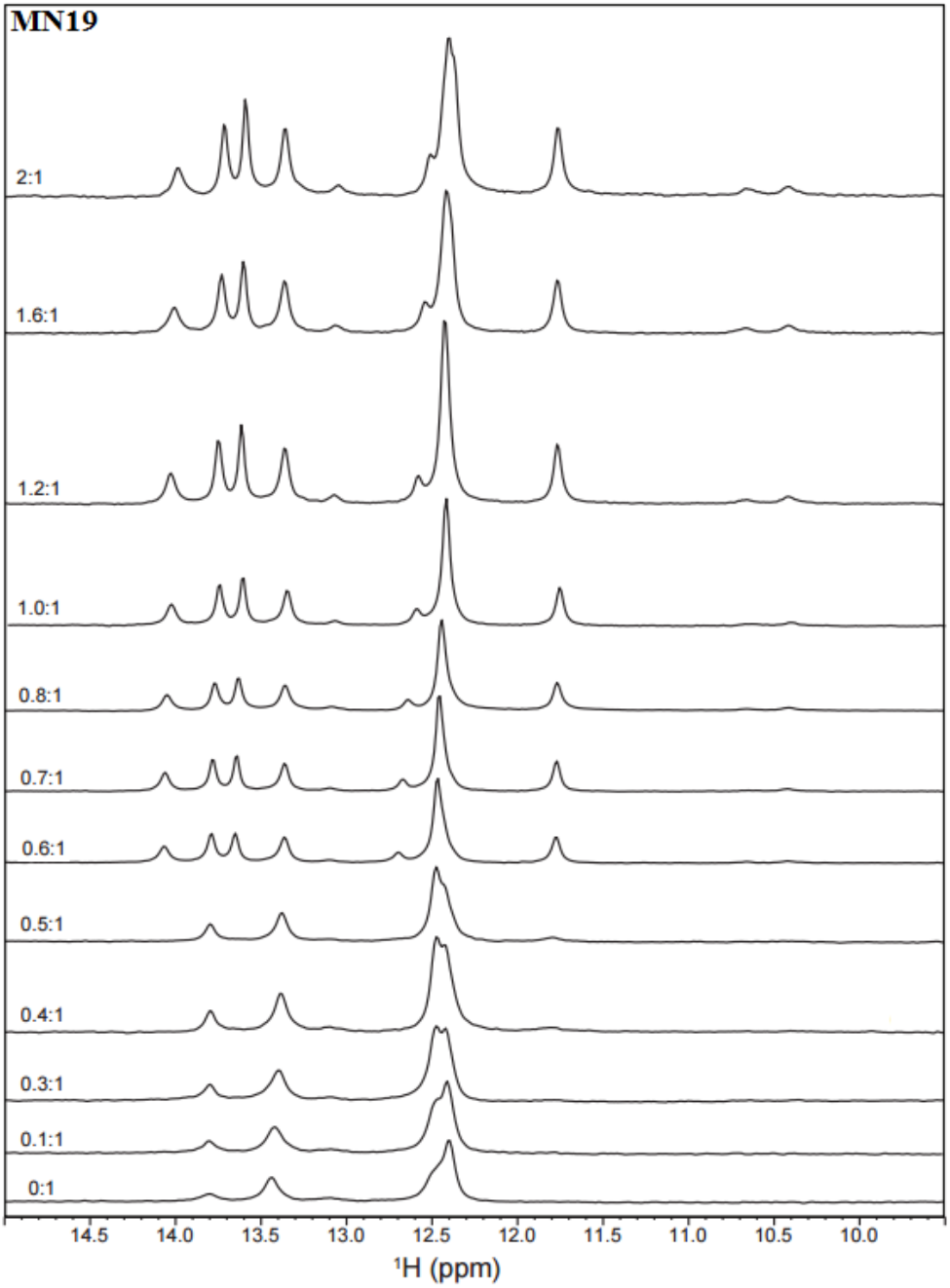

Figure 2.11: Cocaine-binding by the MN19 aptamer monitored by 1D ^{1}H-NMR. Shown is the region of the NMR spectrum focusing on the imino resonances as a function of increasing cocaine concentration. Spectra were acquired in 90% H_2O/10% D_2O at 5 °C. The molar ratios of cocaine**:**aptamer are indicated.

2.3 Discussion

2.3.1 Summary of Initial Results

A primary goal of this research on the cocaine-binding aptamer is to define the structure of the complex using NMR methods. While initial NMR studies on MN1 yielded only very poor quality spectra, substantial improvements were seen in spectra of MN4 where non-canonical base pairs were substituted for Watson-Crick base pairs. This substitution also led to a very slight increase in binding affinity suggesting that the nucleotides at substituted positions are not critical for ligand binding. Additionally, both the MN1 and MN4 aptamers have an enthalpically driven binding mechanism compensated by unfavourable binding entropy; this likely reflects a similar binding mechanism takes place for both aptamers. Similar changes were made in the aptamers with a truncated stem 1, changing the GT non-canonical base pair in stem 3 in MN6 to be a Watson-Crick GC in MN19. This single change significantly increased the affinity of the aptamer for cocaine and demonstrates the importance of having a Watson-Crick base pair at this position to achieve maximal affinity, affinity higher than the originally selected aptamer.

2.3.2 Secondary Structure of the Cocaine-Binding Aptamer

On the basis of the NMR assignments of MN4, a new secondary structure is proposed for the cocaine-binding aptamer that contains adjacent GA base pairs. Additional evidence for this arrangement comes from a construct where all of the non-canonical base pairs present in the originally proposed secondary structure were substituted so as to form Watson-Crick base pairs. In the imino spectrum of this aptamer, two upfield peaks are observed. One due to the G24 in the triloop of stem 3 and a single GA imino peak. The incorporation of a tandem GA into the cocaine-binding aptamer secondary structure is readily accomplished by having the nucleotides T19 and C20 in a bulge. This dinucleotide bulge is consistent with T19 only being observable in the presence of cocaine. Presumably, T19 directly contacts cocaine in the complex in such a way as to result in the imino proton of T19 being protected from exchange and becoming visible or the T19 imino proton becomes involved in a new interaction, such as a base triple, within the aptamer. The proposed arrangement containing tandem GA mismatches is a stable and common motif in DNA structures[143-145]. The tandem GA mismatch has been shown to be the most stable tandem DNA mismatch in the context of having a 5’-C and a 3’-G and, in fact, is more stable in this sequence

context than the corresponding Watson-Crick AT base pairs[146]. Tandem GA base pairs have been identified in eukaryotic centromeric DNA sequences and have been extensively structurally studied[138,142,147,148]. In a crystal structure of a tandem GA pair, the mismatch caused the B-form helix to kink toward the major groove side and extensive interstrand base stacking was observed at the GA mismatch[147]. In the cocaine-binding aptamer, the tandem GA mismatch likely imparts a conformation in the DNA structure required for ligand binding.

2.3.3 A Stem Length-Dependent Binding Mechanism

The binding mechanism employed by the cocaine-binding aptamer depends on the length of stem 1. When stem 1 is short (3 base pairs), the aptamer employs an adaptive binding mechanism and transitions from an unfolded to a folded structure with ligand binding. Alternately, when stem 1 is long (6 base pairs), the secondary structure of the aptamer is preformed and ligand binding induces very little change in secondary structure (Figure 2.12). Presented in this research is both NMR and ITC data to support this stem length dependent binding mechanism.

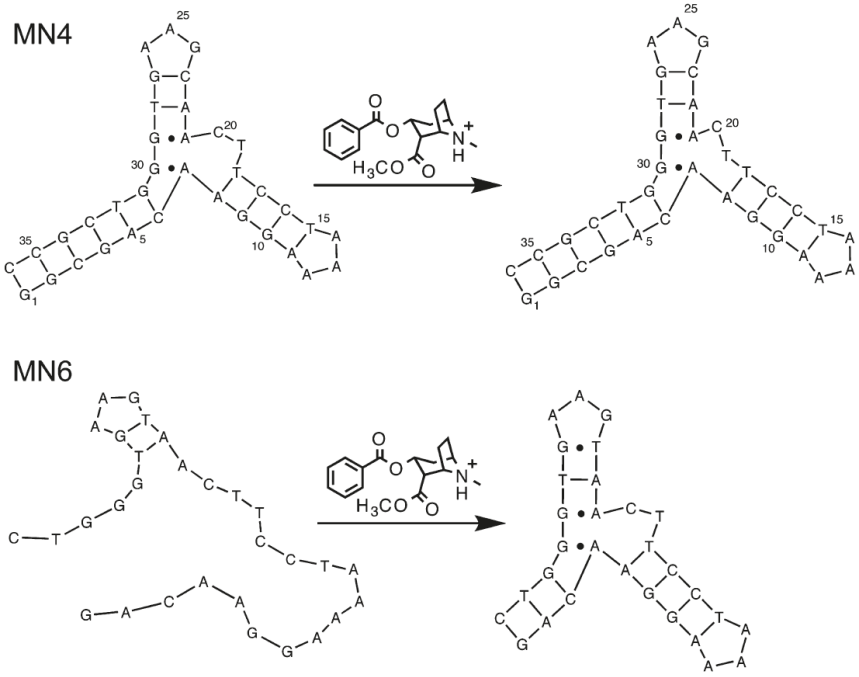

Figure 2.12: Proposed structural changes with ligand binding for the cocaine-binding aptamers with different lengths of stem 1. Aptamers with a long stem 1 (MN1, MN4) undergo tertiary structural changes only with ligand binding. When stem 1 is truncated (MN6, MN19) the aptamer is unfolded when unbound. The secondary structure is established with ligand binding as the aptamer begins to fold.

2.3.3.1 Evidence from Structural Analysis

The NMR spectra of the cocaine-binding aptamer and variants indicate a binding mechanism that is highly dependent on the length of stem 1. For MN1 and MN4 the free aptamer contains the correct number of imino peaks for its secondary structure to be fully formed in the unbound state. Upon addition of ligand, the peaks in the NMR spectrum of both MN1 andMN4 sharpen and become more intense. However, only one new peak appears in the bound form of the aptamer that is not observed in the free form, that of T19. In contrast, for both MN6 and MN19, the ^{1}H-NMR spectrum in the absence of ligand indicates these aptamers contain only a small amount of secondary structure, two or three base pairs being present at most. Upon addition of ligand, the NMR spectrum dramatically changes with numerous narrow peaks from the bound form of the aptamer appearing. These changes indicate the aptamer folds with binding and it is noted that the number of peaks observed for the bound MN6 and MN19 is consistent with their proposed secondary structure.

2.3.3.2 Evidence from Thermodynamics

Additional evidence in support of the stem length-dependent binding mechanism being followed by the cocaine-binding aptamer comes from measurements of the change in heat capacity with ligand binding. For MN4, ΔC_p was determined to be (-557 ± 29) cal mol^{-1} K^{-1}. In contrast, binding data for MN6 resulted in the determination of (-922 ± 51) cal mol^{-1} K^{-1} for the ΔC_p Measuring the ΔC_p value is useful as this parameter is related to the change in polar and apolar surface area between the free ligand, macromolecule, and binary complex[149]. For MN6, the more negative value of ΔC_p indicates a significantly larger amount of nonpolar surface area is buried than is seen with MN4 binding. This observation is consistent with a binding mechanism that involves folding of the macromolecule concurrent with ligand binding. If no structural change in the aptamer occurs with binding, the ΔC_p value will reflect the extent of burial from solvent of the ligand. If cocaine is completely buried, a maximum negative value of (-132.1 ± 21.0) cal mol^{-1} K^{-1} for ΔC_p is predicted. The difference in ΔC_p between experimental values for MN4, MN6 and that of complete burial of cocaine is attributed to structural changes in the aptamer upon binding. For MN4, NMR data suggests little to no secondary structure change occurs with binding. Therefore, the structural change suggested by the ΔC_p value likely reflects tertiary structure compaction. Such changes would be consistent with the improved NMR spectral quality of the bound versus

the free aptamers. For MN6 the ΔC_p of secondary structure formation is coupled to binding and gives rise to the much larger measured value. Similar differences between the measured ΔC_p and the expected ΔC_p based on change in polar and apolar surface area have been previously observed in both small molecule-RNA and small molecule-DNA interaction[150-153].

The experimental values of ΔC_p for MN4 and MN6 lie in the high range reported for these other nucleic acid-small molecule systems. The previously most negative ΔC_p value was -0.81 kcal $mol^{-1}K^{-1}$ for the purine riboswitch aptamer domain,[149] while the least negative was -116 cal $mol^{-1}K^{-1}$ for the L-argininamide- binding DNA aptamer.[153] While the value of ΔC_p arises from numerous factors, it is likely that the larger negative magnitude of ΔC_p tracks the amount of structural change with ligand binding for these systems. Some of the applications of the cocaine-binding aptamer rely on an aptamer with the MN6 sequence transitioning from an unfolded to folded structure with ligand binding.[111-125] This folding transition was also observed in the previously described EPR and fluorescence study.[125] The authors proposed that stems 2 and 3 were formed prior to cocaine binding while stem 1 forms with binding. In contrast, NMR data shows that only two to three base pairs might be formed prior to ligand binding. For aptamers with the long stem 1, an adaptive binding mechanism was previously proposed where stem 3 folds with cocaine binding.[100] NMR reveals that all three stems are folded in the free state with only changes in the tertiary structure potentially taking place upon ligand binding.

2.4 Conclusion

For all of the aptamers studied here, cocaine binding is an enthalpically driven process offset by an unfavorable entropic penalty. Two categories of DNA-small molecule binding interactions have been classified according to their thermodynamic signature. Groove binders display small negative or positive enthalpy with favorable binding entropy, while intercalators have unfavorable entropy and negative enthalpy values.[155] The thermodynamic parameters observed for MN1, MN4, MN6, and MN19 binding cocaine would put this interaction in the "intercalator" category. This is not to propose that these aptamers follow a classic intercalation binding mechanism where the ligand sits between adjacent base pairs. It is proposed that the cocaine-binding aptamer follows a binding mechanism where the DNA rearranges to a more rigid structure. It is this rearrangement which gives rise to the thermodynamic signature of the intercalation mechanism.[155]

It is noted that this rearrangement is consistent with the large negative $\Delta C_p°$ values measured that suggest tertiary structure packing from MN1 and MN4. ITC was used to determine the energetics of cocaine binding for a series of DNA aptamers. This is the first study to look at the binding thermodynamics of the cocaine-binding aptamer, though previous studies have utilized other techniques to measure the binding affinities for some variants of the cocaine-binding aptamer. The affinities reported for MN1 are consistent with previously published binding data on the cocaine-binding aptamer. MN1, having a K_d of (9.15 ± 0.09) μM is comparable to the MNS-4.1 aptamer with a reported K_d value of 5 μM in identical buffer and salt conditions.[100],[112] MN1 and MNS-4.1 are identical with the exception that MN1 is one base pair shorter as it does not have a terminal GA base pair in stem 1. This extra base pair in MNS-4.1 likely contributes little to cocaine binding. An affinity (49 ± 1) μM is reported for the MN6 aptamer which is in line with previous reports of 37 μM[155] and ~20 μM.[112]

In summary, NMR and thermodynamic data demonstrate that the cocaine-binding aptamer follows a stem length dependent binding mechanism. With 6 base pairs in stem 1, the secondary structure of the aptamer is formed when free and ligand binding tightens up or orders the tertiary structure. When stem 1 has three base pairs, the aptamer is unfolded in the free state except for possibly two to three base pairs. Ligand binding induces secondary structure formation and folding of the bound aptamer. This study should provide guidance for the further development of anti-cocaine biosensors.

2.5 Experimental Methods

2.5.1 Materials and Sample Preparation

Cocaine hydrochloride was obtained from Sigma-Aldrich. Aptamer samples were obtained from the University of Calgary DNA Service. DNA samples for NMR analysis were purified by denaturing (8 M urea) 20% polyacrylamide gel electrophoresis. The DNA was separated from the gel by electroelution, and the DNA samples were pooled, exchanged three times in a 3 kDa molecular mass cutoff concentrator with sterilized 1M NaCl, and subsequently washed at least three times with distilled deionized H_2O. DNA samples for ITC and were exchanged with 20 mM Tris (pH 7.4), 140 mM NaCl, and 5 mM KCl (Buffer A) three times before use.

2.5.2 NMR Spectroscopy

All 1D ^{1}H-NMR experiments on aptamer samples were acquired using a 600 MHz Bruker Avance spectrometer. 2D NOESY (τm = 200 ms) spectra in H_2O/D_2O (90%/10%) were recorded at 5 °C. A 2DNOESY (τm=200 ms) spectrum was acquired on the MN4 aptamer in D_2O at 20 °C using a Varian 800 MHz NMR spectrometer. Aptamer concentration for NMR studies ranged from 0.5 to 2.3 mM. Data were analyzed using CcpNmr Analysis.[181]

2.5.3 Isothermal Titration Calorimetry

ITC has been an instrumental technique applied in this investigation and additional detail on its mechanics are provided in Chapter 8: Appendix 1.

2.5.3.1 Standard Titration Procedure and Data Analysis

Isothermal titration calorimetry (ITC) was performed using a MicroCal VP-ITC instrument and the data were analyzed by fitting to a one-site binding model using the accompanying Origin software. Samples were degassed before use with the MicroCal Thermo Vac unit. All experiments were corrected for the heat of dilution of the titrant. Unless otherwise specified, cocaine and aptamer solutions were prepared in Buffer A. Binding experiments were typically performed with 20 μM aptamer solutions using cocaine concentrations of 280 μM at 20 °C. All aptamer samples were heated in a boiling water bath for 3 min and cooled on ice prior to use in a binding experiment to allow the aptamer to anneal. Binding experiments consisted of (1) 30 successive 8 μL injections of cocaine solution every 300 s to a final molar ratio of 2.5**:**1 or (2) 36 injections of 6 μL of cocaine solution spaced every 300 s with a first injection of 1 μL to a final molar ratio of 2**:**1.

2.5.3.2 Low c ITC Procedure

A low c ITC method was developed for use with the weaker binding constructs or conditions.[166,183] In these low c ITC experiments, the running conditions were kept the same; however, titrations consisted of 35 successive injections of a 45 mM cocaine solution. The first 10 injections were 5 μL, and the remaining additions were 8 μL injected every 300 s to a 50-fold

molar excess of cocaine. The raw low c data were also corrected for heat of dilution of the titrant. The constructs fit under these low c conditions are MN6 and MN19.

2.5.3.3 Determination of the Isobaric Heat Capacity of Binding

The isobaric heat capacity (ΔC_p) of cocaine binding for MN4 and MN6 was determined by measuring the thermodynamics of binding over a temperature range of 5-50 °C with an aptamer solution of 20 μM and a cocaine solution of 3.6 mM in Buffer A. The ITC experiments conducted to measure the thermodynamic parameters consisted of 35 successive injections of cocaine spaced every 300 s. The first injection was 1 μL followed by 20 injections of 3 μL and 14 injections of 15 μL to ensure complete binding site saturation. These low c conditions were selected so that all temperatures could be studied using the same experimental parameters. Since all experiments were allowed to reach complete binding site saturation, the observed saturation was used as the dilution reference.[182] ΔC_p was determined by fitting the ITC measured enthalpy and free energy to the equations:

$$\Delta G = \Delta G^\circ + T \int_{\tau^\circ}^{T} \Delta H \, d\tau \qquad (1)$$

$$\Delta H = \Delta H^\circ + \int_{T^\circ}^{T} \Delta C_p \, dT \qquad (2)$$

$$\Delta C_p = \Delta C_p{}^\circ + \Delta \varphi_p (T - T^\circ) \qquad (3)$$

Here ΔG and ΔH are the free energy and enthalpy at the given temperature, ΔG° and ΔH° are the free energy and enthalpy at standard conditions, (T - T°) is the change in temperature, $\tau = 1/T$, and $\Delta\varphi_p$ is a term that represents the linear change in the heat capacity.[136] Under circumstances where $\Delta\varphi_p$ is small, the enthalpy versus temperature curve can be fit linearly to equation 4.

$$\Delta H = \Delta H^\circ + \Delta C_p (T - T^\circ) \qquad (4)$$

Linear regression analysis of the data fit yields the values of ΔC_p and ΔH as well as the associated errors.

2.5.3.4 Surface Area Calculations

In order to determine the polar and nonpolar surface area of cocaine, a PDB file of the molecule was generated using PRODRG.[184] The amount of polar and apolar area was then determined using the VEGA WE online server.[185] The expected ΔC_p based on the change in polar (ΔA_p) and apolar (ΔA_{np}) surface area was calculated using the method of Spolar and Record, where $\Delta C_p = [(0.32 \pm 0.04)\Delta A_{np} - (0.14 \pm 0.04)\Delta Ap]$ cal mol^{-1} K^{-1}.[149] The equation presented here was derived following observed heat capacity changes associated with the transfer of hydrocarbons and amides taken from aqueous into non aqueous phases. Similarly, folding proteins, also exhibiting changes in heat capacity, demonstrated similar proportionalities to the non-polar surface area removed in the presence of water, as in the transfer of hydrocarbons and amides. It was noted that changes in water-accessible non-polar surface area was a major determinant for changes in heat capacity associated with folding. However, polar and non-polar compounds were both able to model the folding behaviour of proteins, essentially indicating that changes both non-polar and polar solvent accessible surface area are determinants in the changes in heat capacity associated with folding.[227]

3 Defining the Sequence Requirements of the Cocaine-Binding Aptamer and Investigation of the Structure Switching Mechanism

All of the content reported within this chapter has been published in the article listed below.[157,158] Results presented in section 3.2.2 are from experiments conducted during my undergraduate research project, however data analysis and conclusions reported here are all part of my graduate work.

Content within section 3.3.5 pertains to structural information about steroid-binding aptamer variants obtained from experiments conducted purely by corresponding authors. It is included to clarify conclusions drawn about the nature of the unbound state of the cocaine-binding aptamer and its variants as well as its implications on the binding mechanism.

- Neves M.A.,, Reinstein O., Saad M., Johnson P.E. (2010) Defining the secondary structural requirements of a cocaine-binding aptamer by a thermodynamic and mutation study, *Biophys Chem* **53** (1), 9-16.

- Reinstein O., Neves M.A., Saad M., Boodram S.N., Lombardo S., Beckham S.A., Brouwer J., Audette G.F., Groves P., Wilce M.C., Johnson P.E. (2011) Engineering a structure switching mechanism into a steroid-binding aptamer and hydrodynamic analysis of the ligand binding mechanism, *Biochemistry* **50** (43), 9368 – 9376.

3.1 Introduction

The widespread use of the cocaine-binding aptamer in biosensing applications is attributed to its engineered structural switching or ligand-induced folding mechanism. Previously described was the dependency on stem length for this binding mechanism. A second method to achieve ligand-induced folding is to divide the aptamer into two separate strands. Cocaine binding results in the assembly of the two strands and the ligand into a single tertiary complex.[111] This two strand assembly mechanism has been exploited to control the assembly of a variety of DNA-based supramolecular complexes.[159-161] Doubtlessly, the rapid development and use of these applications

are limited by the legal and regulatory restrictions placed on the use of the required ligand, cocaine.

The three-way junction that forms the structural and functional core of the cocaine-binding aptamer has a strong similarity to that of a steroid binding aptamer.[162] Subsequently, the bases at the three-way junction of the cocaine aptamer have been modified to result in sets of biosensors with a range of affinity and specificity for alkaloids as well as steroids such as deoxycholic acid (DCA; Figure 3.3). Such versatility in ligand specificity is uncommon among aptamers and prompted the investigation of a series of cocaine-binding aptamer variants in order gauge which regions and nucleotides are important for ligand binding as well as to determine if variants built around a common DNA architecture which bind different ligands follow a similar binding mechanism. This binding mechanism was also studied further by observing binding as a function of both pH and NaCl. With this knowledge it may be possible to alter an aptamer that binds a steroid or other alkaloid to also perform structural switching upon ligand binding. The existence of such a ligand-induced folding mechanism would open up to widespread adoption the biotechnology applications that utilize the ligand-induced folding mechanism of the cocaine-binding aptamer.

3.2 Results

3.2.1 Ligand Binding Mechanism and Buffer Composition

In order to determine the optimal pH value for cocaine binding and investigate the role played by titratable groups on either the ligand or aptamer, binding as a function of pH was measured for MN1. Under the standard buffer conditions used in previous studies with a pH of 7.4, the amine in cocaine is expected to be protonated (Figure 3.3).[163] The importance of the positive charge in aptamer-binding was assayed by measuring binding as a function of ionic strength for both MN1 and MN4. 1D ^{1}H-NMR experiments with varying concentrations of NaCl were conducted to verify if the differences in observed cocaine affinity were due to salt induced structural changes.

3.2.1.1 Effect of pH on Cocaine Binding

Binding was studied at pH values of 5.4, 6.4, 7.4, 9.2 and 9.6 (Table 3.1). Tightest binding was

observed at pH 7.4. At pH values both higher and lower than 7.4 weaker binding is observed. At pH 9.6 no appreciable binding is observed and an estimate is given that binding must be weaker than approximately 2 mM.

Table 3.1: pH dependence of the dissociation constant and thermodynamic parameters of cocaine binding for the MN1 aptamer.[a]

pH	K_d (μM)	ΔH (kcal mol^{-1})	−TΔS (kcal mol^{-1})
5.4	13.0 ± 0.7	−18.2 ± 0.5	7 ± 0.5
6.4	13.9 ± 0.1	−23 ± 1	16 ± 1
7.4	9.15 ± 0.09	−28.1 ± 0.7	21.1 ± 0.7
9.2	22.9 ± 0.9	−11.0 ± 0.8	8 ± 0.8
9.6	>2000	nd	nd

[a]Data acquired at 20 °C at the indicated pH with 140 mM NaCl, 5 mM KCl. The values reported are averages of 2–4 individual experiments. The error range reported is one standard deviation. 'nd' indicates that the value was not determined.

3.2.1.2 Effect of Ionic Strength on Cocaine Binding

Thermodynamic parameters for cocaine binding by MN1 and MN4 at NaCl concentrations from 0 to 1 M are shown in Table 3.2 and representative ITC data is shown in Figure 3.1. Both MN1 and MN4 show a similar trend of having maximum binding affinity when no NaCl is present. A maximum binding affinity of (0.3 ± 0.1) μM is observed for MN4 with the condition of 0 mM NaCl. For MN1 with no added NaCl, the affinity is (1.4 ± 0.3) μM. At higher NaCl concentrations binding weakens. Binding affinity decreases to (31 ± 1) μM for MN1 in the presence of 500 mM NaCl. Further increases in NaCl concentration to 1 M did not significantly weaken the binding affinity of MN1. At each NaCl concentration studied, binding is enthalpically driven and compensated with unfavorable binding entropy (Table 3.2).

From NMR studies it was observed that as the concentration of NaCl increases, the linewidths of the imino protons increase, but the resonances retain their chemical shifts. This indicates no structural changes occur as the salt concentration increases. Instead, the increase in linewidth reflects a change in dynamics of the aptamer with the addition of NaCl.

Table 3.2: Ionic strength dependence of the dissociation constant and thermodynamic parameters of cocaine binding for aptamers MN1 and MN4.[a]				
Aptamer	**NaCl (mM)**	**K_d (μM)**	**ΔH (kcal mol^{-1})**	**−TΔS (kcal mol^{-1})**
MN1	0	1.4 ± 0.3	−22.7 ± 1	14.8 ± 1
	140	9.15 ± 0.09	−28.1 ± 0.7	21.1 ± 0.7
	500	31 ± 1	−21.2 ± 0.7	2 ± 0.7
	1000	27 ± 3	−12.5 ± 0.6	3 ± 0.5
MN4	0	0.3 ± 0.1	−16 ± 3	9.3 ± 0.8
	140	7 ± 1	−14.5 ± 0.4	7.6 ± 0.5
	500	35 ± 8	−8.4 ± 0.8	2.4 ± 0.7

[a]Data acquired at 20 °C in 20 mM Tris (pH 7.4) with the amount of NaCl indicated. The values reported are averages of 2–4 individual experiments. The error range reported is one standard deviation.

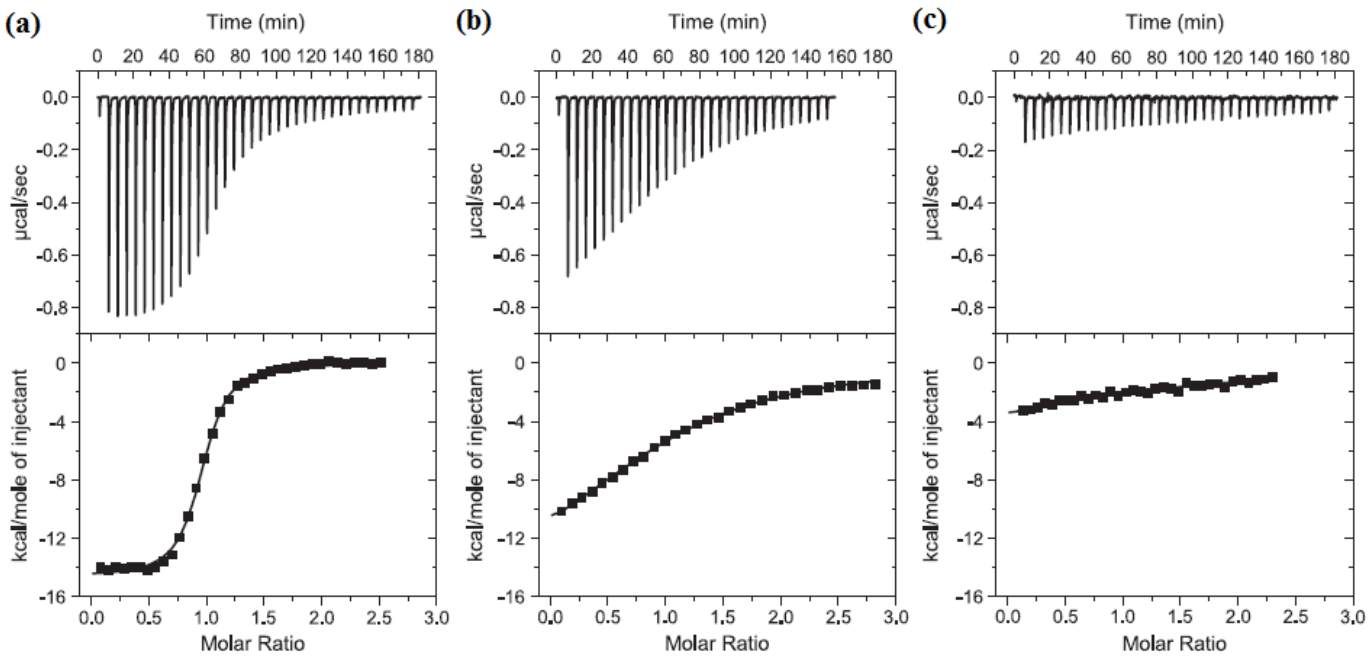

Figure 3.1: Analysis of cocaine binding by the MN4 aptamer using isothermal titration calorimetry. Shown are titrations of cocaine into an MN4 aptamer solution (20 mM Tris, pH 7.4) in the presence of (a) 0 mM NaCl (b) 140 mM NaCl, and (c) 500 mM NaCl, 20 mM Tris, pH 7.4. On top is the raw titration data showing the heat resulting from each injection of cocaine into the aptamer solution. On the bottom are the integrated heats after correcting for the heat of dilution. Binding affinity increases from right to left as per Table 3.2.

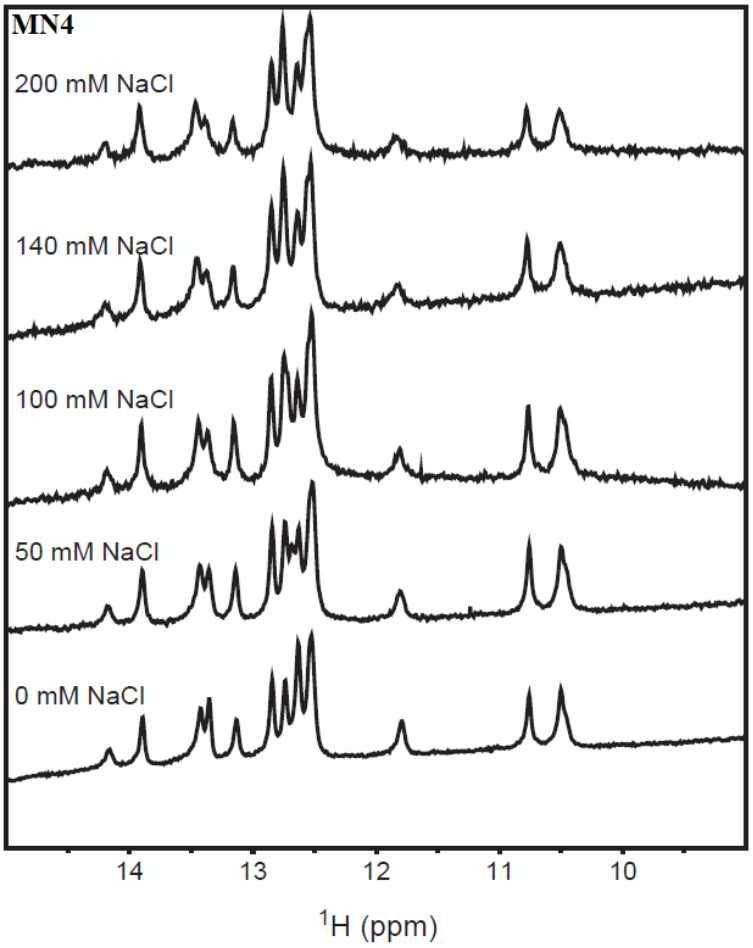

Figure 3.2: Change in the imino proton NMR spectrum of the MN4 aptamer as a function of added NaCl. Shown are the 1D ^{1}H-NMR spectra of cocaine-bound MN4 in conditions of 0 to 500 mM NaCl.

3.2.2 Aptamer Sequence and Ligand Binding Thermodynamics

The importance of the length of the three stems of the cocaine-binding aptamer was analyzed by varying stem length and measuring the cocaine binding affinity of these constructs (Figure 3.3). When stem 3 was eliminated or shortened by two base pairs (S1S2, SS3 and MN2), cocaine binding was eliminated. For the MN5 construct, where stem 3 is shortened by one base pair, missing only the GT base pair adjacent to the triloop, binding occurs but the affinity is reduced to (42 ± 4) μM (Table 3.3). Stem 2 can be shortened to contain a single putative base pair (MN7) and still retain cocaine binding with a reduced affinity of (55 ± 1) μM (Table 3.3). Previously reported here and in other studies, it has been shown that stem 1 can be shortened to consist of three base

pairs and still retain reasonable affinity (MN6 and MN19)[125,157] (Figure 3.3; Table 3.3). The lengths of all three stems were simultaneously decreased to test if there would be an additive effect. The construct MN18 combined the stem shortening mutations of MN5, MN7 and MN6 and the resulting molecule displayed no detectable ligand binding.

The importance of the identity of the non-canonical base pairs for cocaine binding was also analyzed. When all the non-canonical base pairs in the cocaine-binding aptamer, as drawn with the originally proposed secondary structure (Figure 2.1) are changed to Watson-Crick base pairs (construct WC; Figure 3.3) binding is reduced 23 fold to (204 ± 6) μM. This large reduction in binding showed the importance of the non-canonical base pairs for cocaine binding.

To determine if all non-canonical base pairs were important for ligand binding, aptamer variatns MN3, MN4 and MN8 (Figure 3.3) were tested. These variants had affinities of (14 ± 4) μM, (7 ± 1) μM, and (8.6 ± 0.2) μM, respectively. All of these constructs bind with a very similar affinity as MN1 and show that the predicted T23/G27, G2/A35 and A3/G34 base pairs in MN1 are not essential for high affinity binding. In contrast, analysis of MN9, MN10, and MN11 show the importance of the non-canonical G29/A21 base pair. When this GA pair is modified to a GC pair, binding was greatly reduced to (193 ± 1) μM, (148 ± 9) μM and (123 ± 22) μM for MN9, MN10 and MN11, respectively. The importance to binding of the G30/A7 base pair was assayed by construct MN12 (Figure 3.3). In MN12, A7 was substituted for a C. The resultant G30/C7 displayed no binding, even under the low c conditions used to assay weak binders. This indicates that the identity of A7, and retaining the A7/G30 base pair, is essential to maintain ligand binding function of the aptamer.

The newly proposed secondary structure of the cocaine-binding aptamer displays two unpaired nucleotides present at the three-way junction, T19 and C20. The importance of the identity of these nucleotides was tested in constructs MN15, MN16 and MN17 (Figure 3.3). In MN17, C20 was substituted for a G. MN17 retained binding but with a reduced affinity of (59 ± 13) μM, 8.4 times lower than MN4. In MN16, T19 is replaced by an A. This change resulted in no quantifiable binding being observed for this construct. Changes in the thermogram with ligand binding under low c conditions indicated that very weak binding, in the millimolar range, was occurring. Similar very weak binding was observed for MN15 where a double mutant (T19 to C; C20 to T) was

tested. Together these results indicate that the identity of T19 is critical to maintain cocaine binding while the identity of C20 is less crucial.

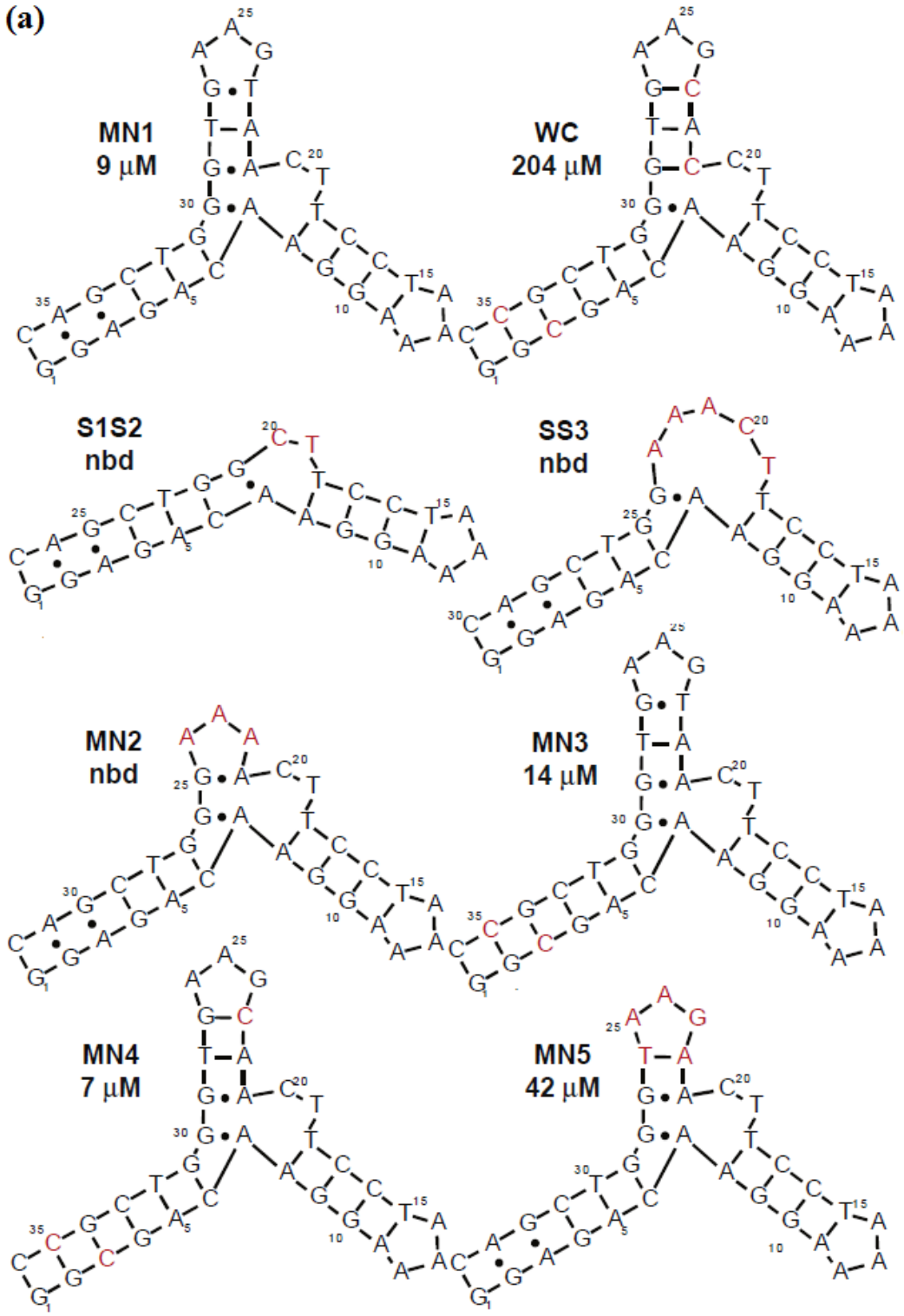

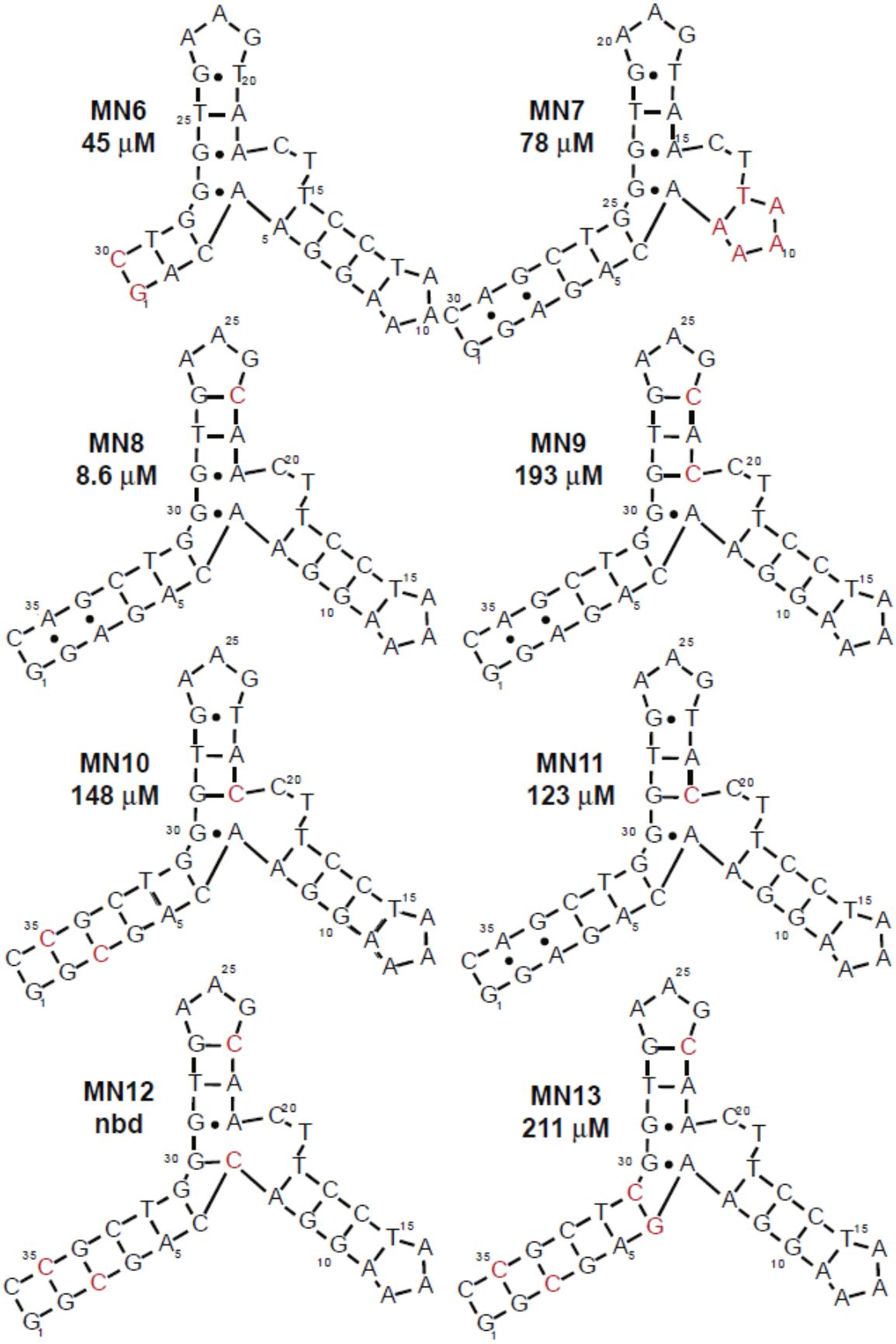
MN6
45 μM
MN7
78 μM
MN8
8.6 μM
MN9
193 μM
MN10
148 μM
MN11
123 μM
MN12
nbd
MN13
211 μM

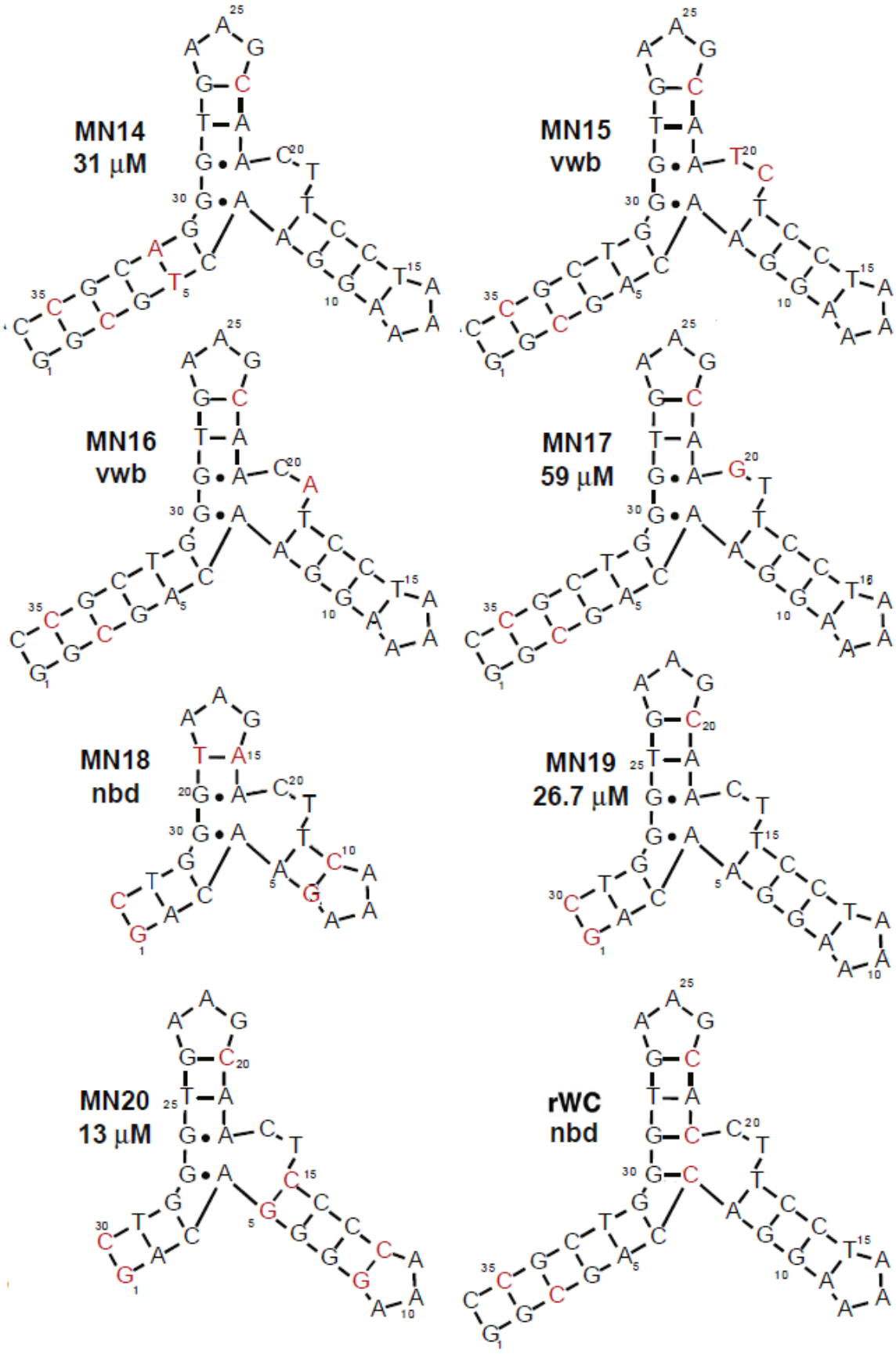
MN14
31 μM
MN15
vwb
MN16
vwb
MN17
59 μM
MN18
nbd
MN19
26.7 μM
MN20
13 μM
rWC
nbd

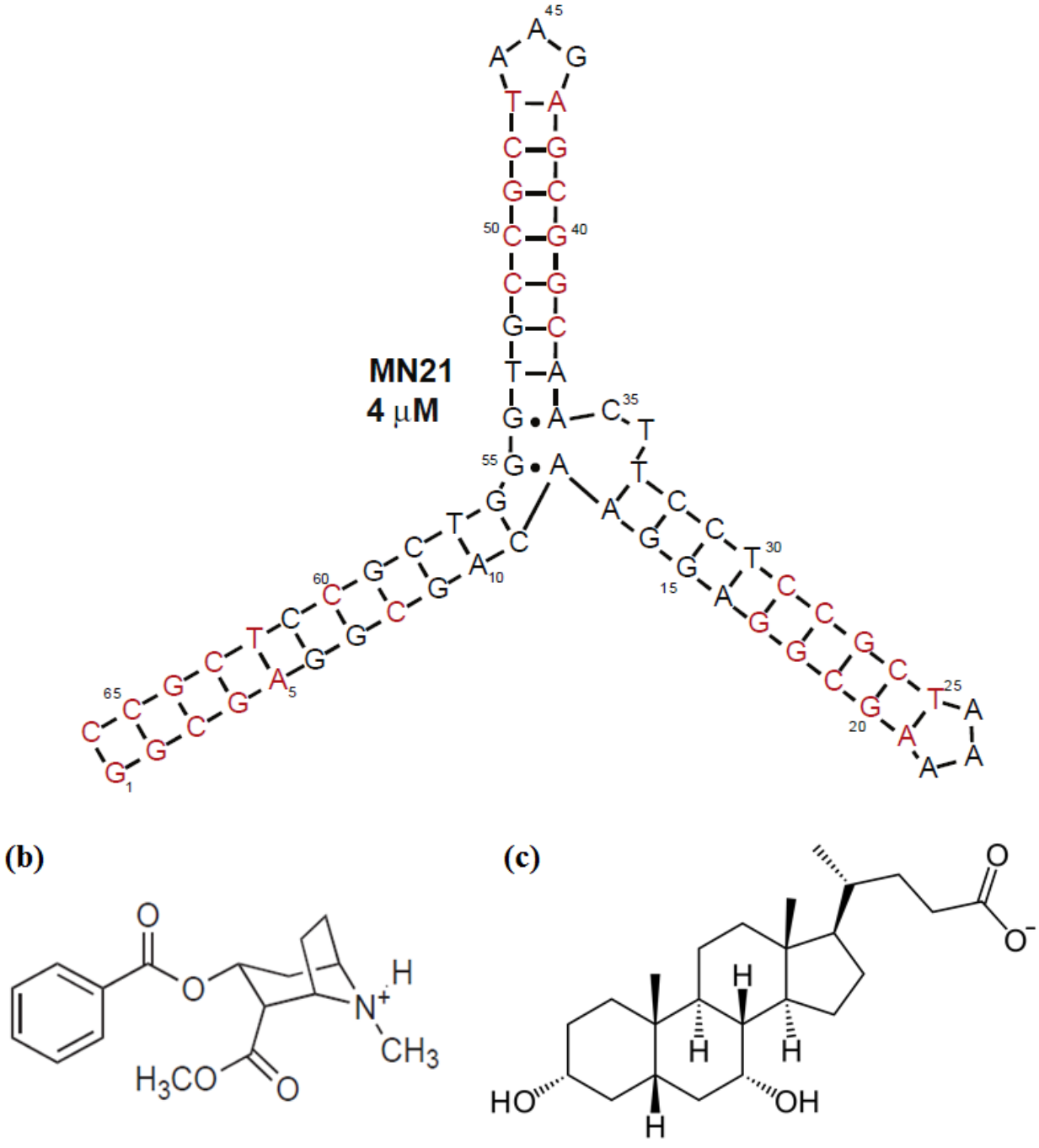

Figure 3.3 (pgs. 54 – 57): (a) Sequence and secondary structures of the different cocaine-binding aptamer constructs analyzed. Nucleotides that are altered compared to MN1 are coloured red. The cocaine binding affinity determined for each construct is indicated under the name. K_d values are provided for each construct. Error in the reported K_d values is indicated in Table 3.3. nbd denotes no binding detected. vwb indicates very weak binding detected, but was not quantifiable. (b) cocaine molecule and (c) deoxycholate molecule as expected at pH 7.4

Table 3.3: The binding affinity and thermodynamic binding parameters of ligand binding by cocaine aptamer constructs as determined by isothermal titration calorimetry.[a]			
Aptamer	**K_d**	**ΔH (kcal mol^{-1})**	**−TΔS (kcal mol^{-1})**
MN1b	9.15 ± 0.09	−28.1 ± 0.7	21.1 ± 0.7
WC	204 ± 6	−12.5 ± 0.9	7.6 ± 0.9
S1S2	nbd[d]	-	-
SS3	nbd[c]	-	-
MN2	nbd[c]	-	-
MN3	14 ± 4	−13.84 ± 0.01	7.3 ± 0.2
MN4[b]	7 ± 1	−14.5 ± 0.4	7.6 ± 0.5
MN5[e]	42 ± 4	−8.5 ± 0.4	2.6 ± 0.4
MN6[b,e]	45.3 ± 0.5	−22 ± 2	16 ± 2
MN7[e]	55 ± 1	−9.9 ± 0.2	4.2 ± 0.2
MN8	8.6 ± 0.2	−13.4 ± 0.5	6.6 ± 0.5
MN9[e]	193 ± 1	−5.23 ± 0.01	0.25 ± 0.02
MN10[e]	148 ± 9	−15.6 ± 0.9	10.5 ± 0.9
MN11[e]	123 ± 22	−12.8 ± 0.2	7.46 ± 0.01
MN12	nbd[c]	-	-
MN13[e]	211 ± 25	−6.7 ± 0.4	1.8 ± 0.4
MN14[e]	31 ± 5	−5.4 ± 0.3	0.6 ± 0.2
MN15	vwb[d]	-	-
MN16	vwb[d]	-	-
MN17[e]	59 ± 13	−8.7 ± 0.2	3.0 ± 0.3
MN18	nbd[c]	-	-
MN19[b]	26.7 ± 0.7	−23.9 ± 0.9	17.7 ± 0.9
MN20	13 ± 7	−16 ± 2	10 ± 2
MN21	4 ± 1	−20.1 ± 1	12 ± 1

[a]Data acquired at 20 °C in 20 mM Tris (pH 7.4), 140 mM NaCl and 5 mM KCl (Buffer A). The values reported are averages of 2–4 individual experiments. The error range reported is one standard deviation.

[b]These data are from Neves et al.[131]

[c]nbd indicates no binding was detected even under low c ITC conditions.

[d]Binding detected but data could not be fit. Very weak binding, on the order of millimolar, is estimated.

[e]Data fit under low c conditions and n was restrained to be 1.

Finally, the cocaine binding ability of an aptamer in which all three stems have been lengthened by five base pairs (MN21) was measured (Figure 3.3). This aptamer has the tightest affinity for cocaine of any aptamer variant studied to date, having a K_d of (4 ± 1) μM in standard buffer conditions (Table 3.3).

3.2.3 NMR Analysis of Aptamer Sequence and Ligand Binding

From the NMR imino proton chemical shift perturbations measured upon cocaine binding it was observed that G31 and T32 experienced the greatest change in chemical shift with ligand binding (Figure 3.4).[131] Compensatory mutations at these positions in the MN4 sequence were analyzed to test the importance of these nucleotides for ligand recognition. In MN13, the G31/C6 base pair was switched to be C31/G6. In this construct weak binding was maintained at (211 ± 25) μM, 30 fold weaker than MN4. This indicates that the spatial positioning of the G and C nucleotides in the G31/C6 base pair is important to maintain high-affinity binding. For MN14 the T32/A5 base pair was inverted to A32/T5. In this construct, fairly tight binding was maintained at (31 ± 5) μM, yet this binding is still over 4 fold weaker than observed for MN4.

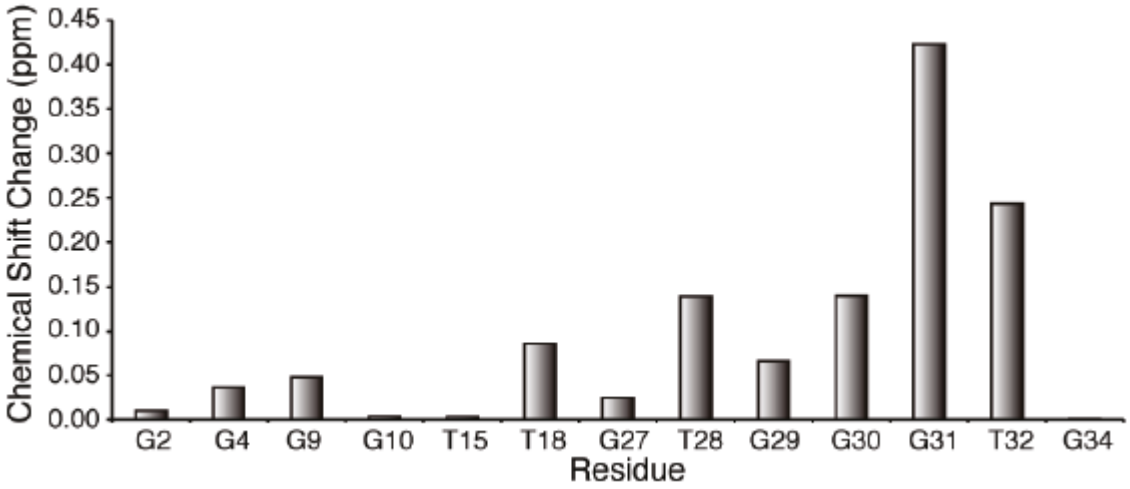

Figure 3.4: Chemical shift perturbations for cocaine binding by MN4. Nucleotides displaying greater changes in chemical shift are hypothesized to be of higher importance for binding.[131]

From the chemical shift perturbation data, the imino proton of T18 showed little change with ligand binding indicating it may be away from the site of cocaine binding. This was tested in construct MN20 where both AT base pairs in stem 2 were changed to GC base pairs. Additionally, this construct had a shortened stem 1 and the AT base pair adjacent to the triloop in stem 3

changed to GC as in MN19. MN20 binds cocaine with a K_d of (13 ± 7) μM, roughly twice as tight as MN19, from which it was based. As MN20 has a short stem 1, NMR methods were applied to see if it undergoes a structural with ligand binding. The 1D ^{1}H-NMR of MN20 in the absence of cocaine shows 5–6 peaks. This indicates that this aptamer is not fully folded in the free state. In the bound form, there are the expected 12 imino peaks from the folded aptamer with three stem loops showing that ligand-induced folding occurs with MN20 (Figure 3.5).

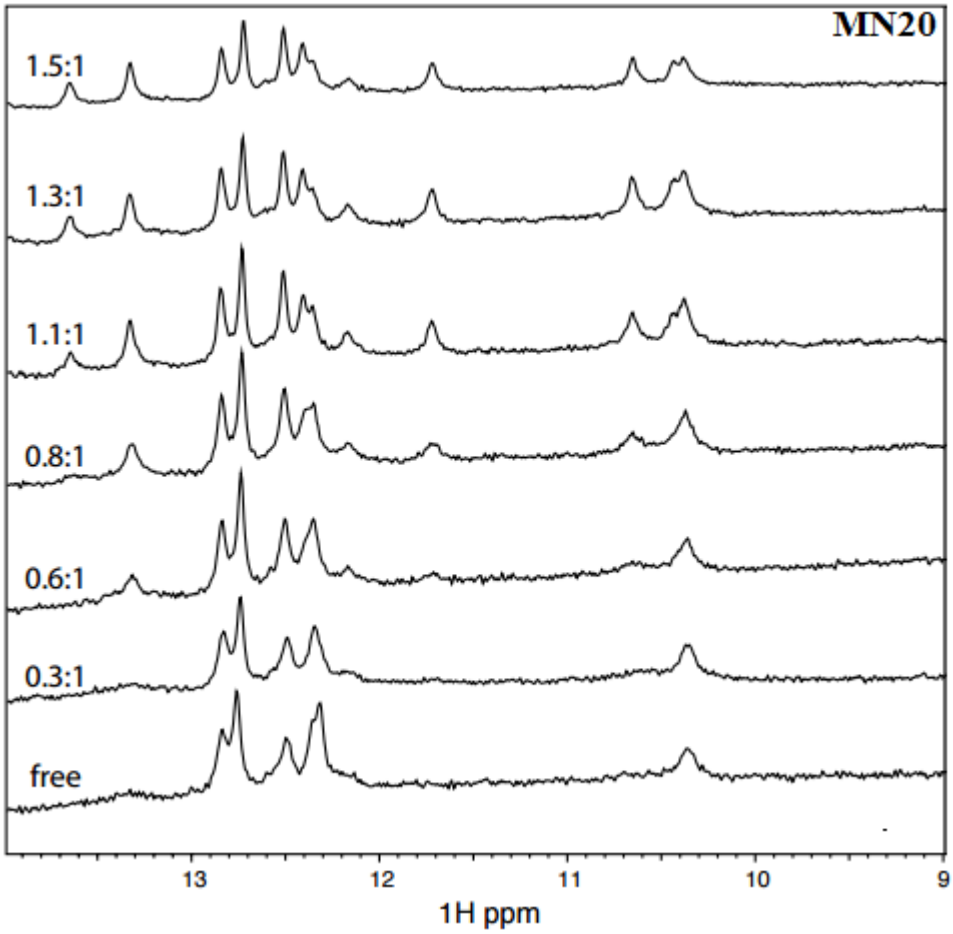

Figure 3.5: Cocaine-binding by the MN20 aptamer monitored by 1D ^{1}H-NMR. Shown is the region of the NMR spectrum focusing on the imino resonances as a function of increasing cocaine concentration. Spectra were acquired in 90% H_2O/10% D_2O at 5 °C. The molar ratios of cocaine:aptamer are indicated.

3.2.4 Sequence Requirements for Steroid Binding

ITC was used to analyze the ability of the WC aptamer and a series of sequence variants (MN6, MN9, MN10, MN11; Figure 3.3, MS1 and MS2; Figure 3.7) to bind DCA (Figure 3.3). Sample ITC binding data is shown in Figure 3.6.

Table 3.4. Thermodynamic parameters and dissociation constants of DCA binding for selected aptamers.[a]

	DCA			cocaine[b]
Aptamer	**K_d (μM)**	**ΔH (kcal mol^{-1})**	**−TΔS (kcal mol^{-1})**	**K_d (μM)**
WC	16 ± 3	−7 ± 1	0.7 ± 1.3	204 ± 6
MN6	nbd	-	-	45.3 ± 0.5
MN8	nbd	-	-	8.6 ± 0.2
MN9	12.2 ± 0.8	-3.7 ± 0.3	2.8 ± 0.1	193 ± 1
MN10	18.6 ± 0.1	−8.4 ± 0.8	2.1 ± 0.8	148 ± 1
MN11	15 ± 0.8	−5.2 ± 0.8	1.2 ± 0.8	123 ± 22
rWC	nbd	-	-	nd
MS1	nbd	-	-	nd
MS2	25 ± 3	−16 ± 1	10 ± 1	nd

[a]Data acquired in Buffer A. Data for WC, MS1, and MS2 were acquired at 15 °C; all others were acquired at 20 °C. The values reported are averages of 2−4 individual experiments. The error range reported is one standard deviation. Nbd indicates no binding detected. nd indicates that binding for that combination was not measured. [b]The corresponding data for cocaine binding are included for comparison.[157]

The affinity and thermodynamic parameters of DCA binding for these constructs are summarized in Table 3.4. The corresponding affinity data for cocaine binding is included in Table 3.4 for comparison. From this binding data there exists a trend where constructs with a cytosine corresponding to position 21 of the WC aptamer, and its equivalent position in other constructs (MN9, MN10, MN11), bind DCA with a K_d of 12 − 19 μM. These same aptamers only weakly bind cocaine. Constructs with an adenine in this position, corresponding to position 21 of WC, are able to bind cocaine but do not bind DCA. Sequence changes outside of the vicinity of the tandem GA mismatch in the aptamer have little impact on ligand binding. The WC, MN9, MN10, and

MN11 constructs contain different combinations of the GT and GA non-Watson−Crick base pairs observed in the originally selected cocaine-binding aptamer.[111] All these aptamers show similar affinity for DCA and uniformly weak affinity for cocaine. We analyzed the importance of the presence of both GA mismatches for DCA binding using the aptamer rWC. In this aptamer, both GA mismatches were changed to GC base pairs. No binding to either DCA or cocaine was observed for this aptamer. Together, these data indicate that the determinants for ligand selectivity lie at the tandem GA mismatch at the three-way junction.

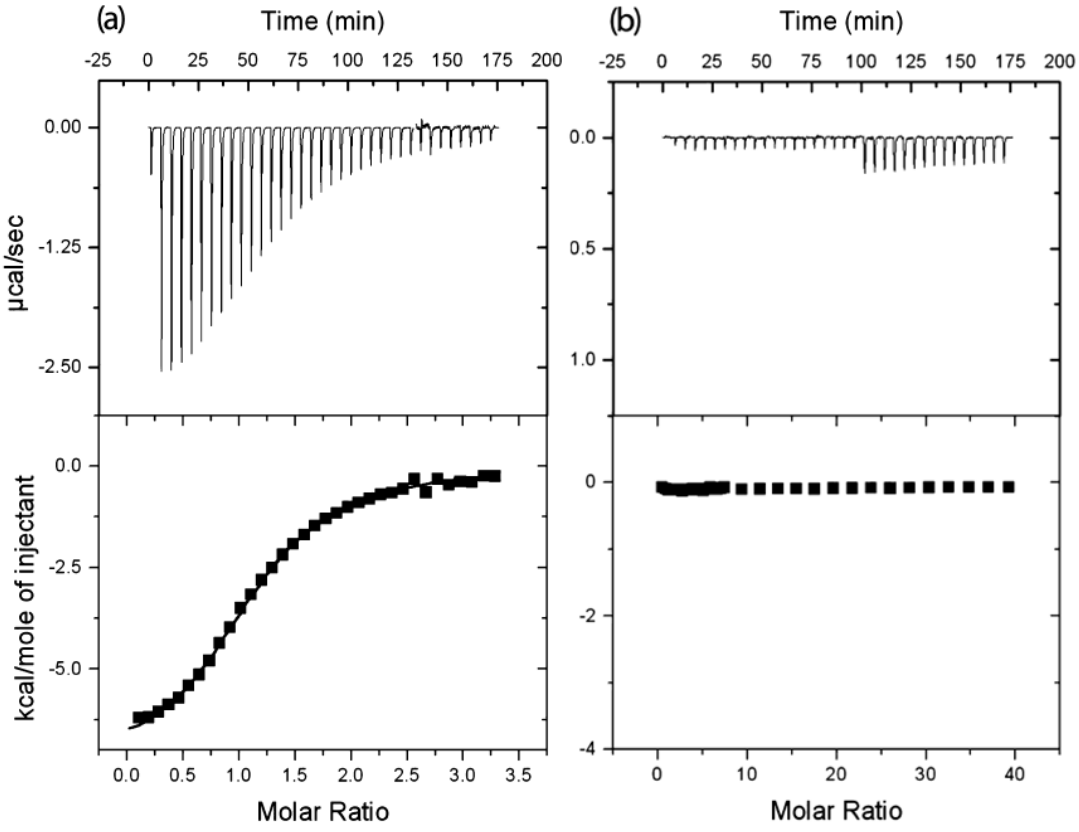

Figure 3.6: Sample of ITC data showing the interaction of the (a) WC and (b) MN6 aptamers with DCA. In (a) the WC aptamer binds DCA with a K_d value of (16 ± 3) µM while in (b) binding is not detected between MN6 and DCA. (top) Raw titration data showing the heat resulting from each injection of DCA into an aptamer solution. (bottom) Integrated heats after correcting for the heat of dilution. Binding experiments were performed at 20 °C in Buffer A.

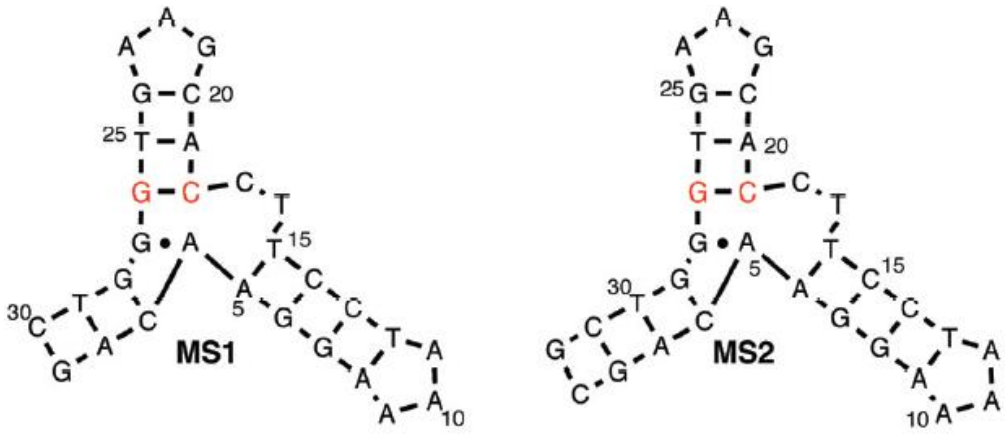

Figure 3.7: (a) Sequence of MS1 and MS2 aptamers. The GC base pair that is important for ligand discrimination between cocaine and DCA binding is shown in red.

3.2.5 Effect of Ionic Strength on DCA Binding

At a pH value of 7.4, the standard condition used in binding studies reported here, DCA is expected to be negatively charged due to the presence of the carboxylate group (Figure 3.3). The effect of this negative charge on ligand binding was studied by measuring the affinity and thermodynamics of DCA binding as a function of NaCl concentration. The DCA-binding parameters for the WC aptamer at NaCl concentrations of 0, 140, and 1000 mM are summarized in Table 3.5. The tightest binding is observed in 140 mM NaCl.

At concentrations of NaCl above or below 140 mM, binding affinity is reduced. Binding remains enthalpically driven with unfavorable entropy of binding under all conditions.

Table 3.5. Dissociation constant and thermodynamics of DCA binding by the WC aptamer as a function of NaCl concentration.[a]

[NaCl] (mM)	K_d (μM)	ΔH (kcal mol^{-1})	−TΔS (kcal mol^{-1})
0	68 ± 2	−9.0 ± 0.7	3.5 ± 0.7
140	16 ± 3	−7 ± 1	0.7 ± 1.3
1000	46 ± 5	−8 ± 1	2 ± 1

[a]Data acquired at 15 °C in Buffer A. The values reported are averages of 2−4 experiments. The error range reported is one standard deviation.

3.2.6 Engineering of a Structure Switching Mechanism in a DCA-Binding Aptamer

Cocaine-binding aptamer variants with three base pairs in stem 1 exhibit a ligand induced folding mechanism (Figure 2.12).[131,157] A DCA-binding aptamer was designed which undergoes a similar unfolded to folded secondary structure transition upon ligand binding. First tested was a WC aptamer variant with stem 1 truncated to 3 base pairs (MS1; Figure 3.7). No DCA binding was detected by either ITC or NMR methods upon the addition of the ligand (Table 3.4). 1D ^{1}H-NMR spectra of MS1 indicate this sequence is unfolded in both the absence and presence of DCA (Figure 3.8).

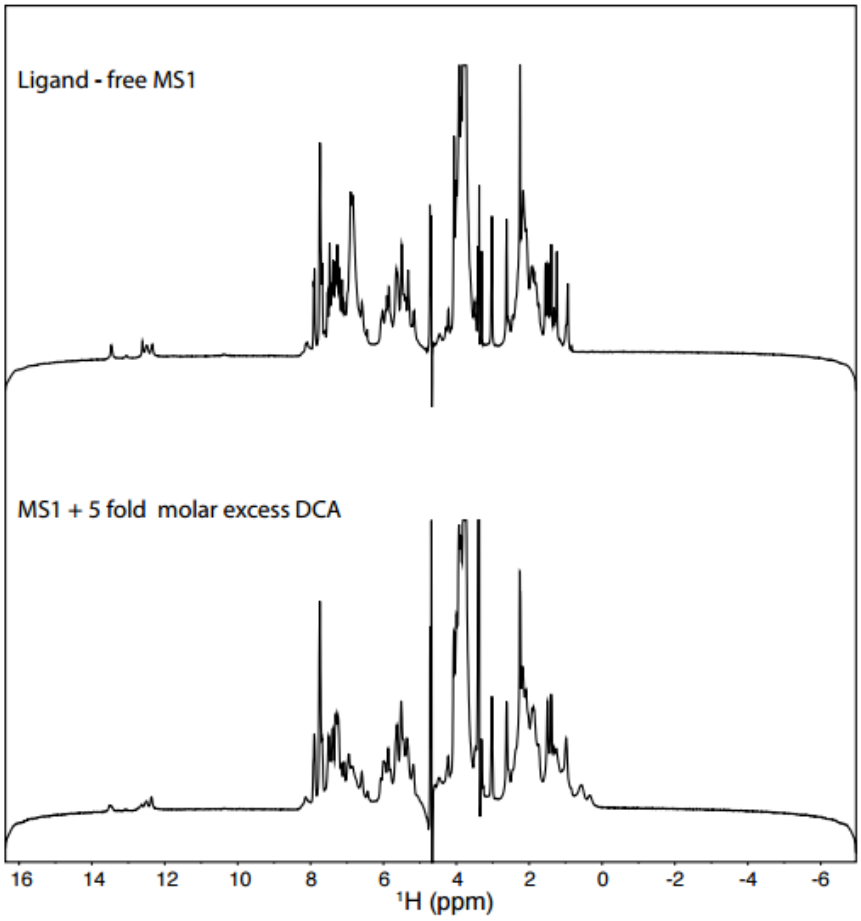

Figure 3.8: 1D ^{1}H-NMR spectra of aptamer MS1 in the absence and presence of a 5 fold molar excess of DCA. Resonances become broadened in the presence of DCA but do not change chemical shift and no new peaks (aside from those of DCA) appear. Together, this indicates MS1 does not bind DCA. Data were acquired in 90% H_2O/10% D_2O.

MS1 was then lengthened by one base pair, making it four base pairs long (MS2; Figure 3.7). The resulting MS2 aptamer binds DCA with a K_d of (25 ± 3) μM (Table 3.4). NMR spectroscopy was again applied to check the extent of secondary structure formation in free and bound MS2 as a function of increasing DCA concentration (Figure 3.9). For free MS2, 4 peaks in the imino region are detected by 1D ^{1}H-NMR. These peaks are assigned to the stem 3 nucleotides G27, T28, G29, and G30 (Figure 3.10). Upon addition of DCA, there is a significant change in the imino region as numerous additional peaks appear. The appearance of 6 − 8 additional dispersed peaks indicates the formation of additional secondary structure elements upon ligand binding. Of particular note is the presence of the upfield imino at 10.4 ppm, indicating the presence of a sheared GA base pair in the aptamer.[131] Addition of DCA to WC results in a number of resonances changing chemical shift when ligand binding occurs, but the same number of peaks are observed in the DCA-bound WC aptamer as in the free aptamer.

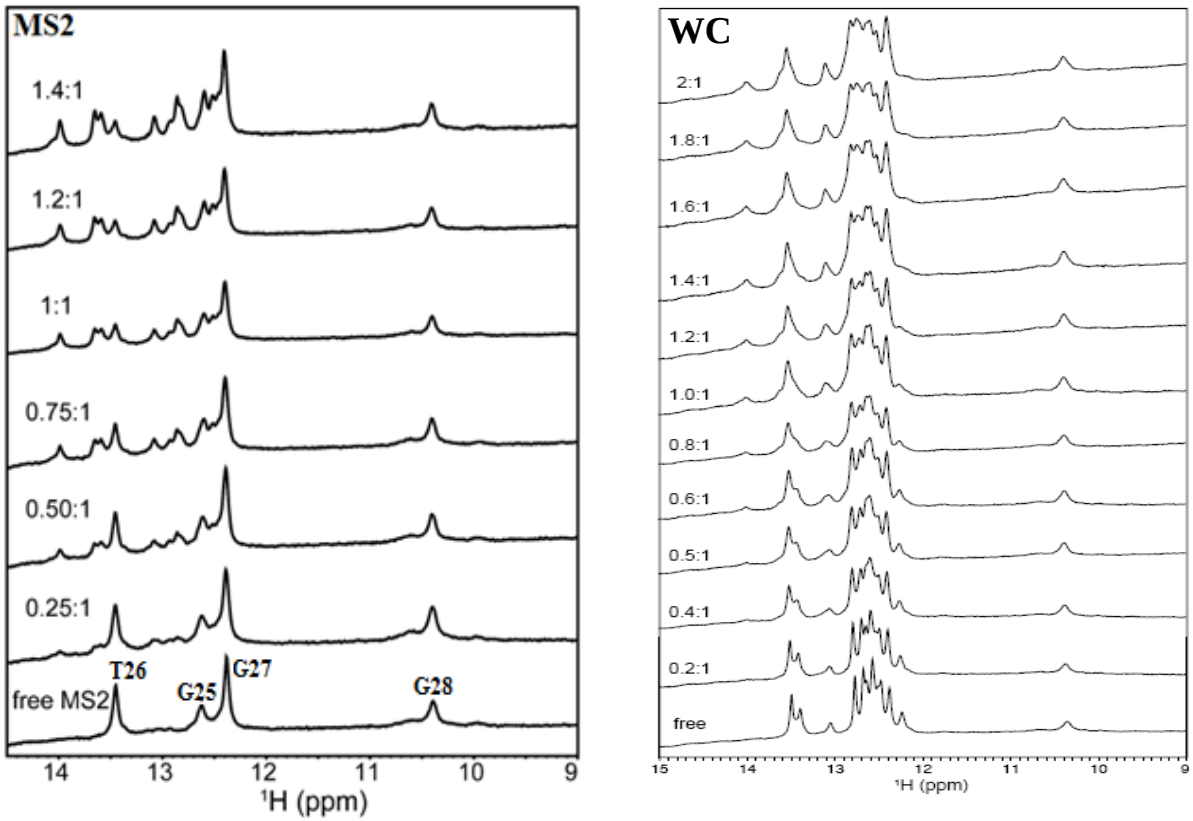

Figure 3.9: Binding of DCA by the MS2 aptamer (left) and the WC aptamer (right), demonstrated by 1D 1H-NMR. Shown is the region of the NMR spectrum focusing on the imino resonances as a function of increasing DCA concentration. Spectra were acquired in 90% H_2O/10% D_2O at 5 °C. The molar ratios of DCA:aptamer are indicated

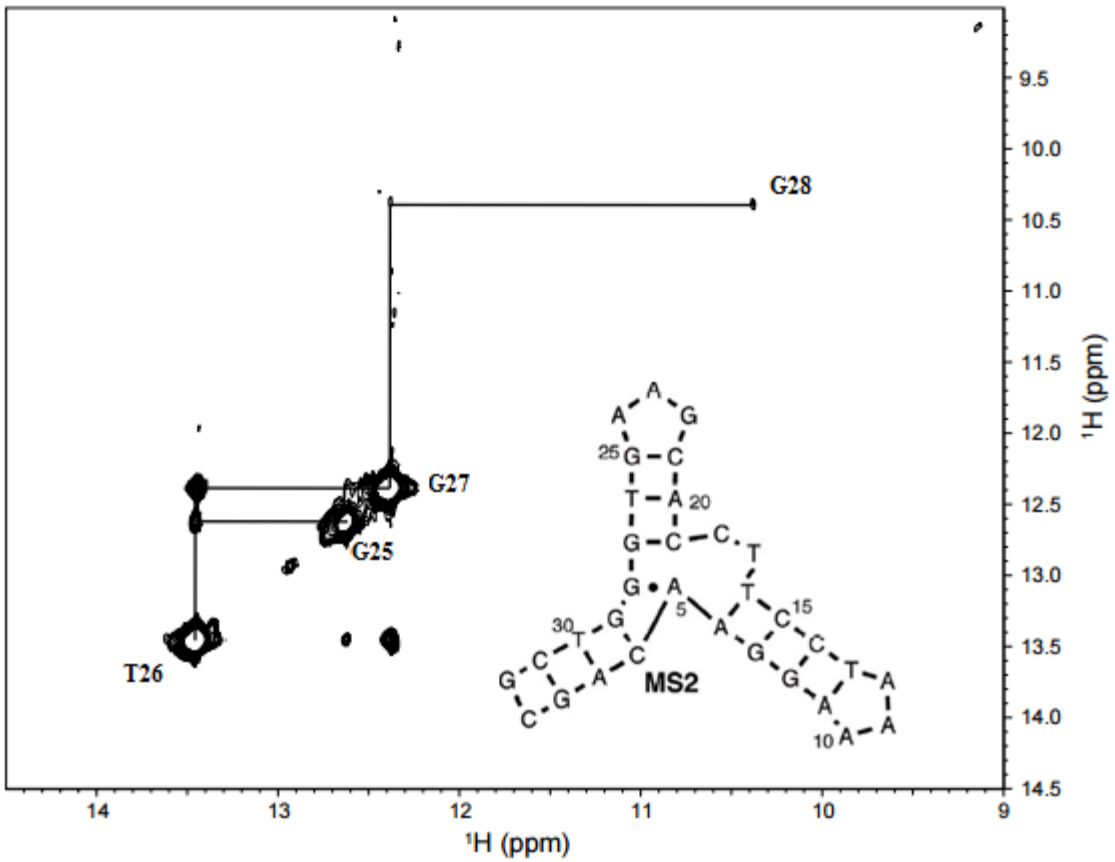

Figure 3.10: Imino-imino region of the 2D NOESY (τm=200 ms) of unbound MS2 recorded at 5 °C. Assignments are labeled in the spectrum. For consistency, nucleotide numbering is consistent with that used for the WC aptamer.

3.2.7 Change in Heat Capacity with Steroid Binding

To gain further insight into the DCA binding mechanism and make comparisons with the cocaine binding mechanism, ITC methods were applied to measure the change in heat capacity of both WC and MS2 aptamers with DCA binding (Figure 3.11). WC and MS2 both had binding data (Table 3.6) obtained at temperatures between 5 and 15 °C to determine ΔC_p. Data acquired at higher temperatures was excluded from the calculation of ΔC_p as the aptamers become thermally destabilized but is included in Table 3.6 for reference. Using NMR, thermal stability of the MS2-DCA complex was estimated to be approximately 20 °C (Figure 3.12). In the plot of enthalpy versus temperature, the measured enthalpy for MS2 reflects both folding and binding events. A fit of these data for MS2 yields a ΔC_p value of (−753 ± 200) cal mol^{-1} K^{-1} for DCA binding. For WC, a fit of the enthalpy data yields a ΔC_p value of (−94 ± 75) cal mol^{-1} K^{-1}.

Table 3.6: The binding affinity and thermodynamic binding parameters of ligand binding by steroid-binding aptamer constructs as determined by isothermal titration calorimetry.[a]				
Aptamer	**Temperature (°C)**	**K_d (μM)**	**ΔH (kcal mol^{-1})**	**−TΔS (kcal mol^{-1})**
WC	5.017	12.2 ± 0.4	-7.3 ± 0.2	1.0 ± 0.2
	10.099	11.5 ± 0.8	-7.1 ± 0.7	0.7 ± 0.7
	12.673	12.2 ± 2.1	-8.8 ± 0.1	2.3 ± 0.2
	15.012	13.3 ± 0.3	-7.8 ± 1.0	1.3 ± 1.0
	17.521	53.5 ± 2.1	-20.7 ± 0.7	15 ± 0.7
MS2	7.556	17.4 ± 0.4	-10.2 ± 1.1	4.1 ± 1.0
	10.022	16.6 ± 1.6	-14.5 ± 1.6	8.3 ± 1.5
	12.512[b]	20.2 ± 0.5	-14.5 ± 0.1	8.3 ± 0.8
	15.012	25.1 ± 2.9	-16.4 ± 1.3	10.4 ± 1.2

[a]Data acquired in Buffer A at the temperatures indicated. The values reported are averages of 2−3 experiments. The error range reported is one standard deviation.

[b]Data provided at this temperature is for a single experiment and corresponding error values are the standard measurement of error (data fit).

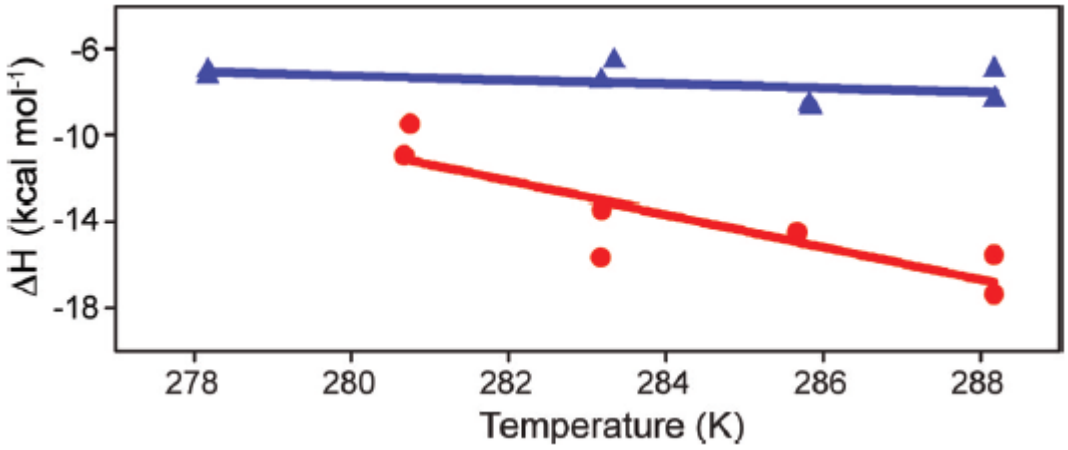

Figure 3.11: Temperature dependence of the enthalpy of DCA binding for the WC (blue) and MS2 (red) aptamers derived by ITC. The data values are shown while the fit of the data is represented by the solid line. For both aptamers only the low-temperature region where effects of bound aptamer unfolding do not contribute to the enthalpy were used in the fit. ΔC_p for WC: (−94 ± 75) cal mol^{-1} K^{-1}. ΔC_p for MS2: (−753 ± 200) cal mol^{-1} K^{-1}.

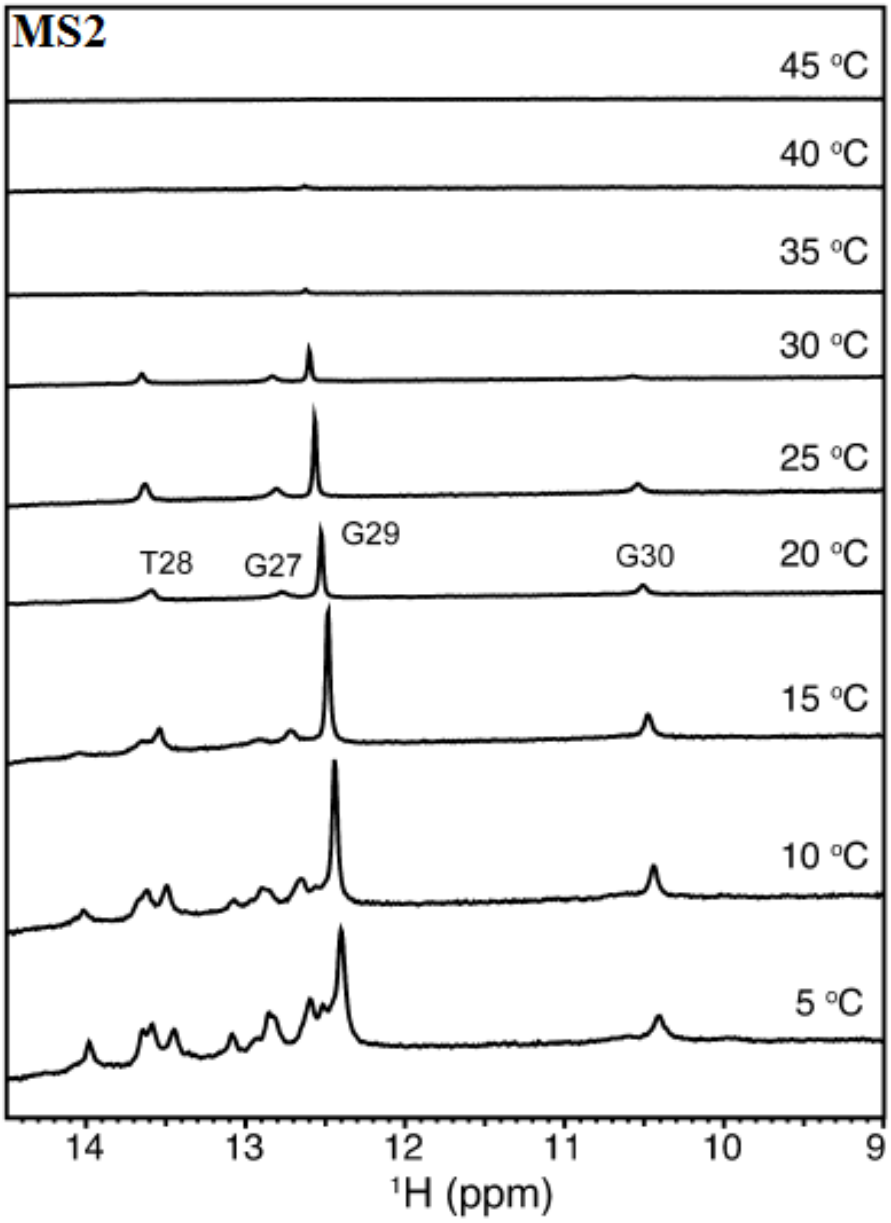

Figure 3.12: Thermal stability of the DCA-MS2 complex assayed by 1D ^{1}H-NMR. Shown is the region of the NMR spectrum focusing on the imino resonances as a function of increasing temperature from 5 to 45 °C. Spectra were acquired in 90% H_2O/10% D_2O.

3.3 Discussion

3.3.1 Buffer Composition and Impact on Ligand Binding

The cocaine-binding aptamer and cocaine contain titrateable groups (Figure 3.3). In order to see what effect protonation of these groups may have on cocaine binding, the MN1 aptamer was analyzed by measuring the binding thermodynamics as a function of pH. The optimal pH value for binding is 7.4. Below this value, binding affinity is slightly decreased. This decrease may result from the change in the buffer used. Above pH 7.4, binding is more significantly decreased. Cocaine is a secondary amine and has an experimentally determined pK_a value of 8.6 and a calculated pK_a value of 8.01 to 9.00 depending on the prediction method used.[163] The decreased binding affinity at pH 9.2 is consistent with deprotonation of the cocaine resulting in a lower affinity and suggests that cocaine needs to be positively charged in order to take advantage of ionic interactions to obtain maximum affinity. The lack of observable binding at pH 9.6 likely results from a combination of having a fully deprotonated cocaine ligand and also potential deprotonation of the guanine imino proton with a pK_a value of 9.2. Changing the protonation of the guanines will almost certainly have a very disruptive effect on the structure of the aptamer.

Having cocaine protonated suggests that ionic interactions are involved in the cocaine binding mechanism. This interaction may involve the negative phosphate backbone of the DNA interacting with the positive charge on cocaine. The importance of ionic interactions was tested by measuring binding affinity as a function of NaCl concentration. Binding affinity decreases as NaCl concentration increases for both aptamers studied. A 22 and 117 fold reduction in affinity was observed between conditions of 0 and 500 mM NaCl, for MN1 and MN4 respectively. This reduced affinity indicates that charge-dependant interactions are important for achieving tight binding as added NaCl should shield ionic interactions and weaken binding. However, as binding still occurs at high NaCl concentrations, cocaine binding by these aptamers is not entirely driven by ionic interactions. Also noted is that the tightest binding was achieved at pH 7.4, the pH at which the aptamer was originally selected.[111] Additionally, binding was tightest with no NaCl present. This is a little surprising as the aptamer was selected at a NaCl concentration of 140 mM and aptamer binding is often thought to be tightest under the same conditions as selection occurs. For other aptamers where ionic interactions are thought to occur, binding conditions of lower

NaCl concentration than originally used for selection should be tested if an increased affinity for the target is desired.

The DCA binding mechanism of the WC aptamer was also analyzed by measuring the affinity of ligand binding as a function of NaCl concentration. Under the experimental conditions applied, both the aptamer and the DCA ligand are negatively charged. The affinity of the aptamer for DCA is reduced at NaCl concentrations of 0 and 1 M compared to 140 mM NaCl. This finding is in contrast to cocaine binding where the affinity is tightest at 0 M NaCl and indicates that for the WC aptamer, electrostatic interactions do not play a positive role in DCA binding as would be expected from ligands carrying the same charge as DNA.

3.3.2 Importance of Stem Length and Nucleotide Identity in Ligand Binding

In order to see which regions of the aptamer and which nucleotides are important for aptamer function the binding ability of several cocaine-binding aptamer variants were analyzed, observing first the effects of changing the lengths of three stems. On an individual basis, each of the three stems can be shortened by one to three base pairs from their original length and still retain reasonable binding affinity where "reasonable" affinity as not more than ~10 fold weaker than the binding affinity observed for MN1. Simultaneous stem length reduction, as in MN18, resulted in the combined loss of binding affinity which, could no longer be measured. These data show that in order to retain high affinity binding, the stem length needs to be maintained at the length of the originally selected aptamer.

A construct where the length of each of the stems is increased by five new base pairs (MN21) was also tested. This change doubles the length of each of the stems. Chapter 2 outlined the subtle structural changes in MN4 that occurred with ligand binding and that binding is accompanied by a more negative ΔC_p than predicted to occur based solely on ligand burial.[131] This suggested a binding mechanism in which tertiary structural changes occur for MN4, and the packing of the three helices provides a positive driving force for binding. It was reasoned that by increasing the length of the stems, larger changes in tertiary structure would occur which would serve as a

stronger driving force for binding. Consistent with this hypothesis, a 1.75 fold increase in affinity for MN21 compared to the shorter stem length MN4 was observed. Additional constructs of this nature and further increases in stem length were not tested, but a further modest increase in affinity would be expected as the length of the three stems increase.

Binding results on individual nucleotide changes in the cocaine-binding aptamer variants presented in this research is consistent with previously published data on the binding ability of cocaine-binding aptamer mutants. When adapting the cocaine-binding aptamer for use in steroid binding, numerous sequence variants of the aptamer were assayed for cocaine binding.[123,127,164] In these studies, cocaine-binding aptamer variants where the G29/A21 base pair was changed to a GC base pair, no cocaine binding was reported.[123] Within this research, a mutation disrupting the same base pair (WC, MN9, MN10, MN11) results in a greatly reduced binding affinity, 14 to 23 fold, compared to MN1. Additionally, for aptamers where double mutations were introduced that disrupted the G30/A7 base pair and altered the identity of T19, cocaine binding was eliminated.[164] Binding studies with constructs MN12 and MN16 contained similar changes and the cocaine binding ability of these aptamers was similarly eliminated or greatly reduced.

The cocaine-binding aptamer core contains a tandem arrangement of GA base pairs. In a crystal structure of a tandem GA arrangement, the mismatch caused the B-form helix to kink toward the major groove side and extensive inter-strand base stacking was observed at the GA mismatch.[147] In the cocaine-binding aptamer, the tandem GA mismatch likely imparts a conformation in the DNA structure required for cocaine binding. This is evident from mutational data obtained for the WC, MN9, MN10, MN11 constructs. When the G30/A7 base pair was disrupted (MN12) no binding was observed. Mutations in the GA base pairs likely result in a structural change in the aptamer that prevents the aptamer binding cocaine. 2D NMR experiments have shown that G30 makes direct contact with the aromatic ring of cocaine.[131] It is possible that substituting A7 for a C alters the hydrogen bonding network and as a result, the spatial positioning of nucleotides so as to prevent cocaine from having a reasonably sized binding pocket. The same reasoning could be provided for the G29/A21 base pair. However an argument against this possibility is that the imino proton of G29 experiences only a relatively small change in chemical shift with cocaine

binding. The nucleotides that change the most in chemical shift with cocaine binding are G31 and T32.

The importance of the imino of T19 is shown by the observation that it is only observable in the ligand-bound form. T19 is known to make direct contacts with cocaine.[131] It is very possible that upon ligand binding, the imino proton becomes protected from hydrogen exchange. Consistent with this proposal, in the construct MN16 where T19 is changed to an A, cocaine binding by the aptamer is eliminated. It is possible that T19 is important for structural reasons in addition to, or instead of making contact with the cocaine ligand.

The large chemical shift change with ligand binding seen in G31 is the result of direct contact with cocaine. The compensatory mutant where the G31/C6 base pair is changed to C31/G6 (MN13) results in a 30 fold decrease in binding affinity when compared to MN4. Binding of MN20 shows that changing the two AT base pairs in stem 2 to GC base pairs results in a moderate increase in affinity of the aptamer compared to MN19, on which it was based. As the imino proton chemical shift perturbation of residues in this stem are small[131] these changes were not expected to hinder binding. It was initially thought this increase in affinity resulted from an increase in stability of the free aptamer, but the temperature at which the last imino is visible in a 1D ^{1}H-NMR spectrum is unchanged from MN19 to MN20 (Figure 3.13).

It is possible that the affinity increase is derived from an increase in the amount of secondary structure of the unbound state of MN20 compared to that of MN19. Consistent with this, there are more imino protons present in the free form of MN20 compared to MN19. Additionally, the enthalpy of binding is lower for MN20 compared to MN19 (Table 3.3) possibly due to fewer hydrogen bonds forming upon folding. This is offset by lower unfavorable binding entropy possibly due to a higher degree of organization in the free state. While such arguments may be valid in this case, the analysis of binding thermodynamics are complicated by hydration effects and similar arguments may not be valid in other cases.

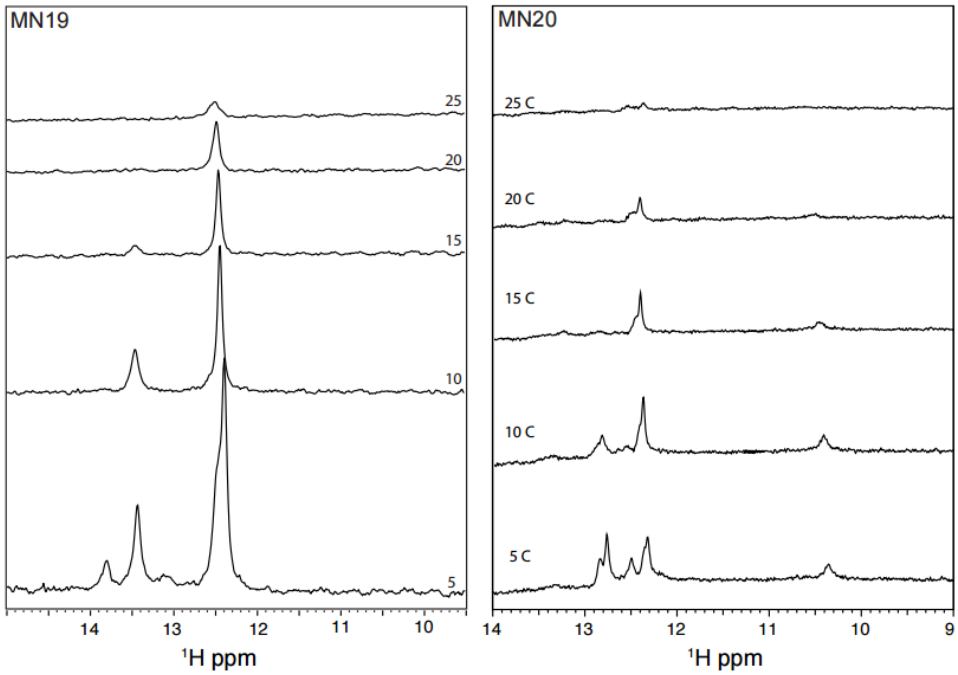

Figure 3.13: Thermal stability of the free MN19 and MN20 aptamers measured by 1D ^{1}H-NMR Shown is the region of the NMR spectrum focusing on the imino resonances as a function of increasing temperature from 5 °C to 35 °C. Spectra were acquired in Buffer A with 10% D_2O.

From a comparison of the enthalpy and entropy values with the affinity data (Table 3.3) for the different aptamers, inferences into which of these thermodynamic parameters are important or not important for binding can be made. For the tightest binding constructs, K_d < 100 μM, the enthalpy and entropy values highly vary. The enthalpy values can range from (−28.1±0.7) kcal mol^{-1} for MN1 to (−5.4 ± 0.3) kcal mol^{-1} for MN14 while the −TΔS values range from (21.1 ± 0.7) kcal mol^{-1} to (0.6 ± 0.2) kcal mol^{-1} for MN1 and MN14, respectively. In contrast, for the constructs that bind cocaine the weakest, K_d > 100 μM, there is not as large of a variation in enthalpy and entropy values. For the weakly binding aptamers, the enthalpy values are not among the most exothermic observed for these aptamers and range from (−15.6 ± 0.9) kcal mol^{-1} to (−5.23 ± 0.01) kcal mol^{-1} for MN10 and MN9, respectively. The corresponding values of −TΔS do not include the most unfavorable values and range from (10.5 ± 0.9) kcal mol^{-1} to (0.25 ± 0.02) kcal mol^{-1} for MN10 and MN9, respectively.

As shown in Table 3.3, binding data for many of the constructs were acquired under low c conditions. When fitting these data to determine the affinity and binding enthalpy, binding stoichiometry (n) had to be fixed the 1.[165] While we include the enthalpy values here we will note that the optimal method to determine ΔH° recommended by Tellinghuisen involves repeating binding at a variety of temperatures and obtaining ΔH° from a van't Hoff analysis. Using this n value is valid for two reasons: 1) data not acquired under low c conditions had fits with n values very close to 1. There are some outliers such as for MN21 where n was determined to be 0.4. These low n values likely result from an inaccurate determination of the aptamer concentration using the calculated extinction coefficient rather than not being a true 1:1 binding ratio. 2) The 1:1 binding ratio for the aptamer-cocaine complex agrees with the NMR data where only one binding site is observed and there are no chemical shift perturbations above a 1:1 molar ratio. Additionally, in a cocaine titration monitored by 2D TOCSY experiments, there was no evidence for multiple binding events. For the H5–H6 correlations that move with ligand binding the resonances move in a straight line as expected for a 1:1 binding ratio. Research on multisite binding, such as the 2:1 ligand:RNA ratio observed for paromomycin binding to a RNA molecule containing a CC mismatch show distinctly curved trajectories for the H5–H6 correlations as ligand was titrated into the RNA and multiple binding sites were populated.[166]

The sequence requirement for the change of binding specificity from cocaine to DCA is the single nucleotide substitution which converts the G29/A21 base pair to a GC. (Figure 3.3, Table 3.4). The identity of the two GA base pairs is critical to retain high affinity cocaine binding.[123,164] As a tandem GA arrangement in a DNA helix is known to distort the helix,[147] it is likely that the disruption of the structure formed by the tandem GA base pairs results in loss of cocaine-binding and conveys DCA-binding ability. Verifying this possible change in structure could be addressed in future studies by employing methods such as SAXS or fluorescence spectroscopy where a 2-aminopurine replaces an adenine to compare a tandem GA-containing aptamer with a WC-type single GA mismatch aptamer. The WC, MN9, MN10, and MN11 constructs all bind DCA within a 2-fold range of affinity (Table 3.4). This demonstrates that nucleotide changes away from the three-way junction have little effect on DCA binding. In a similar manner, changes outside the three-way junction do not affect cocaine binding.[131,157] We also tested the necessity of the presence of a GA base pair for DCA binding through the use of the rWC construct (Figure 3.3). In

this molecule, both GA base pairs were changed to GC base pairs, resulting in elimination of DCA binding ability. This finding shows that the presence of a GA base pair is necessary for DCA binding. The sequence requirements to produce a DCA-binding aptamer presented here are consistent with earlier studies that first identified DCA binding by a modified cocaine-binding aptamer with a fluorophore reporter at the three-way junction.[123,164]

3.3.3 Engineering of a Steroid-Induced Structure Switching Mechanism

A ligand-induced structural switching binding mechanism was engineered in the steroid-binding aptamer MS2. Stem 1 in MS2 is shortened to contain four base pairs, resulting in an aptamer that has secondary structure formed in only stem 3 in the unbound state. Upon addition of DCA, numerous well-dispersed resonances appear, indicating the folding of the aptamer into the predicted secondary structure (Figure 3.5). The steroid-binding aptamer likely contains the same secondary structural elements seen previously in the cocaine-binding aptamer, indicating that this DNA framework of three stems arranged around a three-way junction appears to be a versatile architecture for ligand binding, and shortening of stem 1 enables the engineering of a structural switching mechanism in a predictable manner.

One difference between the MS2 DCA-binding aptamer and the previously studied MN6 and MN19 cocaine-binding aptamers is that for MN6 and MN19, stem 1 contains three base pairs while for MS2, four base pairs are needed to produce an aptamer that is functional. This suggests that cocaine binding has a greater stabilizing effect than DCA binding. Temperature-dependent NMR experiments demonstrate that, in comparison to cocaine-bound MN6 and MN19, DCA-bound MS2 is less thermally stable. The last of the well dispersed imino protons that appear in MS2 due to ligand binding are visible at 10 °C, compared to 15 °C for MN6 and MN19.[131] This lower stability exists despite stem 1 having four base pairs in MS2 while MN6 and MN19 have 3 base pairs in their stem 1. While the disappearance of the imino signals can be due to either the unfolding of the aptamer or an increase in the hydrogen exchange rate as the temperature increases, it is clear that DCA binding does not have as much of a stabilizing effect on the MS2 aptamer as cocaine binding has for MN6 and MN19.

3.3.4 Steroid-Binding vs. Cocaine-Binding Mechanisms

NMR and ITC data indicate a high degree of similarity between the DCA binding mechanisms and the cocaine binding mechanisms described previously. The ^{1}H-NMR spectrum shows that for MS2, only stem 3 is formed in the absence of ligand (Figure 3.9), and upon binding DCA, all three stems form. This behavior is similar to what is seen with short stem 1 variants of the cocaine-binding aptamer. From thermodynamic analysis, MS2 has a much more negative ΔC_p than seen for the WC. As such, more nonpolar surface area becomes buried upon MS2 binding compared with WC binding which implies that a greater degree of structural change occurs for MS2 and constructs of this type than for constructs such as WC.[149] An additional similarity between the DCA and cocaine binding mechanisms is that for all aptamers studied, binding for both ligands is an enthalpically driven process with an unfavorable binding entropy.

3.3.5 Tertiary Structure Analysis of Ligand-Free and Ligand Bound Steroid-Binding Aptamer Constructs

Research reported here is largely the work of collaborators (noted for each subsection). Results and Figures are presented to aid in discussing the overall findings of this study, in which one aim was to understand what tertiary structure changes occur with ligand binding. This first began by considering the WC and MS2 aptamers, observing the changes in hydrodynamics of free and DCA-bound WC and MS2. Additionally, NMR and calorimetry techniques were used in order to help provide a comparison with previous findings with the cocaine-binding aptamer (Chapter 2 and Chapter 3: Section 3.2)

3.3.5.1 Hydrodynamic Analysis Using Quasi-Elastic Light Scattering

Research discussed here was conducted by Stephanie Lombardo and Gerald F. Audette. Quasi-Elastic Light Scattering (QELS) was employed in this study as it has the capability to estimate the size of particles in solution.[211] With observed differences in structural changes for short and long stem aptamer variants studied by ITC and NMR, DLS was applied to obtain further evidence for the observed ligand induced structure switching. Results of this study output a radius of hydration (R_h (z)), which was used as a standard for comparison of the free and bound aptamers. The free WC aptamer had a calculated R_h (z) of (28 ± 1) Å. For DCA bound WC, R_h (z) was calculated to

be (26 ± 1) Å (Table 3.7). It is noted that the R_h (z) of free WC is larger than that of ligand-bound WC. This data indicates a small degree of compaction with DCA binding for WC. The change is quite subtle, but this is then in agreement with data obtained through ITC and NMR which have also indicated a small degree of structural change taking place upon binding of DCA.

3.3.5.2 Analysis of the Effect of Ligand Binding on Diffusion Using Diffusion-Ordered NMR Spectroscopy

Research discussed here was conducted by Patrick Groves. In order to analyze any change in molecule shape upon DCA binding, Diffusion-Ordered NMR Spectroscopy (DOSY) experiments on the free and ligand-bound WC aptamer were performed. Within this entire study, DOSY was a useful technique because of its ability to separate NMR signals based on translational diffusion coefficients (D_t). Through DOSY, information about, but not limited to, particle size and shape can be obtained.

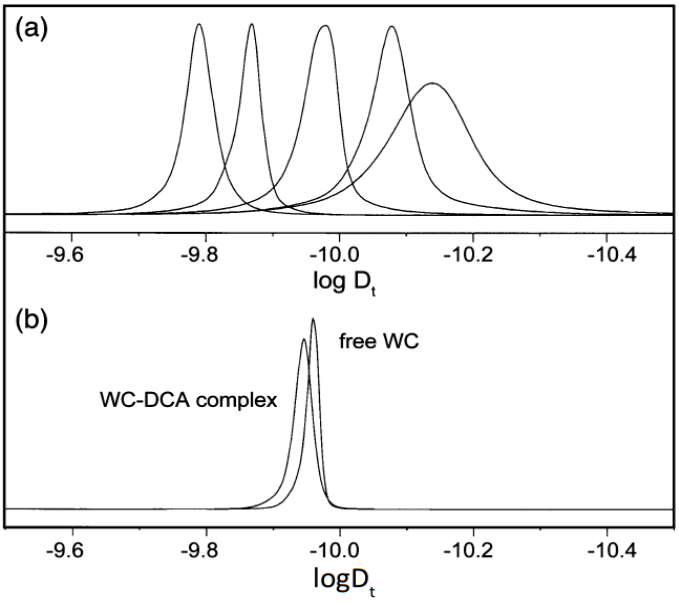

Figure 3.14: Diffusion profiles obtained from DOSY spectra for (left to right), (a) aprotinin (6.6 kDa), α-lactalbumin (14.4 kDa), carbonic anhydrase (29 kDa), ovalbumin (44 kDa), and bovine serum albumin (66 kDa). (b) Diffusion profile of free and DCA-bound WC aptamers. The diffusion coefficient of DCA-bound WC aptamer is less negative. This corresponds to a smaller effective molecular weight and smaller R_g, upon complex formation with ligand.

This observed decrease in log D_t occurs despite the molecular mass of the complex being heavier than for the free aptamer by the weight of DCA (391.6 Da). This decrease in log D_t likely reflects a small compaction in structure upon ligand binding. The radius of gyration (R_g) for the free aptamer is estimated to be 17.1 Å and that of the bound aptamer to be 16.3 Å. (Table 3.7). This decrease in R_g is indicative of compaction of the aptamer with ligand binding and is in agreement with data obtained through QELS, ITC, and NMR.

Table 3.7: Summary of the hydrodynamic data for the free and bound WC and MS2 aptamers.[a]

	SAXS[b]		DOSY	QELS
Sample	**R_g (Å)**	**R_{max} (Å)**	**R_g (Å)**	**R_h (z) (Å)**
WC_{Free}	17.4 ± 0.1	59.4	17.1	28 ± 1
WC_{bound}	17.6 ± 0.1	60.5	16.3	26 ± 1
$MS2_{Free}$	17.6 ± 0.1	61		
$MS2_{bound}$	16.7 ± 0.1	57.2		

[a]Data acquired in Buffer A.

[b]For SAXS-derived R_g values, data from the 1 in 4 dilution is presented.

3.3.5.3 Structural Analysis of DCA Binding Using SAXS

Research presented here is the work of Matthew C.J. Wilce and Simone A. Beckham. SAXS data was very valuable within this study as SAXS is a method refined at resolving information related to particle size and shape.[212] Solution SAXS was conducted on the WC and MS2 aptamers in both the absence and presence of DCA (Figure 3.16a). The R_g and R_{max} are similar for both the bound and free aptamers with a slight reduction in both R_g and R_{max} for the ligand-bound MS2 (Table 3.7). The pair distance distribution function (PDDF), P(r), was calculated using the indirect Fourier transform method (Figure 3.16b).[186] While three of the P(r) functions are essentially the same, there are noticeable differences in the profile of the P(r) function for the WC-DCA sample. Kratky analysis suggests that the WC-DCA structure changes upon binding DCA (Figure 3.16c). Kratky plots for each of the samples are indicative of a partially folded or partially flexible molecule; however, the WC-DCA Kratky plot is suggesting that upon ligand binding, WC becomes more ordered.

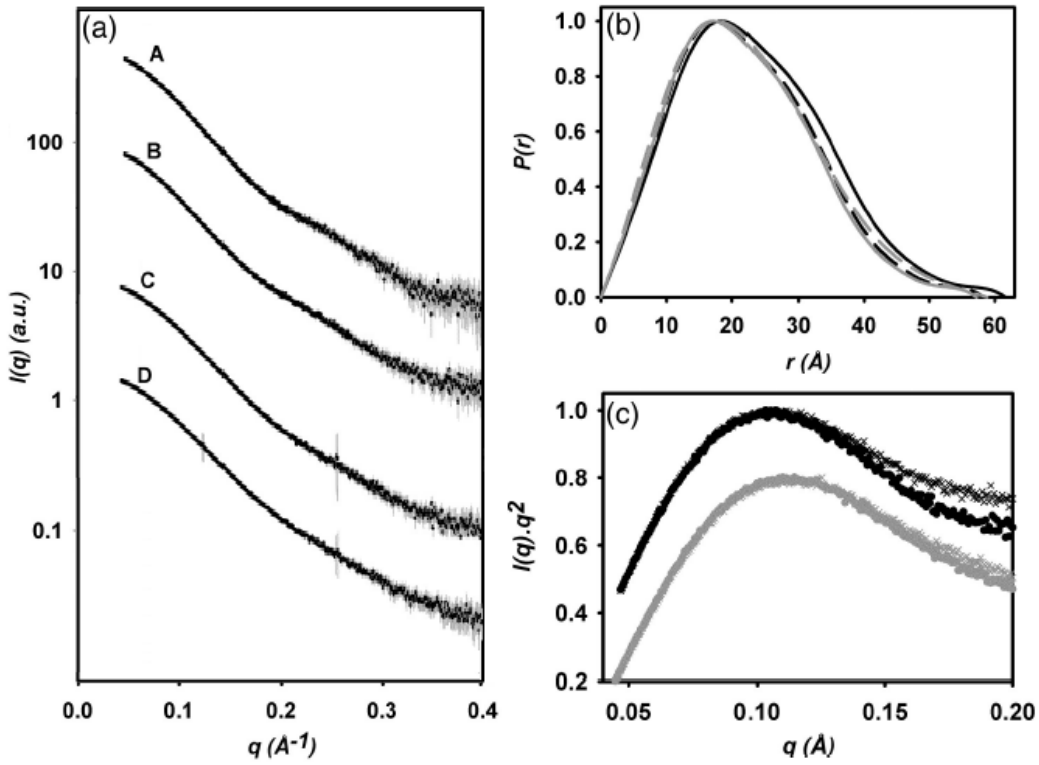

Figure 3.15: (a) SAXS data for WC and MS2 in the presence and absence of ligand. SAXS intensity profile I(q) as a function of the magnitude of the scattering vector q. Error bars indicate the mean, plus or minus one standard deviation. Line A: WC-DCA; B: free WC; C: MS2-DCA; D: free MS2. (b) Pair-distance distribution function (P(r)) for WC and MS2 SAXS data. WC-DCA: black solid line; free WC: black dashed line; MS2-DCA: gray solid line; free MS2: gray dashed line. (c) Kratky plot for WC and MS2 SAXS data. WC-DCA: black circles; free WC: black crosses; MS2-DCA: gray circles; free MS2: gray crosses.

3.3.5.4 Structural Implications of the Hydrodynamic Changes upon Steroid Binding

From the SAXS data, it is evident that no significant change in R_g was observed with DCA binding by the WC aptamer. This difference between methods may arise from small changes in the roughly flat, elongated shape of the aptamer changing the diffusion rate but still giving rise to the same R_g as measured by SAXS. Despite the lack of difference in R_g values between free and DCA-bound WC, analysis of the SAXS data using the P(r) function and the Kratky plot indicates

the presence of structural changes in the WC aptamer with DCA binding an points to the aptamer becoming more ordered upon DCA binding. Together, these results indicate little change in the overall size of the molecule with ligand binding but that structural changes do occur in the WC aptamer with DCA binding. Previously, for cocaine binding, very little secondary structure change was observed with cocaine binding by the MN4 aptamer, but tools to observe tertiary structure were unavailable. Given the similarity in NMR and ITC trends between the cocaine-binding MN4 aptamer and DCA-binding WC aptamer, it is likely that these hydrodynamic findings would be similar for MN4 binding cocaine. SAXS methods were also used to look at what structural changes occur with DCA binding by the MS2 aptamer. A significant decrease in R_g was noted for the MS2 aptamer with ligand binding (Table 3.7) as may be expected given the secondary structure formation in this aptamer with DCA binding. Surprisingly, there is little difference in the Kratky plot between free and DCA-bound MS2, indicating that MS2 does not become significantly more ordered with ligand binding. This apparent discrepancy with the NMR data that shows secondary structure formation in two stems in MS2 can be best explained if the structure of the unbound state is taken into consideration. If the unbound state exits as an unfolded, random, uncoiled single strand, then secondary structure formation of two stems should represent a large increase in order. However, if the unbound form exists in a more compact state, one where the base pairs outside of stem 3 are not yet formed but the strands are already aligned close together, then ligand binding and base pair formation can occur without a large change in order.

In light of this new data, it is proposed that steroid-binding aptamer constructs utilize a similar binding mechanism to that observed for cocaine-binding constructs, however, the possibility of a compact, yet unfolded structure is taken into account and is illustrated in Figure 3.16.

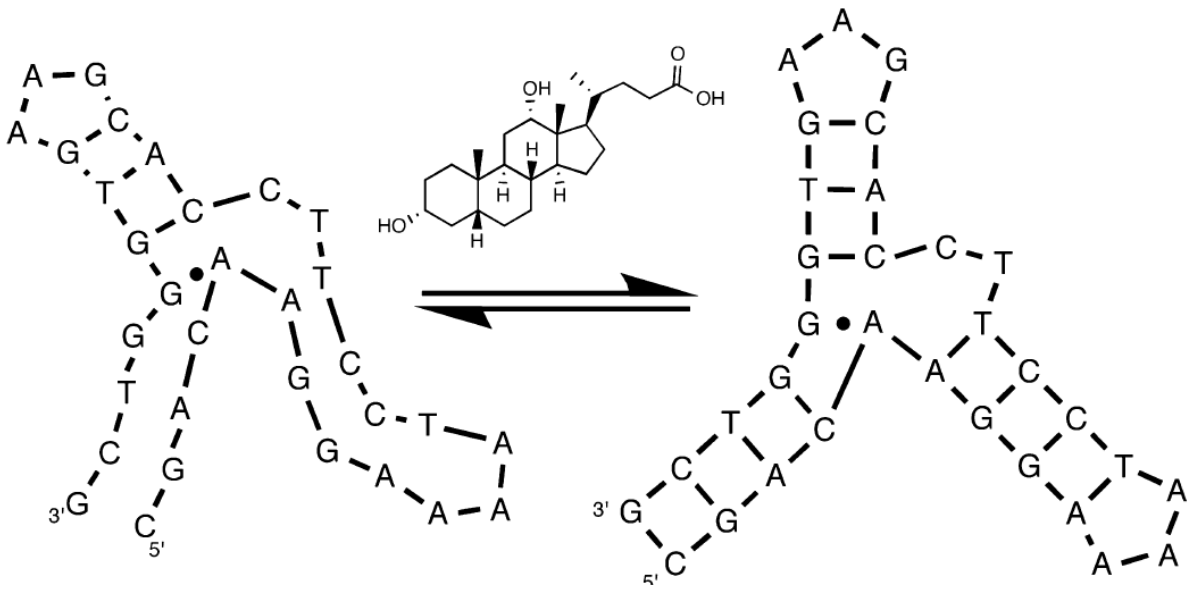

Figure 3.16: Proposed mechanism for the structural changes that occur with ligand binding by the MS2 aptamer. In the free state, stem 3 is formed and the molecule exists in a compact prefolded form where stems 1 and 2 do not exist in a random coil. With ligand binding, base pair formation in stems 1 and 2 take place despite little change in overall order occurring.

3.4 Conclusion

The research presented within this study demonstrates that the cocaine-binding aptamer employs a cocaine-binding mechanism where ionic interactions play an important role, but do not solely govern ligand binding. The length of all three stems in the aptamer is important for ligand binding and cannot be shortened without reducing binding affinity. In contrast, increasing the length of the three stems results in an aptamer with increased ligand binding affinity. This observation is consistent with the hypothesis that tertiary structure formation concurrent with ligand binding provides an important driving force for cocaine recognition. Furthermore, a ligand-induced folding mechanism was engineered into a steroid binding aptamer. This was accomplished by shortening stem 1 in the steroid-binding aptamer in a similar manner as seen in the cocaine-binding aptamer. Only some fine-tuning of the stem 1 length was needed to achieve a mechanism where two stems of the three-way junction form with ligand binding. Given the propensity shown by the DNA architecture of the cocaine-binding aptamer to be selective for different ligands,[123,127,164] it should be possible to use this structure as a general template to obtain a set of

aptamers that exhibit ligand-induced folding specific to a wide array of ligands which need not bear the legal restrictions present for cocaine.

3.5 Experimental Methods

3.5.1 Materials and Sample Preparation

Aptamer samples were obtained from the University of Calgary DNA Service and Integrated DNA Technologies. DNA samples were dissolved in water and then exchanged three times in a 3 kDa molecular weight cutoff concentrator with sterilized 1 M NaCl and then washed at least three times with distilled deionized H_2O. Except where noted, all DNA samples were exchanged with 20 mM Tris (pH 7.4), 140 mM NaCl, and 5 mM KCl (Buffer A) three times before use. Aptamer concentrations were determined by absorbance spectroscopy using the calculated extinction coefficients. Sodium deoxycholate (DCA) was obtained from Sigma-Aldrich (part number D6750). Stock solutions of DCA and cocaine were prepared by weight and dissolved in the desired buffer. Cocaine hydrochloride was obtained from Sigma Aldrich.

3.5.2 NMR Spectroscopy

All 1D ^{1}H-NMR experiments on aptamer samples were acquired using a 600 MHz Bruker Avance spectrometer. 1D ^{1}H-NMR spectra were acquired in 90% H_2O/10% D_2O at 5 °C unless otherwise noted. These sample conditions were chosen to result in spectra showing the sharpest signals.[131] The concentrations of aptamers for NMR studies ranged from 0.3 – 2.3 mM. All 1D and 2D data were processed and analyzed using NMRPipe/NMRDraw.[187]

3.5.3 Isothermal Titration Calorimetry

ITC was performed using a MicroCal VP-ITC. Data was analyzed using accompanying Origin software and fit to a one-site binding model. Samples for ITC analysis were degassed before use with the MicroCal Thermo Vac unit. All experiments were corrected for the heat of dilution of the titrant. Unless otherwise specified, cocaine, DCA, and aptamer solutions were prepared in Buffer A. Steroid binding experiments were performed with aptamer solutions ranging from 20 to 85 μM using DCA concentrations of 1.2 − 4.2 mM at 20 °C. Cocaine binding experiments were

performed with aptamer solutions of 20 μM using cocaine concentrations of 280 μM at 20 °C. All aptamer samples were heated in a boiling water bath for 3 min and cooled on ice prior to use in a binding experiment to allow the DNA aptamer to anneal. Unless otherwise noted, binding experiments were carried out in Buffer A.

3.5.3.1 ITC Binding Studies as a Function of Ionic Strength

For binding studies conducted at pH 5.4 and 6.4, buffers of 20 mM sodium acetate and sodium phosphate, respectively, were used and contained the same NaCl and KCl conditions as Buffer A. Binding studies above pH 7.4 were conducted in 20 mM Tris at the indicated pH. Experiments conducted where the NaCl concentration was varied were conducted with the aptamer in pH 7.4 Tris buffer containing the indicated amount of NaCl. Binding experiments typically consisted of either (i) 30 successive 8 μL injections of cocaine every 300 s to a final molar ratio of 2.5**:**1. Or (ii) 36 injections of 6 μL cocaine spaced every 300 s to a final molar ratio of 2**:**1. For all experiments, the first injection volume was 1 μL. The raw ITC data was corrected for heat of dilution of the titrant.

3.5.3.2 Low c ITC Studies of Aptamer Variants

Some constructs only bind weakly at the previously indicated aptamer and cocaine concentrations due to low affinity of the aptamer for ligand. A low c ITC procedure was applied for these constructs.[165,183] The running conditions of low c experiments were kept the same, however these experiments consisted of 35 successive injections of 45 mM cocaine. The first 10 injections were 5 μL and the remaining additions were 8 μL injected every 300 s to a 50 fold molar excess of cocaine. The raw low c data was also corrected for heat of dilution of the titrant. The constructs fit under these low c conditions are WC, MN5, MN6, MN7, MN9, MN10, MN11, MN13, M14 and MN17. For constructs MN15 and MN16, even lower c conditions were attempted using a 400**:**1 molar excess of ligand.

3.5.3.3 Affinity Determination of Steroid Binding Constructs

For the affinity determination experiments of steroid binding aptamers, a low c ITC method was used to enable all conditions to be studied using the same experimental parameters.[165,182] These low c ITC experiments consisted of 35 successive injections spaced every 300 s where the first

injection was 1 μL, the next 20 injections were 3 μL, and the remaining additions were 15 μL going to a 30−50-fold molar excess of DCA. For the data fitting of the low c ITC experiments, the stoichiometry of the interaction (n) was fixed at 1.

3.5.3.4 Heat Capacity of Binding

ΔC_p of DCA-binding for WC and MS2 was determined by measuring the thermodynamics of binding over a temperature range of 5−40 °C in Buffer A. The pH of Tris buffer was not corrected for changes due to temperature effects. For these experiments, low c methods were not used. Standard binding experiments consisted of 35 successive 8 μL injections spaced every 300 s where the first injection was 2 μL. Each experiment had a c value of 5.

4 Quinine Binding by the Cocaine-Binding Aptamer. Thermodynamic and Hydrodynamic Analysis of High-Affinity Binding of an Off-Target Ligand

All of the content reported within this chapter has been published in the article listed below.[167] Information on contributing authors is provided in the corresponding section.

- Reinstein, O., Yoo, M., Han, C., Palmo, T., Beckham, S.A., Wilce, M.C.J., Johnson, P.E. (2013) Quinine Binding by the Cocaine-Binding Aptamer. Thermodynamic and Hydrodynamic Analysis of High-Affinity Binding of an Off-Target Ligand, *Biochemistry* **52**, 8652−8662.

4.1 Introduction

One feature of the cocaine-binding aptamer that sets it apart from other aptamers is its binding promiscuity. Though selected for cocaine binding, this aptamer also binds other alkaloids and even binds quinine with higher affinity than it binds cocaine.[127,168,169] Such versatility in ligand binding is uncommon among aptamers and is not a desirable characteristic for a biosensor, but it may be a useful property for the biotechnology applications of the cocaine-binding aptamer. The binding versatility of this aptamer leads to questions such as "How does the same sequence bind to different ligands?" and "Does the aptamer use the same binding site and binding mechanism for all ligands?" In this study, the interaction of the cocaine-binding aptamer with quinine was investigated. Aptamer variants used in previous studies (all constructs can be found in Figure 3.3) have been employed here to demonstrate that quinine binds approximately 30-fold more tightly than does cocaine. Furthermore, structural studies using NMR methods in conjunction with thermodynamic studies using isothermal titration calorimetry (ITC) have demonstrated that the ligand-induced folding of the short stem 1 constructs of the cocaine-binding aptamer is retained with the binding of quinine. Noting the similarities between cocaine and quinine (Figure 4.1), the extent of electrostatic interactions taking place with ligand binding is also reported.

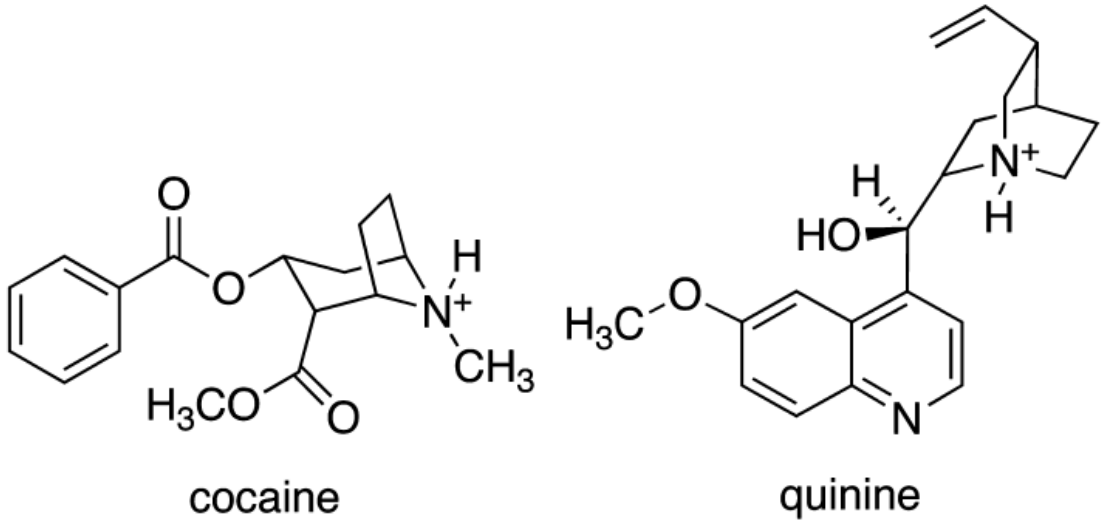

Figure 4.1: Molecular structure of cocaine and quinine.

4.2 Results

4.2.1 Affinity and Thermodynamics of Quinine Binding

ITC methods were used to establish the affinity and thermodynamics of binding by a set of cocaine-binding aptamer variants, WC, MN4, MN16, and MN19 (Figure 3.3), for the ligand quinine (Figure 4.1). The constructs studied were chosen to include the most commonly studied versions of the cocaine-binding aptamer used in previous studies.[131,157,158] Figure 4.2 provides a sample thermogram of MN4 binding quinine acquired using ITC. The affinity and thermodynamic parameters of quinine binding for these constructs are summarized in Table 4.1. These data show that the binding affinity for quinine of the aptamer variants used in this study is consistently significantly higher than that for cocaine. The affinity of MN4 for quinine is 30 times that for cocaine, while the MN19 and WC variants show a 38- and 17- fold increased affinity for quinine over cocaine, respectively.

These data also demonstrate that the relative order of affinity for these aptamers remains the same for both the quinine and the cocaine ligands. Among the variants studied, MN4 exhibits the highest affinity. The ITC data further demonstrate that, for all aptamer variants used in this study, quinine binding is an enthalpically driven process with unfavorable binding entropy.

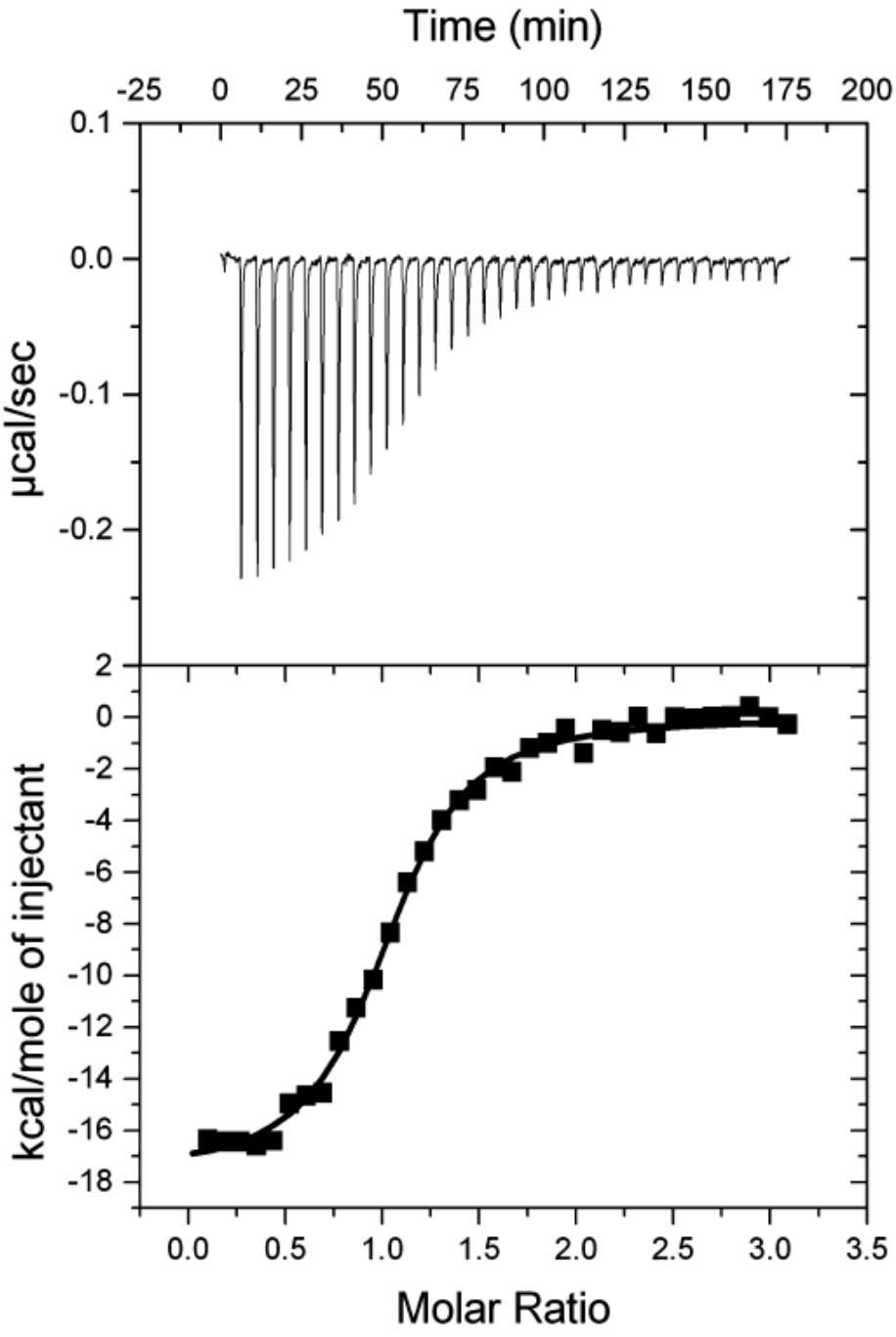

Figure 4.2: Sample of ITC data showing the interaction of MN4 with quinine. A one-site fit to the data yields a K_d value of (0.16 ± 0.01) µM and an enthalpy of −17.7 kcal mol^{-1}. (Top) The raw titration data showing the heat resulting from each injection of quinine into aptamer solution. (Bottom) The integrated heat plot after correcting for the heat of dilution. This binding experiment was performed at 20 °C in 20 mM Tris (pH 7.4), 140 mM NaCl, and 5 mM KCl (Buffer A).

Table 4.1 Thermodynamic parameters for the interaction between quinine and the aptamers presented in this Study.[a]				
	Quinine			Cocaine
Aptamer	**K_d (μM)**	**ΔH (kcal mol^{-1})**	**−TΔS (kcal mol^{-1})**	**K_d (μM)**
MN4	0.23 ± 0.03	−14.5 ± 0.4	5.6 ± 0.4	7 ± 1
MN19	0.7 ± 0.2	−22.2 ± 0.4	14.0 ± 0.4	26.7 ± 0.7
WC	12 ± 4	−21 ± 4	15 ± 4	204 ± 6
MN16	51 ± 3	−6.9 ± 0.5	1.1 ± 0.4	vwb[c]
MN4 + Mg^{2+}	0.42 ± 0.02	−10.9 ± 0.7	2.4 ± 0.7	nd[c]
MN19 + Mg^{2+}	0.6 ± 0.4	−14.6 ± 1.6	6.4 ± 1.4	nd[c]

[a]Data acquired in Buffer A. Data for WC, MN4, and MN16 were acquired at 20 °C; data for MN19 were acquired at 17.5 °C; data for MN4 and MN19 with Mg^{2+} were acquired at 15 °C. The values reported are averages of 2−5 individual experiments. The error range reported is one standard deviation.

[b]The corresponding data for cocaine binding are included for the purpose of comparison (Table 3.3 contains cocaine binding data for additional aptamers)

[c]vwb denotes that only very weak binding was observed; nd denotes not determined, the experiment was not performed.

Previous studies have indicated that DNA structures containing three-way junctions are more stable in the presence of Mg^{2+}.[170] To see if the presence of Mg^{2+} affects quinine binding, ITC experiments were conducted using MN4 and MN19 in standard buffer conditions that also contained 5 mM $MgCl_2$. Results are presented in Table 4.1 and show that the addition of $MgCl_2$ has a negligible effect on the affinity of these aptamers for quinine.

4.2.2 Change in Heat Capacity with Quinine Binding

To gain a greater level of insight into the mechanism by which the MN4 and MN19 aptamers bind quinine, enthalpy of binding by these aptamers was measured as a function of temperature to determine ΔC_p. Titration data is provided in Table 4.2 and plotted in Figure 4.3. For MN4, temperature data were obtained from 10 to 35 °C. Binding data for MN19 was acquired from 7.5 to 17.5 °C. At temperatures above 17.5 °C, MN19 exhibited signs of incomplete folding upon

binding as the enthalpy rapidly became less negative, and it is not possible to separate the enthalpy of folding from that of binding. From the slopes of the lines in Figure 4.3, ΔC_p can be computed and is (−377 ± 55) cal mol^{-1} K^{-1} for MN4 and (−798 ± 91) cal mol^{-1} K^{-1} MN19.

Table 4.2: Binding affinity and thermodynamic binding parameters of quinine binding by the cocaine-binding aptamer as determined by ITC.[a]

Aptamer	Temperature	K_d (uM)	ΔH (kcal/mol)	-TΔS (kcal/mol)
MN4	10.017	0.5 ± 0.1	-13.7 ± 0.4	5.5 ± 0.5
	15.016	0.3 ± 0.1	-13.8 ± 0.8	5.1 ± 0.6
	20.016	0.9 ± 0.5	-15.0 ± 0.1	6.8 ± 0.2
	25.016	1.1 ± 0.3	-19.1 ± 0.3	10.9 ± 0.2
	30.014	1.4 ± 0.1	-19.4 ± 0.2	11.3 ± 0.2
	35.010	1.6 ± 0.7	-22.7 ± 0.5	14.5 ± 0.7
MN19	7.515	0.69 ± 0.04	-15 ± 1	7.0 ± 0.9
	10.021	0.9 ± 0.2	-15.4 ± 0.1	7.3 ± 0.1
	12.515	1.1 ± 0.1	-18.6 ± 0.2	10.8 ± 0.2
	15.035	0.61 ± 0.04	-20.5 ± 0.1	7.3 ± 0.1
	17.514	0.5 ± 0.2	-22.5 ± 0.4	14.0 ± 0.5

[a]Binding experiments were performed in Buffer A. The values reported are averages of 2−3 individual experiments. The error range reported is one standard deviation.

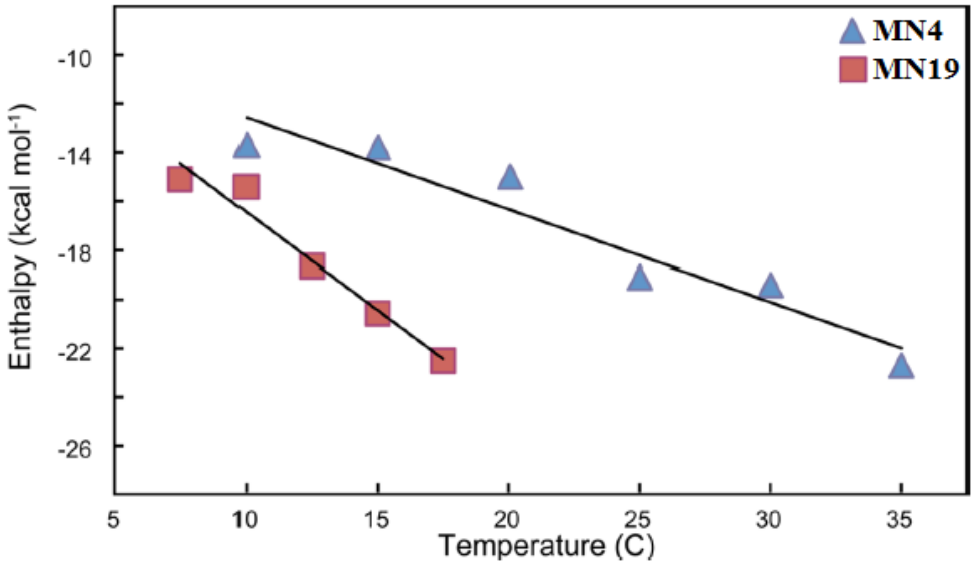

Figure 4.3: Temperature dependence of the enthalpy of MN4and MN19 binding quinine. The slope of the line represents ΔC_p, which was determined to be (−377 ± 55) cal mol^{-1} K^{-1} for MN4 and (−798 ± 91) cal mol^{-1} K^{-1} for MN19.

4.2.3 Buffer Identity and Quinine Binding

ITC methods were used to test for changes in the protonation state of quinine during binding. Change in protonation is detected by measuring the binding enthalpy in different buffers at a constant pH value. If the protonation state changes during binding, different binding enthalpy values will be obtained that differ by the number of protons lost or gained, multiplied by the protonation enthalpy of the buffer.[213,214] Enthalpies of MN4 binding to quinine were measured in both N-(2- hydroxyethyl)piperazine-N′-ethanesulfonic acid (HEPES) and phosphate buffer at a pH value of 7.4 to be (−15.2 ± 0.8) kcal mol^{-1} and (−14.4 ± 1.4) kcal mol^{-1}, respectively. Binding at pH 8.5 was also measured using HEPES and Tris buffer which resulted in ΔH values of (−14.2 ± 0.5) kcal mol^{-1} and (−16.7 ± 1.6) kcal mol^{-1}, respectively. The similarity of the binding enthalpies in the two buffers at each of these pH values indicates that little to no change in protonation state is taking place with quinine binding. Had the protonation state been affected, the difference in ΔH values expected is 16 and 11 kcal mol^{-1}, respectively.

4.2.4 Effect of Ionic Strength on Quinine Binding

To quantify the contribution that electrostatic interactions play in quinine binding, the enthalpy of MN4 binding quinine was determined at a range of NaCl concentrations from 50 to 500 mM (Table 4.3) In general, the affinity of the aptamer for quinine increases as the NaCl concentration decreases. The contribution of electrostatics to ligand binding is measured by equation 4.1, where Z is the apparent charge on the bound ligand and φ is the fraction of Na^+ bound per nucleic acid phosphate.[171]

$$\left(\frac{\partial \log K_a}{\partial \log[Na^+]}\right) = -Z\varphi \qquad (4.1)$$

From a plot of log K_a versus log [NaCl], the slope gives the value of −Zφ. For MN4 binding quinine (Figure 4.4) this value is −0.45 ± 0.14. The contribution of electrostatics to the free energy of binding can then be determined from equation 4.2.

$$\Delta G_{elec} = Z\varphi RT \ln[Na^+] \qquad (4.2)$$

Table 4.3: Binding thermodynamics of the MN4 aptamer as measured by ITC to determine contribution of electrostatic forces in quinine binding.[a]		
[NaCl] mM	**K_a (MM^{-1})**	**ΔG_{tot} (kcal mol^{-1})**
50	4.3 ± 2.4	-8.8 ± 0.3
75	4 ± 0.1	-8.84 ± 0.01
140	4.4 ± 0.6	-8.9 ± 0.1
200	3.0 ± 0.1	-8.68 ± 0.01
500	1.4 ± 0.5	-8.2 ± 0.2

[a]Binding experiments were performed in a solution of 20 mM Tris (pH 7.4) and 5 mM KCl at the indicated NaCl concentration. The values reported are averages of 2−3 individual experiments. The error range reported is one standard deviation

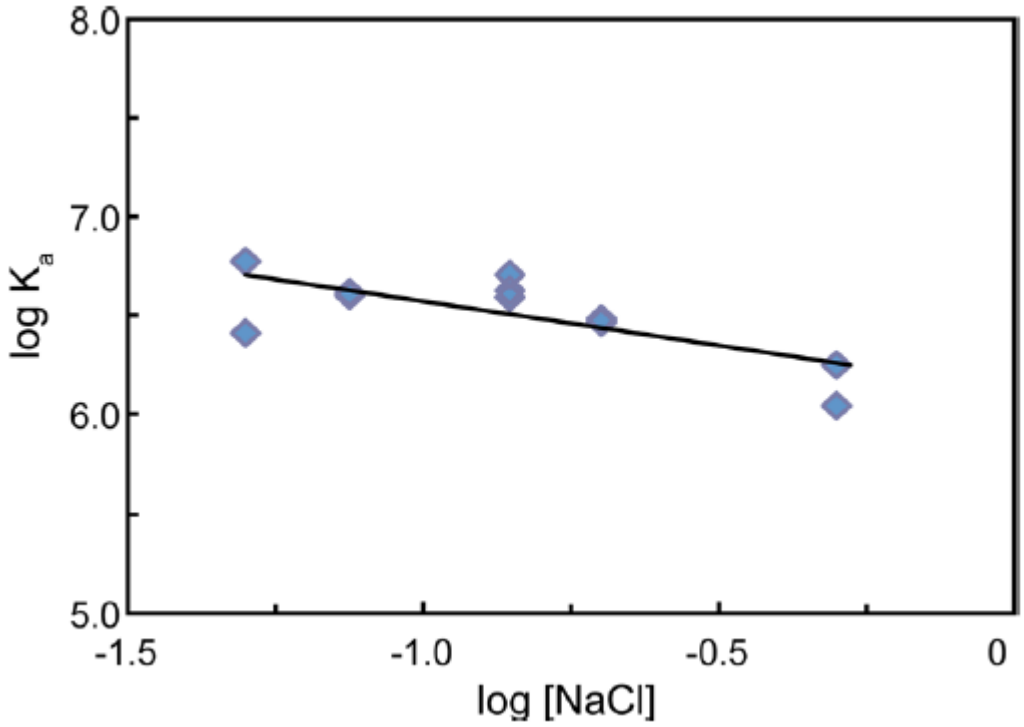

Figure 4.4: Log K_a vs log [NaCl] for MN4 binding to quinine. The slope of this line was used to determine the contribution to the free energy of binding by electrostatic (ΔG_{elec}) interactions. At 140 mM NaCl, ΔG_{elec} comprises only 6% of the overall binding ΔG.

For the MN4−quinine pair the value of ΔG_{elec} is −0.51 kcal mol^{-1} at 140 mM NaCl. Knowing the binding affinity at this NaCl concentration (Table 4.1) the overall binding free energy is calculated

to be (−8.90 ± 0.1) kcal mol^{-1}. This reveals that electrostatic interactions represent 6% of the overall free energy of MN4 binding quinine at 140 mM NaCl.

4.2.5 NMR Assignments and Quinine-Induced Chemical Shift Perturbations

The ^{1}H-NMR assignment of the imino protons of the quinine-bound MN4 and MN19 aptamers were obtained from 2D homonuclear NOESY experiments. The quality of the NMR data was excellent and complete assignments of the imino protons were obtained for the spectra of both quinine-bound MN4 and quinine-bound MN19 (Figures 4.5 – 4.7).

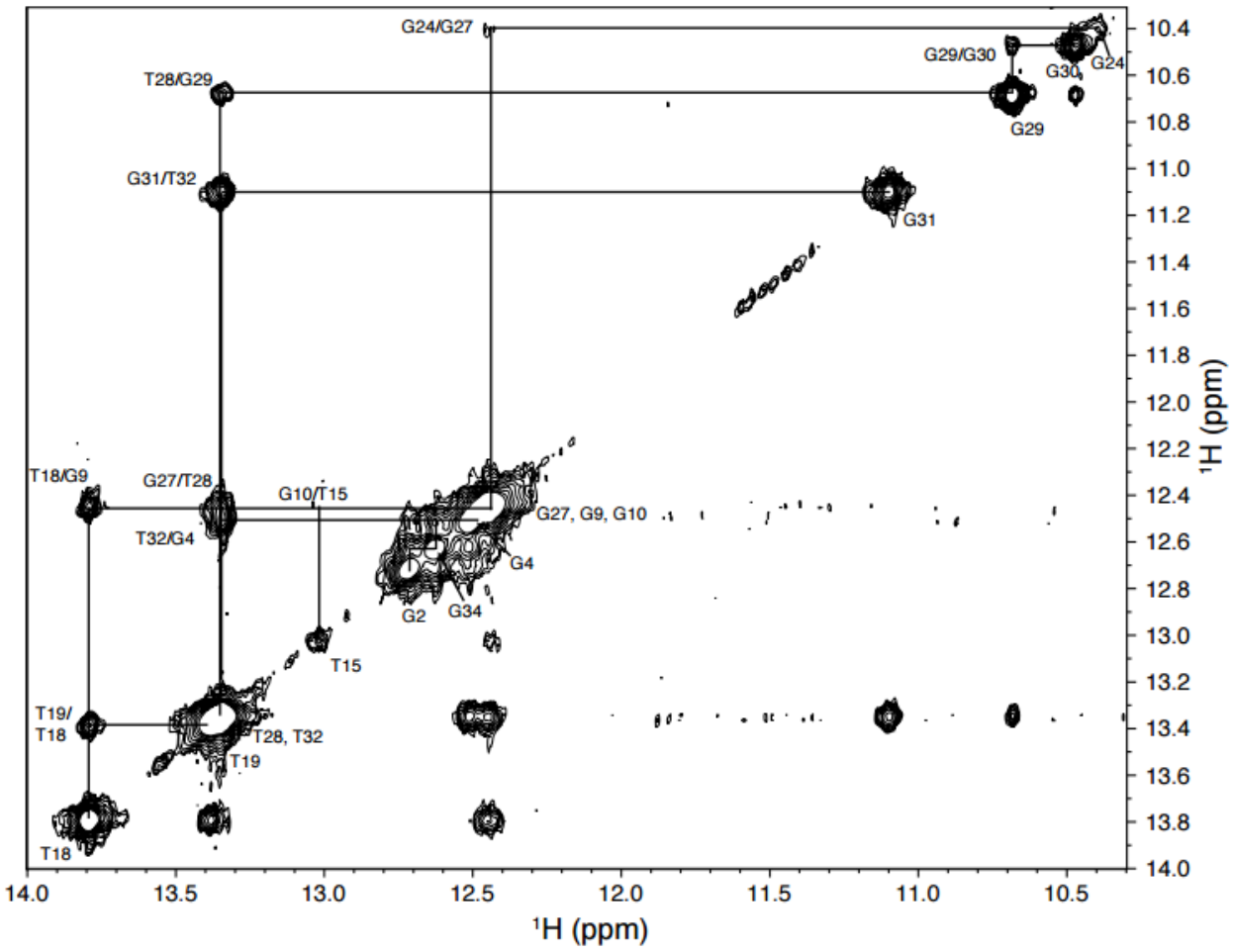

Figure 4.5: Imino−imino region of the 2D NOESY spectrum (τ_m = 200 ms) of MN4 bound to quinine acquired in 90% H_2O/10% D_2O at 5 °C. Assignments are traced out in the spectrum.

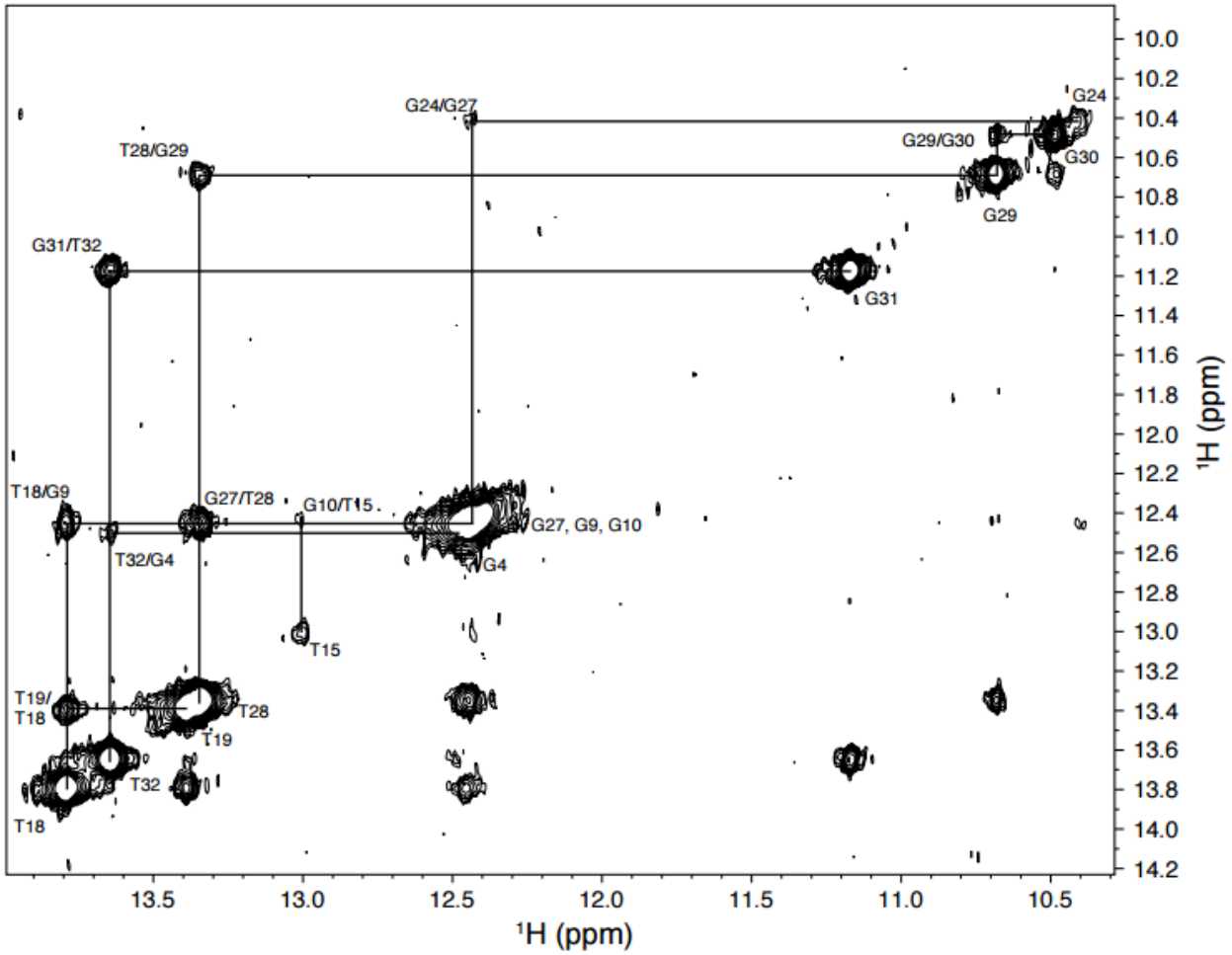

Figure 4.6: Imino-imino region of the 2D NOESY (τ_m = 200 ms) of quinine-bound MN19 recorded at 5 °C. Assignments are labeled in the spectrum.

Figure 4.7b illustrates the unfolded to folded transition taking place with MN19 for quinine binding evidenced by the appearance of several imino proton signals as quinine is titrated into the sample. The number of new signals observed account for all the expected peaks in the equimolar sample of MN19 with quinine. Insights into the location of the quinine-binding site in the MN4 aptamer can be deduced from the chemical-shift perturbations of the imino protons observed with ligand binding. Assignments of free MN4 were outlined in Chapter 2 and match what was observed for this sample of free MN4.

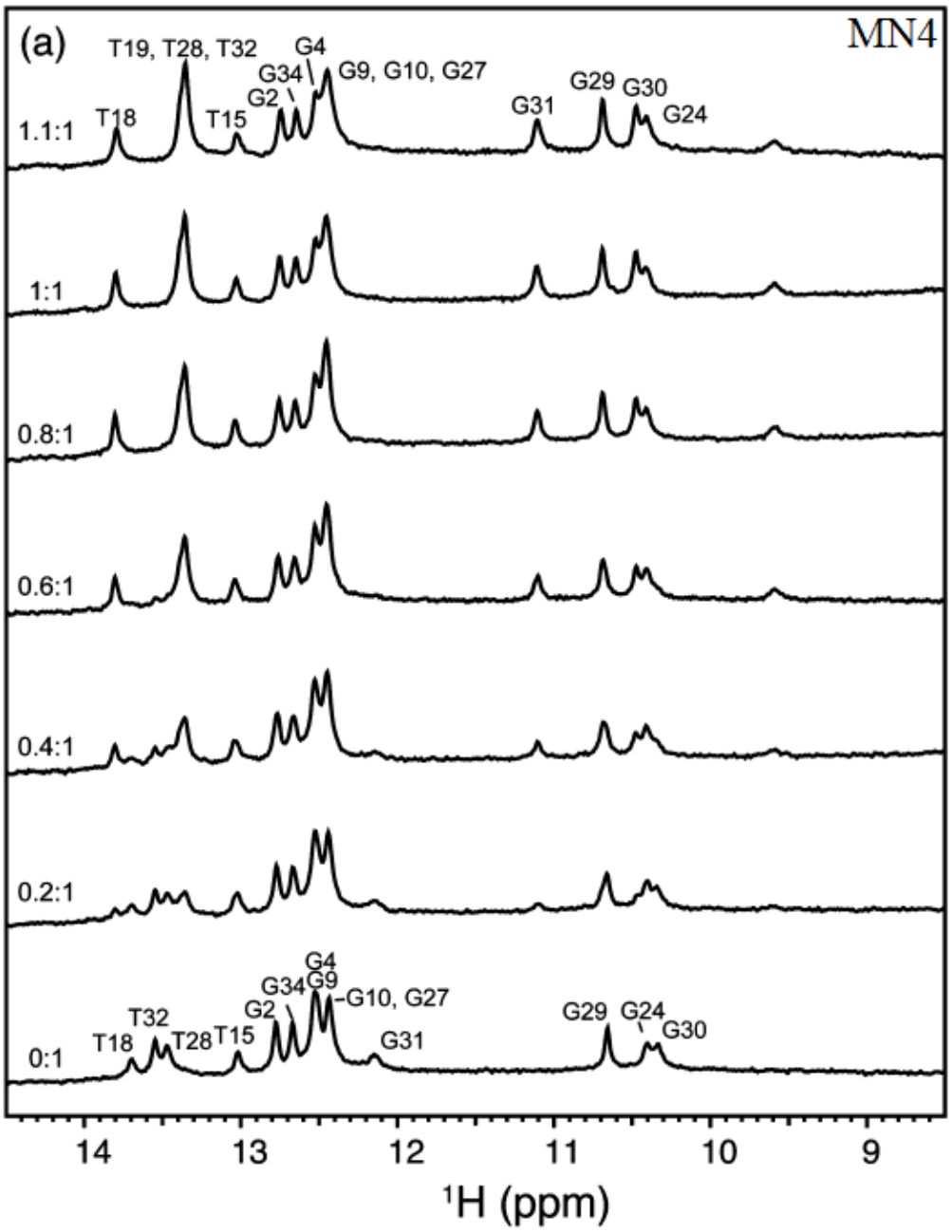

Figure 4.7a: Quinine binding by MN4 monitored by 1D ^{1}H-NMR. Displayed is the region of the NMR spectrum focusing on the imino resonances as a function of increasing quinine concentration. All spectra were acquired in 90% H_2O/10% D_2O at 5 °C at the quinine:aptamer molar ratios indicated.

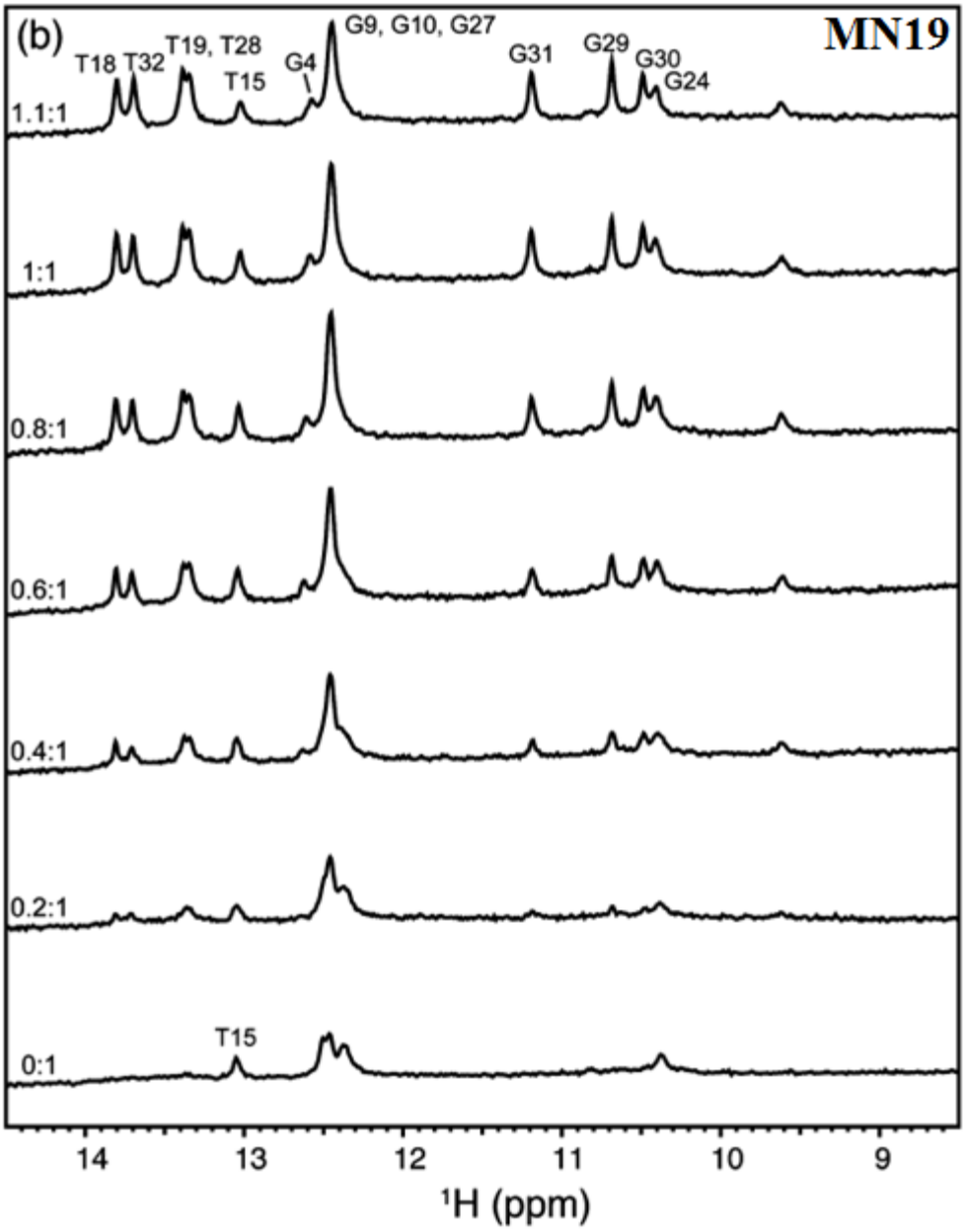

Figure 4.7b: Quinine binding by MN19 monitored by 1D ^{1}H-NMR. Displayed is the region of the NMR spectrum focusing on the imino resonances as a function of increasing quinine concentration. Note that for MN19 only a few broad peaks are observed in the free spectrum. Upon binding, sharp resonances from the quinine-bound MN19 aptamer appear. All spectra were acquired in 90% H_2O/10% D_2O at 5 °C at the quinine:aptamer molar ratios indicated.

The binding of quinine is in slow exchange on the NMR time scale, with signals for both the free and bound resonances observed simultaneously upon addition of quinine. The difference in chemical shift between the free and quinine-bound states can be determined and is plotted in Figure 4.7. Upon binding, G31 showed the greatest difference in chemical shift, followed by T32 and T28. As seen previously with MN4, the imino proton signal of T19 is not observed in the free sample, but appears with ligand binding.

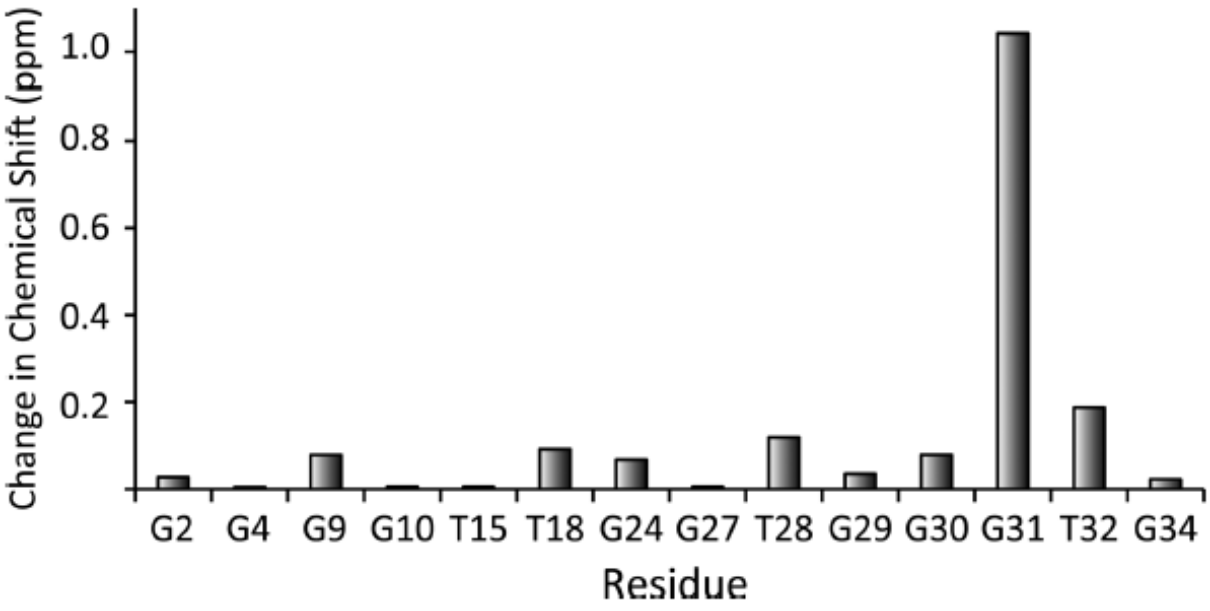

Figure 4.8: Histogram showing the chemical shift perturbations of the imino protons in MN4 upon quinine binding.

4.2.6 ITC and NMR-Monitored Competition Binding Experiments

To determine if the cocaine and quinine ligands bind at the same location in the aptamer, a set of ITC competitive-binding experiments were conducted (Figure 4.9). First quinine was added to a solution of free MN4 (Figure 4.9a). From fitting the data to a single-site binding model, a K_d value of (0.35 ± 0.04) μM and a ΔH value of (−15.2 ± 0.2) kcal mol^{-1} were obtained at 15 °C. Following this experiment, cocaine was titrated into the solution of quinine-bound MN4. As seen in Figure 4.9b, no detectable binding was observed. This inability of cocaine to bind MN4 in the presence of quinine is consistent with quinine being bound tighter by MN4 and with both ligands binding at the same site in the aptamer. Additionally, the reverse titration was performed in which cocaine was added first to free MN4 (Figure 4.9c), resulting in a K_d value of (2.2 ± 0.1) μM and a

ΔH value of (−7.96 ± 0.08) kcal mol^{-1} at 15 °C. Quinine was then titrated into the cocaine-bound MN4 and binding was observed (Figure 4.9d). The data was fit to a competitive-binding model,[172] which resulted in a K_d value of (0.14 ± 0.02) μM and a ΔH value of (−11.2 ± 0.1) kcal mol^{-1} at 15 °C for quinine binding to MN4.

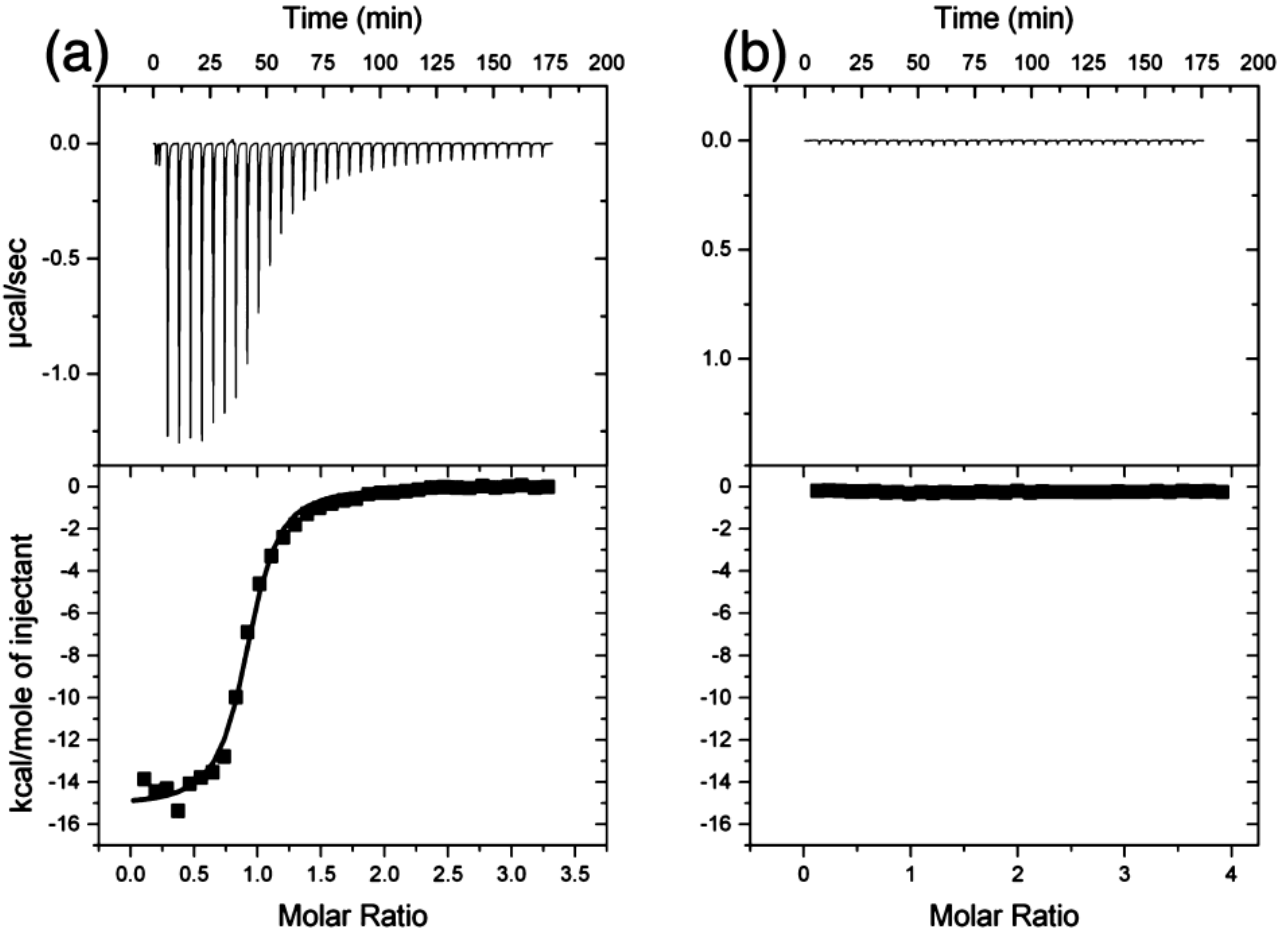

Figure 4.9 (a & b): ITC-based competitive-binding data. Shown are the interactions of (a) quinine with unbound MN4, (b) cocaine with quinine-bound MN4. On the bottom of each panel is the integrated heat plot after correcting for the heat of dilution. Titrations (a) was fit to a single-site binding model Experiments were performed at 15 °C in Buffer A.

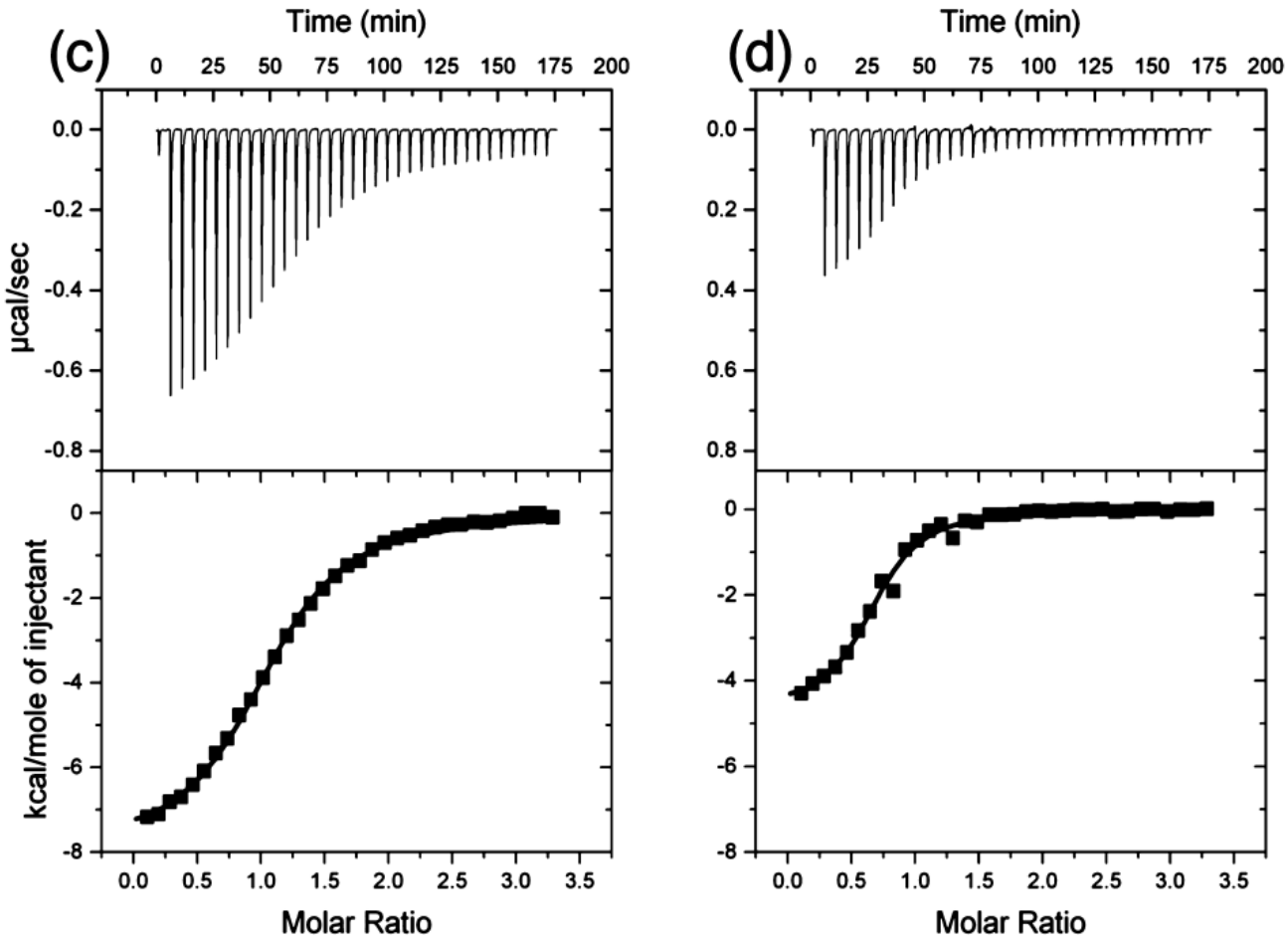

Figure 4.9 (c & d): ITC-based competitive-binding data. Shown are the interactions (c) cocaine with unbound MN4, and (d) quinine into cocaine-bound MN4. On the top of each panel is the raw titration data showing the heat resulting from each injection of quinine into aptamer solution. On the bottom of each panel is the integrated heat plot after correcting for the heat of dilution. Titrations (c) was fit to a single-site binding model, while the titration in (d) was fit to a competitive-binding model. Binding experiments were performed at 15 °C in Buffer A.

Competitive binding by cocaine and quinine for MN4 was also observed in NMR-monitored titrations. Three different titrations were performed. First, quinine was added to MN4 followed by addition of cocaine (Figure 4.10). During the addition of quinine, similar changes were observed, as seen in Figure 4.7a. During the addition of cocaine to the quinine-bound MN4, no changes in chemical shift were observed; however, peaks due to G31, T15, and T18 experienced significant line broadening.

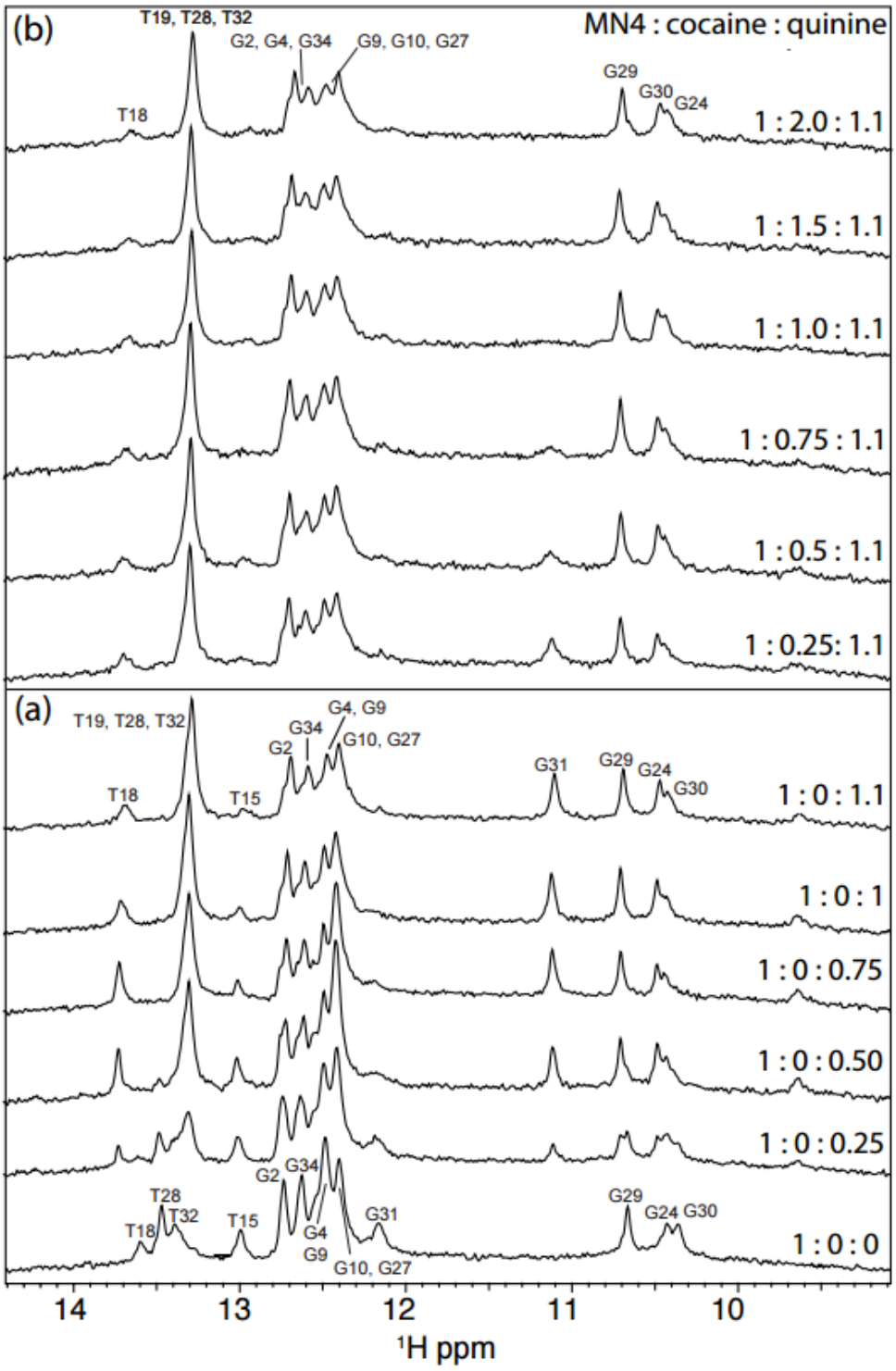

Figure 4.10: Competitive ligand binding monitored by 1D ^{1}H-NMR. Displayed is the region of the NMR spectrum focusing on the imino resonances of MN4 as a function of (a) increasing quinine concentration and (b) increasing cocaine concentration in the quinine-bound MN4. All spectra were acquired in 90% H_2O/10% D_2O at 5 °C at the molar ratios indicated.

In the second NMR monitored titration, cocaine was first added to MN4, followed by the addition of quinine to the MN4-cocaine complex (Figure 4.11). The first part of this titration resulted in spectra that are very similar to those we observed previously for the addition of cocaine to MN4.[131] When quinine was added to the MN4−cocaine complex, changes in chemical shift were noted for some peaks. Namely, the peak due to G31 shifted to its frequency indicative of the quinine-bound MN4, and the peak due to T19 shifted to its quinine-bound frequency. Additionally, in the spectrum acquired with a molar ratio of 1**:**1.1**:**3 (MN4/cocaine/quinine) all the peaks experience line broadening and resonances from T18, and T15 experienced line broadening to an extent the peaks are no longer observable.

Table 4.4: Fraction of cocaine and quinine bound by MN4 in an equimolar titration.[a]

Molar Ratios (MN4:Cocaine:Quinine)	**Fraction bound by cocaine (%)**	**Fraction bound by quinine (%)**
1 **:** 0 **:** 0	0	0
1 **:** 0.125 **:** 0.125	12	12
1 **:** 0.25 **:** 0.25	24	25
1 **:** 0.375 **:** 0.375	35	37
1 **:** 0.5 **:** 0.5	41	50
1 **:** 0.625 **:** 0.625	36	61
1 **:** 0.750 **:** 0.750	20	79
1 **:** 0.825 **:** 0.825	15	84
1 **:** 1 **:** 1	12	87

[a]Fraction bound calculated as outlined in ref. 173

Finally, a titration was performed where an equimolar mixture of cocaine and quinine was added to MN4 (Figure 4.12). In this titration, at sub saturating amounts of total ligand concentration, peaks from both quinine-bound G31 and cocaine-bound G31 were simultaneously observed. These peaks are best observed at a molar ratio of 1**:**0.375**:**0.375 (MN4/cocaine/quinine). As the total ligand concentration increases, the proportion of MN4 bound to the more tightly binding quinine increases and the amount of cocaine-bound MN4 decreases. Note that all three titrations include a spectrum in which the molar ratios of MN4 and the two ligands are essentially the same. This is the 1**:**1**:**1 (MN4/ cocaine/quinine) spectrum that corresponds to MN4 87.4% quinine-bound and 12.4% cocaine-bound (Table 4.4). The spectrum of MN4 at this ratio appears very

similar in all three titrations which demonstrates the repeatability of these titrations despite the different titration schemes used.

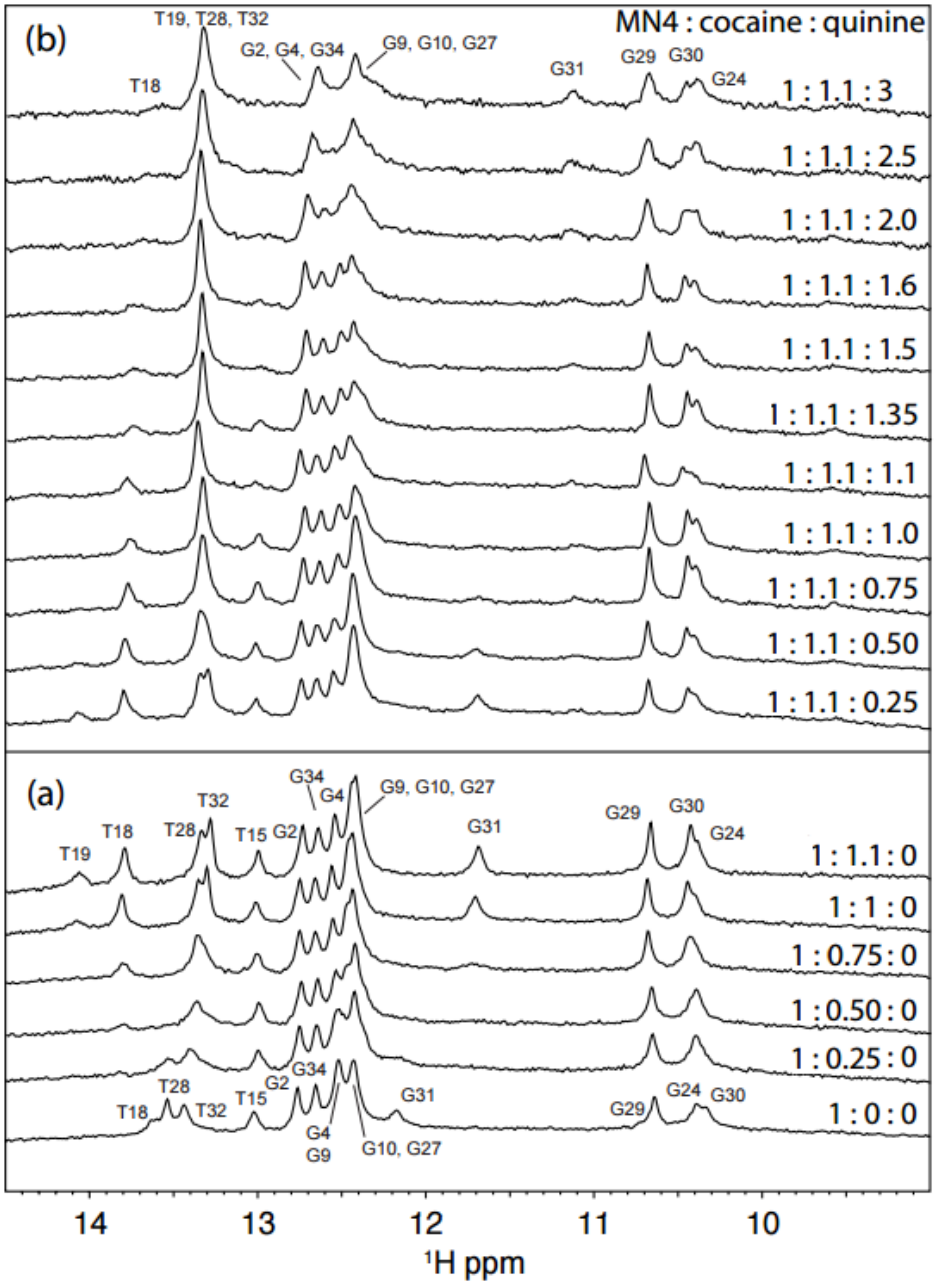

Figure 4.11: Competitive ligand binding monitored by 1D ^{1}H-NMR. Displayed is the region of the NMR spectrum focusing on the imino resonances of MN4 as a function of (a) increasing cocaine concentration and (b) increasing quinine concentration in the cocaine-bound MN4. All spectra were acquired in 90% H_2O/10% D_2O at 5 °C at the molar ratios indicated.

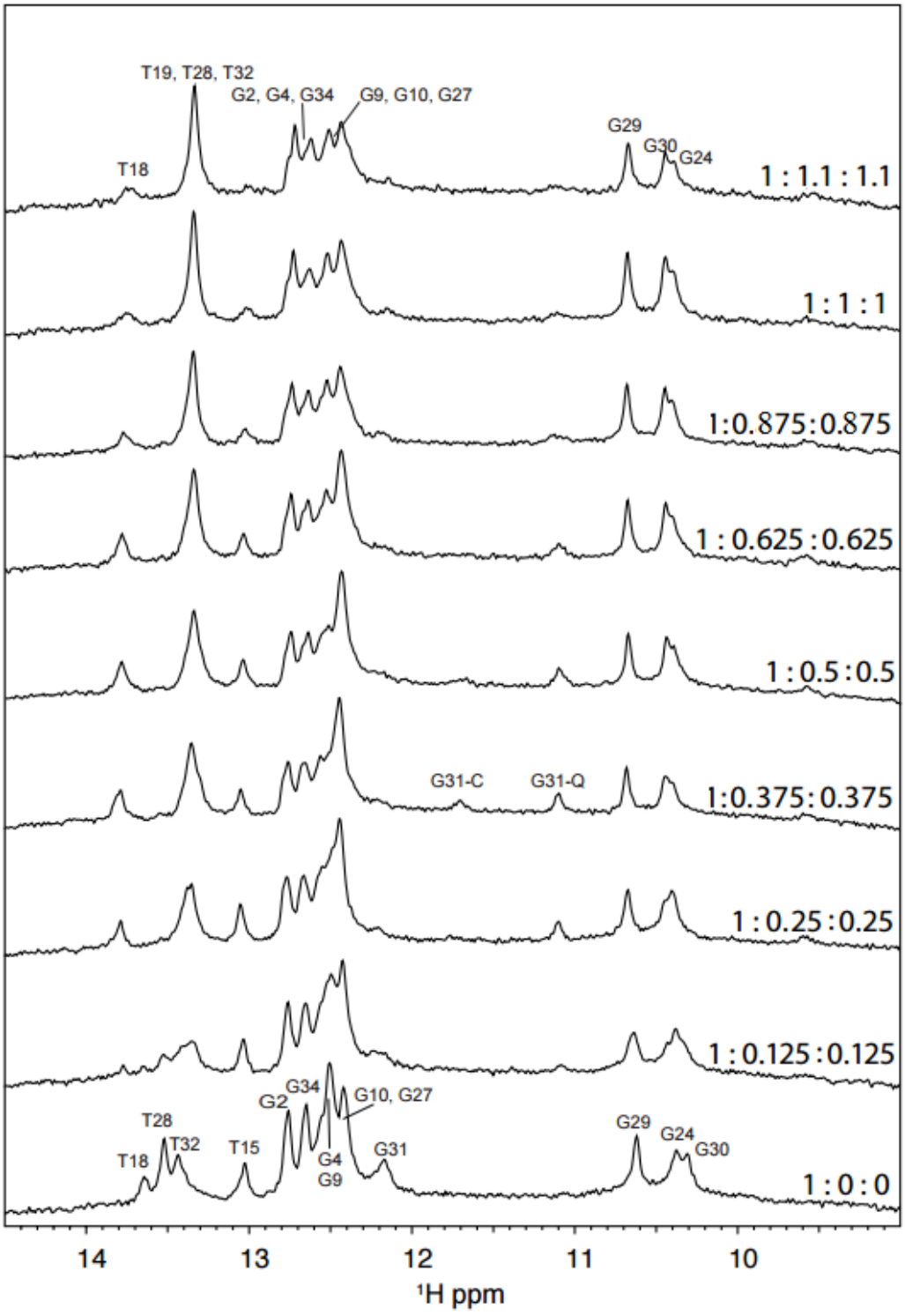

Figure 4.12: Competitive ligand binding monitored by 1D 1H-NMR. Displayed is the region of the NMR spectrum focusing on the imino resonances of MN4 as a function of increasing both quinine and cocaine concentrations using a equimolar mixture of quinine and cocaine. All spectra were acquired in 90% H_2O/10% D_2O at 5 °C at the molar ratios indicated.

Table 4.5: Structural parameters calculated from SAXS data.				
Sample	**R_g (Å)[a]**	**R_g (Å)[b]**	**R_{max} (Å)**	**NSD[c]**
MN4	17.5	17.6	57	0.83
MN4/quinine	17.8	17.8	57	0.72
MN4/cocaine	17.6	17.5	58	0.76
MN19	15.7	15.7	45	0.64
MN19/quinine	15.5	15.4	46	0.56
MN19/cocaine	15.8	15.8	47	0.55

[a]R_g calculated from Guinier plot of desmeared scattering data. [b]R_g calculated from PDDF.
[c]Normalized spatial discrepancy.

4.3 Discussion

In this study the binding of quinine by the cocaine-binding aptamer was analyzed. This work provides a basis for comparing the binding thermodynamics of the aptamers MN4 and MN19 for cocaine, the ligand originally used to select these aptamers, and research presented here for quinine. There are many similarities in the binding mechanism between the two ligands and also some differences.

4.3.1 Ligand Structure and Binding Affinity

From the competition binding experiments (Figure 4.9), it is shown that cocaine and quinine share a common binding site in the aptamer as opposed to binding at separate sites. Perhaps of most significance is that MN4 and MN19 bind quinine 30−40 times more tightly than they bind cocaine (Table 4.1). It is unusual for an aptamer to bind an off-target ligand much more tightly than the ligand it has been selected for. Quinine and cocaine do share some common structural features in that they both have an aromatic ring attached to an aliphatic nitrogen containing eight-atom bridged ring structure (Figure 4.1). However, these two structures are significantly different in the location of the substituents on the aliphatic ring. When the aliphatic ring portions of the molecule are superimposed to align the nitrogen atoms, there is little overlap of the aromatic rings. Similarly, overlaying the aromatic rings results in the aliphatic portion of the molecule not being aligned to any significant extent. However, it is possible that in the binding site, bonds in the ligands rotate into conformations other than those most favored in the free state. Detailed structural analysis of the complexes formed between the ligands and the aptamer are needed to

understand how the cocaine binding aptamer interacts with both cocaine and quinine. The exact reason for the observed increased affinity for quinine over cocaine is still unknown, but may be, in part, due more to the presence of the larger bicyclic aromatic ring on quinine in place of the monocyclic aromatic ring found in cocaine (Figure 4.1). The larger aromatic group in quinine may provide an increase in stacking interactions with the DNA bases in the aptamer compared to those seen in cocaine. In support of stacking interactions playing a role in the cocaine binding aptamer−ligand interactions, noted is the combination of binding enthalpy and entropy for both quinine and cocaine by this aptamer (Table 4.1) which falls into the intercalator category by the classification of Chaires (Figure 4.13).[155]

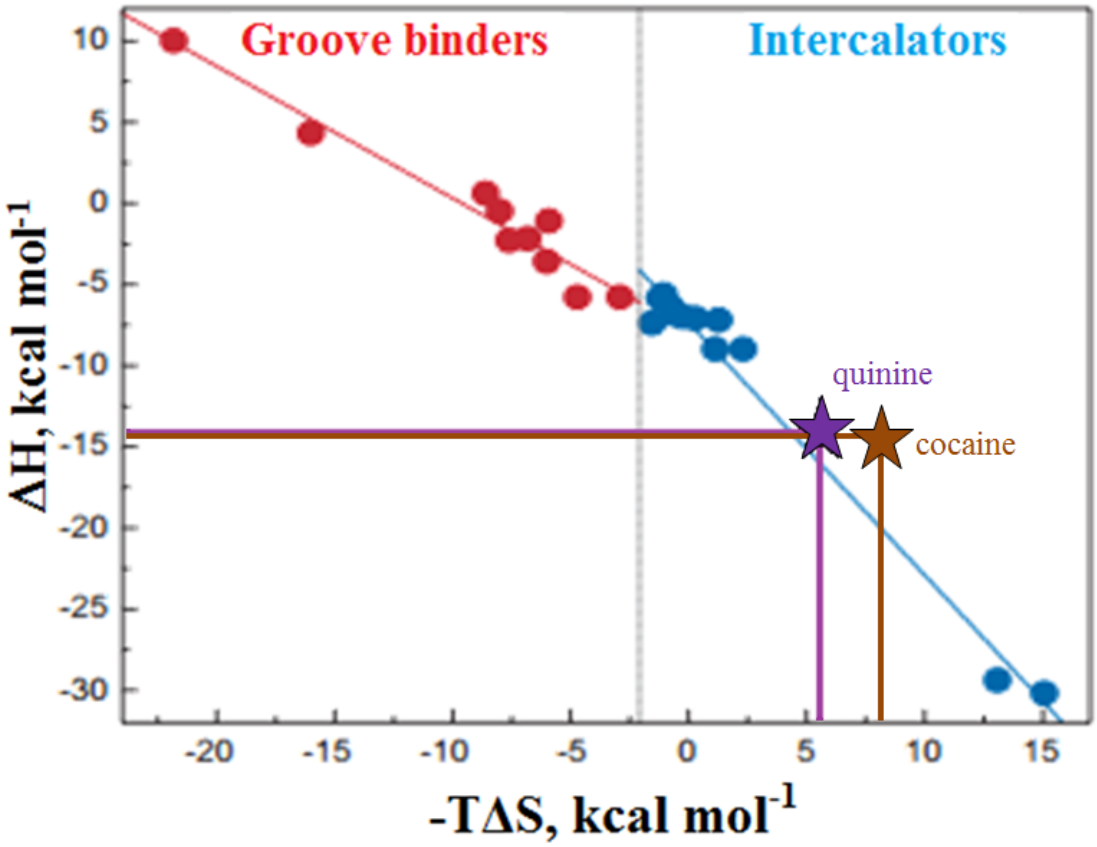

Figure 4.13: Thermodynamic profiles for a variety of groove binding (red) and intercalating (blue) molecules. The thermodynamic profiles of MN4 binding to quinine and cocaine are marked by purple and brown stars, respectively. Both fall within the intercalator region.

Additional support of the importance of the aromatic ring in ligand binding by the cocaine-binding aptamer is found when comparing the binding of quinine and cocaine to that of their structural analogues. The quinine analogues cinchonine and cinchonidine are identical to quinine except they are missing the methoxy group present in quinine on the aromatic ring (Figure 4.14). Both of these ligands are bound significantly more weakly than quinine despite this minor change.[127,169] In comparison, data consistent with changes to the aliphatic portion of the ligand not being important for binding come from studies by the Heemstra group in which both cocaine and norcocaine have equal effect in their split aptamer proximity ligation assay.[175,176]

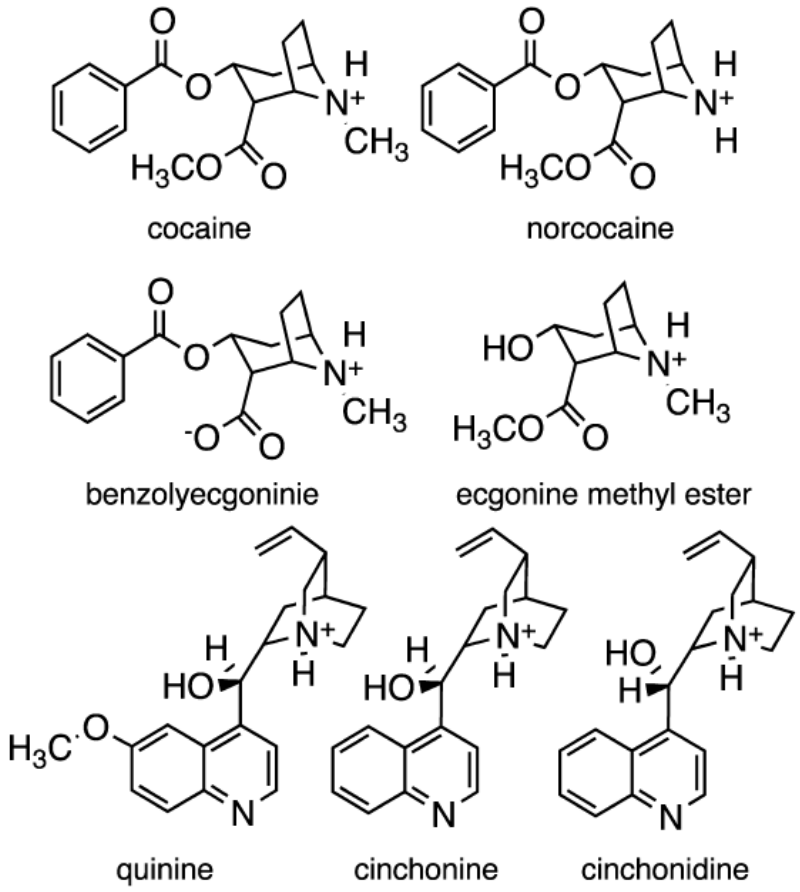

Figure 4.14: Chemical structures of quinine, cocaine, and a series of structural analogues.

In contrast, removal of the aromatic group from cocaine (ecgonine methyl ester) and the creation of a negatively charged carboxylic acid by the removal of a methyl group on cocaine to make benzoylecgonine both result in very little ligation due to these ligands not being bound by the aptamer.[175,176] Together, these data indicate that changes to the aromatic portion of the ligand result in a significant decrease in binding affinity.

4.3.2 A Consistent Structure Switching Mechanism

The functionally important structural-switching binding mechanism for MN19 is retained for both the cocaine and the quinine ligands. With stem one being 3 base pairs in this aptamer, only few imino signals are observed in the 1D ^{1}H-NMR (Figure 4.7b), indicating the aptamer has a limited number of base pairs stably formed in the unbound state. Upon addition of quinine, all the expected imino signals for the secondary structure appear. For MN4, the aptamer is folded in the free state, and quinine binding, like cocaine binding, does not appear to significantly change the secondary structure of the aptamer (Figure 4.7a). Additional evidence for the structure switching mechanism is displayed by the ΔC_p data for MN4 and MN19. A more negative ΔC_p is observed for MN19 binding quinine than for MN4 (Figure 4.3). The basis for a negative ΔC_p is the burying of nonpolar surface area.[149] This can result directly from burying the ligand as well as indirectly by triggering folding in the aptamer, resulting in an increase in nonpolar surface being buried as base stacking increases. In this case, it is expected that quinine binding by both MN4 and MN19 results in a similar amount of nonpolar surface area burial on the ligand, and any difference between MN4 and MN19 aptamers to reflect differences in nonpolar burial due to folding. For MN19, if the aptamer starts off more unfolded in the free state than the bound state, and aptamer folding occurs with quinine binding, a more negative ΔC_p is expected than if the aptamer is folded in both the free and bound state. Demonstrated here, quinine binding to MN19 has a ΔC_p of (-798 ± 91) cal mol^{-1} K^{-1}, while the ΔC_p for MN4 is (-377 ± 55) cal mol^{-1} K^{-1}. This more negative ΔC_p for MN19 is consistent with a ligand-induced folding mechanism. A more negative ΔC_p was similarly seen for the MN6 construct binding cocaine compared to MN4 binding cocaine.[131] This same trend was also observed for the binding of deoxycholic acid by the MS2 construct when compared to the WC construct. This structural-switching binding mechanism is likely inherent in this aptamer and can be triggered by binding any ligand that provides enough binding free energy to trigger folding.

4.3.3 Evidence of the Structure Switching Mechanism from SAXS

SAXS studies were conducted in collaboration with this research project by Matthew C.J. Wilce and Simone A. Beckham. As in Chapter 3, SAXS studied were pursued again to obtain additional information that could characterize the solution structure of the MN4 and MN19 aptamers.

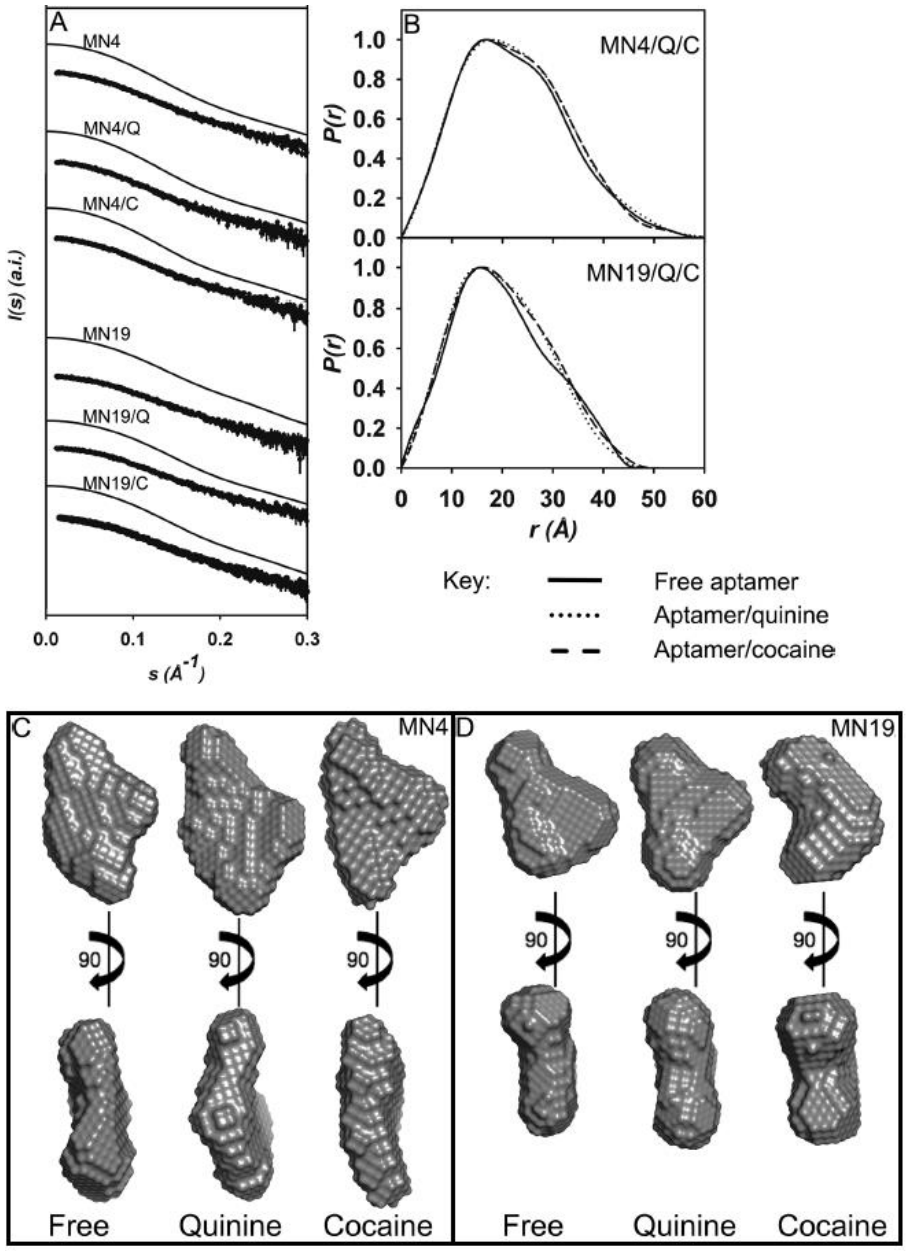

Figure 4.15: SAXS analysis of MN4 and MN19 free and bound to quinine or cocaine. (a) Scattering data for each sample showing raw scattering data with error bars; above this, the desmeared scattering curve. (b) PDDF plots. Top panel MN4; MN4/Q and MN4/C indicate MN4 bound to quinine and cocaine, respectively. Bottom panel MN19; MN19/Q and MN19/C indicate MN19 bound to quinine and cocaine, respectively. (c) Ab initio reconstructions of free MN4 and MN4 with quinine or cocaine bound. (d) Ab initio reconstructions of free MN19 and MN19 with quinine or cocaine bound. Two orientations rotated 90° about the y axis are presented. The reconstructions were aligned using the program supcomb.[174]

Analysis of data shown in Figure 4.15b revealed that the R_g was consistently larger for MN4 than it was for MN19 in both free and bound forms. R_g for MN4 ranged from 17.5 to 17.8 Å and 15.5 to 15.8 Å for MN19. Additionally, these PDDFs indicate that MN4 free and the quinine- and cocaine-bound samples exhibit similar solution structures, while the MN19 samples are quite different. This is particularly evident when comparing the free MN19 data with that of the two bound aptamer samples. The free MN19 aptamer exhibits a shoulder around 35 Å not seen in the quinine- and cocaine-bound forms of the aptamer. For MN4, the PDDF plot shows little difference between the free MN4 form and the two ligand bound complexes, indicating that only small structural changes, if any, occur upon ligand binding. The *ab initio* shape reconstruction of the MN4 and MN19 aptamers shows that these molecules form non-globular, elongated, and flat structures (Figure 4.15(c & d)). The three MN4 structures are fairly similar, containing a bulge off to one side, while the three MN19 structures form variations of an elongated flat structure. This data provides additional evidence for the previously proposed ligand-binding mechanism used by MN4 and MN19.

4.3.4 NMR Evidence for the Quinine Binding Site

From the NMR chemical shift perturbation data, it can be concluded that quinine and cocaine share a common ligand binding site. The signals that shift the most with quinine binding are G31 and T32 (Figures 4.7. 4.8, 4.16). These are the same resonances that move the most with cocaine binding.[131] Additionally, the T19 imino signal appears in the quinine bound sample, while it is not observable in the free MN4 state. The main difference in the imino-proton NMR spectrum of the cocaine- and quinine-bound aptamer is that G31 has a greater change in chemical shift with quinine binding than it does when binding cocaine. Also, the position of the bound T19 is significantly different in these two forms (Figure 4.15).

Changes in chemical shifts can be due to the spatial proximity of the ligand and the observed proton or to structural changes with ligand binding at a site away from the location of the observed proton resonance. In this particular case, it is hypothesized that perturbation is due to direct contact: if ligand binding was occurring at a site away from the site of the greatest change in chemical shift, signals other than G31, T32, and T19 would be affected by the binding event.

Together this implies not only that the ligand binding location in the aptamer is the same for both cocaine and quinine but also that the binding site is close to T32, G31, and T19.

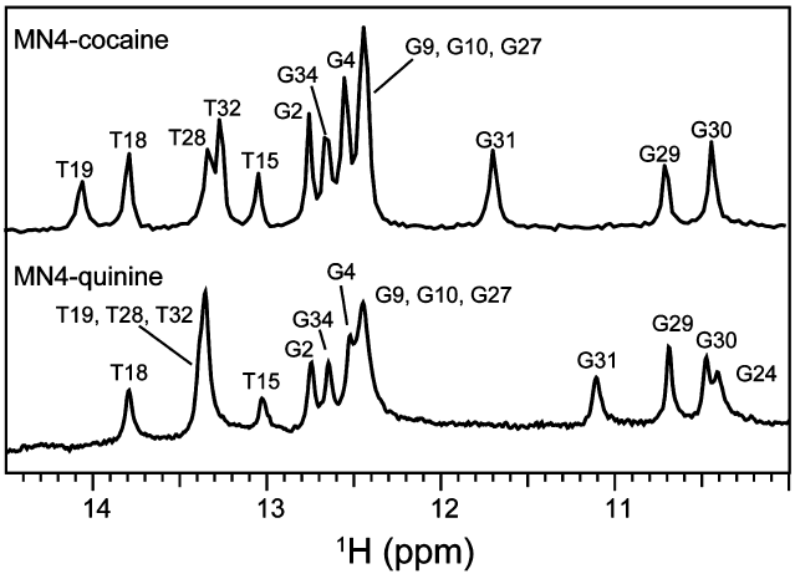

Figure 4.16: Comparison of the imino region of the 1D ^{1}H-NMR spectra of cocaine- and quinine-bound MN4. For most imino protons, resonances occur at the same position in both spectra, indicating the similarity of the structure for both aptamers. The only significant differences between these two spectra are the positions of the G31 and T19 imino protons. These protons lie at the binding site, and the change in frequency of these imino resonances in the two samples reflects the different bound ligand.

4.3.5 Electrostatic Contributions to Binding

The salt-dependent behavior of the quinine-binding association constant shows that the MN4 aptamer uses electrostatics for only about 6% of the binding free energy at a NaCl concentration of 140 mM. This is small compared with the binding of aminoglycosides to the A-site RNA, in which electrostatics make up >50% of the binding free energy.[177] This difference reflects the number of charged amino groups involved in the interaction between the ligand and nucleic acid binding partners, but it also likely reflects the need for aptamers to use more shape-specific interactions, such as hydrogen bonds, to specifically recognize their desired ligand, even though this aptamer distinguishes poorly between cocaine and quinine.

4.4 Conclusion

In summary, it has been demonstrated that quinine binding by the cocaine-binding aptamer is similar to the enthalpy-driven binding mechanism the aptamer has for cocaine, follows a ligand-induced folding similar to that for cocaine when stem 1 is three base pairs long, and shares with cocaine the same ligand-binding site in the aptamer. Furthermore, much like in the research presented for the steroid-binding variants (chapter 3), it is proposed that all short stem 1 constructs of the cocaine-binding aptamer that are capable of binding a ligand are quite likely to exist in a loosely arranged configuration in the absence of any ligand, as evidenced by SAXS. The major difference between the two ligands used within this study is the significantly higher affinity of the aptamer for quinine over cocaine. While the lack of ligand binding specificity of the cocaine-binding aptamer raises doubts about the suitability of this aptamer for biosensor applications, it does allow the non-biosensor uses of this aptamer to be developed using quinine as opposed to cocaine.

4.5 Experimental Methods

4.5.1 Materials and Sample Preparation

Aptamer samples were obtained from Integrated DNA Technologies (IDT). The DNA samples were dissolved in distilled deionized H_2O (ddH2O) and then exchanged three times using a 3 kDa molecular weight cutoff concentrator with sterilized 1 M NaCl followed by three exchanges into ddH2O. Except where noted, all DNA samples were exchanged with 20 mM Tris (pH 7.4), 140 mM NaCl, and 5 mM KCl (Buffer A) three times before use. The aptamer concentrations were determined by absorbance spectroscopy using the extinction coefficients supplied by the manufacturer. Quinine hemisulfate monohydrate was obtained from Sigma-Aldrich (catalog number 145912 Aldrich). Stock solutions of quinine hemisulfate were prepared by dissolving the appropriate weight of quinine-hemisulfate monohydrate in Buffer A.

4.5.2 Isothermal Titration Calorimetry

4.5.2.1 Thermodynamics of Quinine Binding

ITC was performed using a MicroCal VP-ITC instrument. Data were fit to a one site binding model using Origin 5.0 software. Samples were degassed prior to use with the MicroCal Thermo Vac unit. All experiments were corrected for the heat of dilution of the titrant. Unless otherwise specified, the quinine and aptamer solutions were prepared in Buffer A. The binding experiments were performed with aptamer solutions ranging from 15 to 150 μM using quinine concentrations of 0.23−2.25 mM at the indicated temperatures. All titrations were performed with the aptamer in the cell and with the ligand, as the titrant, in the needle. All aptamer samples were heated in a boiling water bath for 3 min and cooled on ice before use in an ITC experiment, to allow the DNA aptamer to anneal. The standard binding experiments consisted of 35 successive 8 μL injections every 300 s; the first injection was 2 μL. The experimental concentration for the MN4 construct was established using a fixed c value[190] of 50, while the experiments for the MN19 construct used c values ranging from 2 to 7.5. A low c ITC method was adopted for the weak-binding MN16 construct.[165,182] This method used 20 μM MN16, which was titrated with 3.6 mM quinine to 30-fold molar excess. Experiments using the low c method consisted of 35 injections in which the first injection was 2 μL, followed by 19 injections of 3 μL and finishing with 15 injections of 15 μL. The injections were made every 300 s.

4.5.2.2 Heat Capacity of Binding

ΔC_p of quinine binding for MN4 and MN19 was determined by measuring the thermodynamics of binding over temperature ranges of 7.5−35 °C in Buffer A. The pH of the Tris buffer was not corrected for changes due to temperature effects.

4.5.2.3 Competitive Binding Studies

For the ITC-based competitive-binding experiments, the initial titration was performed as described above. Following completion of the first titration, the sample was collected, degassed, and loaded back into the cell; the second titration was then performed with the appropriate ligand.

4.5.3 NMR Spectroscopy

NMR experiments on the aptamer samples were performed using a 600 MHz Bruker Avance spectrometer equipped with a $^{1}H-^{13}C-^{15}N$ triple-resonance probe equipped with triple-axis magnetic-field gradients. All NMR spectra were acquired in H_2O/D_2O (90%/10%) at 5 °C. These sample conditions, with no NaCl added, were chosen to result in spectra with the smallest linewidths. Nuclear Overhauser Enhancement Spectroscopy (NOESY) spectra[191,192] were obtained using a mixing time (τ_m) of 200 ms. Water suppression was achieved through the use of the WATERGATE sequence.[193] The aptamer concentration for the NMR studies ranged from 0.4 to 2.3 mM. 2D NOESY spectra were processed and analyzed using NMRPipe and NMRDraw.[187]

5 Folding Studies of the Cocaine-Binding Aptamer Show Remarkable Stability Against Urea Denaturation

The content reported within this chapter includes experimental results and data analysis which is in preparation for publication.

5.1 Introduction

The number of cocaine biosensing platforms has steadily grown since the cocaine-binding aptamer was first isolated. The surge in new biosensing platforms as well as other applications which utilize the cocaine-binding aptamer presents a variety of experimental conditions which may affect the functionality of the aptamer. Understanding the functional limits of the cocaine-binding aptamer would reinforce its reliability for a variety of applications, whether these applications are novel biosensing platforms or apply the aptamer as a scaffold as part of a large complex. Research presented here first outlines the structural stability of the cocaine-binding aptamer in the presence of harsh denaturing conditions.

Following the studies on steroid-binding variants of the cocaine-binding aptamer, it was established that the short stem 1 constructs which undergo unfolded to folded transitions are unlikely to exist as completely solvent exposed single stranded molecules (chapter 3). This finding suggested that the nature of the unbound state for short stem 1 constructs may not be very well understood and that additional structural modelling may be required to better understand the behaviour of the aptamer in the ligand free state. Using molecular beacons and a fluorescence spectroscopy-based approach, the ligand free state of the aptamer was studied in greater detail.

5.2 Results

5.2.1 Gauging Resistance to Chemical Denaturation

In order to make comparisons between long stem 1 and short stem 1 aptamers, stability measurements were focused on two aptamers, MN4 and MN19. Preliminary measurements of aptamer stability were conducted by means of ITC where binding was measured as a function of urea concentration (Figure 5.1). Both aptamers appeared to follow the same trend where functionality would be retained and only minor changes in binding activity were observed.

Beyond a specific concentration of urea, 5M for MN4 and 4M for MN19, a significant reduction in binding activity was observed.

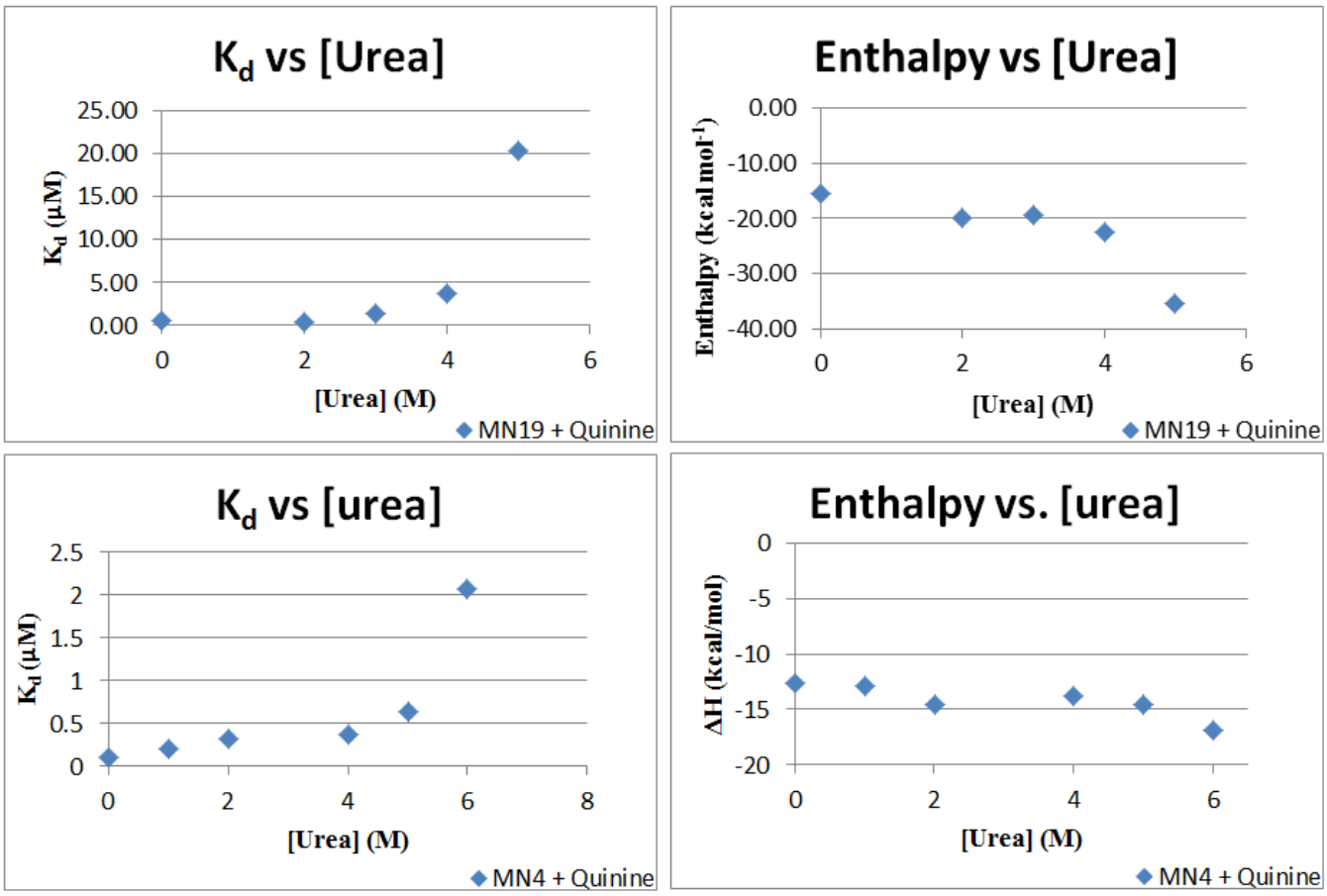

Figure 5.1: ITC binding experiments conducted for MN19 (top) and MN4 (bottom) binding quinine in the presence of varying concentrations of urea. All binding experiments were conducted in a buffer of 20 mM Tris, 140 mM NaCl, and 5 mM KCl (Buffer A) at 10 °C with the indicated concentration of urea. Individual data points are obtained from single ITC experiments.

NMR methods were similarly applied in attempts to obtain a more accurate denaturation point for the aptamers. Ideally, a completely denatured, strand-like, solvent exposed aptamer would display far fewer peaks than one that is folded up due to the fewer number of chemical environments that could be present under such conditions. While some clues as to a denaturation point were obtained, NMR spectra never produced clean spectra that allowed for a definite determination of complete denaturation of the aptamers. (Figures 5.2, 5.3) However, a downfield peak around 8.5 ppm began to appear in spectra of both MN4 and MN19 at higher concentrations of urea. The first

appearance of these peaks was used as estimates for the denaturation point of the aptamers which were in modest agreement with ITC results: 4 M for MN4 and 3 M for MN19.

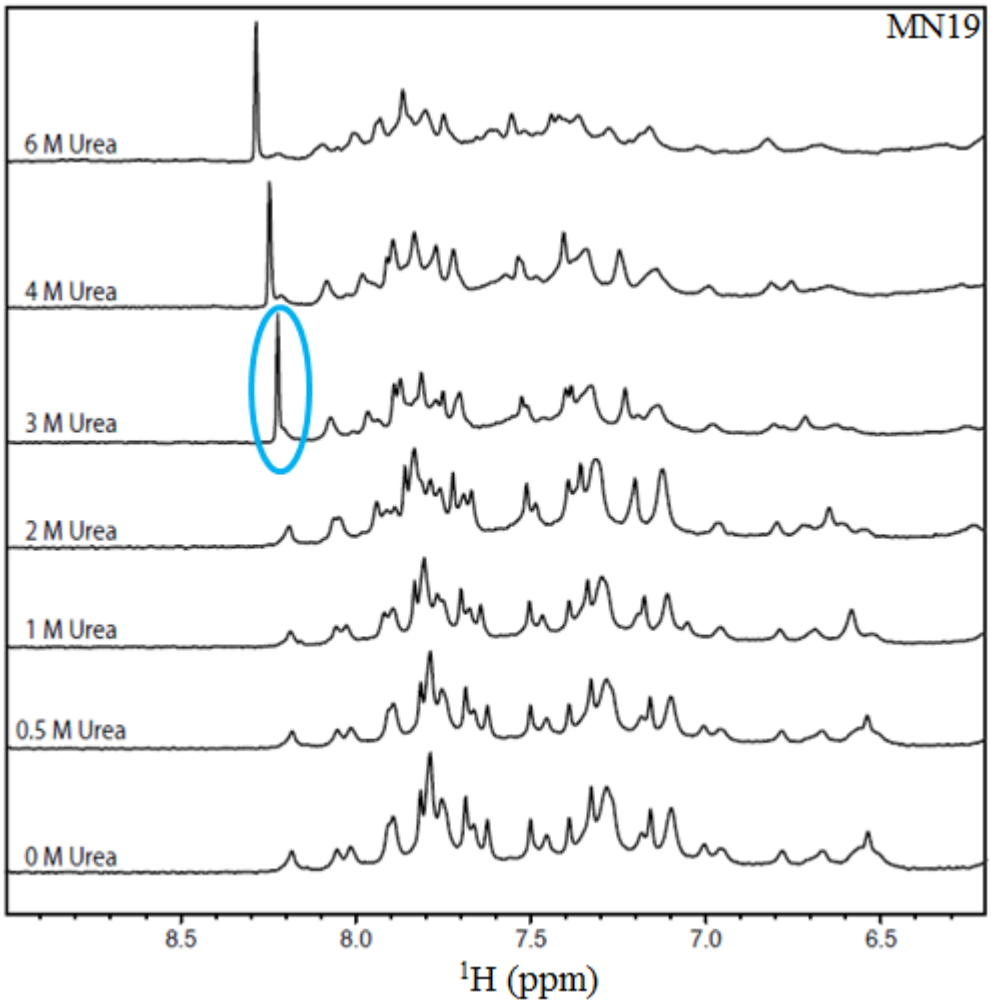

Figure 5.2: Chemical denaturation of MN19 monitored by 1D ^{1}H-NMR**.** Spectra were acquired in 99.99% D_2O at 5 °C with the concentrations of urea indicated. The peak showing up at 8.2 ppm is hypothesized to be that of quinine and appears as a result of a significant loss in the binding affinity of MN19.

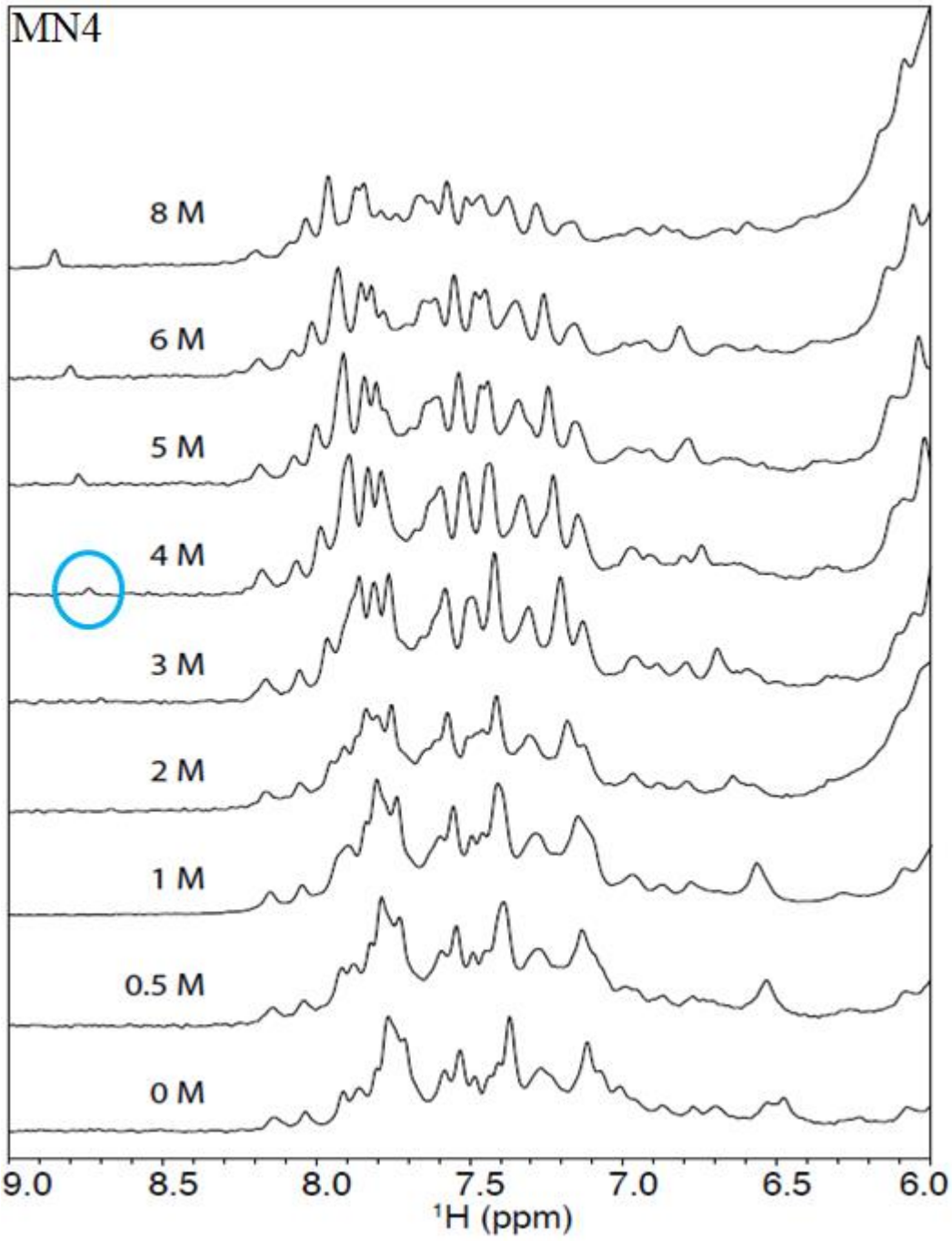

Figure 5.3: Chemical denaturation of MN4 monitored by 1D ^{1}H-NMR**.** Spectra were acquired in 99.99% D_2O at 5 °C with the concentrations of urea indicated. The peak showing up at 8.7 ppm is hypothesized to be that of quinine and appears as a result of a significant loss in the binding affinity of MN4.

5.2.2 Fluorescence Studies of Aptamer Secondary Structure

To determine whether short stem 1 aptamers exist as entirely solvent exposed single strands in the absence of ligand or as partially folded molecules with some loosely folded stems, both MN4 and MN19 were developed into molecular beacons. As shown in Figure 5.4, a molecular beacon consists of a molecule which contains both a fluorescent tag and quencher. For this study, a fluorescein tag was placed at the 5' terminus of the aptamer and a Dabcyl quencher at the 3' terminus.

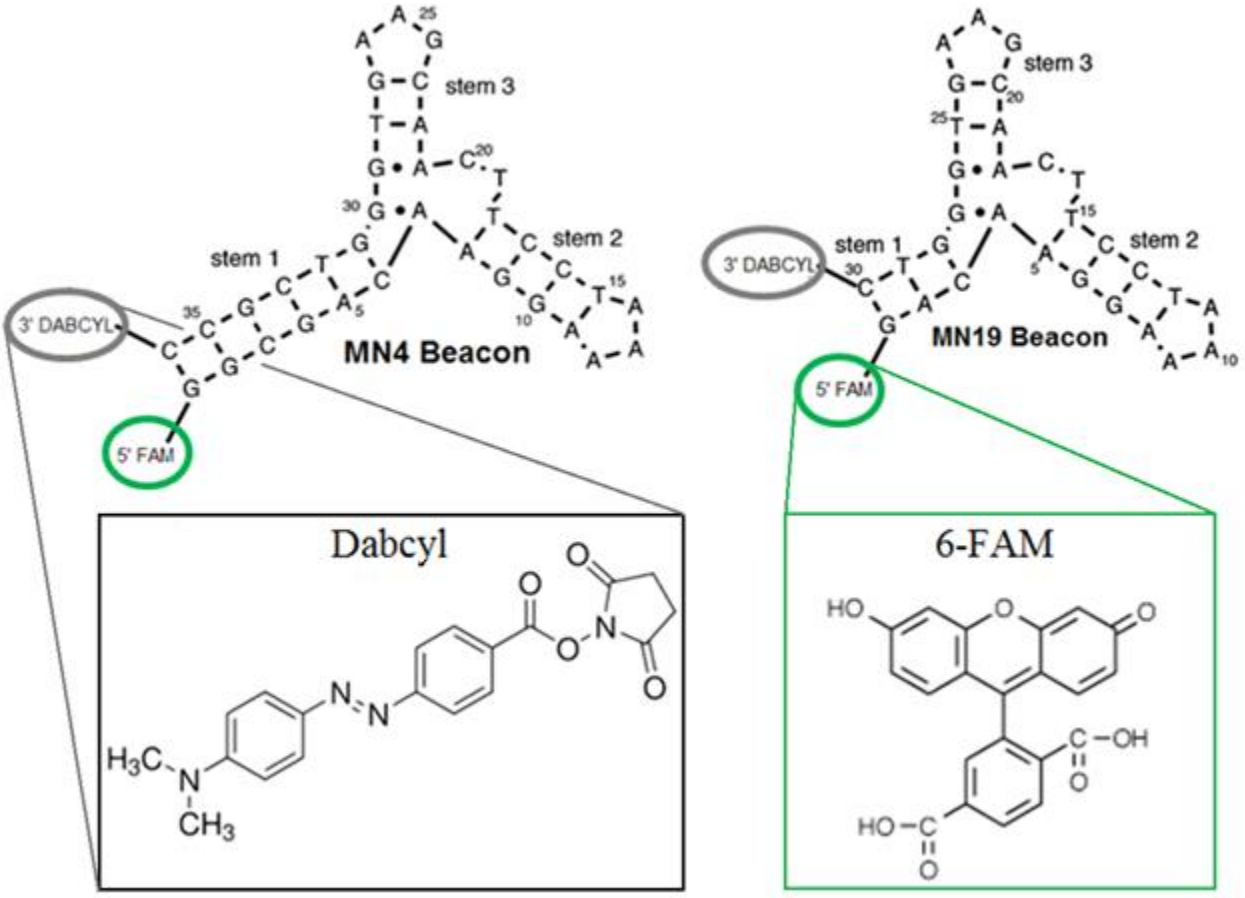

Figure 5.4: MN4 and MN19 molecular beacon constructs. Each contain a 5' fluorescein attachment and 3' Dabcyl universal quencher. The chemical structure of Dabcyl and fluorescein are included.

The underlying assumption in this study was that unbound MN19 should be almost entirely unfolded as demonstrated by NMR studies reported in chapter 4. However, SAXS data has so far been somewhat contradictory to this conclusion. Under the assumption of unbound MN19 being completely unfolded, a relatively high background fluorescence should be observed for the aptamer where increasing the concentration of urea should have little to no effect on the level of observed fluorescence. Conversely, MN4 should display relatively low background fluorescence that rises as the concentration of urea is increased as a result of the secondary structure destabilization. Quite interestingly, both MN4 and MN19 exhibited unfolding curves where MN4 was 50% unfolded by approximately 4 M, 4.8 M and 6 M urea (ligand free, cocaine bound, quinine bound), respectively (Figure 5.5) MN19 was determined to be 50% unfolded by at 2.3 M, 2.4 M, and 4.4 M urea (ligand free, cocaine bound, quinine bound), respectively. (Figure 5.6)

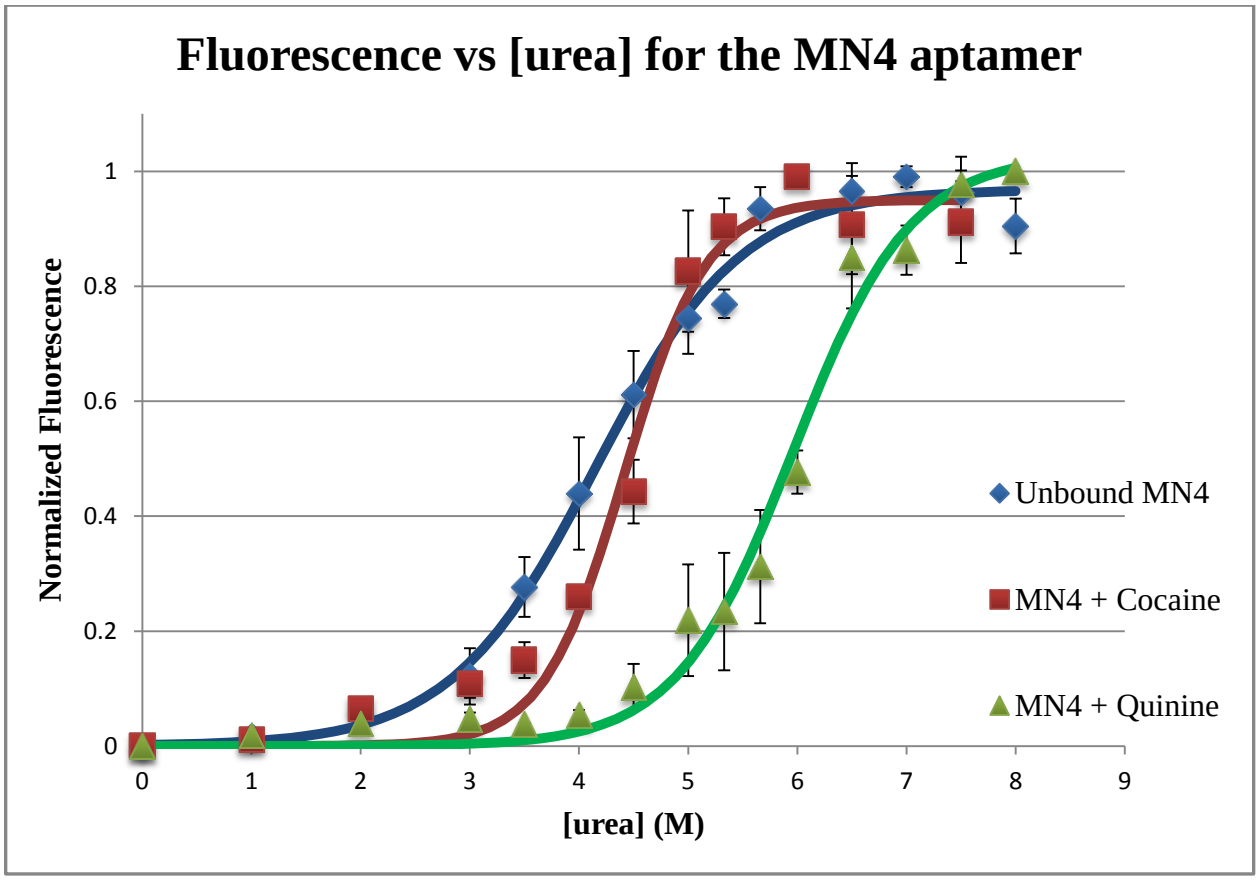

Figure 5.5: Fluorescence vs [urea] for free, cocaine, and quinine bound MN4. Samples were prepared with a 40 fold molar excess of ligand in bound samples. Readings were acquired at room temperature Stability measurements were taken to be the point at which 50% of the aptamer is unfolded represented by the inflection points of the curves.

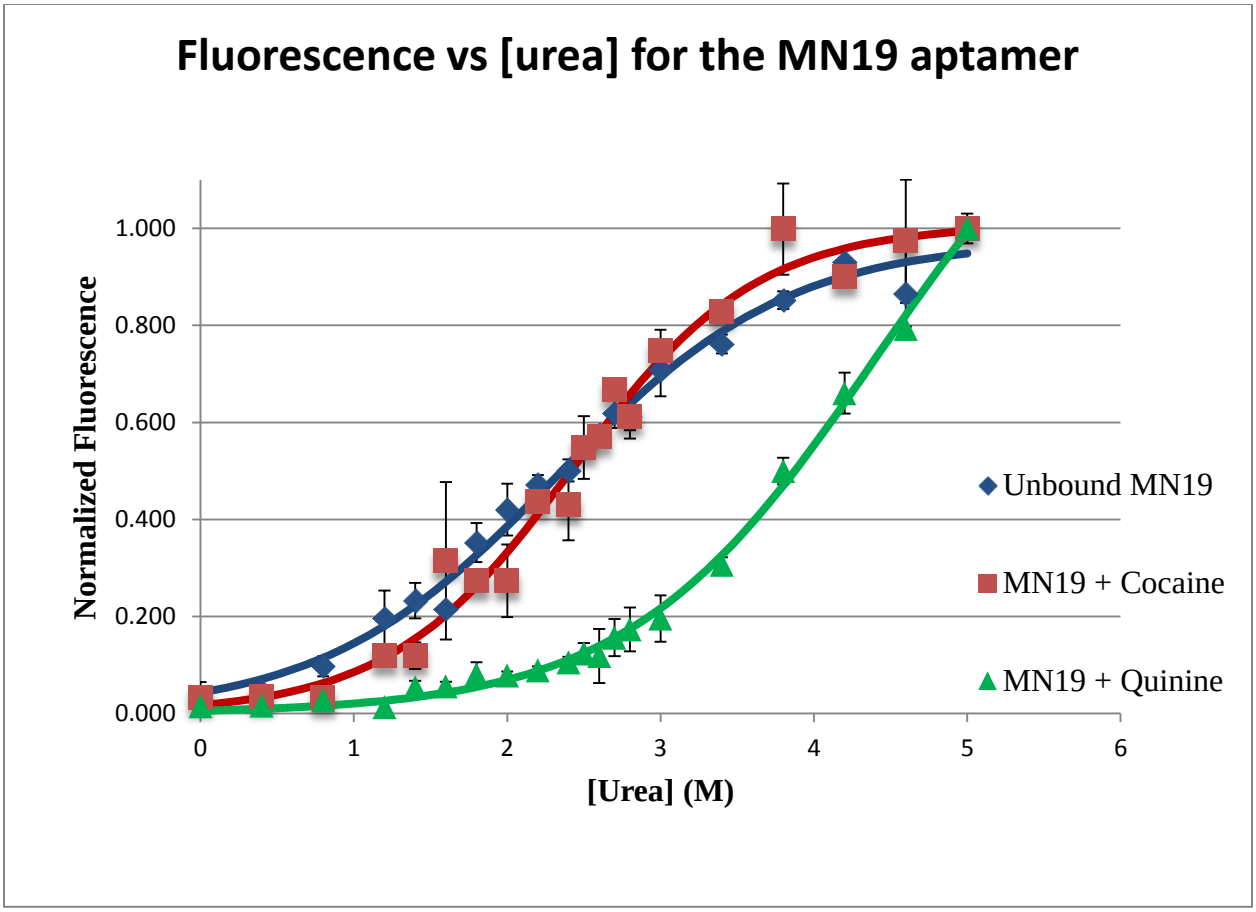

Figure 5.6: Fluorescence vs [urea] for free, cocaine, and quinine bound MN19. Samples were prepared with a 40 fold molar excess of ligand in bound samples. Readings were acquired at room temperature Stability measurements were taken to be the point at which 50% of the aptamer is unfolded represented by the inflection points of the curves.

5.3 Discussion

5.3.1 Resolving the Discrepancy between ITC and NMR Data

Due to the absence of any observable peaks in the 1D NMR studies of MN19, it was always hypothesized that MN19 is mostly unfolded in the unbound state. Studies with urea were undertaken to verify this hypothesis. By observing enthalpy of binding at varying concentrations of urea, ITC studies were able to verify that MN19 may not be as unfolded as it was previously assumed to be. By the proposed mechanism, in the presence of ligand, aptamers must both bind and fold. Both processes have an associated enthalpy. Had MN19 been completely unfolded to begin with, the trends in enthalpy vs urea concentration would not have been as apparent as they

are in Figure 5.1. It is noted that as urea concentration is increased, the enthalpy value becomes increasingly more negative, suggesting that more folding must be taking place, up to a point where binding is no longer observed due to severe structural destabilization. Such a trend would be unlikely to exist if MN19 was completely unfolded, as the enthalpy of folding would always be nearly identical under all concentrations of urea. This is perhaps better illustrated in Figure 5.7, an ITC derived result which demonstrates a much larger ΔC_p associated with binding of MN19 in the presence of urea.

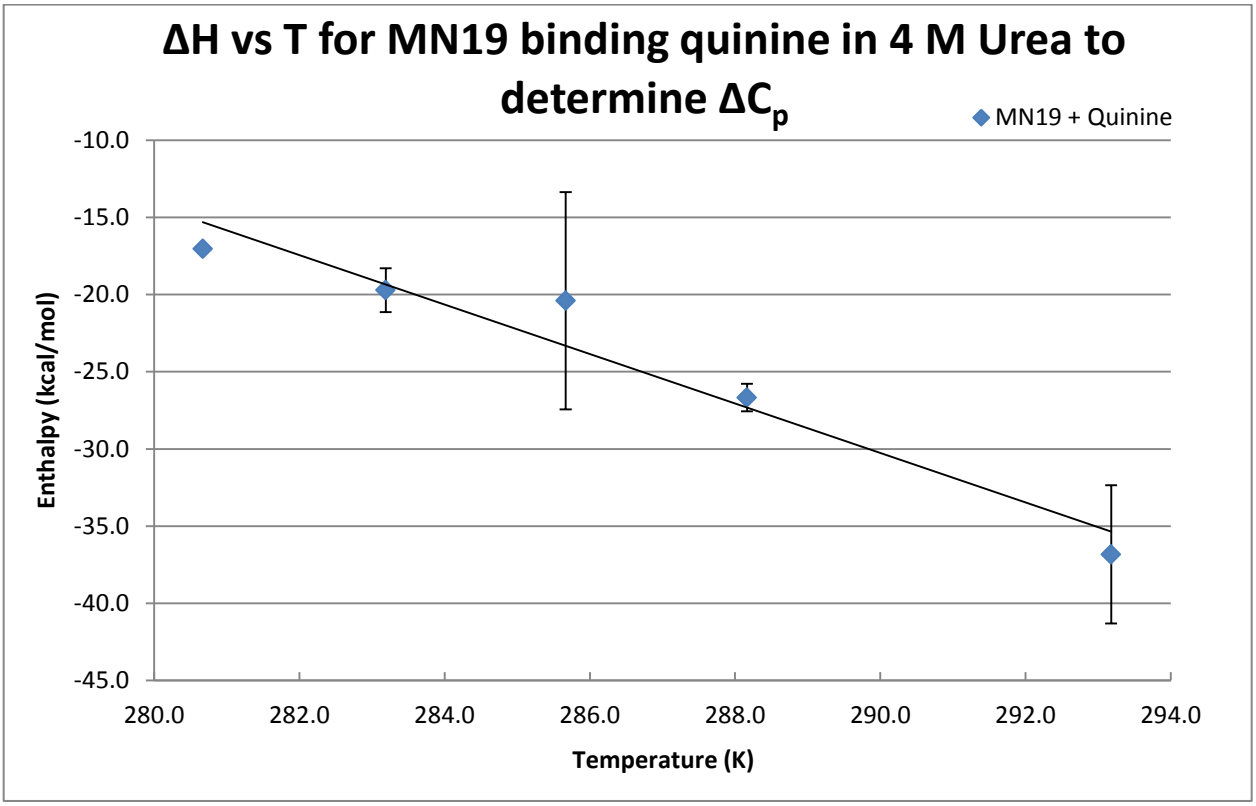

Figure 5.7: ΔC_p obtained for MN19 binding quinine in the presence of 4 M urea. Linear regression of this data yields a ΔC_p value of (-1.6 ± 0.9) kcal mol^{-1} K^{-1}. Data points are resultant of singular experiments and were conducted at the indicated temperatures in Buffer A in the presence of 4 M urea.

The value of ΔC_p obtained for MN19 binding quinine in the presence of 4 M urea is (-1.6 ± 0.9) kcal mol^{-1} K^{-1}. Compared to the ΔC_p of (-922 ± 51) cal mol^{-1} K^{-1} obtained for MN19 in previous studies that took place in the absence of urea (Chapter 2) it becomes evident that MN19 exhibits a greater degree of folding with urea present. This points to the fact that MN19 very likely exists in a loosely folded state in the absence of ligand. Although previous NMR studies of MN19 showed a clear transition from unfolded to folded, it is more apparent now that the lack of observable imino signals in the unbound state of MN19 is not direct evidence of the lack of a secondary structure. Rather, it is very likely the case that in the unbound state, the imino protons are in a loosely folded configuration that allows for rapid hydrogen exchange due to increased solvent accessibility. Introducing the ligand then imparts some rigidity to the aptamer, limiting the rate of exchange and giving rise to the signals that are typically observed.

5.3.2 NMR Evidence for a Partially Folded Structure in MN19

NMR data acquired in the presence of urea was seeking to establish a clear transition between bound and unbound aptamer states. Unfortunately, the spectra did not produce very conclusive results. Instead of seeing peaks coalesce at high concentrations of urea, they simply broadened out leading to messier spectra which were more difficult to interpret. The transition from folded to unfolded is somewhat apparent when the region around 8.7 ppm in the MN4 spectrum and 8.2 ppm in the MN19 spectrum are noted. The upfield peaks are observable in 3 M urea for MN19 and 4 M urea for MN4. These peaks are attributed to free quinine in solution resultant of the aptamer becoming destabilized, however this is not stated with 100% confidence. A ^{1}H-NMR spectrum of free quinine displays the most downfield peak at roughly 8.4 ppm. This corresponds to a proton within the aromatic ring system of quinine.[226] While Figure 5.3 might support this hypothesis on the basis of a single peak which changes intensity as urea concentration is increased, Figure 5.4 shows the sudden appearance of a single peak with unchanging intensity with addition of urea. The difference in observed behaviour for this peak in the two spectra makes it somewhat difficult to draw any clear conclusion about the true nature of this peak. If these peaks do correspond to quinine, they may serve as a strong indication for the transition between folded and unfolded aptamer states and reflects well on MN19 having some loosely folded structure in the unbound state. Gauging the exact point at which the aptamer becomes unfolded by

NMR has not been accomplished given the rather poor quality of the data. This makes it somewhat difficult to correlate with the ITC and fluorescence data. However, all three of these methods have suggested that MN4 exhibits higher resistance to urea denaturation than MN19.

5.3.3 Fluorescence Spectroscopy Reveals the Partially Folded Unbound State of MN19

The fluorescence data acquired was produced with the assumption that the MN4 and MN19 molecular beacons would begin to unfold as the concentration of urea was gradually increased. This would slowly disrupt the hydrogen bonding network within the aptamer forcing the fluorescein and Dabcyl to become separated. As their separation grew, a rise in fluorescence was expected. Figures 5.5 & 5.6 demonstrate the results of this study and are in line with what was predicted. The data obtained was fit to the equation described originally by Santoro & Bolen,[178] and redefined by Lawrence et al.[179]

The point at which the aptamer was 50% unfolded was taken to be the inflection point in the curve and reflects overall aptamer stability. The first set of fluorescence experiments demonstrated primarily that the aptamers are stable to unusually high concentrations of urea. Such high resistance to chemical denaturation is a rather unusual property. Most enzymes lose most functionality beyond 1 M urea.[180] MN4 shows greater resistance to denaturation by urea over MN19, as demonstrated previously by ITC and NMR.

The most important conclusion drawn from the data however is that if MN19 was almost entirely unfolded in the absence of ligand as predicted by early NMR studies, it would not have produced the unfolding curve displayed in Figure 5.6. This is very strong evidence for the existence of some type of loosely folded structure which may contain all of the expected secondary structure elements but with weakly established hydrogen bonds with direct implications on acquiring NMR spectra as described in 5.3.1.

5.4 Conclusion

The fluorescence unfolding studies reported here provide strong evidence for MN19 (and by extension probably all short stem cocaine-binding aptamer constructs) existing in a loosely folded configuration. Very similar evidence of this loosely folded state was established by SAXS discussed in Chapter 3. The relatively high resistance to chemical denaturation by the cocaine-binding aptamer has also been demonstrated. This property is rather unusual but adds a tremendous amount of functionality to the aptamer. Both biosensing and non-biosensing studies may be able to take advantage of the fact that the cocaine-binding aptamer retains most of its functionality in harsh denaturing conditions where a majority of other functional biomolecules lose their functionality.

5.5 Experimental Methods

5.5.1 Materials and Sample Preparation

MN4 and MN19 aptamers and molecular beacons (5' Fluorescein and 3' Dabycl modifications) were obtained from IDT. Aptamer samples were dissolved in water and then exchanged three times in a 3 kDa molecular weight cutoff concentrator with sterilized 1 M NaCl and then washed at least three times with ddH_2O. Molecular beacons were not purified prior to use in fluorescence-based experiments. Aptamer concentrations were determined by absorbance spectroscopy using the calculated extinction coefficients. Urea was obtained from Bioshop (cat. no. URE002). Cocaine hydrochloride and quinine hemisulfate monohydrate (cat. no. 145912 Aldrich) were obtained from Sigma Aldrich. Stock solutions of urea, cocaine, and quinine were prepared by dissolving the appropriate weight of cocaine or quinine-hemisulfate monohydrate in ddH_2O.

5.5.2 Fluorescence Spectroscopy

Fluorescence-based experiments were conducted using both a Cary Eclipse Fluorescence Spectrophotometer equipped with 4 cell changer and a Nanodrop 3300 Fluorospectrometer. Data were analyzed using the accompanying Cary WinUV and Nanodrop ND-3300 (version 2.6.0) software. Molecular beacon samples were prepared at a concentration of 450 nM and cocaine- and quinine-bound samples contained a 200 – 400 fold molar excess of quinine or cocaine so as to

ensure samples were at least 90% bound. All samples were annealed prior to addition of ligand by heating in a hot water bath for 3 minutes followed by cooling on ice for 10 - 15 minutes. All samples were prepared in ddH_2O to which the appropriate volume of 8.5 M stock urea (at pH 7.4) was added, generating a gradient from 0 – 8 M. 500 μL samples were prepared and placed into quartz cuvettes of 1 cm path length for analysis on the Cary spectrophotometer. Data was acquired using simple reads with a single ddH_2O blank and all samples with one replicate each at absorption of 495 nm and emission at 520 nm. 3 μL of the working solutions were used for analysis on the Nanodrop fluorospectrometer. Data was acquired in a manner very similar to that already described but did not include replicate measurements.

5.5.3 Isothermal Titration Calorimetry

ITC was performed using a MicroCal VP-ITC instrument. Data were fit to a one-site binding model using Origin 5.0 software. Samples were degassed prior to use with the MicroCal Thermo Vac unit. All experiments were corrected for the heat of dilution of the titrant. Quinine and aptamer solutions were prepared in 20 mM Tris (pH 7.4), 140 mM NaCl, and 5 mM KCl (Buffer A) with the appropriate amount of urea (obtained from an 8 M stock solution). Binding experiments were performed with aptamer solutions of 20 μM using quinine concentrations of 0.312 mM at indicated temperatures. All titrations were performed with the aptamer in the cell and the ligand, as the titrant, in the needle. Aptamer samples were heated in a boiling water bath for 3 minutes and cooled on ice before use in an ITC experiment to allow the DNA aptamer to anneal. Standard binding experiments consisted of 35 successive 8 μL injections spaced every 300 s where the first injection was 2 μL. Experimental concentration for the MN4 construct was established using a c value of 50.

5.5.4 NMR Spectroscopy

NMR experiments on the aptamer samples were performed using a 600 MHz Bruker Avance spectrometer equipped with a $^{1}H–^{13}C–^{15}N$ triple-resonance probe equipped with triple-axis magnetic-field gradients. All NMR spectra were acquired in 99.99% D_2O at 5 °C. This condition was accomplished by lyophilizing samples of quinine-bound MN4 and MN19 and appropriate volumes of urea (separately) followed by resuspension in D_2O. Aptamer samples were then

lyophilized a second time and resuspended in 99.99% D_2O prior to their use on the NMR spectrometer. Generating the urea gradients shown was then accomplished by mixing the resuspended aptamer sample directly with the previously lyophilized urea. Aptamer sample volumes were 500 μL and were prepared at 0.4 mM with a 1.1 fold excess of quinine. All data were processed and analyzed using NMRPipe/NMRDraw.[187]

6 A Bifunctional Aptamer Binding Cocaine and Deoxycholic Acid Has Potential as a Nucleic Acid Logic Gate

The content reported within this chapter includes experimental results and data analysis which is in preparation for publication.

6.1 Introduction

A number of research studies have been conducted in recent years outlining the development and use of bifunctional aptamers. A fair amount of these studies have applied bifunctional aptamers in biosensing platforms, quoting their high affinities and bifunctional recognition.[195-197] Other studies have presented bifunctional aptamers as a means of molecular separation and strategies for purification.[198] In a majority of cases, aptamers that independently recognized a target can be modified to incorporate regions that promote hybridization with other aptamers, or aptamer sequences can simply be fused into a single subunit, all while retaining recognition of their native targets. The research presented in this study extends the use of bifunctional aptamers to the realm of DNA computing. Over the past two decades, with new tools, a large interest has grown in the computational power of DNA. Investigations with respect to this field showed that DNA machines were capable of solving a variety of computational problems within a reasonable time frame and with the right framework, could rival the computational speeds of some of the most powerful supercomputers.[199,200] In 2003, Stojanovic and Stefanovic demonstrated a DNA based machine capable of playing through a game of Tic Tac Toe using a deoxyribozyme as a core component.[201] Although the framework of this DNA machine was fluorescence based and as such, required ample time to complete a single game, it implemented DNA based logic function and was a significant advancement within the field.[201] Unfortunately, this DNA gaming machine was not reusable and cannot be extended beyond the function for which it was designed.

The research presented here outlines the potential for using aptamers, specifically a bifunctional steroid- and cocaine-binding aptamer (Figure 6.1) as a DNA logic gate which may allow for both rapid and reusable framework in a DNA based machine. With the structure switching nature of some of the aptamers presented in previous studies as well as in the numerous biosensing studies,

it is hypothesized that electrical transmission can be used as the primary source of information transfer in a DNA based machine. The unfolded and folded states of the aptamers may effectively direct an electrical signal. The premise here would be effective charge transfer along a DNA strand – a phenomenon well studied and known to occur.[202]

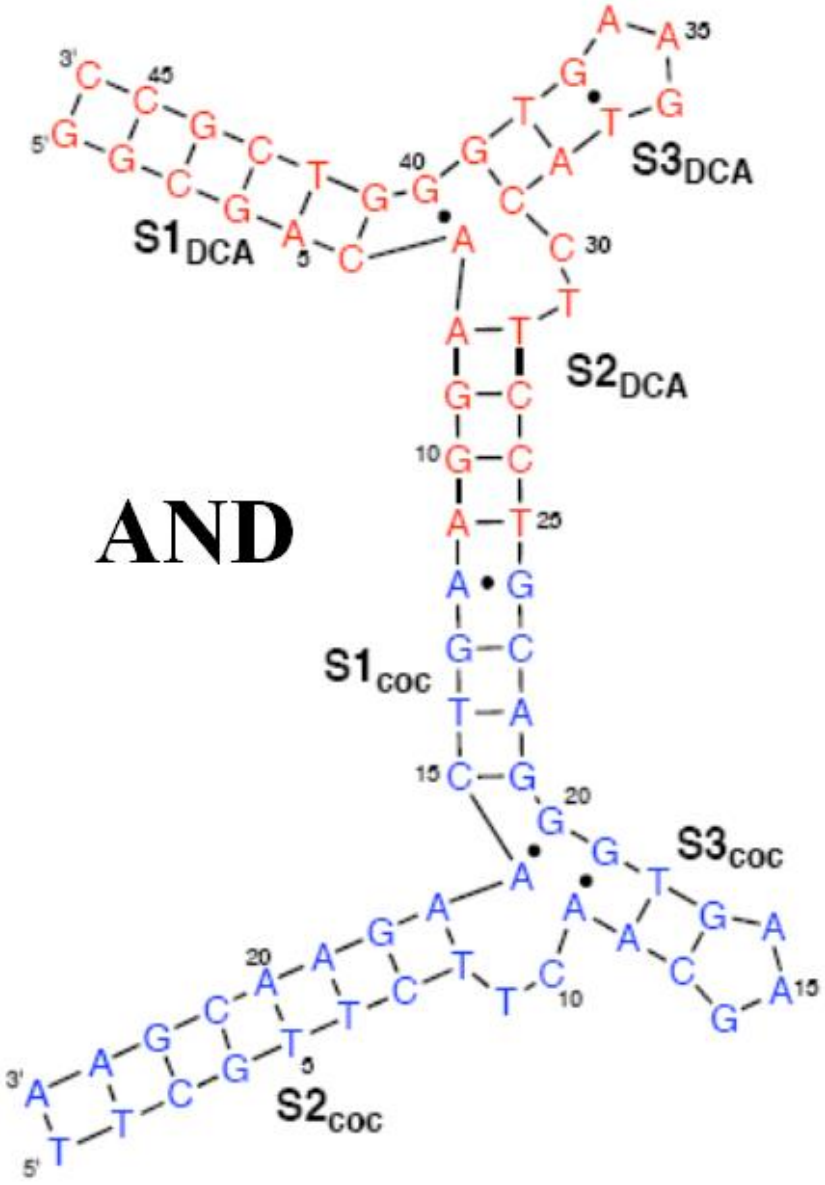

Figure 6.1: Secondary structure and sequence of a split bifunctional "AND" aptamer. Aptamers are split by removing the triloop sequences and fused through stem 2 of the steroid binding construct and stem 1 of the cocaine-binding construct. The DCA-binding "WC" aptamer and a cocaine-binding aptamer are utilized in this bifunctional construct.

6.2 Results and Discussion

6.2.1 Thermodynamics of Binding for the AND Aptamer

The 'AND' bifunctional aptamer was developed on the premise that the two strands hybridize and fold in the presence of both, DCA and cocaine. To test whether the aptamer displayed bifunctionality, ITC studies were employed to measure thermodynamics of binding in the presence of DCA and cocaine. Results are summarized in Table 6.1 below.

Table 6.1 Thermodynamic parameters for the interaction of the bifunctional 'AND' aptamer construct with cocaine and DCA.[a]

Sample and Titrant	K_d (μM)	ΔH (kcal mol^{-1})	−TΔS (kcal mol^{-1})
AND + cocaine	12 ± 3	-12 ± 5	7 ± 5
AND + DCA	16 ± 7	-11 ± 2	5 ± 3
[AND•cocaine] + DCA[b]	15	-5.3	-1.1
[AND•DCA] + cocaine	27 ± 1	-11 ± 2	6 ± 1
AND + equimolar cocaine/DCA	11 ± 1	-32.5 ± 0.2	25.9 ± 0.1

[a]Data acquired at 20 °C in 20 mM Tris (pH 7.4), 140 mM NaCl, and 5 mM KCl (Buffer A). The values reported are averages of 2–3 individual experiments. The error range reported is one standard deviation. [b]Data reported is of a single experiment which did not yield meaningful error values through the fitting procedure. All data was processed using a 1 site binding model.

Looking at the enthalpy of binding, titrations of the AND aptamer with cocaine and DCA yield values of (-12 ± 5) and (-11 ± 2) kcal mol^{-1}, respectively. In the event that the aptamer binds both ligands, a minimum of the sum of these enthalpies is expected, calculated here to be -23 ± 7 kcal mol^{-1} It is noted then that a titration of the AND aptamer with an equimolar mixture of DCA and cocaine yielded an enthalpy value of (-32.5 ± 0.2) kcal mol^{-1}. This provides strong evidence for the bifunctional nature of the aptamer. Additionally, titrations of one ligand into the aptamer already complexed with the other ligand resulted in binding with thermodynamic parameters in the expected ranges obtained previously (Table 3.3, Table 3.4).

6.2.2 Bifunctional Aptamer Constructs as Logic Gates

While the results in this study do not test the practical application of the bifunctional AND aptamer in a DNA based machine, the ITC results do present strong evidence for the bifunctional

nature of the aptamer which may have potential to function as an AND logic gate. In the absence of one or both ligands, the 3 way junction within the aptamer might be unstable such that effective charge transfer along the DNA strand would be very limited. It is hypothesized that effective charge transfer could only take place when the 3 way junctions are stabilized in presence of both ligands. Hence the requirement for cocaine *AND* DCA. Under these same principles, it is also possible to construct a variety of other bifunctional aptamer logic gates, such as an OR gate illustrated in Figure 6.2 below.

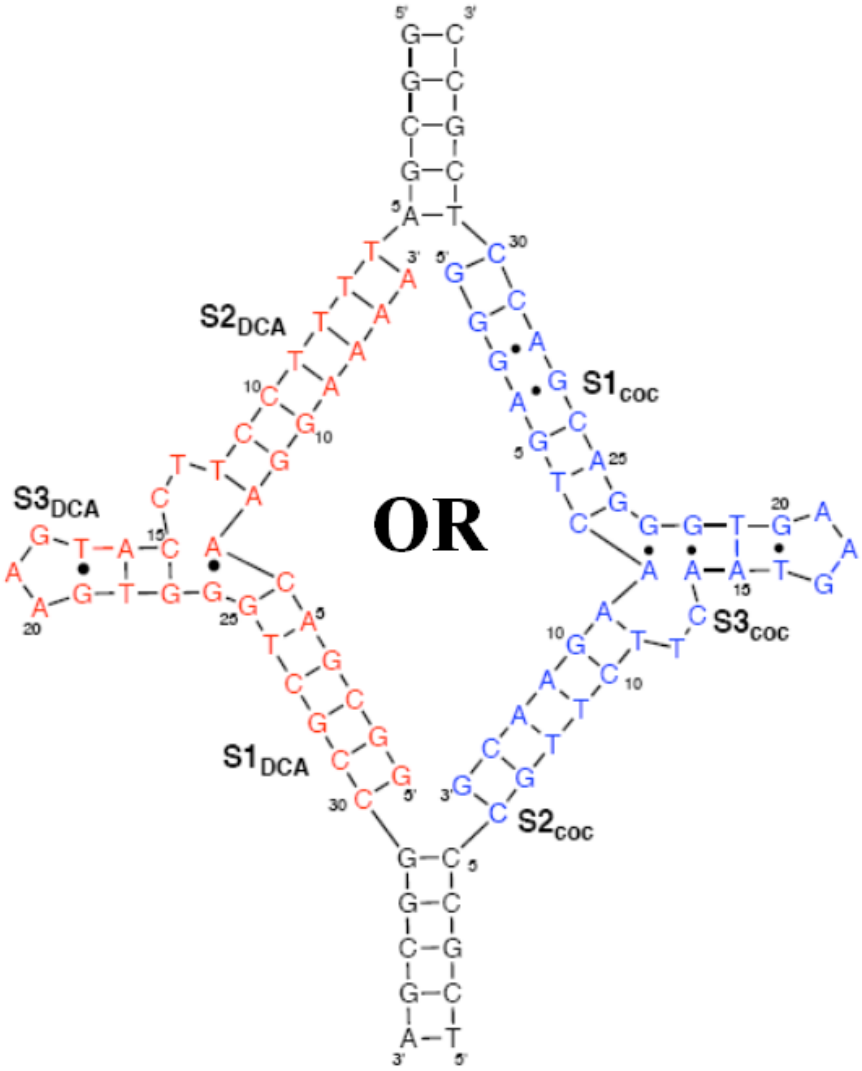

Figure 6.2: Secondary structure and sequence of a split bifunctional "OR" aptamer. The DCA-binding (WC) aptamer and the cocaine-binding aptamer (MN4) are utilized in this bifunctional construct with linker regions allowing for the hybridization of the two. The OR gate, as presented, would only require the presence of one ligand, either cocaine or DCA to effectively transfer charge along the DNA strand.

6.3 Conclusion

In summary, a bifunctional aptamer was developed utilizing the frame work of the cocaine-binding aptamer. Various configurations of the aptamers can be used to produce a variety of logic gates with potential uses in DNA based machines that function on electrical transmission.

6.4 Experimental Methods

6.4.1 Materials and Sample Preparation

Aptamer samples were obtained from the University of Calgary DNA Service. DNA samples were dissolved in water and then exchanged three times in a 3 kDa molecular weight cutoff concentrator with sterilized 1 M NaCl and then washed at least three times with distilled deionized H_2O. Except where noted, all DNA samples were exchanged with 20 mM Tris (pH 7.4), 140 mM NaCl, and 5 mM KCl (Buffer A) three times before use. Aptamer concentrations were determined by absorbance spectroscopy using the calculated extinction coefficients. Sodium deoxycholate (DCA) was obtained from Sigma-Aldrich (part number D6750). Stock solutions of DCA and cocaine were prepared by weight and dissolved in the desired buffer. Cocaine hydrochloride was obtained from Sigma Aldrich.

6.4.2 Isothermal Titration Calorimetry

ITC was performed using a MicroCal VP-ITC. Data was analyzed using accompanying Origin software and fit to a one-site binding model. Samples for ITC analysis were degassed before use with the MicroCal Thermo Vac unit. All experiments were corrected for the heat of dilution of the titrant. Unless otherwise specified, cocaine, DCA, and aptamer solutions were prepared in Buffer A. All binding experiments were performed at 20 °C with aptamer solutions ranging from 20 to 85 μM. Cocaine and DCA concentrations used were 0.3 – 1.3 mM. All aptamer samples were heated in a boiling water bath for 3 min and cooled on ice prior to use in a binding experiment to allow the DNA aptamer to anneal. Binding experiments consisted of 35 successive 8 μL injections every 300 s where the first injection was 2 μL. Tests for bifunctionality were conducted by first performing titrations of either cocaine or DCA into the free aptamer followed by titration of the unused ligand into an aptamer-ligand complex. Finally, titrations using equimolar mixtures of DCA and cocaine were performed.

7 Concluding Remarks

7.1 Summary of Research

This research project started off exploring what is very often referred to as a "black box" within the realm of biomolecular interactions – functional studies of biomolecules. Although the functional study of biomolecules in general is not a brand new area of research, the functional study of aptamers is a largely unexplored domain within the field of biomolecular interactions and is largely due to the emergence of aptamers only two and a half decades ago. Technological advancements over the years have allowed for (looking at aptamers specifically) the development of novel laboratory techniques which have started to shed some light on the behaviour of aptamers and also see their practical application as presented in Chapter 1.

ITC is one such novel technique, which within this research has allowed for a complete thermodynamic profile of the cocaine-binding aptamer. Of course, ITC is hardly limited to the study of aptamers and can be utilized to study other ligand-target systems. Chapter 2 illustrated the use of ITC in obtaining the thermodynamics of binding for the cocaine-binding aptamer to its original cocaine ligand. Results in this chapter established a ligand-binding mechanism consistent with what was seen by NMR studies. Although NMR predates the use of ITC in the study of biomolecular interactions, it has been an invaluable tool in assisting with characterizing the behaviour of the cocaine-binding aptamer and also served to establish the secondary structure illustrated throughout all of the research studies presented here.

Chapter 3 added additional techniques into the mix, exploring aptamer behaviour using DOSY-NMR, SAXS, and QELS. All of these techniques have a relatively recent emergence, but allow for the characterization of two very important properties of biomolecules – shape and size. A major goal of this research project was to attain a 3-dimensional snapshot of the cocaine-binding aptamer (or any of its variants). While these methods, individually or collectively, did not supply the complete 3-dimensional package, they did send the research down a critical path – understanding the nature of the unbound state of short stem 1 variants of the cocaine-binding aptamer. These short stem 1 constructs have led to some inconsistencies among the various techniques discussed and a more in depth study of these constructs was completed in chapter 5.

Chapter 4 revisited the cocaine-binding aptamer but studied binding thermodynamics with a new ligand – quinine. Using the aforementioned tools, the study identified the ligand-binding site in the aptamer and went far more in depth with respect to how the aptamer binds its ligand, looking specifically at intermolecular forces. Also noteworthy was the striking similarity between cocaine and quinine binding by the aptamer which allows for further study of the aptamer without the worry of any legal implications associated with obtaining its original ligand – cocaine.

The results discussed in chapter 3 served as the impetus for all of the studies undertaken in chapter 5. The transitions seen for short stem 1 constructs were quite puzzling and the fluorescence study that was conducted served to piece it all together. Although previous studies using NMR suggested an unfolded to folded transition, it is now understood that the aptamer is unlikely to exist as a completely uncoiled strand in solution. Rather, there is some degree of order that exists but is not clearly identifiable by means of NMR.

Chapter 6 served to provide some ideas of practical applications using the cocaine-binding aptamer. While DNA computing was a hot topic for a brief period, aptamers could very well serve as a scaffold to revitalize this idea. While the research outlined here does not outline the means by which one could construct a DNA based machine using aptamers, given that binding sites function independently, it does suggest that bifunctional aptamers can be used as logic gates – a critical component to functional computers. ITC results within this study demonstrated the bifunctionality of the AND aptamer. It is likely that the suggested DNA charge transfer experiments would need to be conducted prior to its considerations in an actual DNA based machine.

7.2 Future Directions

One of the primary focuses of this research was to obtain a clear 3-dimensional perspective of the cocaine-binding aptamer. The research began with crystal screens in which hundreds of conditions were tested. Although some conditions yielded microcrystals were, even with optimization of these conditions, crystals suitable for diffraction could not be isolated. The conditions which yielded these microcrystals were then optimized by means of robotic screening which performed several thousand new optimized screens but none to date have yielded crystals suitable for

diffraction. As a potential solution, future research on the crystallization of the cocaine-binding aptamer is focused on using a chimeric aptamer consisting of DNA and RNA domain. One such chimera is the MN4 aptamer fused with the U1A RNA tag – a tag which is known to crystallize well under specified conditions. It is with much hope that the aptamer would then co-crystalize with this domain allowing for crystals that are suitable for diffraction.

An alternative method to the elusive crystal screen was to utilize NMR. 3D-NMR techniques using ^{13}C-^{15}N-labelled DNA was a potential avenue in structural elucidation of the cocaine-binding aptamer. However, the approach to generating labelled DNA of this type has its own drawbacks. A procedure detailing the synthesis of ^{13}C-^{15}N-labelled RNA is detailed, but it is uncertain whether this can be extended directly to the synthesis of similarly labelled DNA.

Whichever route is taken or ends up being successful, the rationale behind any of these structural studies would be to obtain critical information with respect to how the aptamer is arranged both in the absence and presence of a ligand. Although previous studies have identified the binding site, obtaining evidence for the proposed binding site by means of a 3-dimensional structure would serve to both reinforce our confidence in the various techniques applied previously and also greatly improve our understanding of the behaviour of the cocaine-binding aptamer. We would ultimately seek a better understanding of how the aptamer binds its ligand and the basis for the established interaction. Through this, it might be possible to identify an even better ligand, although, it was previously suggested that if the cocaine-binding aptamer interacts with so many ligands, perhaps it was never the best aptamer in the first place and warrants the use of SELEX to identify a better aptamer for cocaine.

Ultimately, the research within this dissertation has demonstrated the application of a number of biophysical tools in the functional study of the cocaine-binding aptamer. It has shed some light on the interaction of the aptamer with several ligands and this information may find its use in the study and application of other DNA structures based on 3-way or multi-way junctions. It is with the greatest hope that it may even find its usefulness in the field of aptamers as a whole.

8 Appendix 1: Application and Mechanics of Isothermal Titration Calorimetry

ITC is an instrument well attuned to studying bimolecular interactions. With this instrument, heat released or absorbed during a binding event can be directly measured and using this data, thermodynamic parameters such as reaction stoichiometry (n), K_a, ΔH, ΔS, and hence ΔG, can all be determined from a single binding experiment.[190] The convenience of obtaining all of this information from a single titration has made the ITC a useful technique for studying all facets of biomolecular interaction including, but not limited to, protein/ligand, protein/protein, protein/nucleic acid, and perhaps more recently, nucleic acid/ligand interactions.[203,204] More recent developments have also allowed for the application of ITC in the study of enzyme kinetics, biological activity assessment, as well as binding mechanisms and the impact of conformational changes that take place with binding.[205]

ITC has become a rather popular analytical tool since its emergence due to major improvements in instrument sensitivity. This is a major advantage for modern day ITC instruments where the standard machine can quite easily measure a K_a within the range of 10^8 - 10^9 M^{-1}. From the perspective of K_d, this is binding in approximately the nanomolar range. The breakthrough comes from a design using extremely sensitive electronic parts capable of detecting heat changes as small as 0.1 μcal with reasonable accuracy. For a binding event, the instrument typically reports a heat rate and as little as 0.1 μcal/sec is detectable with a detection limit at roughly half of this. This reinforces the ITC as an instrument that is ideal for characterizing reaction rates.[206]

Another great advantage of the ITC came with improvement in data analysis which has allowed for its use in the study of multi-site binding. Software that accompanies the ITC now typically allows for the processing of independent, sequential, cooperative (positive and negative) or competitive binding data.[207]

The VP-ITC instrument used in this research was manufactured by Microcal (USA), now part of Malvern (Malvern, UK). Major manufacturers of ITC instruments currently include Malvern and TA instruments.

A typical ITC experiment consists of titrating a solution of a chosen biomolecule (X) from the syringe into a sample cell which contains a solution of a potential binding candidate (Y).[207] For titrations involving small molecules and macromolecules, it is very common to place the small molecule in the syringe while the macromolecule is held within the sample cell. This, however, is not a necessity and a reverse titration is equally feasible.[204] Part of the rationale behind using the small molecule as the titrant is the attainable concentration and the cost factor. Figure 8.1 presents a cross sectional scheme of a typical ITC instrument.

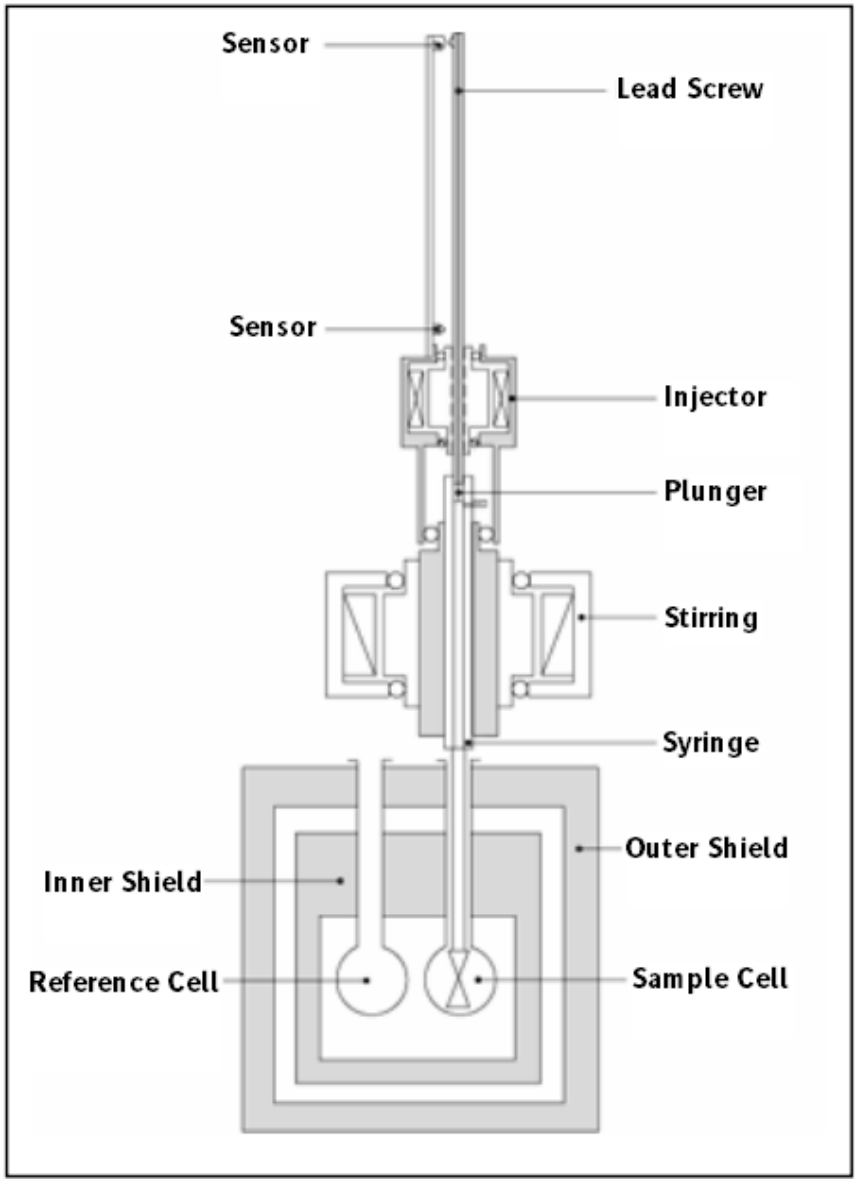

Figure 8.1: Cross section of a basic ITC instrument. Over a standard experiment, titrant stored in the syringe is injected into the sample cell which is constantly stirred. Image adapted from ref. 207.

Any heat released or absorbed from a binding event throughout a titration is detected by means of a feedback heater that maintains contact with the sample cell (Figure 8.2). Figure 8.1 reveals the presence of two cells, the sample cell and the reference cell. The reference cell does not house any reaction over the course of a titration and usually only contains water or an identical buffer solution to the sample cell. The ITC instrument attempts to maintain an identical temperature for both cells over the course of a titration. Generally, a user decided power level is input prior to a titration (dependent on how endothermic or exothermic one assumes the reaction to be) and the instrument establishes an equilibrium with the selected power level and chosen experimental temperature.[207]

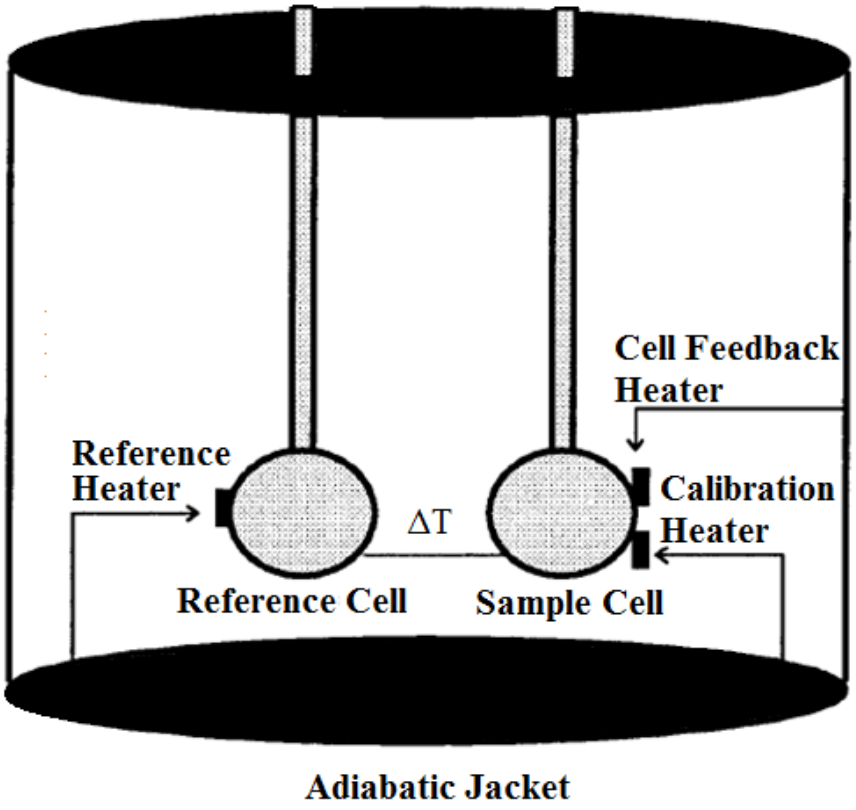

Figure 8.2: Layout of the sample and reference cell within the ITC instrument. The instrument attempts to maintain $\Delta T = 0$ by means of the cell feedback heater – also responsible for the data output by the instrument. Figure adapted from ref. 208.

The data output by the instrument is obtained directly from the cell feedback heater. As an example, an exothermic reaction would cause the temperature of the sample cell to rise slightly. With a newly established temperature difference between the sample and reference cell, the feedback heater cuts back on the power level which then appears as a dip in the computer generated thermogram. Conversely, an endothermic reaction would cause the feedback heater to require additional power to compensate for a loss in temperature, appearing as a spike in the thermogram. Figure 8.3 provides illustrations of thermograms for endothermic and exothermic reactions.

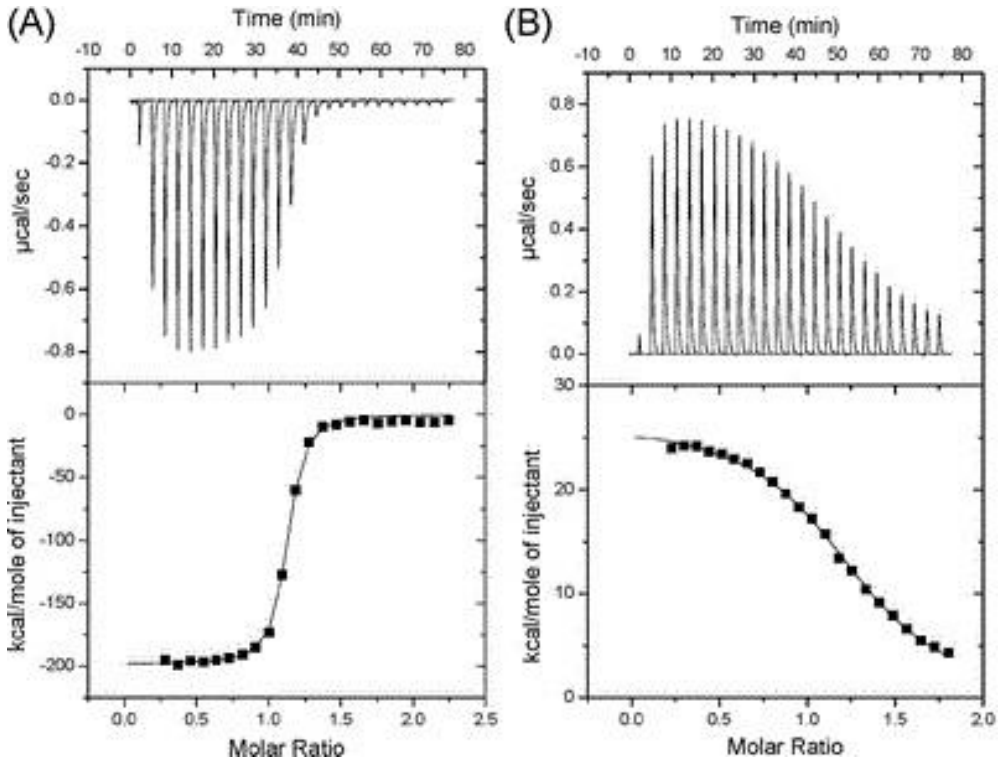

Figure 8.3: (A) Sample thermogram of an exothermic binding event measured by ITC. (B) Sample thermogram of an endothermic binding event measured by ITC. The top half of the thermogram displays the raw data acquired by the computer from the cell feedback heater. The bottom half is processed data obtained through integration of the raw data over time. Data can then be fit to a binding model suitable for the binding event generating the solid sigmoidal curve which also outputs all of the thermodynamic parameters for the binding event. Figure adapted from ref. 209.

As the titration progresses, less heat is absorbed or released. This is the most general trend observed for titration reactions of this nature as the components being titrated form complexes. All injection volumes being equal, the initial injection will usually have the greatest amount of heat absorbed or released as all of the macromolecule is available to react with the titrant. In the final steps of the titration, most of the macromolecule is no longer available for binding, and so most of the titrant remains unreacted. Dependent on the K_a of the reaction, at a large enough molar excess of the titrant, the reaction is said to be saturated. All observed heat absorbed or released at this point is due to that of diluting the titrant in buffer and not of additional binding events, also a component of the titration reaction which must also be accounted for as a part of standard data processing procedures.[207]

Basic data processing using the ITC involves the use of Gibbs free energy to compute the thermodynamic parameters for a binding event. Gibbs free energy is described in two ways: $\Delta G = -RT\ln K_a$ and $\Delta G = \Delta H - T\Delta S$ where R is the gas constant and T is the temperature of the system in Kelvin. Knowing K_a and ΔH, the instrument is able to output ΔS. Values for K_a and ΔH are obtained through an iterative algorithm that utilizes nonlinear least squares fitting. The procedure also attempts to fit reaction stoichiometry at the same time. Good titration data (operating within the detection window) usually provides an accurate initial guess for ΔH and n. This makes the iterative procedure to obtain K_a rather quick. Poorer titration data however quite often requires the user's best initial guess prior to initiating the iterative process.[203,208]

For this reason, a guideline has been established to help users choose an appropriate concentration for titration experiments which is defined as the ITC "c" value. This value is defined as follows: $c = n \times K_a \times [\text{macromolecule}]$.[207] Experiments conducted with c values ranging between 10 and 500 typically yield titration data which is fairly easy to fit. Figure 8.4 illustrates how titration curves vary with different c values. Often times a user may not know the values of n or K_a. Under such conditions, it is often best to make an initial guess (typically micromolar binding with 1:1 reaction stoichiometry) as the shape of the thermogram following the first experiment will very often give the user an idea of what c value they are operating at. From this point it becomes more apparent in which direction sample concentrations should be altered.

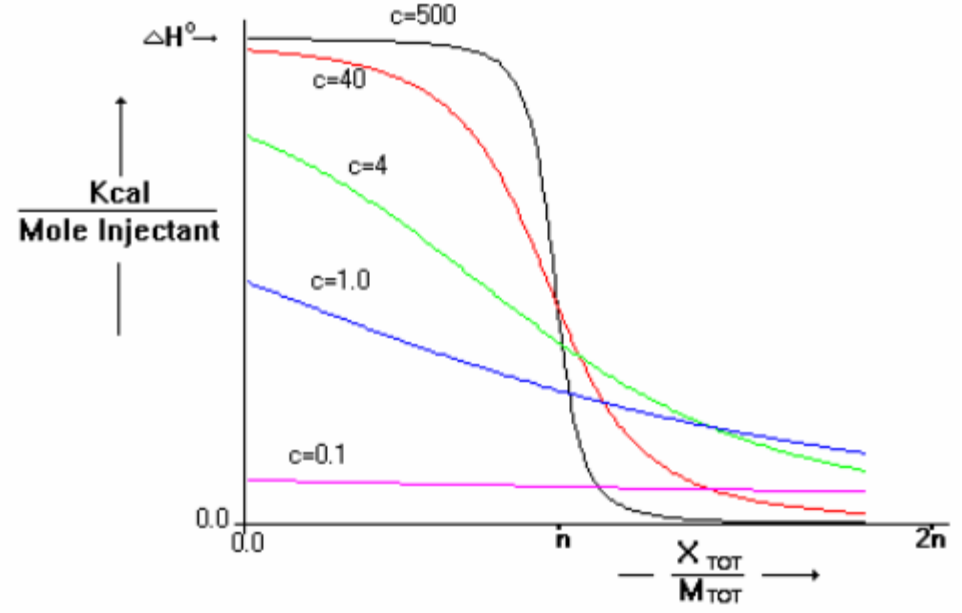

Figure 8.4: A representation of how the shape of the thermogram changes for an experiment conducted at different c values. The ideal experimental c value ranges from 10 – 500. Below 10, data fitting becomes difficult as establishing an initial guess for ΔH becomes increasingly difficult and thus has the potential to make this value inaccurate. Above 500, data fitting also becomes difficult as computing K_a accurately become problematic. A reaction which saturates too quickly cannot supply enough data near the inflection of the curve which is necessary for accurate computation of K_a. Figure obtained from ref. 207.

It should be noted that although experiments are best contained within a c range of 10 – 500, operating outside of this range can have its benefits, as outlined by some of the low-c titration procedures used within the research presented.[165] Likewise, competitive binding can be used to study tight binding ligands which would not make it possible to attain c values below 1000 or more.[210]

References

1) Mills, D.R., Peterson, R.L., Spiegelman, S. (1967) An extracellular Darwinian experiment with a self-duplicating nucleic acid molecule. PNAS **58**(1), 217–224.

2) Spiegelman, S., Haruna, I. (1965) PNAS **54**(4), 1189-1193.

3) Miele, E.A., Mills, D.R., Kramer, F.R. (1983) Autocatalytic replication of a recombinant RNA. J. Mol. Biol. **171**(3), 281-295.

4) Kramer, F.R., Mills, D.R., Cole, P.E., Nishihara, T., Spiegelman, S. (1974) Evolution in vitro: sequence and phenotype of a mutant RNA resistant to ethidium bromide. J Mol. Biol. **89**, 719-736.

5) Tuerk C., Gold, L. (1990) Systematic evolution of ligands by exponential enrichment: RNA ligands to bacteriophage T4 DNA polymerase. Science **249**(4968), 505-510.

6) Ellington, A.D., Szostak, J.W. (1990) In vitro selection of RNA molecules that bind specific ligands. Nature **346**, 6287, 818-822.

7) Gold, L., Janjic, N., Jarvis, T., Schneider, D., Walker, J.J., Wilcox, S.K., Zichi, D. (2012) Aptamers and the RNA World, Past and Present. Cold Spring Harb Perspectives in Biology **4**, a003582

8) Cech, T.R., Zaug, A.J., Grabowski, P. J. (1981) In vitro splicing of the ribosomal RNA precursor of Tetrahymena: involvement of a guanosine nucleotide in the excision of the intervening sequence. Cell **27**, 487–496.

9) Guerrier-Takada C, Gardiner K, Marsh T, Pace N, Altman S. (1983) The RNA moiety of ribonuclease P is the catalytic subunit of the enzyme. Cell **35**(3 pt 2), 849-857.

10) Woese, C. (1967) The genetic code. New York: Harper and Row.

11) Djordjevic M. (2007) SELEX experiments: new prospects, applications and data analysis in inferring regulatory pathways. Biomol Eng. **24**(2), 179-189.

12) Sun, H., Zhu, X., Lu, P.Y., Rosato, R.R., Tan, W., Zu, Y. (2014) Oligonucleotide Aptamers: New Tools for Targeted Cancer Therapy. Molecular Therapy Nucleic Acids **3**, e182.

13) Klussmann, Sven. (2006) The Aptamer Handbook: Functional Oligonucleotides and Their Applications. Weinheim: Wiley-VCH, Print.

14) Gold, L. (1995) Oligonucleotides as research, diagnostic, and therapeutic agents. J. Biol. Chem **270**(23), 13581-13584.

15) Reader, J.S., Joyce, G.F. (2002) A ribozyme composed of only two different nucleotides. Nature **420**, 841–844.

16) Rogers, J., Joyce, G.F. (1999) A ribozyme that lacks cytidine. Nature **402**, 323–325.

17) Anderson, J.R., Mukherjee, D., Muthukumaraswamy, K., Moraes, K.C.M., Wilusz, C.J., Wilusz, J. (2006) Sequence-specific RNA binding mediated by the RNase PH domain of components of the exosome. RNA **12**(10), 1810–1816.

18) Bock, L.C., Griffin, L.C., Latham, J.A., Vermaas, E.H., Toole, J.J. (1992) Selection of single-stranded DNA molecules that bind and inhibit human thrombin. Nature **355**(6360), 564 - 566.

19) Stoltenburg, R., Reinemann C., Strehlitz B. (2007) SELEX—A (r)evolutionary method to generate high-affinity nucleic acid ligands. Biomolecular Engineering **24**, 381–403.

20) Rockey et al. (2011) Rational truncation of an RNA aptamer to prostate-specific membrane antigen using computational structural modeling. Nucleic Acid Therapeutics **21**(5), 299-314.

21) Dassie et al. (2009) Systemic administration of optimized aptamer-siRNA chimeras promotes regression of PSMA-expressing tumors. Nature Biotechnology **27**, 839–846.

22) Kaur H., Yung, L-Y.L. (2012) Probing High Affinity Sequences of DNA Aptamer against VEGF165. PLoS ONE **7**(2), e31196.

23) Liu, X., Cao, G., Ding, H., Zhang, D., Yang, G., Liu, N., Fan, M., Shen, B., Shao, N. (2004) Screening of functional antidotes of RNA aptamers against bovine thrombin. FEBS Letters **562**(1), 125–128.

24) Cong, X. (2006) Development of aptamer based targeted reversibly attenuated probes. Retrospective Theses and Dissertations. Paper 1500.

25) Lee, C.H., Lee, Y.J., Kim, J.H., Lim, J.H., Kim, J.-H., Han, W., Lee, S.-H., Noh, G.-J., Lee, S.W. (2013) Inhibition of Hepatitis C Virus (HCV) Replication by Specific RNA Aptamers against HCV NS5B RNA Replicase. J. Virol. **87**(12), 7064-7074.

26) Dey, A.K., Griffiths, C., Lea, S.M., James, W. (2005) Structural characterization of an anti-gp120 RNA aptamer that neutralizes R5 strains of HIV-1. RNA **11**, 873-884.

27) Blind, M., Blank, M. (2015) Aptamer Selection Technology and Recent Advances. Molecular Therapy Nucleic Acids **4**, e223.

28) Hamula, C.L.A., Guthrie, J.W., Zhang, H., Li, X.-F., Le, X.C. (2006) Selection and analytical applications of aptamers. Trends in Analytical Chemistry **25**(7), 681-691.

29) Lorenz, C., von Pelchrzim, F., Schroeder, R. (2006) Genomic systematic evolution of ligands by exponential enrichment (Genomic SELEX) for the identification of protein-binding RNAs independent of their expression levels. Nature Protocols **1**(5), 2202–2212.

30) Kim M.Y., Jeong, S. (2011) In vitro selection of RNA aptamer and specific targeting of ErbB2 in breast cancer cells. Nucleic Acid Therapeutics **21**, 173–178.

31) Kuwahara, M., Ohsawa, K., Kasamatsu, T., Shoji, A., Sawai, H., Ozaki, H. (2005) Screening of a glutamic acid-binding aptamer from arginine-modified DNA library. Nucleic Acids Symposium Series (Oxf.) **49**, 81–82.

32) Ohsawa, K., Kasamatsu, T., Nagashima, J., Hanawa, K., Kuwahara, M., Ozaki, H., Sawai, H. (2008) Arginine-modified DNA aptamers that show enantioselective recognition of the dicarboxylic acid moiety of glutamic acid. Anal. Sci. **24**, 167–172.

33) Janas, T. (2011) The selection of aptamers specific for membrane molecular targets. Cell Mol. Biol. Lett. **16**(1), 25-39.

34) Guyer, R., Koshland Jr., D.R. (1989) The molecule of the year. Science **246** (4937), 1543-1546.

35) Garibyan, L., Avashia, N. (2013) Polymerase Chain Reaction. Journal of Investigative Dermatology **133**, e6.

36) Rahman, Md.T., Uddin, M.S., Sultana, R., Moue, A., Setu, M. (2013) Polymerase Chain Reaction (PCR): A Short Review. Anwer Khan Modern Medical College Journal **4**(1), 30-36.

37) Ishmael, F.T., Stellato, C. (2008) Principles and applications of polymerase chain reaction: basic science for the practicing physician. Ann Allergy Asthma Immunol. **101**(4), 437-443.

38) Musheev, M.U., Krylov, S.N. (2006) Selection of aptamers by systematic evolution of ligands by exponential enrichment: Addressing the polymerase chain reaction issue. Analytica Chimica Acta **564**, 91–96.

39) Tolle, F., Wilke, J., Wengel, J., Mayer, G. (2014) By-Product Formation in Repetitive PCR Amplification of DNA Libraries during SELEX. PLoS One **9**(12), e114693.

40) Conrad, R.C., Baskerville, S., Ellington, A.D. (1995) In vitro selection methodologies to probe RNA function and structure. Mol. Div. **1**, 69–78.

41) Krylov, S.N. (2005) NECEEM for development, characterisation and analytical utilisation of aptamers. LabPlus International.

42) Cibiel, A., Quang, N.N., Gombert, K., Thézé, B., Garofalakis, A., Ducongé, F. (2014) From ugly duckling to swan: unexpected identification from cell-SELEX of an anti-Annexin A2 aptamer targeting tumors. PLoS One **9**(1), e87002.

43) Sefah, K., Shangguan, D., Xiong, X., O'Donoghue, M.B., Tan, W. (2010) Development of DNA aptamers using Cell-SELEX. Nature Protocols **5**, 1169–1185.

44) Gold, L., Brown, D., He, Y.-Y., Shtatland, T., Singer, B.S., Wu, Y. (1997) From oligonucleotide shapes to genomic SELEX: Novel biological regulatory loops. PNAS **94**, 59–64.

45) Patel, D.J., Suri, A.K., Jiang, F., Jiang, L., Fan P.R., Kumar, A., Nonin, S. (1997) Structure, recognition and adaptive binding in RNA aptamer complex. J. Mol. Biol. **272**, 645–664.

46) Osborne, S.E., Ellington, A.E., (1997) Nucleic acid selection and the challenge of combinatorial chemistry. Chem. Rev. **97**, 349–370.

47) Hermann, T., Patel, D.J. (2000) Adaptive recognition by nucleic acid aptamers. Science **87**, 820–825.

48) Nadal, P., Pinto, A., Svobodova, M., Canela, N., O'Sullivan, C.K. (2012) DNA Aptamers against the Lup an 1 Food Allergen. PLoS ONE **7**(4), e35253.

49) Guo, H.C-T., De Abreu, D.M., Tillier, E.R.M., Saville, B.J., Olive, J.E. and Collins, R.A. (1993) Nucleotide sequence requirements for self-cleavage of Neurospora VS RNA. J Mol Biol **232**(2), 351-361.

50) Lafontaine, D.A., Norman, D.G., Lilley, D.M.J. (2001) Structure, folding and activity of the VS ribozyme: importance of the 2-3-6 helical junction. EMBO J. **20**(6), 1415–1424.

51) Jhaveri, S., Olwin, B., Ellington, A.D. (1998) In vitro selection of phosphorothiolated aptamers. Bioorg. Med. Chem. Lett. **8**, 2285–2290.

52) Keefe, A.D., Cload, S.T. (2008) SELEX with modified nucleotides. Current Opinion in Chemical Biology **12**, 448-456.

53) Ono, T., Scalf, M., Smith, L.M. (1997) 2'-Fluoro modified nucleic acids: polymerase-directed synthesis, properties and stability to analysis by matrix-assisted laser desorption/ionization mass spectrometry. Nucleic Acids Research **25**(22), 4581 – 4588.

54) Kuwahara, M., Hanawa, K., Ohsawa, K., Kitagata, R., Ozaki, H., Sawai, H. (2006) Direct PCR amplification of various modified DNAs having aminoacids: convenient preparation of DNA libraries with high-potential activities for in vitro selection. Bioorg. Med. Chem. **14**, 2518–2526.

55) Wilson, C., Szostak, J.W. (1995) In vitro evolution of a self-alkylating ribozyme. Nature **374**, 777–782.

56) Wilson, C., Szostak, J.W. (1998) Isolation of a fluorophore-specific DNA aptamer with weak redox activity. Chem. Biol. **5**, 609–617.

57) Wilson, D.S., Szostak, J.W. (1999) In vitro selection of functional nucleic acids. Ann. Rev. Biochem. **68**, 611–647.

58) Javaherian, S., Musheev, M.U., Kanoatov, M., Berezovski, M.V., Krylov, S.N. (2009) Selection of aptamers for a protein target in cell lysate and their application to protein purification. Nucleic Acids Res. **37**(8), e62.

59) Kanoatov, M., Javaherian, S., Krylov, S.N. (2010) Selection of aptamers for a non-DNA binding protein in the context of cell lysate. Analytica Chimica Acta **681**, 92–97.

60) Kim, Y.S., Gu, M.B. (2014) Advances in aptamer screening and small molecule aptasensors. Adv. Biochem. Eng. Biotechnol. **140**, 29–67.

61) Stoltenburg, R., Reinemann, C., Strehlitz, B. (2005). FluMag-SELEX as an advantageous method for DNA aptamer selection. Anal. Bioanal. Chem. **383**, 83–91.

62) Shangguan, D., Cao, Z., Meng, L., Mallikaratchy, P., Sefah, K., Wang, H., Li, Y., Tan, W. (2008) Cell-specific aptamer probes for membrane protein elucidation in cancer cells. J. Proteome Res. **7**, 2133–2139.

63) Ngubane, N.A., Gresh, L., Pym, A., Rubin, E.J., Khati, M. (2014) Selection of RNA aptamers against the M. tuberculosis EsxG protein using surface plasmon resonance-based SELEX. Biochem Biophys Res Commun. **449**(1), 114-9.

64) Mosing, R.K., Bowser, M.T. Isolating aptamers using capillary electrophoresis-SELEX (CE-SELEX). Methods Mol. Biol. **535**, 33-43.

65) Mayer, G., Ahmed, M.-S.L., Dolf, A, Endl, E., Knolle, P.A., Famulok, M. (2010) Fluorescence-activated cell sorting for aptamer SELEX with cell mixtures. Nature Protocols **12**, 1993-2004.

66) Viguera, E., Canceill, D., Ehrlich, S.D. (2001). Replication slippage involves DNA polymerase pausing and dissociation. The EMBO Journal **20**(10), 2587–2595.

67) Tabarzad, M., Kazemi, B., Vahidi, H., Aboofazeli, R., Shahhosseini, S., Nafissi-Varcheh, N. (2014) Challenges to Design and Develop of DNA Aptamers for Protein Targets. I. Optimization of Asymmetric PCR for Generation of a Single Stranded DNA Library. J. Pharm. Res. **13**(Suppl), 133–141.

68) Citartan, M., Tang, T.-H., Tan, S.-C., Hoe, C.-H., Saini, R., Tominaga, J,. Gopinath, S.C.B. (2012) Asymmetric PCR for good quality ssDNA generation towards DNA aptamer production. J. Sci. Technol. **34**(2), 125-131.

69) Berezovski, M.V., Musheev, M.U., Drabovich, A.P., Jitkova, J.V., Krylov, S.N. (2006) Non-SELEX: selection of aptamers without intermediate amplification of candidate oligonucleotides. Nature Protocols **1**, 1359–1369.

70) Tolle. F., Wilke, J., Wengel, J., Mayer, G. (2014) By-Product Formation in Repetitive PCR Amplification of DNA Libraries during SELEX. PLoS ONE **9**(12), e114693.

71) Fan, Chunhai. (2013) DNA Nanotechnology: From Structure to Function. Heidelberg: Springer, Print.

72) Md. Ashrafuzzaman. (2014) Aptamers as Both Drugs and Drug-Carriers. BioMed Research International **2014**, Article ID 697923, 21 pages.

73) MarketsandMarkets: Aptamers Market by Type (DNA, RNA, XNA), Application (Diagnostics, Therapeutics, R&D), Technology (SELEX, Other Technologies) & by End Users (Academic Research Institutes, Biotechnology & Pharmaceutical Companies, CRO) - Global Forecast to 2020." Top Market Reports. N.p., June 2015. Web. 23 July 2015.

74) Tuerk, C., MacDougal, S., Gold, L. (1992) RNA pseudoknots that inhibit human immunodeficiency virus type 1 reverse transcriptase. PNAS. **89**(15), 6988-6992.

75) Giver, L., Bartel, D.P., Zapp, M.L., Green, M.R., Ellington, A.D. (1993) Selection and design of high-affinity RNA ligands for HIV-1 Rev. Gene. **137**(1), 19-24.

76) Pan, W., Craven, R.C., Qiu, Q., Wilson, C.B., Wills, J.W., Golovine, S., Wang, J.F. (1995). Isolation of virus-neutralizing RNAs from a large pool of random sequences. PNAS **92**(25), 11509–11513.

77) Vater, A., Jarosch, F., Buchner, K., Klussmann, S. (2003) Short bioactive Spiegelmers to migraine-associated calcitonin gene-related peptide rapidly identified by a novel approach: tailored-SELEX. Nucleic Acids Research **31**(21), e130.

78) Vater, A., Klussmann, S. (20150) Turning mirror-image oligonucleotides into drugs: the evolution of Spiegelmer® therapeutics. Drug Discovery Today **20**(1), 147-155.

79) Jayasena, S.D. (1999) Aptamers: an emerging class of molecules that rival antibodies in diagnostics Clinical Chemistry **45**(9), 1628-1650.

80) Rohloff, J.C., Gelinas, A.D., Jarvis, T.C., Ochsner, U.A., Schneider, D.J., Gold, L., Janjic, N. (2014) Nucleic Acid Ligands With Protein-like Side Chains: Modified Aptamers and Their Use as Diagnostic and Therapeutic Agents. Molecular Therapy Nucleic Acids **3**, e201.

81) Ochsner, U.A., Green, L.S., Gold, L., Janjic, N. (2014) Systematic selection of modified aptamer pairs for diagnostic sandwich assays. BioTechniques **56**(3), 125–133.

82) Anthony D. Keefe, Supriya Pai & Andrew Ellington Nature Reviews Drug Discovery **9**, 537–550 and references therein.

83) Liu, J., Cao, Z., and Lu, Y. (2009) Functional Nucleic Acid Sensors. Chem. Rev. **109**, 1948−1998.

84) Cho, E. J., Lee, J.-W., Ellington, A. D. (2009) Applications of Aptamers As Sensors. Annu. Rev. Anal. Chem. **2**, 241−264.

85) Li, D., Song, S., and Fan, C. (2010) Target-Responsive Structural Switching for Nucleic Acid-Based Sensors. Acc. Chem. Res. **43**, 631−641.

86) Vallee-Belisle, A., Plaxco, K. W. (2010) Structure-Switching Biosensors: Inspired by Nature. Curr. Opin. Struct. Biol. **20**, 518−526.

87) Iliuk, A.B., Hu, L., Tao, W.A. (2011) Aptamer in Bioanalytical Applications. Anal. Chem. **83**, 4440−4452.

88) Famulok, M., Mayer, G. (2011) Aptamer Modules As Sensors and Detectors. Acc. Chem. Res. **44**, 1349−1358.

89) Du, Y., Li, B., and Wang, E. (2012) "Fitting" Makes "Sensing" Simple: Label-Free Detection Strategies Based on Nucleic Acid Aptamers. Acc. Chem. Res. **46**, 203−213.

90) Xing, H., Wong, N.Y., Xiang, Y., Lu, Y. (2012) DNA Aptamer Functionalized Nanomaterials for Intracellular Analysis, Cancer Cell Imaging and Drug Delivery. Curr. Opin. Chem. Biol. **16**, 429−435.

91) Zhou, W., Huang P.J., Ding J., Liu J. (2014) Aptamer-based biosensors for biomedical diagnostics. Analyst **139**(11), 2627 – 2640.

92) Song K.-M., Lee, S., Ban, C. (2012) Aptamers and Their Biological Applications. Sensors (Basel). **12**(1), 612–631.

93) Han, K., Liang, Z., Zhou, N. (2010) Design Strategies for Aptamer-Based Biosensors. Sensors **10**, 4541-4557.

94) Bruno, J.G. (2015) Predicting the Uncertain Future of Aptamer-Based Diagnostics and Therapeutics. Molecules **20**, 6866-6887.

95) Neumann, O., Zhang, D., Tam, F., La, S., Wittung-Stafshede, P., Halas, N.J. (2009) Direct Optical Detection of Aptamer Conformational Changes Induced by Target Molecules. Analytical Chem. **81**(24), 10002–10006.

96) Lou, K.-J. (2011) Imaging with aptamers. SciBX **4**(11).

97) Tan, X., Chen, W., Lu, S., Zhu, Z., Chen, T., Zhu, G., You, M., Tan, W. (2012) Molecular Beacon Aptamers for Direct and Universal Quantitation of Recombinant Proteins from Cell Lysates. Anal. Chem. **84**(19), 8272–8276.

98) Yamamoto, R., Baba, T., Kumar, P.K. (2000) Molecular beacon aptamer fluoresces in the presence of Tat protein of HIV-1. Genes to Cells. **5**(5), 389-96.

99) Hamaguchi, N., Ellington, A., Stanton, M. (2001) Aptamer beacons for the direct detection of proteins. Anal. Biochem. **294**(2), 126-31.

100) Stojanovic, M.N., Landry, D.W. (2002) Aptamer-based colorimetric probe for cocaine. JACS **124**(33), 9678-9679.

101) Xia et al. (2010) Colorimetric detection of DNA, small molecules, proteins, and ions using unmodified gold nanoparticles and conjugated polyelectrolytes. PNAS **107**(24), 10837–10841.

102) Zhao, W., Chiuman, W., Brook, M.A., Li, Y. (2007) Simple and Rapid Colorimetric Biosensors Based on DNA Aptamer and Non-crosslinking Gold Nanoparticle Aggregation. ChemBioChem **8**(7), 727–731.

103) Chen, Z., Tan, T., Zhang, C.,Yin, L., Ma, H., Ye, N., Qiang, H., Lin, Y. (2014) A colorimetric aptamer biosensor based on cationic polymer and gold nanoparticles for the ultrasensitive detection of thrombin. Biosensors and Bioelectronics. **56**, 46–50.

104) Savinov, A., Perez, C.F., Block, S.M. (2014) Single-molecule studies of riboswitch folding. Biochim. Biophys. Acta. **1839**(10), 1030-1045.

105) Garst, A.D., Edwards, A.L., Batey, R.T. (2011). Riboswitches: Structures and mechanisms. Cold Spring Harbor Perspectives in Biology **3**(6), a003533.

106) McDaniel, B.A., Grundy, F.J., Artsimovitch, I., Henkin, T.M. (2003) Transcription termination control of the S box system: direct measurement of S-adenosylmethionine by the leader RNA. PNAS **100**(6), 3083-3088.

107) Breaker, R.R. (2012) Riboswitches and the RNA World. Cold Spring Harbor Perspectives in Biology **4**(2), a003566.

108) Nahvi, A., Sudarsan, N., Ebert, M.S., Zou, X., Brown, K.L., Breaker, R.R. (2002) Genetic control by a metabolite binding mRNA. Chem. Biol. **9**(9), 1043–1049.

109) Mignone, F., Gissi, C., Liuni, S., Pesole, G. (2002) Untranslated regions of mRNAs. Genome Biology **3**(3), reviews(0004.1–0004.10)

110) Ray, P.S., Jia, J., Yao, P., Majumder, M., Hatzoglou, M., Fox, P.L. (2009) A stress-responsive RNA switch regulates VEGFA expression. Nature **457**, 915-919.

111) Stojanovic, M.N., de Prada, P., Landry, D.W. (2000) Fluorescent Sensors Based on Aptamer Self-Assembly. JACS **122**, 11547-11548.

112) Stojanovic, M.N., de Prada, P., Landry, D.W. (2001) Aptamer-Based Folding Fluorescent Sensor for Cocaine. JACS **123**, 4928-4931.

113) Huizenga, D.E., Szostak, J.W. (1995) DNA Aptamer that Binds Adenosine and ATP. Biochemistry **34**, 656-665.

114) Canada Border Services Agency. 2014. CBSA seizes 244 kg of suspected cocaine at the Port of Montréal. Retrieved from http://www.cbsa-asfc.gc.ca/media/release-communique/2014/018-eng.html accessed: 03/08/2015

115) Daniel Tencer. Cocaine Prices Dropping: Weak Economy, Streamlined Smuggling Operations Drive Down Cost Of 'White Lines'. The Huffington Post Canada. 04/18/2012. Retrieved from http://www.huffingtonpost.ca/2012/04/18/cocaine-prices-business-smuggling_n_1435028.html accessed: 03/08/2015

116) Baker, B.R., Lai, R.Y., Wood, McC.S., Doctor, E.H., Heeger, A.J., Plaxco, K.W. (2006) An Electronic, Aptamer-Based Small-Molecule Sensor for the Rapid, Label-Free Detection of Cocaine in Adulterated Samples and Biological Fluids. JACS **128**, 3138-3139.

117) Jufer, R.A., Wstadik, A., Walsh, S.L., Levine, B.S., Cone, E.J. (2000) Elimination of Cocaine and Metabolites in Plasma, Saliva, and Urine Following Repeated Oral Administration to Human Volunteers. Journal of Analytical Toxicology **24**(7), 467-477.

118) Liu, J., Lu, Y. (2006) Fast Colorimetric Sensing of Adenosine and Cocaine Based on a General Sensor Design Involving Aptamers and Nanoparticles. Angew. Chem. Int. Ed. **45**, 90 –94.

119) Yan, X., Cao, Z., Laub, C., Lu, J. (2010) DNA aptamer folding on magnetic beads for sequential detection of adenosine and cocaine by substrate-resolved chemiluminescence technology. Analyst, **135**, 2400–2407.

120) Kawano, R., Osaki, T., Sasaki, H., Takinoue, M., Yoshizawa, S.,Takeuchi, S. (2011) Rapid Detection of a Cocaine-Binding Aptamer Using Biological Nanopores on a Chip. JACS **133**, 8474–8477.

121) Sheng, Q., Liu, R., Zhang, S., Zheng, J. (2014) Ultrasensitive electrochemical cocaine biosensor based on reversible DNA nanostructure. Biosensors and Bioelectronics **51**, 191–194

122) Peters, J.E., Chou, J.Z., Ho, A., Reid, K., Borg, L., Kreek, M.J. (1996) Simplified quantitation of urinary benzoylecgonine in cocaine addiction research and for related pharmacotherapeutic trials. Addiction **91**(11), 1687-1697.

123) Stojanović, M.N., Green, E.G., Semova, S., Nikić, D.B., Landry, D.W. (2003) Cross-Reactive Arrays Based on Three-Way Junctions. JACS **125**(20), 6085–6089.

124) Elbaz, J., Shlyahovsky, B., Li, D., Willner, I. (2008) Parallel analysis of two analytes in solutions or on surfaces by using a bifunctional aptamer: applications for biosensing and logic gate operations. Chembiochem **9**(2), 232-239.

125) Cekan, P., Jonsson, E.O., Sigurdsson, S.T. (2009) Folding of the cocaine aptamer studied by EPR and fluorescence spectroscopies using the bifunctional spectroscopic probe Ç. Nucleic Acids Resesarch **37**(12), 3990-3995.

126) Porchetta, A., Vallée-Bélisle, A., Plaxco, K.W., Ricci, F. (2012) Using Distal-Site Mutations and Allosteric Inhibition To Tune, Extend, and Narrow the Useful Dynamic Range of Aptamer-Based Sensors. JACS **134** (51), 20601–20604.

127) Pei, R., Shen, A., Olah, M.J., Stefanovic, D., Worgall, T., Stojanovic, M.N. (2009) High-resolution cross-reactive array for alkaloids. Chemical Communications (22), 3193-3195.

128) Doherty, E.A., Doudna, J.A. (2000) Ribozyme structures and mechanisms. Annu. Rev. Biochem. **69**, 597–615.

129) Joyce, G.F. (2002) The antiquity of RNA-based evolution. Nature **418**, 214-221.

130) White, H.B. (1976) Coenzymes as fossils of an earlier metabolic state. J. Mol. Evol. **7**, 101–104.

131) Neves M.A., Reinstein O., Johnson P.E. (2010) Defining a stem length-dependent binding mechanism for the cocaine-binding aptamer. A combined NMR and calorimetry study. Biochemistry **49**(39), 8478-8487.

132) Lin, C.H., Patel, D.J. (1997) Structural basis of DNA folding andrecognition in an AMP-DNA aptamer complex: distinct architectures but common recognition motifs for DNA and RNA aptamers complexed to AMP. Chem. Biol. **4**, 817–832.

133) Williamson, J.R. (2000) Induced fit in RNA-protein recognition. Nat. Struct. Biol. **7**, 834–837.

134) Leulliot, N., Varani, G. (2001) Current topics in RNA-protein recognition: control of specificity and biological function through induced fit and conformational capture. Biochemistry **40**, 7946–7956.

135) Latham, M.P., Zimmermann, G.R., Pardi, A. (2009) NMR chemical exchange as a probe for ligand-binding kinetics in a theophylline-binding RNA aptamer. JACS **131**, 5052–5053.

136) Gilbert, S.D., Stoddard, C.D., Wise, S.J. (2006) Thermodynamic and kinetic characterization of ligand binding to the purine riboswitch aptamer domain. J. Mol. Biol. **359**, 754–768.

137) Garst, A.D., Heroux, A., Rambo, R.P., Batey, R.T. (2008) Crystal structure of the lysine riboswitch regulatory mRNA element. J. Biol. Chem. **283**, 22347–22351.

138) Lane, A., Martin, S.R., Ebel, S., Brown, T. (1992) Solution conformation of a deoxynucleotide containing tandem GA mismatched base pairs and 30-overhanging ends in d(GTGAACTT)2. Biochemistry **31**, 12087–12095.

139) Chou, S.-H., Chin, K.-H. (2001) Solution structure of a DNA double helix incorporating four consecutive non-Watson-Crick basepairs. J. Mol. Biol. **312**, 769–781.

140) Cheng, J.-W., Chou, S.-H., Reid, B.R. (1992) Base pairing geometry in GA mismatches depends entirely on the neighboring sequence. J. Mol. Biol. **228**, 1037–1041.

141) Greene, K.L., Jones, R.L., Li, Y., Robinson, H., Wang, A.H.-J., Zon, G., Wilson, W.D. (1994) Solution structure of a GA mismatch DNA sequence, d(CCATGAATGG)2 determined by 2D NMR and structural refinement methods. Biochemistry **33**, 1053–1062.

142) Li, Y., Zon, G., Wilson, W.D. (1991) NMR and molecular modeling evidence for a GA mismatch base pair in a purine-rich DNA duplex. PNAS **88**, 26–30.

143) Chou, S.-H., Chin, K.-H., and Wang, A. H.-L. (2003) Unusual DNA duplex and hairpin motifs. Nucleic Acids Research **31**, 2461–2474.

144) Ortiz-Lombardía, M., Cortés, A., Huertas, D., Eritja, R., Azorín, F. (1998) Tandem 5'-GA:GA-3' mismatches account for the high stability of the fold-back structures formed by the centromeric Drosophila dodeca-satellite. J. Mol. Biol. **277**, 757–762.

145) Ebel, S., Lane, A., and Brown, T. (1992) Very stable mismatch duplexes: structural and thermodynamic studies on tandem GA mismatches in DNA. Biochemistry **31**, 12083–12086.

146) Ke, S.-H., Wartell, R.M. (1996) The thermal stability of DNA fragments with tandem mismatches at a d(CXYG)d(CY0X0G) site. Nucleic Acids Research **24**, 707–712.

147) Gao, Y.G., Robinson, H., Sanishvili, R., Joachimiak, A., Wang, A.H.1999) Structure and recognition of sheared tandem GA base pairs associated with human centromere DNA sequence at atomic resolution. Biochemistry **38**, 16452 -16460.

148) Chou, S.-H., Cheng, J.-W., Fedoroff, O., Reid, B. R. (1994) DNA sequence GCGAATGAGC containing the human centromere core sequence GAAT forms a self-complementary duplex with sheared GA pairs in solution. J. Mol. Biol. **241**, 467–479.

149) Spolar, R. S., and Record, M., Jr. (1994) Coupling of local folding to site-specific binding of proteins to DNA. Science **263**, 777–784.

150) Gilbert, S.D., Stoddard, C.D., Wise, S.J. (2006) Thermodynamic and kinetic characterization of ligand binding to the purine riboswitch aptamer domain. J. Mol. Biol. **359**, 754–768.

151) Bishop, G.R., Ren, J., Polander, B.C., Jeanfreau, B.D., Trent, J.O., Chaires, J.B. (2007) Energetic basis of molecular recognition in a DNA aptamer. Biophys. Chem. **126**, 165–175.

152) Lin, P.-H., Yen, S.-L., Lin, M.-S., Chang, Y., Louis, S. R., Higuchi, A., and Chen, W.-Y. (2008) Microcalorimetrics studies of the thermodynamics and binding mechanism between L-tyrosinamide and aptamer. J. Phys. Chem. B **112**(21), 6665–6673.

153) Pilch, D.S., Kaul, M., Barbieri, C.M., and Kerrigan, J.E. (2003) Thermodynamics of aminoglycoside-rRNA recognition. Biopolymers **70**, 58–79.

154) Cowan, J.A., Ohyama, T., Wang, D., and Natarajan, K. (2000) Recognition of a cognate RNA aptamer by neomycin B: quantitative evaluation of hydrogen bonding and electrostatic interactions. Nucleic Acids Research **28**, 2935–2942.

155) Chaires, J.B. (2008) Calorimetry and thermodynamics in drug design. Annu. Rev. Biophys. **37**, 135–151.

156) Li, T., Li, B., and Dong, S. (2007) Adaptive recognition of small molecules by nucleic acid aptamers through a label-free approach. Chem. Eur. J. **13**, 6718–6723.

157) Neves M.A., Reinstein, O., Saad, M., Johnson P.E. (2010) Defining the secondary structural requirements of a cocaine-binding aptamer by a thermodynamic and mutation study. Biophys Chem. **53**(1), 9-16.

158) Reinstein et al. (2011) Engineering a structure switching mechanism into a steroid-binding aptamer and hydrodynamic analysis of the ligand binding mechanism. Biochemistry **50**(43), 9368 – 9376.

159) Freeman, R., Li, Y., Tel-Vered, R., Sharon, E., Elbaz, J., Willner, I. (2009) Self-assembly of supramolecular aptamer structures for optical or electrochemical sensing. Analyst **134**, 653–656.

160) Freeman, R., Sharon, E., Tel-Vered, R., Willner, I. (2009) Supramolecular cocaine-aptamer complexes activate biocatalytic cascades. JACS **131**, 5028–5029.

161) Z.-G. Wang, O.I. Wilner, I. Willner, Self-assembly of aptamer-circular DNA nanostructures for controlled biocatalysis, Nano Lett. 9 (2009) 4098–4102.

162) Kato, T., Yano, K., Ikebukuro, K., Karube, I. (2000) Interaction of three-way DNA junctions with steroids. Nucleic Acids Res. **28**, 1963−1968.

163) Lu, H., Chen, X., Zhan, C.-G. (2007) First-principles calculation of pK for cocaine, nicotine, neurotransmitters, and anilines in aqueous solution, J. Phys. Chem. B **111**, 10599 – 10605.

164) Green, E. Olah, M.J., Abramova, T,. Williams, L.R., Stefanovic, D., Worgall, T., Stojanovic, M.N. (2006) A rational approach to minimal high-resolution cross-reactive arrays. JACS **128**, 15278–15282.

165) Tellinghuisen, J. (2008) Isothermal titration calorimetry at very low c. Analytical Biochem. **373**, 395–397.

166) Tavares, T.J., Beribisky, A.V., Johnson, P.E. (2009) Structure of the Cytosine–Cytosine mismatch in the thymidylate synthase mRNA binding site and analysis of its interaction with the aminoglycoside paromomycin, RNA **15**, 911–922.

167) Reinstein, O., Yoo, M., Han, C., Palmo, T., Beckham, S.A., Wilce, M.C.J., Johnson, P.E. (2013) Quinine Binding by the Cocaine-Binding Aptamer. Thermodynamic and Hydrodynamic Analysis of High-Affinity Binding of an Off-Target Ligand, Biochemistry **52**, 8652−8662.

168) Bao, J., Krylova, S.M., Reinstein, O., Johnson, P. E., and Krylov, S.N. (2011) Label-Free Solution-Based Kinetic Study of Aptamer- Small-Molecule Interactions Reveals How Kinetics Control Equilibrium. Analytical Chem. **83**, 8387−8390.

169) Spiropulos, N.G., and Heemstra, J.M. (2012) Templating Effect in DNA Proximity Ligation Enables Use of Non-Bioorthogonal Chemistry in Biological Fluids. Artificial DNA: RNA & XNA **3**, 123− 128.

170) Muhuri, S., Mimura, K., Miyoshi, D., Sugimoto, N. (2009) Stabilization of Three-Way Junctions of DNA under Molecular Crowding Conditions. JACS **131**, 9268−9280.

171) Record, M. T., Jr., Anderson, C. F., and Lohman, T. M. (1978) Thermodynamic Analysis of Ion Effects on the Binding and Conformational Equilibria of Proteins and Nucleic Acids: The Roles of Ion Association or Release, Screening, and Ion Effects on Water Activity. Q. Rev. Biophys. **11**, 103−178.

172) Sigurskjold, B.W. (2000) Exact Analysis of Competition Ligand Binding by Displacement Isothermal Titration Calorimetry. Analytical Biochem. **277**, 260−266.

173) Wang, Z.-X. (1995) An exact mathematical expression for describing competitive binding of two different ligands to a protein molecule. FEBS Letters **360**(2), 111-114.

174) Kozin, M., Svergun, D.I. (2001) Automated Matching of High- And Low-Resolution Structural Models. J. Appl. Crystallogr. **34**, 33−41.

175) Sharma, A.K., Heemstra, J.M. (2011) Small-Molecule- Dependent Split Aptamer Ligation. JACS **133**, 12426− 12429.

176) Sharma, A.K., Kent, A.D., Heemstra, J.M. (2012) Enzyme-Linked Small-Molecule Detection Using Split Aptamer Ligation. Analytical Chem. **84**, 6104−6109.

177) Kaul, M., Barbieri, C.M., Pilch, D.S. (2005) Defining the Basis for the Specificity of Aminoglycoside-rRNA Recogntion: A Comparative Study of Drug Binding to the A Sites of Escherichia coli and Human rRNA. J. Mol. Biol. **346**, 119−134.

178) Santoro, M.M., Bolen, D.W. (1992) A test of the linear extrapolation of unfolding free energy changes over an extended denaturant concentration range. Biochemistry **3**, 4901-4907

179) Lawrence, C., Vallée-Bélisle, A., Pfeil, S.H., de Mornay, D., Lipman, E.A., Plaxco, K.W. (2014) A comparison of the folding kinetics of a small, artificially selected DNA aptamer with those of equivalently simple naturally occurring proteins. Protein Science **23**(1), 56 - 66.

180) Canchi, D.R., Paschek, D., García, A.E. (2010) Equilibrium Study of Protein Denaturation by Urea. JACS **132**(7), 2338 – 2344

181) Vranken, W.F., Boucher, W., Stevens, T.J., Fogh, R.H., Pajon, A., Llinas, M., Ulrich, E.L., Markley, J.L., Ionides, J., Laue, E.D. (2005) The CCPN data model for NMR spectroscopy: development of a software pipeline. Proteins **59**, 687–696.

182) Turnbull, W.B., and Daranas, A.H. (2003) On the value of c: can low affinity systems be studied by isothermal titration calorimetry? JACS **125**, 14859–14866.

183) Recht, M.I., Ryder, S.P., and Williamson, J.R. (2008) Monitoring assembly of ribonucleoprotein complexes by isothermal titration calorimetry. Methods in Molecular Biology (Lin, R.-J., Ed.) pp 117-127, Humana Press, Totowa, NJ.

184) Schuttelkopf, A.W., van Aalten, D.M.F. (2004) PRODRG: a tool for high-throughput crystallography of protein-ligand complexes. Acta. Crystallogr. Sect. D **D60**, 1355–1363.

185) Pedretti, A., Villa, L., Vistoli, G. (2004) VEGA;An open platform to develop chemo-bio-informatics applications, using plug-in architecture and script programming. J. Comput.-Aided Mol. Des. **18**, 167–173.

186) Svergun, D.I. (1991) Mathematical methods in small-angle scattering data analysis. J. Appl. Crystallogr. **24**, 485−492.

187) Delaglio, F., Grzesiek, S., Vuister, G.W., Zhu, G., Pfeifer, J., Bax, A. (1995) NMRPipe: A multidimensional spectral processing system based on UNIX pipes. J. Biomol. NMR **6**, 277−293.

188) Groves et al. (2004) Protein Molecular weight standards can compensate systematic errors in Diffusion Ordered Spectroscopy. Analytical Biochem. **331**, 395−397.

189) Konarev, P.V., Volkov, V.V., Sokolova, A.V., Koch, M.H.J., Svergun, D.I. (2003) PRIMUS - a Windows-PC based system for small-angle scattering data analysis. J. Appl. Crystallogr. **36**, 1277−1282.

190) Wiseman, T., Williston, S., Brandts, J.F., and Lin, L.-N. (1989) Rapid Measurement of Binding Constants and Heats of Binding Using a New Titration Calorimeter. Analytical Biochem. **179**, 131−137.

191) Jeener, J., Meier, B.H., Bachmann, P., and Ernst, R.R. (1979) Investigation of Exchange Processes by Two-Dimensional NMR Spectroscopy. J. Chem. Phys. **71**, 4546−4553.

192) Macura, S., and Ernst, R.R. (1980) Elucidation of Cross Relaxation in Liquids by Two-Dimensional NMR Spectroscopy. Mol. Phys. **41**, 95−117.

193) Piotto, M., Saudek, V., Sklenar, V. (1992) Gradient-Tailored Excitation for Single-Quantum NMR Spectroscopy of Aqueous Solutions. J. Biomol. NMR **2**, 661−665.

194) Freyer, M.W., Lewis, E.A. (2008) Isothermal Titration Calorimetry: Experimental Design, Data Analysis, and Probing Macromolecule/Ligand Binding and Kinetic Interactions. Methods in Cell Biology **84**, 79 – 113.

195) Deng, C., Chen, J., Nie, L., Nie, Z., Yao, S. (2009) Sensitive Bifunctional Aptamer-Based Electrochemical Biosensor for Small Molecules and Protein. Analytical Chem. **81**(24) 9972-9978.

196) Wang, J.,Cao, Y., Chen, G., Li, G. (2009) Regulation of Thrombin Activity with a Bifunctional Aptamer and Hemin: Development of a New Anticoagulant and Antidote Pair. ChemBioChem **10**(13), 2171-2176.

197) Le T.T., Scott, S, Cass A.E. (2013) Streptavidin binding bifunctional aptamers and their interaction with low molecular weight ligands. Anal Chim Acta. **761**, 143 – 148.

198) Bing, T., Liu, X., Cheng, X., Cao, Z., Shangguan, D. (2009) Bifunctional combined aptamer for simultaneous separation and detection of thrombin. Biosensors & Bioelectronics **25**(6), 1487-92.

199) Adleman L.M. (1994) Molecular computation of solutions to combinatorial problems. Science **266**(5187), 1021 - 1024.

200) Boneh, D., Dunworth, C., Lipton, R.J., Sgall, J. (1996) On the computational power of DNA. Discrete Applied Mathematics **71**(1–3), 79–94.

201) Stojanovic, M.N., Stefanovic, D. (2003) A deoxyribozyme-based molecular automaton. Nature Biotechnology **21**, 1069 – 1074.

202) Wagenknecht, Hans-Achim. Charge Transfer in DNA: From Mechanism to Application. Weinheim: Wiley-VCH, 2005. Print.

203) Campoy, A.V., Freire, E. (2005) ITC in the post-genomic era...? Priceless. Biophysical Chemistry **115**, 115 – 124

204) Liang, Y., (2008) Applications of isothermal titration calorimetry in protein science. Acta Biochim. Biophys. Sin. **40**(7): p. 565-76.

205) Freyer, M.W., Lewis, E.A. (2008) Isothermal Titration Calorimetry: Experimental Design, Data Analysis, and Probing Macromolecule/Ligand Binding and Kinetic Interactions. Methods in Cell Biology **84**, 79 – 113.

206) Herrera, I., Winnik, M.A. (2013) Differential Binding Models for Isothermal Titration Calorimetry: Moving beyond the Wiseman Isotherm. J. Phys. Chem. B **117**(29), 8659 – 8672.

207) VP-ITC Microcalorimeter. User's manual MAU130030 Rev. E. Microcal, LLC

208) Pierce, M.M., Raman, C.S., Nall, B.T. (1999) Isothermal Titration Calorimetry of Protein–Protein Interactions. Methods **19**, 213–221.

209) Nagatoishi, S., Tanaka, Y., Kudou, M., Tsumoto, K. (2009) The interaction of hyperthermophilic TATA-box binding protein with single-stranded DNA is entropically favorable and exhibits a large negative heat capacity change at high salt concentration. Mol. BioSyst. **5**, 957-961.

210) Velazquez-Campoy A, Freire E. (2006) Isothermal titration calorimetry to determine association constants for high-affinity ligands. Nat. Protoc. **1**, 186–191.

211) Bloomfield, V.A. (1981) Quasi-Elastic Light Scattering Applications in Biochemistry and Biology. Annual Review of Biophysics and Bioengineering **10**, 421 – 450.

212) Boldon, L., Laliberte, F., Liu, Li. (2015) Review of the fundamental theories behind small angle X-ray scattering, molecular dynamics simulations, and relevant integrated application. Nano Reviews **6**: 25661.

213) Fukada, H., and Takahashi, K. (1998) Enthalpy and Heat Capacity Changes for the Proton Dissociation of Various Buffer Components in 0.1 M Potassium Chloride. Proteins **33**, 159−166.

214) Feig, A. L. (2009) Studying RNA−RNA and RNA−Protein Interactions by Isothermal Titration Calorimetry. Methods Enzymol. **468**, 409−422.

215) Sampson, T. (2003) Aptamers and SELEX: the technology.World Patent Inf. **25**, 123–129.

216) Misono, T.S., Kumar, P.K.R. (2005) Selection of RNA aptamers against human influenza virus hemagglutinin using surface plasmon resonance. Anal. Biochem. **342**, 312–317.

217) Chakrabarti, R., & Schutt, C. E. (2001). The enhancement of PCR amplification by low molecular weight amides. Nucleic Acids Research, **29**(11), 2377–2381.

218) Fadhil, A.M.A., Al-Jeboory, M.R., Al-Jailawi, M.H. (2014) Improving and enhancement of PCR amplification by using ZnO and TiO_2 nanoparticles. Int. J. Curr. Microbiol. App. Sci **3**(11) 549-557.

219) SomaLogic, Inc. (2015) SSM017 Rev 3 DCN 14-194. SOMAmer® Technical note. http://www.somalogic.com/somalogic/media/Assets/PDFs/SSM-017-Rev-3-SOMAmer-Technical-Note-3-7-15.pdf. Date accessed: 23-04-2016

220) Han, K., Chen, L., Lin, Z., Li, G. (2009) Target induced dissociation (TID) strategy for the development of electrochemical aptamer-based biosensor. Electrochem. Commun. **11**, 157-160.

221) Zhao, W., Chiuman, W., Lam, J.C., McManus, S.A., Chen, W., Cui, Y., Pelton, R., Brook, M.A., Li, Y. (2008) DNA aptamer folding on gold nanoparticles: From colloid chemistry to biosensors. JACS **130**, 3610-3618.

222) Ferapontova, E.E., Olsen, E.M., Gothelf, K.V. (2008) An RNA aptamer-based electrochemical biosensor for detection of theophylline in serum. JACS **130**, 4256-4258.

223) Sakamoto, T., Oguro, A., Kawai, G., Ohtsu, T., Nakamura, Y. (2005) NMR structures of double loops of an RNA aptamer against mammalian initiation factor 4A. Nucleic Acids Res. **33**(2), 745-54.

224) Ray, P.S., Jia, J., Yao, P., Majumder, M., Hatzoglou, M., Fox, P.L. (2008) A stress-responsive RNA switch regulates VEGFA expression. Nature **457**, 915-919

225) Yildirim, I., Stern, H.A., Sponer, J., Spackova, N., Turner, D.H. (2009) Effects of Restrained Sampling Space and Nonplanar Amino Groups on Free-Energy Predictions for RNA with Imino and Sheared Tandem GA Base Pairs Flanked by GC, CG, iGiC or iCiG Base Pairs. J Chem Theory Comput. **5**(8), 2088-2100.

226) Spectral Database for Organic Compounds (SDBS); ^{1}H-NMR Spectrum ; SDBS No.: 2170; RN 130-95-0; http://sdbs.db.aist.go.jp/sdbs/cgi-bin/cre_index.cgi (Date accessed: 24-04-2015).

227) Spolar, R.S., Livingstone, J.R., and Record, M.T. Jr. (1992) Use of liquid hydrocarbon and amide transfer data to estimate contributions to thermodynamic functions of protein folding from the removal of nonpolar and polar surface from water. Biochemistry **31**(16), 3947-55.